SMiRT-12 / K. Kussmaul (Editor)
1993 Elsevier Science Publishers B.V.

K23/3

SEISMIC RESPONSE OF BASE-ISOLATED BUILDINGS USING A VISCOELASTIC MODEL

R. Aziz Uras

Reactor Engineering Division, Argonne National Laboratory, 9700 South Cass Avenue, Argonne, IL 60439, USA

1 INTRODUCTION

Due to recent developments in elastomer technology, seismic isolation using elastomer bearings is rapidly gaining acceptance as a design tool to enhance structural seismic margins and to protect people and equipment from earthquake damage. With proper design of isolators, the fundamental frequency of the structure can be reduced to a value that is lower than the dominant frequencies of earthquake ground motions. The other feature of an isolation system is that it can provide a mechanism for energy dissipation.

In the USA, the use of seismic base-isolation has become an alternate strategy for advanced Liquid Metal-cooled Reactors (LMRs). ANL has been deeply involved in the development and implementation of seismic isolation for use in both nuclear facilities and civil structures for the past decade. Shimizu Corporation of Japan has a test facility at Tohoku University in Sendai, Japan. The test facility has two buildings: one is base isolated and the other is conventionally founded. The buildings are full-size, three-story reinforced concrete structures. The dimensions and construction of the superstructures are identical. They were built side by side in a seismically active area. In 1988, the ANL/Shimizu Joint Program was established to study the differences in behavior of base-isolated and ordinarily founded structures when subjected to earthquake loading. A more comprehensive description of this joint program is presented in a companion paper (Wang et al. 1993).

With the increased use of elastomeric polymers in industrial applications such as isolation bearings, the importance of constitutive modeling of viscoelastic materials is more and more pronounced. A realistic representation of material behavior is essential for computer simulations to replicate the response observed in experiments.

2 COMPUTER SIMULATIONS

Three-dimensional space frames are employed to represent the superstructures of the ordinary building and isolated buildings. The beams, columns and girders of the buildings are represented by 3-D beam elements. No stiffness contribution is considered from the outer walls and partitions. However, the masses of these components are added into the appropriate nodal points. Three beam elements which also include the stiffness of the basement reinforced concrete wall are used to model each basement column for the ordinary building. The finite element configuration used in the simulation is shown in Fig. 1 where the three locations labeled

by numbers 111, 63, and 9 indicate the elevations of the basement, first floor and roof, respectively.

As a part of the above mentioned joint program the main focus of this study is set on a comparison of the computer simulation results of two different material models with the measured response during actual earthquakes. The base-isolation bearings considered here were designed to have a frequency of 0.75 Hz at 50% shear strain. The vertical and horizontal stiffnesses are 13.6×10^5 and 961 kgf/cm, respectively.

Here, a fully three-dimensional finite-strain viscoelastic model developed by Simo and Taylor 1983, is employed to characterize the behavior of isolator bearings. In the Simo and Taylor model, the material is assumed to be isotropic in its virgin as well as in its deformed or damaged state. Volumetric and deviatoric responses are uncoupled over any range of deformation. The volumetric response is purely elastic. The proposed damage mechanism incorporates the softening behavior of rubber undergoing deformation (Mullin's effect). In the cyclic test, this translates into progressive degradation of the storage modulus with increasing maximum strain amplitude. The analytical hysteresis curve simulated by this model is given in Fig. 2.

The bilinear constitutive model is a simplified representation of the hysteretic curve for strain-softening rubber material. The linear elastic modulus is determined from the first cycle of loading in a cycling loading test, and the plastic modulus is extracted from the later stages of the same test.

The structural elements and the two constitutive models mentioned above have been incorporated in the ANL-developed computer program SISEC (Seismic Isolation System Evaluation Code) (Wang et al. 1991).

3 RESULTS AND DISCUSSION

During the testing period, thirty-seven (37) earthquakes had occurred in the Sendai area. Three of these earthquakes, No. 2, No. 6 and No. 17, are of significance for numerical simulation and comparison with observed data. Earthquake No. 6 (EQ #06) has the largest amplitude accelerations. Earthquake No. 17 (EQ #17) has the longest duration and a broad frequency spectrum. The range of frequencies in that earthquake indicates that the soil-structure interaction may be of importance. Earthquake No. 2 (EQ #02) has the same order of magnitude as EQ #06 and EQ #17. It occurred right after the installation of bearings, and the bearings were still in the virgin state. It is felt that the dynamic characteristics of the bearings can be obtained from the responses of the isolated building under those three earthquakes. Due to space limitations, comparisons among the observed response, the simulation results obtained using the viscoelastic and bilinear spring models are presented for one earthquake only, *viz.* for EQ #06.

In the longitudinal direction, the input acceleration of the Earthquake #6 has one dominant frequency of 2.23 Hz. The maximum response amplitude for the first floor of the viscoelastic model is 25% greater than the observed one. The results of the bilinear model yields a 22% larger amplitude (Figs. 3 and 4). The frequency spectrum of the viscoelastic model derived from the time history computations through FFT yields a response frequency of 2.23 Hz for the first floor and the roof whereas the observed frequency is 2.27 Hz. It should be noted that a comparably large peak is found at 2.40 Hz both in the observed and computed frequency spectra. The dominant frequencies for the bilinear case are 2.23 Hz for both floors.

Similarly, in the transverse direction, comparably large peaks (dominant frequency at 2.57 Hz) are encountered in the input record. The first floor maximum response amplitude from the viscoelastic model is 15% smaller than that of the observed. Bilinear model yields 18% smaller results. In the viscoelastic model, both the first floor and the roof have a computed frequency

of 2.30 Hz. However, the observed data yields 2.07 Hz for the first floor and 2.17 Hz for the roof with several closely-spaced frequencies in 2.07-2.42 Hz range. The frequencies obtained with the bilinear model are 2.13 Hz and 2.17 Hz for the first floor and the roof, respectively.

4 CONCLUSIONS

The comparison of results shows that the viscoelastic model can predict the actual behavior of highly-filled rubber material used in isolator bearings rather accurately. However, the effectiveness of this model is somewhat dependent on the input spectrum. When the spectrum of the input motion has a clear dominant frequency, the simulation results are in excellent agreement with the experimentally observed data. When the input motion has a wide range of frequencies and no visible dominant frequency exists in the spectrum, the maximum response predicted by the model is shown to be off about 30%. However, the frequency of the superstructure is well retained in the simulations.

The bilinear model originally proposed is found to be fairly effective. However, the performance of the viscoelastic model in most of the test cases presented here is better than that of the bilinear model. The reliability of the viscoelastic model over the bilinear model is also consistently higher. However, the implementation of the viscoelastic model depends on the availability of two types of test data: cyclic shear and relaxation tests. This is different in the bilinear case, where the data needed to construct the bilinear model are derived only from cyclic shear tests. Thus, the bilinear model becomes very attractive when the relaxation data is not available for the rubber material. Nevertheless, it is highly recommended that the viscoelastic model be used in the future seismic response analysis if all the required data of cyclic shear and relaxation tests are available.

ACKNOWLEDGMENTS

Work supported by the National Science Foundation, Agreement No. CES-8800871.

REFERENCES

Simo, J. C. and Taylor, R. L. (1983). A Simple Three Dimensional Model Accounting for Damage Effects, Report No. UCB/SESM/83-10, Department of Civil Engineering, University of California, Berkeley.

Wang, C. Y. et al. (1991). System Response Analyses of Base-isolated Structure to Earthquake Ground Motions, Trans. SMIRT-11, paper K26/6.

Wang, C. Y. et al. (1993). System Response of a Base-isolated Building with High Damping-Low Shear Modulus Elastomeric Bearings, Trans. SMIRT-12, paper K23/6.

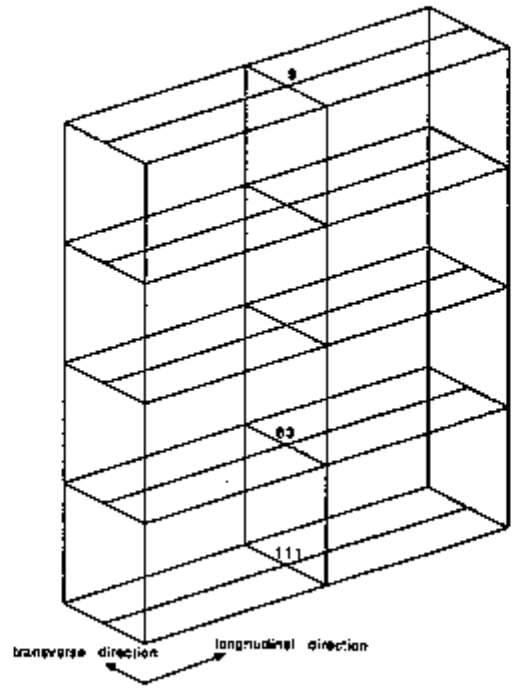

Figure 1. Finite Element Mesh

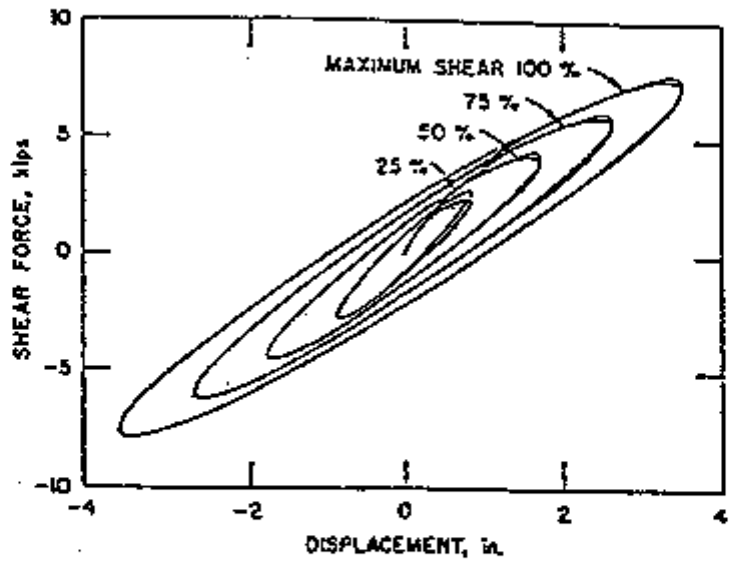

Figure 2. Analytically Simulated Hysteresis Curve

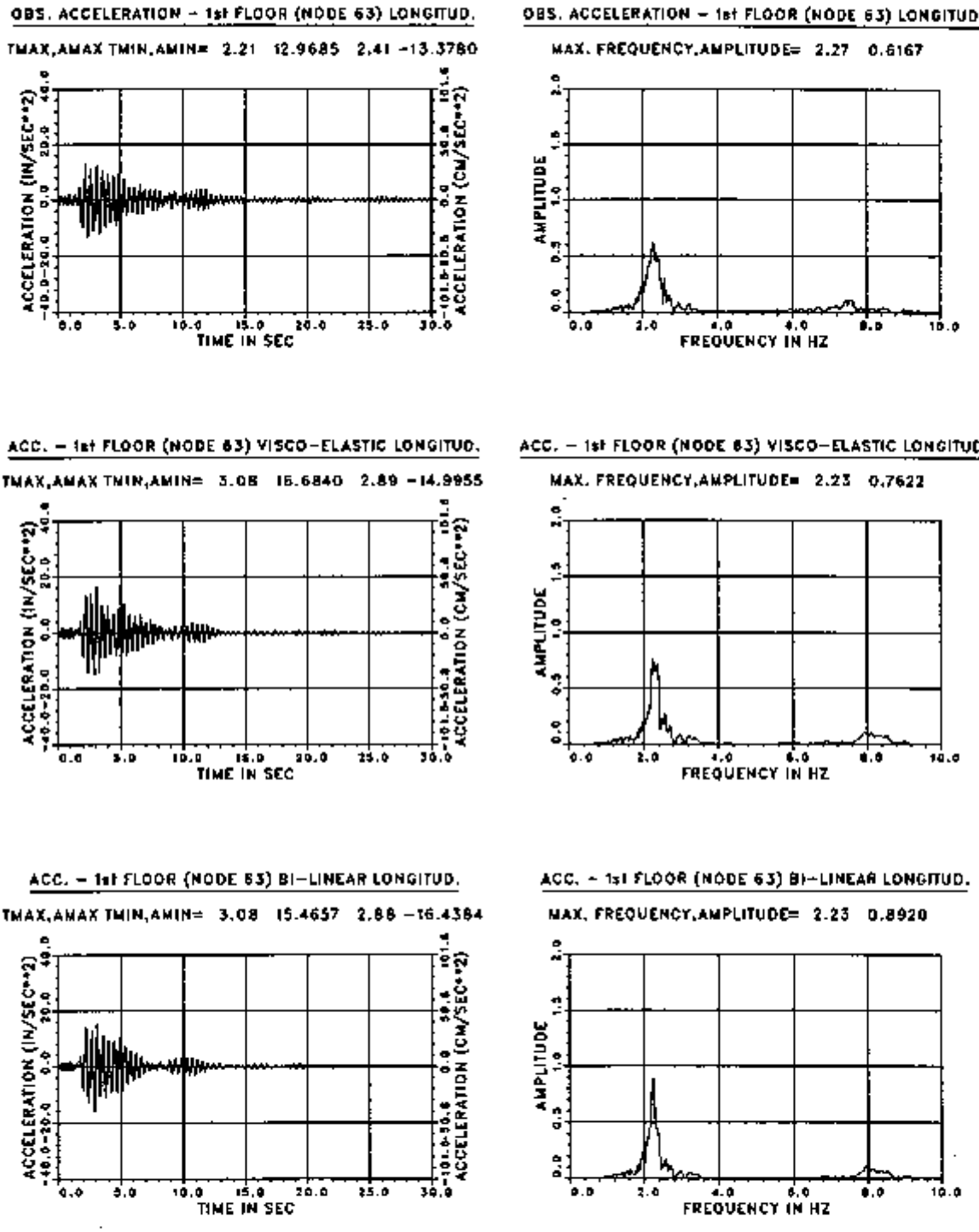

Figure 3. Comparison of Simulation Results with Experimental Observation - First Floor

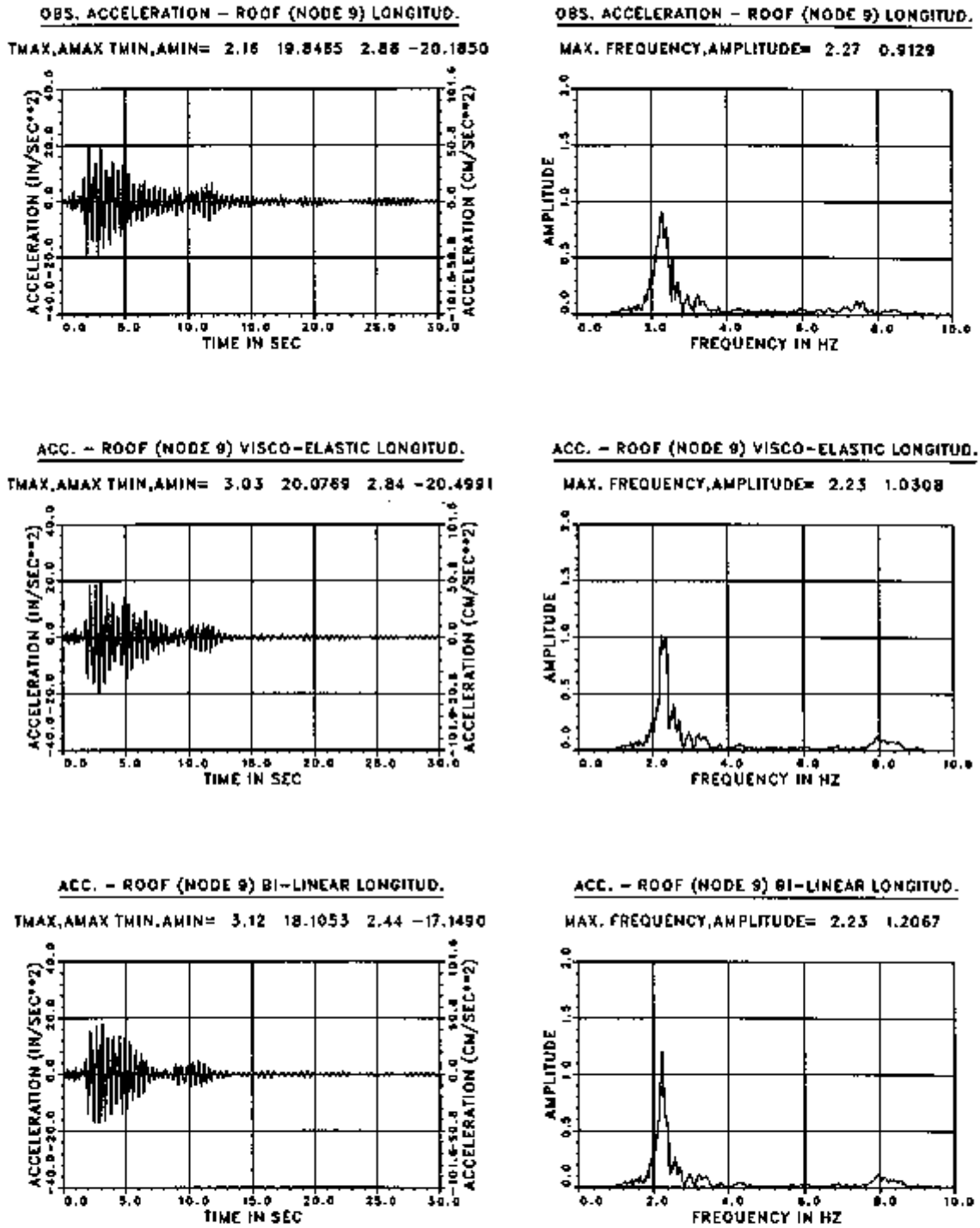

Figure 4. Comparison of Simulation Results with Experimental Observation - Roof

SMiRT-12 / K. Kussmaul (Editor)

K25/4

DEVELOPMENT OF PERIPHERALLY RESTRAINING TYPE SEISMIC ISOLATOR

H. Matsushita, K. Fujisawa and T. Sasaki

Research Department, Research and Development HQ, Sumitomo Rubber Industries, Ltd., 1-1, 1-chome, Tsutsui-cho, Chuo-ku, Kobe 651, Japan

1. Abstract

This paper deals with the development of a peripherally restraining type seismic isolator. Experiments were carried out on a full scale model of 5400 kN rated load capacity, and on contracted models thereof with contraction ratios of 0.3 and 0.18 in dimensions in terms of horizontal and vertical properties and destructive properties.

As the results, the newly developed peripherally restraining type seismic isolator proved to have larger damping capability than that of the existing high-damping rubber bearings, and its destructive properties proved to be satisfactory in its actual application to buildings. The comparison between the data scaled up from the results with contracted models and those with the full scale model showed good agreements to convince that the performance of the contracted models might provide the good prediction of the full scale model.

2. Introduction

It has been regarded as very important for critical facilities such as nuclear reactors that the seismic acceleration, if it should arise, be reduced. In recent years, the high-damping rubber bearings, which have damping capability for themselves, have been attracting attention and several research works are reported(1). In general,the larger the damping capability of rubber bearings, the more effective in reducing the seismic acceleration, thus reducing the response of the upper structures in terms of displacement and acceleration. Accordingly, the development of rubber bearings having ever higher damping capability has been hoped for.

In carrying out the dynamic test of the full scale rubber bearings under the same conditions as they are actually used, a testing machine having an unrealistically large actuator will be required. In fact, most researches on full scale models have been carried out at lower frequencies than those may be encountered in the actual use, or estimations have been made from the test results with contracted models at the same frequencies as the actual use.

However, there are few reports available which focus on whether or not the results with such contracted models should correctly predict the dynamic properties of the full scale model.

This paper deals with the development of a peripherally restraining type rubber bearing which has larger damping capability than that of the existing high-damping rubber bearings. It also refers to the experiment to study whether or not the test results with contracted models correctly provide the good prediction of dynamic properties of full scale models.

3. Experimental

3.1. Specimens

The full scale model of a peripherally restraining type seismic isolator (hereinafter referred to as "PRB") of 5400 kN rated load, shown in Fig.1(a), was tested in terms of the horizontal dynamic properties and the vertical compression. The "PRB" comprises a core block made of a synthetic rubber compound (hereinafter referred to as the "core block"), the damping of which is even higher than that of the high-damping rubber compound used in the multilayers, and a peripherally restraining ring (hereinafter referred to as the "restraining ring") made of multilayers of alternately stacked high-damping rubber sheet bonded to a steel plate surrounding the aforesaid core block. Under the vertical load on the "PRB", the "restraining ring" effectively restrains the homogeneous "core block" from its bulging out thus making the vertical stiffness of "PRB" almost identical with that of the existing high-damping rubber bearing (hereinafter referred to as "HDB"). (This suggests that "PRB" will be usable in the same way as "HDB"). In Fig.1(b) is shown the dimensions of the "PRB" of 5400 kN rated load, which was used as the specimen for the destructive test, the number of rubber layers of which was reduced to some degree so that the specimen might successfully break down within the maximum horizontal stroke of the testing machine. The dimensions and profiles of the contracted "PRB" models with contraction ratios of 0.3 and 0.18 are shown in Figs.1(C) and 1(d).

The dimensions and profiles of "HDB" models, used for the comparison with "PRB" models, are shown in Figs.2(a),2(b),2(c) and 2(d); for the model sizes of full scale (5400 kN rated load), 0.3 contraction ratio, and 0.18 contraction ratio, respectively.

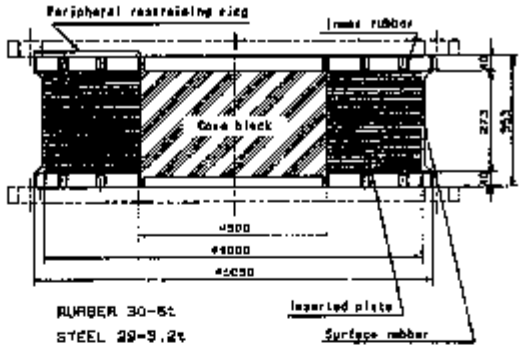

(a) Full scale model (ϕ 1000-500 PRB)

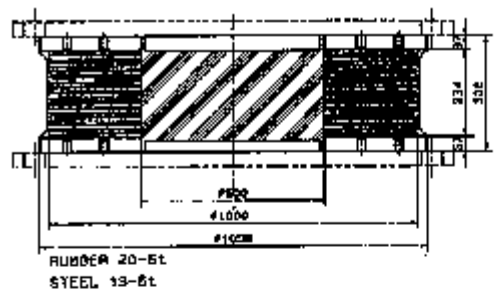

(b) Full scale model for the destructive test (ϕ 1000-500 PRB/L)

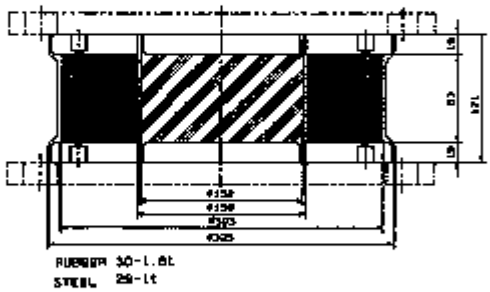

(c) 0.3 contraction ratio model (ϕ 303-152 PRB)

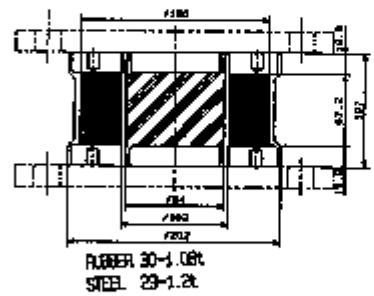

(d) 0.18 contraction ratio model (ϕ 180-94 PRB)

Fig.1 Dimension of the "PRB"

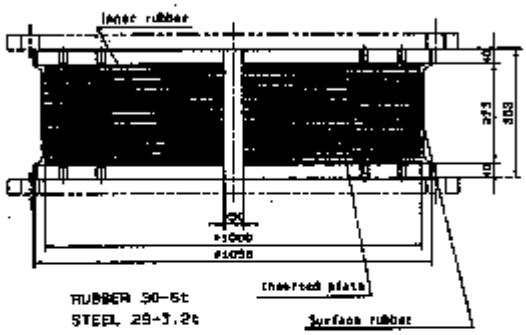

(a) Full scale model (ϕ 1000 HDB)

(b) Full scale model for the destructive test (ϕ 1000 HDB/L)

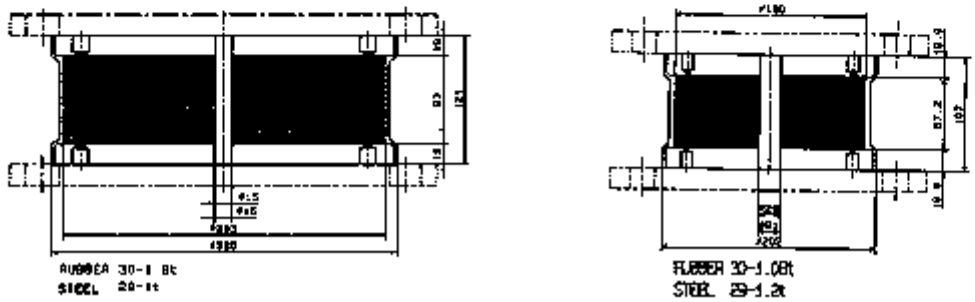

(c) 0.3 contraction ratio model (ϕ 303 HDB)

(d) 0.18 contraction ratio model (ϕ 180 HDB)

Fig.2 Dimension of the "HDB"

3.2. Loading Facilities And Loading Method

The large biaxial testing machine used for the full scale models is shown in Fig.3. The small biaxial testing machine as used for the contracted models is shown in Fig.4.

The dynamic horizontal loading tests were carried out under the conditions as given in Table 1. The loading in these tests were given from the smaller shear strain to the larger one, with three waves for each strain, and the overall test was repeated twice.

It has been known that the properties of high-damping rubbers are affected by the history of the shear strains experienced. Therefore, following discussions are based on the data of the second loading cycle above because the data in the horizontal direction were more stable in that cycle.

Table 1. The dynamic horizontal loading test conditions.

	Contraction ratio	Pressure (MPa)	Frequency (Hz) *
Full scale models	——	5.6	0.01
Contracted models (1)	0.3	3.2	0.01
Contracted models (2)	0.18	5.6	0.01
		7.4	0.5

* sinusoidal

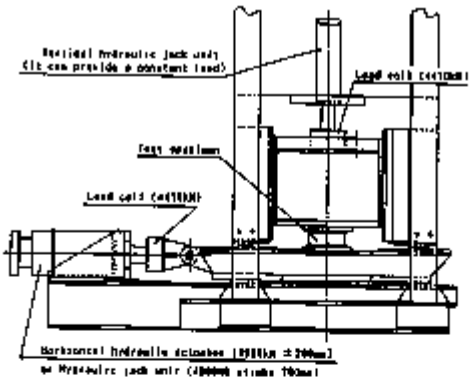

Fig.3 The large biaxial testing machine

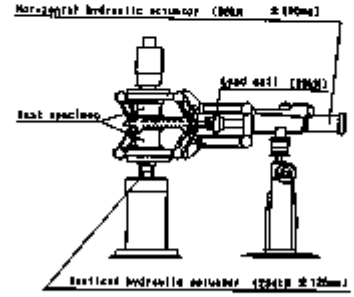

Fig.4 The small biaxial testing machine

4. Results and Discussion

4.1. Static Compressive Tests

The vertical compressive test results of full scale models of "PRB" and "HDB" are shown in Fig.5. The vertical spring constant of "PRB" proved to belower than that of "HDB" by only 9%, which may be defined as almost identical.

4.2. Dynamic Horizontal Loading Tests

Fig.6 shows the horizontal restoring forces of the "PRB" models with full scale and 0.3 contraction ratio in which the data are taken from the third waves. These data were used for the calculation of the horizontal spring constants and the equivalent damping ratios of "PRB" models, and the results are shown as a function of shear strains in Fig.7; however, it should be noted that the calculation results shown for the contracted models are the scaled up ones to equate with the full scale models. The horizontal spring constants and the equivalent damping ratios of "HDB" are shown in Fig.8 as a function of shear strains wherein again the results shown for the contracted models are the scaled up ones to equate with the full scale models. With regard both to "PRB" and "HDB", the scaled up data of the contracted models are in good agreement with those of the full scale models.

As regards the shear strain dependence of the horizontal spring constants, the scaled up data of the contracted models seem of provide the good prediction of the full scale models.

In Fig.9 is shown, as a function of

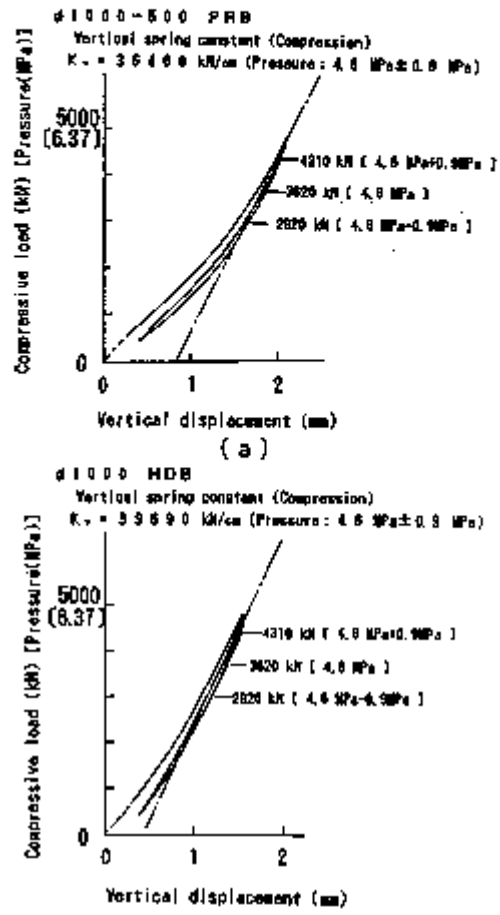

Fig.5 Compressive load vs. vertical displacement
(a) Full scale model (φ 1000-500 PRB)
(b) Full scale model (φ 1000 HDB)

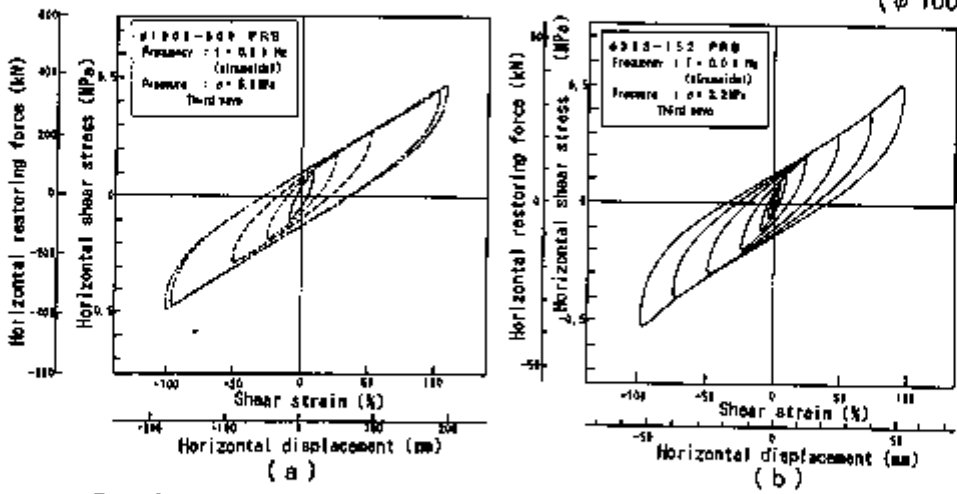

Fig.6 The horizontal restoring forces vs. shear strain
(a) Full scale model (φ 1000-500 PRB)
(b) 0.3 contraction ratio model (φ 303-152 PRB)

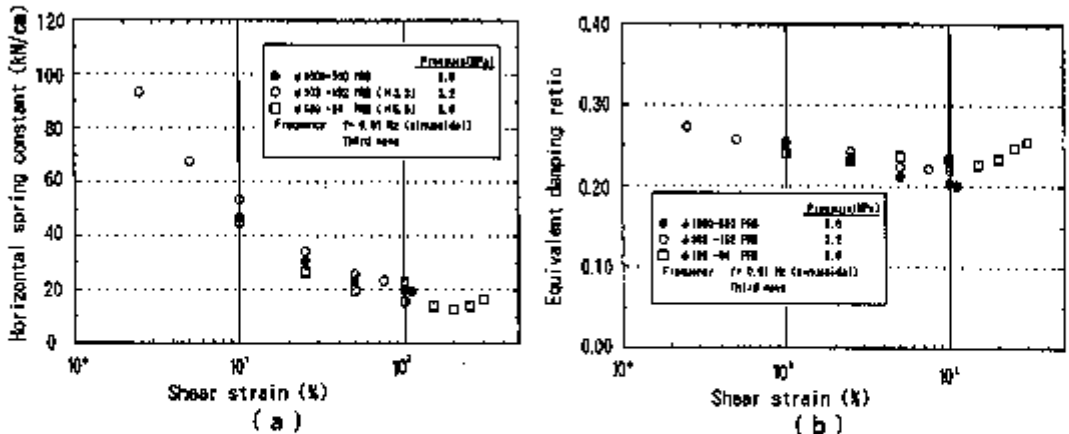

(a) (b)

Fig.7 (a) Horizontal spring constant vs. shear strain (PRB)
(b) Equivalent damping ratio vs. shear strain (PRB)

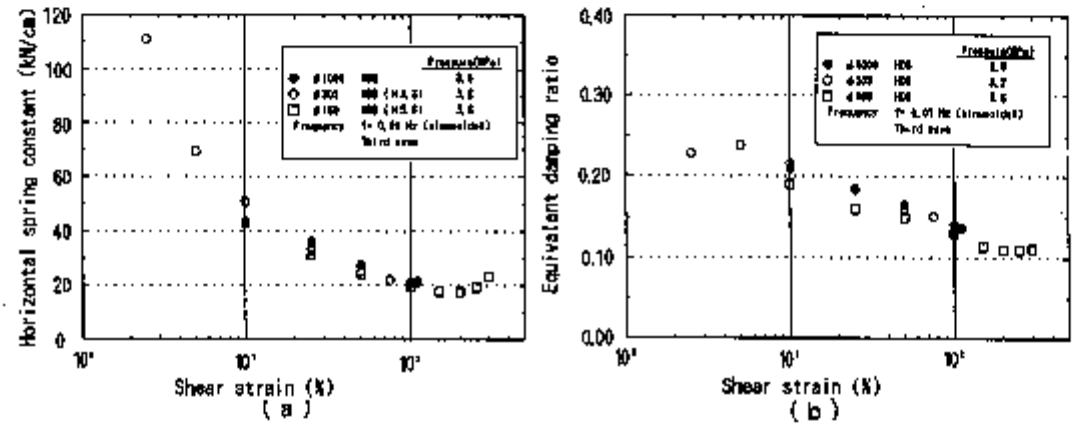

(a) (b)

Fig.8 (a) Horizontal spring constant vs. shear strain (HDB)
(b) Equivalent damping ratio vs. shear strain (HDB)

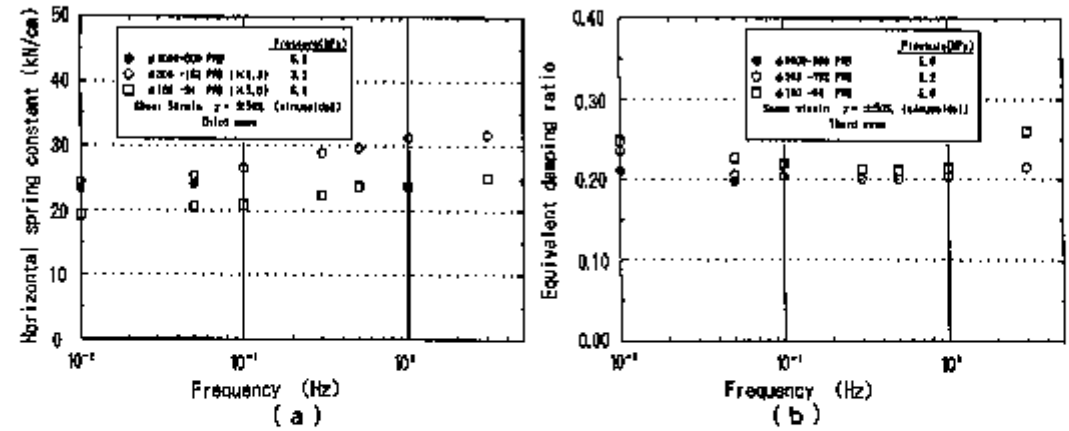

(a) (b)

Fig.9 (a) Horizontal spring constant vs. frequency (PRB)
(b) Equivalent damping ratio vs. frequency (PRB)

frequencies, the horizontal spring constants and the equivalent damping ratios of "PRB" in the shear strain range of ±50%. The data of the full scale models, although not so many in number, seem to show a similar tendency to the contracted models. In Fig.10 are shown the restoring forces of "PRB" of the 0.18 contracted model as measured at 0.5Hz (equivalent to the frequency which may be experienced by a full scale model during an earthquake) under the pres-

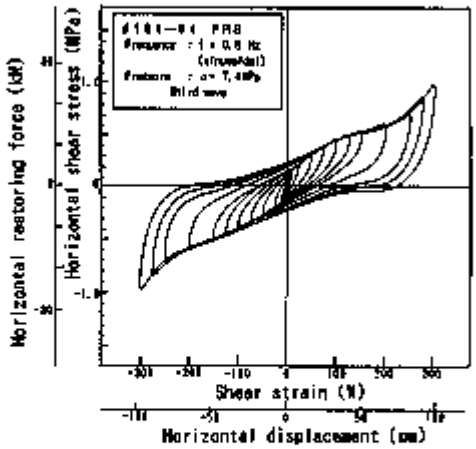

Fig.10 The horizontal restoring forces of the 0.18 contracted "PRB" model

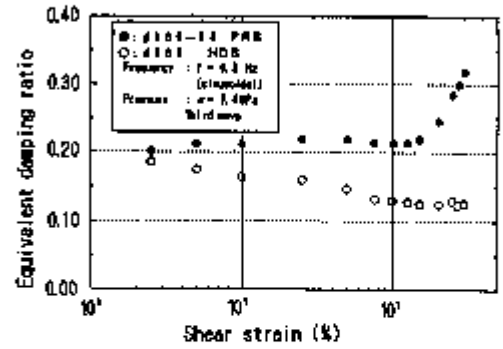

Fig.11 Equivalent damping ratio vs. shear strain for the 0.18 contracted model

sure of 7.4MPa , wherefrom the equivalent damping ratios were calculated and the results are shown in Fig.11 as a function of the shear strains. And also the equivalent damping ratios of the 0.18 contraction model of "HDB" are shown in Fig.11. The equivalent damping ratios of "PRB" was about 0.2, in the shear strain range of ±50% , which was higher than thatof "HDB".

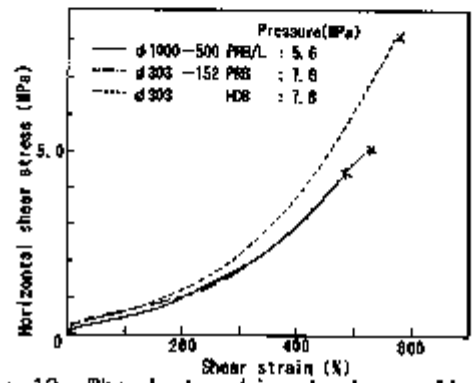

Fig.12 The destructive test results of full scale "PRB" model, 0.3 contracted models of "PRB" and "HDB"

4.3. Destructive Tests

The destructive test results of full scale "PRB" model are shown in Fig.12 wherein the results of 0.3 contracted models of both "HDB" and "PRB" are also shown. The relationship of the shear strain and the horizontal load of the full scale "PRB" model were in good agreement with that of the contracted model. The shear strain at the failure of "PRB" was smaller than that of "HDB", however, this critical strain is more than twice as large as about 170% strain (about 30cm in the horizontal displacement) which equates with the Level 2. Therefore,"PRB" will be satisfactory in the actual use without any problem.

5. Conclusions

From these results, it is concluded that:

(1) The vertical spring constant of "PRB" is on the equivalent level to that of an existing "HDB".
(2) The equivalent damping ratios of "PRB" is higher than that of an existing "HDB".
(3) The rather lower critical shear strain of "PRB" than that of "HDB" will have no problem in its actual use.
(4) The performance of dimensionally contracted models might provide the prediction of that of the full scale model.

6. References

1. T.Fujita et al., Proceedings of a post-conference seminar of the 10th SMIRT, 268-295 (1989)

SMiRT-12 / K. Kussmaul (Editor)

K25/6

APPLICATION OF ACCELERATED LIQUID FLOW DAMPERS TO BASE ISOLATION OF REACTOR BUILDINGS

S. Kawamata[1], M. Ohnuma[1], T. Toda[2] and T. Makita[2]

[1]Tohoku Institute of Technology, Sendai, Japan
[2]Technical Research Institute, Hazama Corporation, Tsukuba, Japan

ABSTRACT

"Accelerated liquid flow damper" utilizes turbulent flow resistance of liquid which is driven into small tubes by a piston-cylinder system and is characterized by very large force capacity and nonlinearly increasing resistance against structural vibration of large amplitude. Resisting force rules are derived by excitation test of the damper and applicability of the damper to base-isolated reactor buildings is examined by earthquake response analyses of the damped system.

1. INTRODUCTION

It has been widely recognized that base isolation is a powerful mean of seismic design of reactor buildings. Being characterized by enormous mass of the building and very high design earthquake, the isolation system necessitates installation of effective damping devices.

The authors developed "accelerated liquid mass damper" for the purpose of passive control of structural vibration[1), 2)] and its effectiveness was proved by tests of small scaled structural models.

To apply the dampers of this type to structures having large mass, the ratio of sectional area of the cylinder to the one of the discharge tube must be large enough to obtain high velocity and high pressure gradient of liquid flow. By excitation of a damper of half scale to prototype, it was found that, for very rapid flow in tubes, inertial resistance of liquid mass became negligible compared to high viscous resistance of turbulent flow and the latter exhibited strong nonlinearity to flow velocity.

In virtue of the nonlinearity of its resistance, the damper is able to suppress the amplitude of resonant response to earthquakes without detracting the action of isolators to filter the earthquake components of high frequency. This property, together with its large capacity of resisting force and displacement stroke, provides the accelerated liquid flow damper with noteworthy advantages in the application to base-isolated reactor buildings.

In this paper, empirical rules of pressure gradient of liquid flow in a tube are derived based on the results of excitation tests of the damper and the damping factor of single mass vibration system is evaluated. Also, applicability of the damper to base-isolated reactor buildings is examined by analyzed steady and earthquake responses of model structures.

2. RESISTING FORCE TEST OF DAMPER

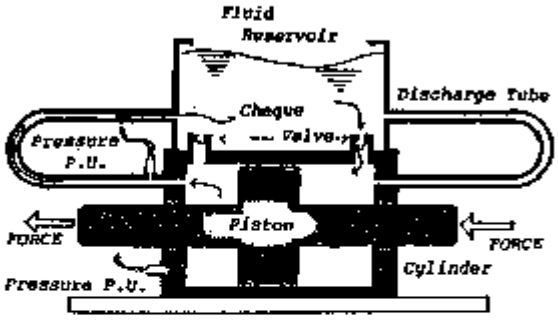

Fig.1 Scheme of accelerated liquid flow damper

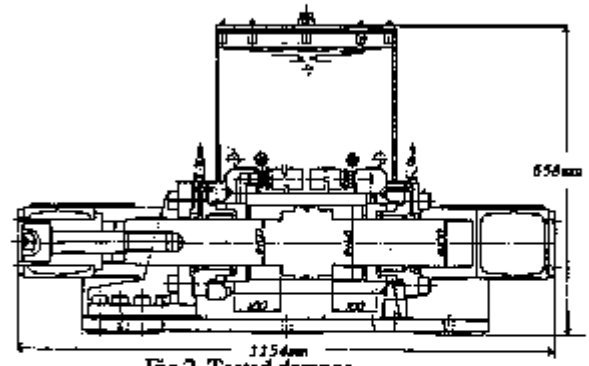

Fig.2 Tested damper

As shown in the scheme of Fig.1, an accelerated liquid flow damper is composed of a fluid reservoir with cheque valves, piston-cylinder and discharge tubes. The liquid flow in the tubes becomes intermittent transient one by the action of the cheque valves and its flow rule is not known.

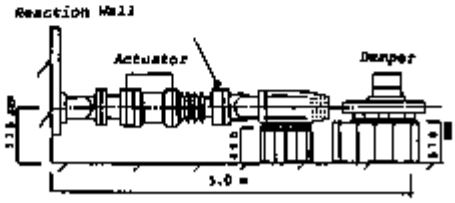

Fig.3 Test setup

To investigate the flow resistance rule, a damper shown in Fig.2, which was designed in half prototype scale, was subjected to sinusoidal excitation by the use of a hydraulic actuator in a manner shown in Fig.3. Damper oil was filled in and discharge tubes of 6.25*mm* and 9.4*mm* inner diameter were used. Exciting frequency ranged from 0.33 to 3.0Hz with displacement amplitude up to ±60*mm*.

Fig.4 shows an example of loops of actuator force and inner pressure in relation to piston displacement. Relation of pressure in discharge tube at zero displacement to piston velocity, shown in Fig.5, indicates that the pressure gradient along tubes does not depend on the exciting frequency and it has strong nonlinearity to sectional mean velocity of the fluid flow.

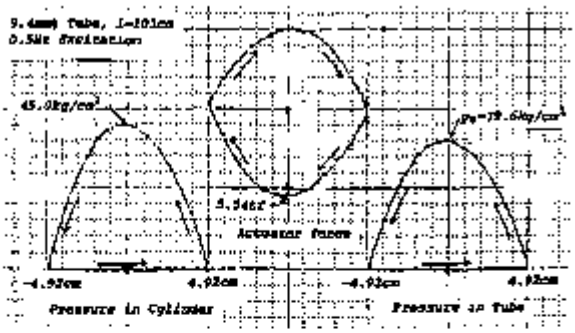

Fig.4 Force / pressure- displacement loops

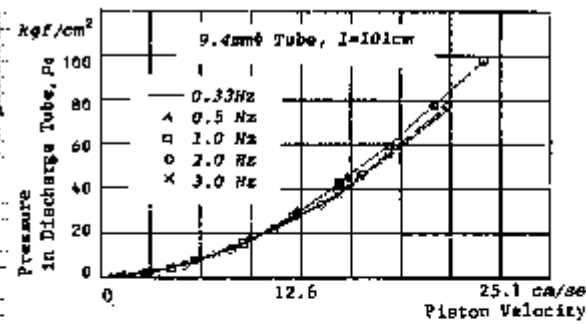

Fig.5 Pressure-velocity relation

As practiced in the analysis of steady flow data, the measured pressure in the tube at zero displacement was represented in term of pipe friction factor, by which the pressure drop along tube is given as

$$\Delta p_T = \frac{\rho l}{2D} \cdot u_m^2 f \tag{1}$$

where, Δp_T : pressure drop in tube; D : inner diameter of tube; ρ : density of fluid; u_m : mean velocity of pipe flow; l : length of tube; f : friction factor

Fig.6 shows the friction factors obtained for both the tubes in terms of Reynolds number defined by diameter of tube, R, where

$$R = u_m D / \nu , \qquad \nu : \text{kinematic viscousity} \tag{2}$$

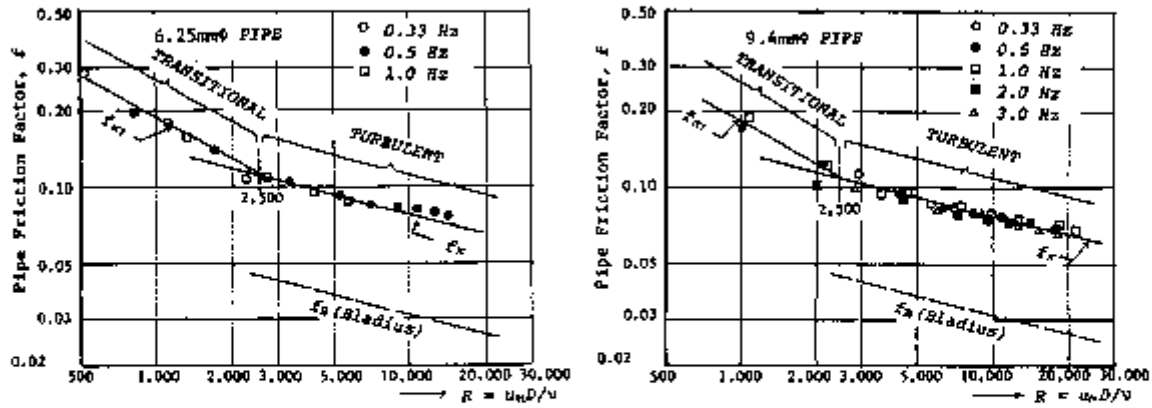

Fig.6 Relation of pipe friction factor to Reynolds number

3. FLOW RULES AND EVALUATION OF DAMPING FACTOR

As shown in Fig.6, plots of pipe friction factor to Reynolds number can be represented by two straight lines: f_K corresponding to turbulent flow region and f_{KI} for transitional region, which can be formulated as

$$f_K = 0.762\,R^{-0.25} \qquad \text{for } 2{,}500 \le R \text{ (turbulent)} \tag{3}$$

$$f_{KI} = 9.49\,R^{-0.57} \qquad \text{for } R < 2{,}500 \text{ (transitional)} \tag{4}$$

Comparing to the known H. Bladius' formula for turbulent steady flow in circular pipes,

$$f_B = 0.316\,R^{-0.25} \qquad \text{for } 2{,}300 \le R \text{ (turbulent)} \tag{5}$$

f_K in Eq.(3) has the same dependence on Reynolds number but has 2.4 times greater coefficient.

In the excitation test, the pressure drop from the outlet of the discharge tube to the surface of the liquid reservoir was not observed separately and was included in the pressure drop in the tube. Therefor, Eq.s (3) and (4) should be interpreted as tentative representations. Transition points from flow resistance linear to velocity into the transitional phase were not recognized in the test: they seemed to be in the region of very small displacement amplitude.

The pressure drop from inside of the cylinder up to inlet of the discharge tube was obtained as the pressure difference between pick up points in the cylinder and in the tube. It can be represented in the term of mean velocity of fluid in the tube as

$$\Delta p_C = 0.661\,\rho\,u_m^2 \tag{6}$$

where, Δp_C : pressure drop in cylinder

The pressure drop in the cylinder may vary according to the design of fluid conduit up to the inlet of the tube.

According to Eq.s (1), (2) and (3), pressure in the tube is proportional to the 1.75th power of mean velocity of fluid in the point of zero displacement. However, for the whole phase of sinusoidal flow, the flow rules should be examined separately.

By the analysis of the shape of observed pressure-displacement loops, it was concluded that the 1.75th power rule of pipe flow could be applied for the whole process of the flow without losing accuracy of response analyses of structural systems. By the same reasoning, flow rules of Eq.s (4) and (6) were also assumed to be valid for the whole flow process.

Now, let the damping factor for a single mass vibration system with the damper shown in Fig.7 be evaluated. Resisting force of the damper is given by

$$F_D = A\,(\Delta p_C + \Delta p_T) \tag{7}$$

where, F_D : resisting force of damper
A : pressure receiving area of piston-cylinder

The mean velocity of liquid flow in the tube is represented in the term of responding velocity of the structural system as

$$u_m = \frac{A}{a}\dot{x} = \frac{4A}{\pi D^2}\dot{x} \qquad (8)$$

where, a : sectional area of discharge tube
x : relative displacement of system

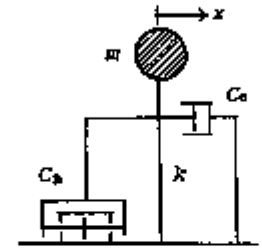

Fig.7 Damped system

The resisting force of Eq. (7) can be evaluated by the use of Eq.s(1)~(6) and Eq.(8). Consequently, damping coefficient and damping ratio to the critical can be obtained as follows:

$$C_D = F_D / \dot{x}, \quad h_D = C_D / 2\omega_0 m \qquad (9)$$

where, C_D : damping coefficient, h_D : damping ratio
m : mass of system, ω_0 : natural frequency

As the resisting force of the damper is nonlinear to velocity, the damping ratio of Eq.(9) should be evaluated in every step of time integration for response analysis and be added to a viscous damping ratio, $h_0 = C_0 / 2\omega_0 m$, proper to the structural system.

4. ANALYSIS OF STEADY RESPONSE TO GROUND MOTION

To investigate the response characteristics of structures provided with the accelerated liquid flow dampers to ground motion, steady response of a single mass system with the damper to sinusoidal ground acceleration was analyzed. Parameters of the subject system is given in Table 1.

Table 1. Parameters of analyzed system

Structure		Damper (1/2 scale model)	
Weight of mass, W	$500ton$*	Pressure area, A	$122.5cm^2$
Natural period, T_0	$2.0sec$	Diameter of tube, D	$0.94cm$
Proper damping, h_0	0.02	Length of tube, l	$200cm$
		Density of liquid, ρ	$0.88gram/cm^3$
		Kinematic viscosity, ν	$0.26cm^2/sec$

* Weight of area covered by single unit of damper

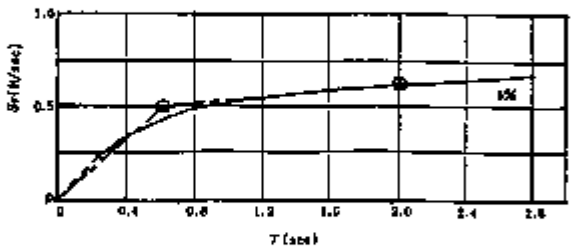

Fig.8 Mean velocity response spectrum (H. Umemura)

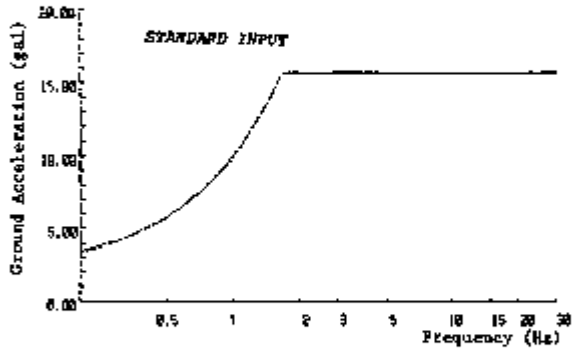

Fig.9 Standard ground-acceleration spectrum

To reflect general character of earthquake motion, a standard input acceleration spectrum was prepared. Mean velocity response spectrum of 5% damping system by H. Umemura, shown in Fig.8, was represented by bi-linear approximation as shown in the

same figure. The standard input ground acceleration spectrum shown in Fig.9 was decided as the one by which a single mass system with the same damping produces the specified velocity response in resonance. Steady vibration was analyzed not only with regard to the standard input but also to those amplified by 2 times and 4 times to see the effect of nonlinear resistance of the damper.

Resonance curves were obtained applying the well known theory of steady vibration, where harmonic response was assumed and viscous damping whose energy dissipation was equivalent to the nonlinear resistance of the damper was searched for by an iterative procedure of prediction and correction.

Fig.10 shows resulted transmissibility for the three levels of input acceleration compared with the cases of constant viscous damping, the corresponding equivalent viscous damping of the system being presented in Fig.11.

It is worthwhile noting that the peak transmissibility in resonance decreases to the input of higher level, while the one to the components of higher frequency is kept far smaller than the cases of viscous damping.

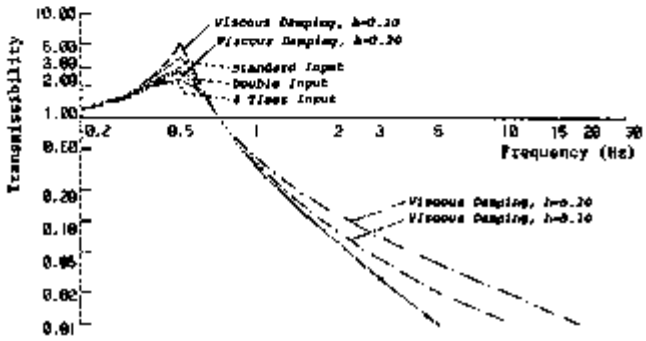

Fig.10 Transmissibility

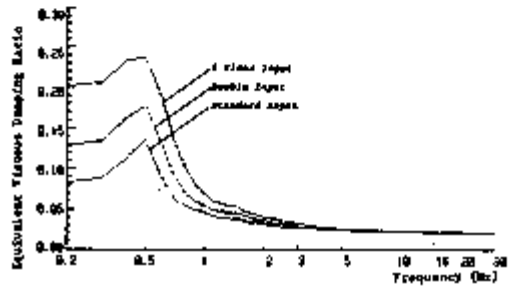

Fig.11 Equivalent damping ratio

5. ANALYSIS OF RESPONSE TO EARTHQUAKE

Single mass systems with an accelerated liquid flow damper of full scale were subjected to analyses of response to two representative recorded earthquakes. Time histories of response were obtained by Runge-Kutta method.

Parameters of the analysis are listed in Table 2. In all cases $h_0 = 0.02$ was assumed.

Table 2. Parameters of full scale damper and structural systems

Inner Diameter of cylinder:	30cm*	Diameter of tube:	2.5cm	Liquid density:	$0.88 gram/cm^3$
Diameter of piston rod:	15cm*	Length of tube:	4.0m	Kinem. viscosity:	$0.23 cm^2/sec$

System *A*	Natural period:	$T_0 = 2.0sec$	Weight of mass:	W = 1,000*ton* **
System *B*	Natural period:	$T_0 = 4.0sec$	Weight of mass:	W = 2,000*ton* **

* Pressure receiving area: 350 cm^2

** Weight covered by a unit of damper

Ground acceleration of El Centro-NS and Hachinohe-EW was input in real amplitude and in double amplitude. Table 3 shows the maximum values of the inputs and resulted responses. An example of the time histories of response is presented in Fig.12.

From the results of the analysis, it can be seen that the base-isolated systems with the damper realize very low amplification factors of responding acceleration with the displacement of isolators well within their allowable limit, and also that factors of responding acceleration and displacement decrease to the higher level of input in general. The maximum inner pressure of the damper is the order of $300 kgf/cm^2$ and is acceptable in the design of the damper.

Table 3. Maximum responses to earthquake inputs

Input earthquake		ELCentro-NS		Hachinohe-EW	
		Real amplitude	Double amplitude	Real amplitude	Double amplitude
	Acceleration	342 *gal*	683 *gal*	183 *gal*	366 *gal*
System *A* $T_O = 2.0$ *sec* $W = 1{,}000$*ton*	Acceleration	144 *gal*	269 *gal*	145 *gal*	262 *gal*
	Amplification factor	0.421	0.394	0.792	0.719
	Displacement	14.0 *cm*	23.9 *cm*	14.4 *cm*	23.8 *cm*
	Inner pressure	$102kgf/cm^2$	$253kgf/cm^2$	$107kgf/cm^2$	$314kgf/cm^2$
System *B* $T_O = 4.0$ *sec* $W = 2{,}000$*ton*	Acceleration	45 *gal*	84 *gal*	51 *gal*	102 *gal*
	Amplification factor	0.132	0.123	0.279	0.279
	Displacement	14.1 *cm*	23.3 *cm*	19.1 *cm*	33.1 *cm*
	Inner pressure	$111kgf/cm^2$	$337kgf/cm^2$	$85kgf/cm^2$	$261kgf/cm^2$

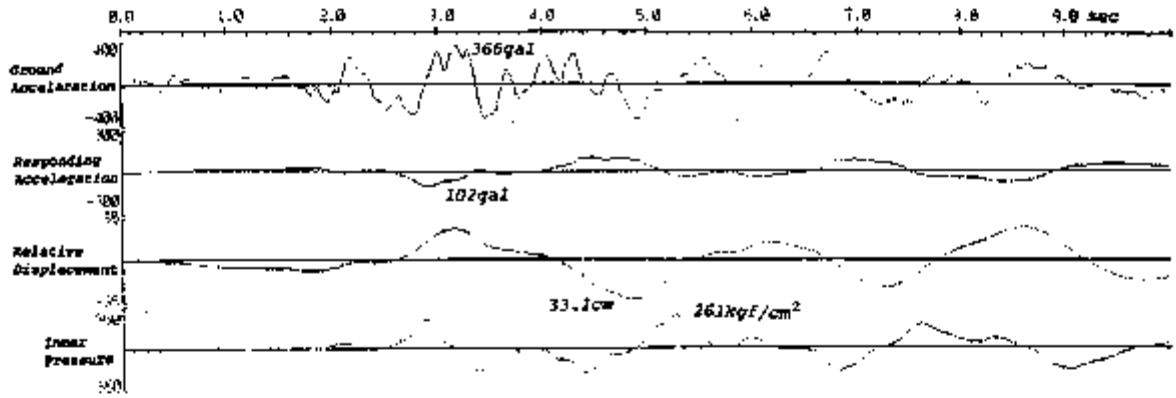

Fig.12 Response time history of System *B* to Hachinohe-EW, double amplitude

6. CONCLUSION

Resisting force rules of the accelerated liquid flow dampers in turbulent and transitional phases were derived from the results of excitation tests of a 1/2 scale model. Also, damping factors of single mass systems provided with the dampers were evaluated.

Analyses of response to ground motion demonstrated the effectiveness of the damper to control structural response for wide range of input level. The damper whose resisting force increases nonlinearly to responding velocity, together with its large capacity of resisting force, seems to provide many advantages for the use in base isolation of reactor buildings.

REFERENCES

1) Kawamata,S.,1987. Accelerated liquid mass damper and principles of structural vibration control. Trans. SMiRT-9, Lausanne, Vol.K: pp.737-742
2) Kawamata,S.,1992. Seismic control of multi-storied buildings by means of accelerated liquid mass damper. Proc. 10WCEE, Madrid, Vol.4: pp.2319-2324

SMiRT-12 / K. Kussmaul (Editor)

MK04/1

EVALUATION OF COMPONENT FRAGILITY IN ISOLATED STRUCTURE

K. Hirata[1], A. Yamamoto[2] and K. Ishida[1]

[1]CRIEPI Abiko Lab., 1646 Abiko, Abiko-city, Chiba 270-11, Japan
[2]Hitachi Eng. Co. Ltd., 3-2-1 Saiwai-chou, Hitachi-city, Ibaraki 317, Japan

ABSTRACT

This paper deals with a methodology evaluating seismic fragility of components in base isolated structure in terms of both ZPA and ground motion parameter, in which functional relationship between both input parameters are made use of, and response non-linearity of the base isolated structure is taken into account. The proposed method is applied to fragility evaluation of FBR reactor vessel.

1 INTRODUCTION

Seismic fragility of components in nuclear power plant is evaluated in terms of zero period acceleration (ZPA) at the floor and/or ground motion parameter (e.g., peak ground acceleration). The former one is advantageous to the latter one in that fragility of various components can be evaluated independent of the response of the structure, especially in the case where the fragilities are applied to design procedure. However, to evaluate annual probability of failure of the component in connection with seismic hazard, or for comparative study of the fragilities regarding the structure and the component, the component fragility should be evaluated with the ground motion parameter.

For base isolated reactor building (R/B) where isolation device shows inelastic response under design earthquake motion, linear relationship between ground motion intensity and the structural response does not hold, and the application of the methodology developed in past seismic PSA's is difficult. In this paper proposed is a method evaluating seismic fragility of the component in the base isolated structure in terms of ground motion parameter considering the response non-linearity of the structure.

2 EVALUATION METHOD

2.1 Formulation of fragility in terms of ZPA

In the fragility analysis of the component, below formulation proposed by Kennedy and Ravindra[1] is widely used.

$$Pf(a) = \Phi\left[\frac{ln(a/Am) + \beta u \Phi^{-1}(Q)}{\beta r}\right] \qquad (1)$$

where, $Pf(\cdot)$ is the failure probability of the component, a is the maximum acceleration of input earthquake motion, $\Phi(\cdot)$ is the cumulative normal distribution function, Am is the median of the acceleration capacity A of

the component, βu and βr are log-standard deviations respectively accounting for the system uncertainty and the inherent randomness. When desired to evaluate the fragility in terms of ZPA, a and Am in the above equation correspond to ZPA and the acceleration capacity evaluated in terms of ZPA. Acceleration capacity A is expressed as a product of ZPA of design floor response, Ad, component response factor Fre and component capacity factor Fc as

$$A = Ad \cdot Fre \cdot Fc \tag{2}$$

where, Fre and Fc respectively evaluating randomness, uncertainty and estimation error of the median included in estimated response and capacity. These factors are expressed as products of sub-factors, e.g., capacity factor Fc is expressed as follows.

$$Fc = Fs \cdot F\mu \tag{3}$$

where, Fs is the ratio of the ultimate strength to the stress response for design floor response, $F\mu$ is the inelastic energy absorption factor that accounts for the reduction of the response in the inelastic region of the component.

2.2 Evaluation of $F\mu$ for reactor vessel

High frequency contents of input earthquake motion to the base isolated structure are filtered off, and the components in the structure are subjected to long period motion compared to their natural frequencies. The base isolated R/B considered herein has natural period of 1～2 second, and for example, the natural period of the reactor vessel is around 0.2 second. In such a case, seismic load could be considered static rather than dynamic, and $F\mu$ is overestimated if one uses Newmark's formula[3] in which $F\mu$ is expressed as a function of allowable ductility ratio μ as

$$F\mu = \sqrt{2\mu - 1} \tag{4}$$

In this study, $F\mu$ for reactor vessel of planned fast breeder reactor (FBR) is evaluated by inelastic response analysis of a single degree of freedom system modelling the reactor vessel, and considering shear buckling as a failure mode. Hysteresis rule of the reactor vessel[2] is used as shown in Fig. 1. Three kinds of floor response waves are used which are obtained from the response analyses of the base isolated R/B for artificial earthquake waves satisfying the target design response spectrum. Each floor response wave is scaled up and used for the response analysis. $F\mu$, in this case, is given as

$$F\mu = Acr/Ae \tag{5}$$

where, Acr and Ae are respectively ZPA, where buckling occurs for inelastic system (Fig. 1 (a)) and elastic system (Fig. 1 (b)). Fig. 2 shows an example of the relationship between ZPA and the response displacement of the reactor vessel. As shown in this figure, for the reactor vessel in the base isolated structure, after response displacement exceeds the buckling displacement (Dcr), the response increases steeply with the increase of ZPA, implying the value of $F\mu$ small. Median value of $F\mu$ thus estimated is shown in Table 1.

2.3 Formulation of component fragility using ground motion parameter

Using Eq. (1), one can evaluate component fragility in the base isolated R/B in terms of ZPA. For the base isolated structure, due to its inelastic response for the design earthquake motion (due to damping device) and hardening effect of the isolation device (elastomer bearing) in the

ultimate state, linear relationship between the ground motion parameter and the response does not hold. Here, non-linear functional relationship between the ground motion parameter and the response is estimated by regression analysis, and the result is incorporated into Eq. (1).

As to the ground motion parameter for the base isolated structure, it is pointed out that the spectral response at its natural period is highly correlated with the response[4]. Figs. 3 and 4 show the relationship between the velocity spectral response Sv(T=2sec, h=5%) and the maximum response displacement of the isolation device, and ZPA at the floor level of the base isolated R/B where the reactor vessel is installed. In these response analyses, artificial earthquake motions are used generated from 12 different power spectra with 25 different random phase characteristics for each spectrum, i.e., 300 waves in all. In this case study, linear limit of 50 cm for the isolation device is assumed, and maximum displacement response of the isolation device for design earthquake motion (Amax = 483cm/sec^2, Sv(T=2sec, h=5%) = 150cm/sec)) is 31.2cm having enough margin for the linear limit of the rubber bearing.

Multiple regression analysis between Sv(T=2sec, h=5%) and the maximum response acceleration (ZPA) is conducted using trilinear function as

$$Zm(s) = \beta 0 + \beta 1 \cdot s1 + \beta 2 \cdot s2 + \beta 3 \cdot s3 \qquad (6)$$

where, Zm(·) is the median of ZPA for given s, s is Sv(T=2sec, h=5%) of the ground motion, $\beta 0$, $\beta 1$, $\beta 2$ and $\beta 3$ are the regression coefficients. s1, s2 and s3 are defined as

$$\begin{aligned} s1 &= s \\ s2 &= 0(s < sH1),\ s - sH1(s > sH1) \\ s3 &= 0(s < sH2),\ s - sH2(s > sH2) \end{aligned} \qquad (7)$$

with sH1 and sH2 being corner points of the trilinear function. The first corner point sH1 corresponds to the elastic limit of the isolation device above which isolating function decreases, and sH2 corresponds to the yield point of the super structure above which owing to the energy absorption of the super structure gradient of the regression line decreases (Fig. 4). Also the variance of the response around the regression curve is evaluated. Substituting Eq. (6) into Eq. (1) one can obtain

$$Pf(s) = \Phi\left[\frac{ln(Z(s)/Am) + \beta' u \Phi^{-1}(Q)}{\beta' r}\right] \qquad (8)$$

in which $\beta' u$ and $\beta' r$ are the revised values where the uncertainty and the randomness regarding the structural response are taken into account.

3 NUMERICAL EXAMPLE

Using Eqs. (1) and (8), seismic fragility of the reactor vessel for shear buckling mode is evaluated. Parameters regarding randomness and uncertainty on the response and the capacity used in the analysis are shown in Table 1. Some of these parameters are evaluated from the experimental study and the numerical simulation, some are quoted from PRA study conducted for LWR (non-isolated)[1], and the rest are assumed. Figs. 5 and 6 respectively show fragilities evaluated in terms of ZPA and Sv of the ground motion. Effect of change in the tendency of the structural response with the increase of the ground motion intensity appears in the fragility curve evaluated in terms of Sv, whereas in the fragility curve in terms of ZPA such singular points do not appear.

For the earthquake motion intensity corresponding to that of the design earthquake (Sv(T=2sec, h=5%) = 150cm/sec) and the response (ZPA = 0.36G) probability of failure (Pf) of the reactor vessel for the shear buckling mode is evaluated as follows.

[Probability of failure in terms of ZPA]
Pf = 4.7×10^{-23} (Q: Non-exceedence probability = 50%)
1.5×10^{-11} (Q = 95%)
HCLPF = 0.69G

[Probability of failure in terms of Sv(T=2sec, h=5%)]
Pf = 2.1×10^{-6} (Q = 50%)
1.3×10^{-3} (Q = 95%)
HCLPF = 203cm/sec

As can be expected Pf in terms of Sv, in which the effect of the response randomness of the structure is considered, increases compared to Pf in terms of ZPA. Considering the probability of the occurrence of the earthquake with the intensity of the design earthquake (it is considered less than 10^{-4}/year), reliability level of the reactor vessel for earthquake is shown considerably high.

4 Conclusions

Conclusions of this study are summarized as follows.

1) A method for fragility evaluation of components in base isolated structure in terms of ground motion parameter is proposed.
2) For the base isolated structure, spectral response around its fundamental frequency (e.g., Sv(T=2sec, h=5%)) is proper as a ground motion parameter.
3) For the shear buckling of the reactor vessel, which is the dominant failure mode, seismic fragility is evaluated both in terms of ZPA and Sv(T=2sec, h=5%) by the proposed method.

5 Acknowledgment

This study was carried out as part of the project of the Ministry of International Trade and Industry titled "Verification Tests of Fast Breeder Reactor Technology", which has been conducted since 1987.

REFERENCES

[1] Kennedy, R.P. and Ravindra, M.K. 1984. Seismic Fragilities for Nuclear Power Plant Risk Studies, Nuc. Eng. and Design 79, pp. 47-68
[2] Hagiwara, Y., Akiyama, H., et al. 1991. Post-buckling Behavior during Earthquakes and Seismic Margin of FBR Main Vessels, Int. J. Pres. Ves. & Piping 45, pp.259-271
[3] Newmark, N. M. 1977. Inelastic Design of Nuclear Reactor Structures and Its Implications on Design of Critical Equipment, Trans. SMiRT K4/1, San Francisco
[4] Hirata, K. and Ohtori, Y. 1992. Seismic Reliability Analysis of Isolated Structure and its Application to Reliability-based Design (in Japanese), CRIEPI Report, No. U92021

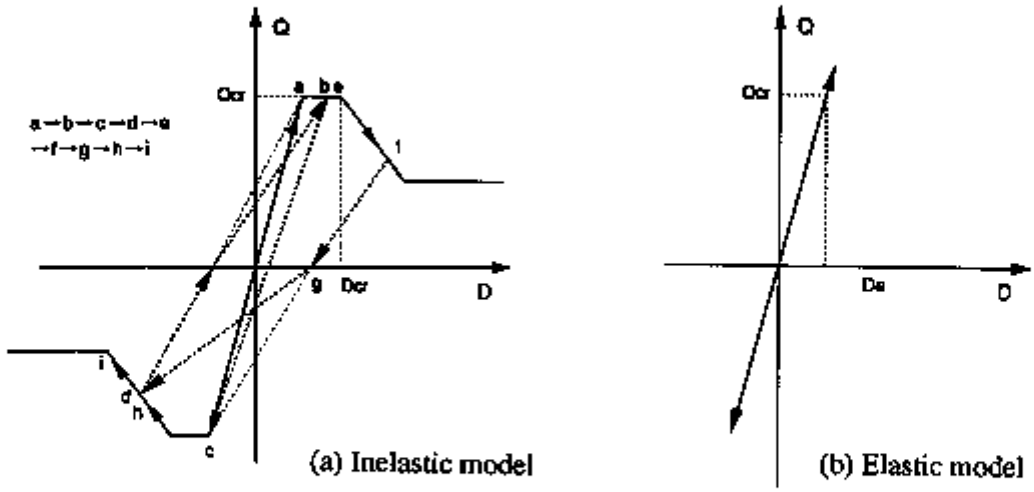

Fig. 1 Hyteresis Rule used for S-D-O-F Model

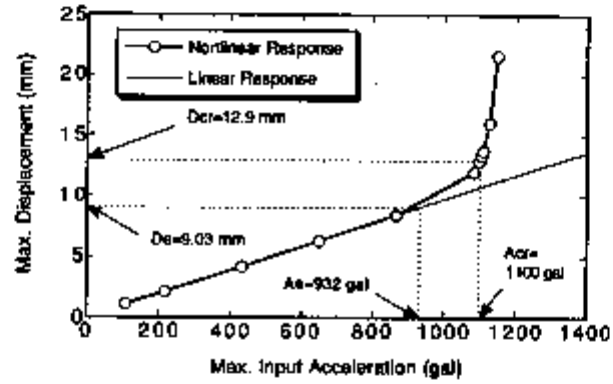

Fig. 2 Max. Input Acceleration vs. Max. Displacement
(Comparison of Response between Liear and Non-linear System)

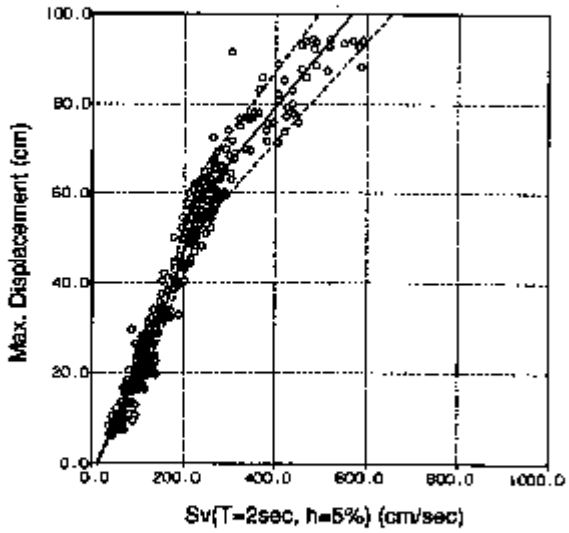

Fig. 3 Sv(T=2sec, h=5%) vs. Displacement Response of Isolation Device

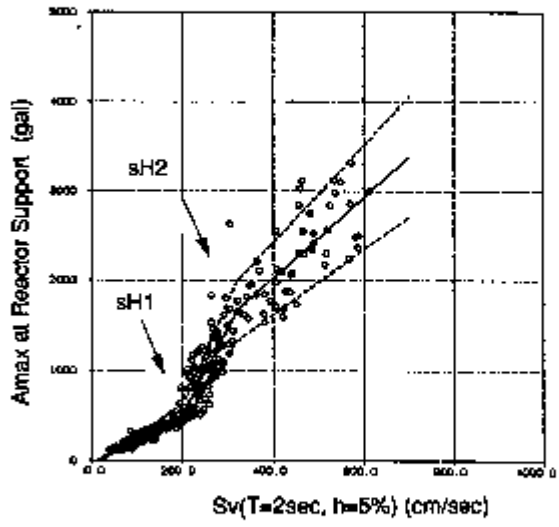

Fig. 4 Sv(T=2sec, h=5%) vs. ZPA

Table 1 Parameters used for Fragility Analysis

Factors	Median	Random βr	Uncertain βu
Response (Fr)e			
Component	0.82	0.11	0.23
Structure	1.00	0.23	0.0
Capacity (Fc)			
Fs	3.71	0.06	0.10
$F\mu$	1.18	0.0	0.0

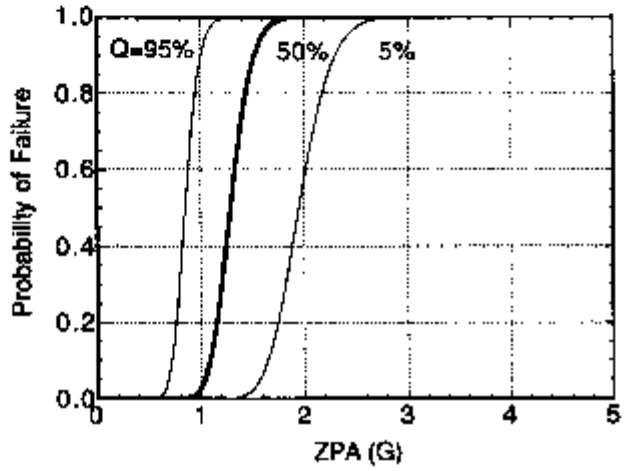

Fig. 5 Prbability of Failure for Reactor Vessel
(Pf - ZPA Relationship)

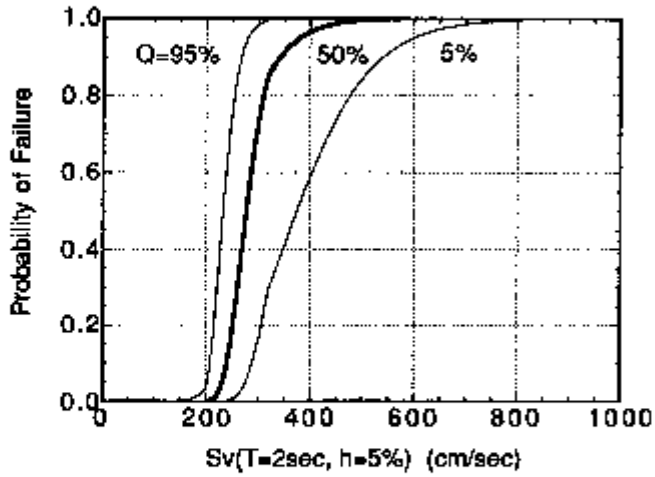

Fig. 6 Prbability of Failure for Reactor Vessel
(Pf - Sv Relationship)

SMiRT-12 / K. Kussmaul (Editor)

MK04/5

FRAGILITY ESTIMATION FOR SEISMICALLY ISOLATED NUCLEAR STRUCTURES BY HCLPF VALUES AND BI-LINEAR REGRESSION

A. Cărăuşu[1] and A. Vulpe[2]

[1]Department of Mathematics, Polytechnic Institute of Iasi, Romania
[2]Department of Structural Mechanics, Polytechnic Institute of Iasi, Romania

ABSTRACT

A method for the fragility estimation of seismically isolated NPP structures is proposed, based upon both HCLPF (high confidence low probability of failure) values and bi-linear regression. LHS (Latin Hypercube Sampling) techniques are also involved.

1 INTRODUCTION

The fragility concept has been increasingly used in the seismic PRA (Probabilistic Risk Assessment) of nuclear plant structures during the last decade. Specific problems are encountered in the case of seismically isolated NPP structures [1,2], e.g., the necessity to consider both bi- and tri-linear hysteretic models for isolation layer / upper structure behaviour under earthquake input motion.

The method presented in [1,2] is based on the regression analysis between the response and the intensity of the input motion. The peak ground velocity V_{max} is taken as 'explanatory variable' in this regression analysis due to its strong correlation with the seismic response of isolated nuclear structures.The relationship between V_{max} and the response of the isolation layer and a member of super structure (respectively) is expressed by the bi-linear function

$$Q = b_o + b_1 x_{o1} + z \cdot b_2 x_{o2} \tag{1}$$

where b_o, b_1, b_2 = regression coefficients and x_{o1}, x_{o2} are independent variables given by

$$\begin{aligned} x_{o1} &= V_{max} \\ x_{o2} &= 0 \qquad\qquad , \; z = 0 \quad \text{if} \quad V_{max} \leqq V_{max_h} \\ &= V_{max} - V_{max_h} , \; z = 1 \quad \text{if} \quad V_{max} > V_{max_h} \end{aligned} \tag{2}$$

In Eqs.(2), z is a dummy variable and V_{max_h} is the value of

V_{max} at the intersection of two line segments, determined so that it will give the largest multiple correlation coefficient.

Assuming the the ultimate capacity R of both the isolation layer and the member of the upper structure, as well as the maximum response Q, are lognormally distributed, the reliability index β for each component is given as a function of V_{max} by

$$\beta(V_{max}) = \frac{E[\ln R - \ln Q(V_{max})]}{\sqrt{D^2[\ln R] + D^2[\ln Q(V_{max})]}} \tag{3}$$

It is specified in [2] that the uncertainty of response Q (or its linear equivalent Q^*) is assumed as resulting from: (i) randomness of response due to material randomness, (ii) modeling uncertainty, and (iii) randomness of response due to random characteristics of earthquake wave. As for (i), it is quantified by $D[\ln Q(V_{max})]$ in Eq.(3), (ii) is neglected while the effect of (iii) is evaluated from the estimation interval for the response Q in the multiple regression analysis (expressed by Eq.(1)). The response corresponding to a non-exceedence level a% is evaluated by

$$Q_a = \hat{a}_o + \hat{a}_1 x_{o1} + z \cdot \hat{a}_2 x_{o2} + t(n-p-1,a)\sqrt{[1+1/n+D_o^2/(n-1)]V_e} \tag{4}$$

where $\hat{a}_o$, $\hat{a}_1$, $\hat{a}_2$ are the least squares estimates of regression coefficients, $t(n-p-1,a)$ is the a-percentile of Student's t distribution with $n-p-1$ degrees of freedom (n = number of data/waves, p= number of explanatory variables in regression analysis) D_o is Mahalanobis' distance given by

$$D_o^2 = \sum_{i=1}^{2}\sum_{j=1}^{2}(x_{oi} - x_i)(x_{oj} - x_j)s^{ij} \tag{5}$$

with s^{ij} = the current entry of the inverse of sum of products of deviations. Finally V_e is the unbiased estimate of conditional variance given by

$$V_e = \sum_{i=1}^{n}[Q_i - (\hat{a}_o + \hat{a}_1(x_{o1})_i + z \cdot \hat{a}_2(x_{o2})_i)]^2/(n-p-1) \ . \tag{6}$$

The fragility is defined in [2] as the conditional probability of failure under given peak ground velocity :

$$P_f(V_{max}) = 1 - \Phi[\beta(V_{max})] \ . \tag{7}$$

2 ALTERNATIVE FRAGILITY ESTIMATIONS FOR ISOLATED NPP STRUCTURES

The above presented fragility estimated method (due to Hirata et al [2]) has to be compared with other fragility models developed in, e.g., [3,4,5], in view of several reasons. For instance, the

HCLPF (high confidence low probability of failure) values have been rather widely used in seismic margins study (according to [6], for instance), and the approach in [1,2] is essentialy based on seismic margins. On another hand, it is argued in [7] that the LHS (Latin Hypercube Simulation / Sampling) method reduces the number of required trials and it can better handle partial correlation in uncertainty between components than the classical MCS (Monte Carlo Simulation). That is why we are going to propose a way to make use of HCLPF values and LHS in fragility estimation for seismically isolated nuclear structures.

The HCLPF values are introduced in terms of the so-called double lognormal format. The PGA (peak ground acceleration) A is usually accepted as the intensity parameter of the earthquake and a fragility curve is expressed (as in [5]) by

$$F(A) = \Phi\left[\frac{\ln(A/C)}{\beta_R}\right] \tag{8}$$

where Φ is the standard normal cdf (as in Eq.(7), too), C is the median PGA capacity and β_R is the variability of the fragility associated with randomness. The median capacity C is assumed to be itself lognormally distributed, with its pdf given by

$$f(C) = \frac{1}{\sqrt{2\pi}\,\beta_U C}\exp\left[-\tfrac{1}{2}\left[\frac{\ln(C/A_m)}{\beta_U}\right]^2\right] \tag{9}$$

where A_m is the median and β_U is the Log-N standard deviation of C. Now, the HCLPF value (of the component fragility) can be expressed as

$$HCLPF = A_m \exp[-1.645(\beta_R + \beta_U)] \ . \tag{10}$$

With the composite variability β_C defined as the norm of (β_R, β_U) the probability of failure P_f can be determined as follows :

$$P_f = \Phi\left[\frac{\ln HCLPF - \ln A_m}{\beta_C}\right] \ . \tag{11}$$

Let us now compare Eqs.(3),(7) with Eqs.(8),(11) but taking care of possible misleading notations : β in (3) and (7) is a reliability index, while subscripted β's in Eqs.(8) thru (11) are variabilities or (more precisely) logarithmic standard deviations and R in (3) is the ultimate capacity, while R in (8) and (10) stands for 'randomness'. Eq.(7) may be equivalently written as

$$P_f(V_{max}) = \Phi[-\beta(V_{max})] \tag{12}$$

where $\beta(V_{max})$ is given by Eq.(3). Since $\ln(A/C) = \ln A -$

- ln C, a difference appears between Eqs.(3) and (8) : the expectation E is not taken in the latter one. Instead, the numerator under Φ in Eq.(11) may be considered as an average logarithmic safety margin since both HCLPF and A_m are central values. As regards the denominators in the two equations, the similarity becomes clear as the composite variability β_C is given by

$$\beta_C = \sqrt{\beta_R^2 + \beta_U^2} \ . \tag{13}$$

These remarks (and other details not given here) have led us to a proposal for an alternative method for fragility estimation of seismically isolated NPP structures. The main points are given below.

1° Both ultimate capacity R and structural response (of isolation layer / upper structure component) Q are assumed to be lognormmaly distributed, and included in a fragility model as the one given by Eqs.(8) and (9). A is replaced by R and its variability (due to randomness) is quantified by D[ln R]. C is replaced by the median response Q with the variability (due to model uncertainty) quantified by D[ln Q].

2° The regression coefficients b_i in Eq.(1) are estimated by LHS (instead of MCS) and they are employed in evaluation of the response for a non-exceedence level a% like in Eq.(4), that is,

$$Q_a \doteq \hat{b}_o + \hat{b}_1 x_{o1} + z\, \hat{b}_{o2} x_{o2} + \ldots \tag{14}$$

where $\hat{b}_i$ are the LHS estimates of b_i (i = o,1,2).

3° Tolerance intervals including three response values evaluated by Eq.(14) are determined ; the middle one corresponds to the point where the regression line changes its slope (see Eqs.(2)). A lower and an upper bilinear regression lines are thus obtained, corresponding to non-exceedance levels a-σ and a+σ, respectively. The resulting regression lines are illustrated in Fig.1.

4° The probability of failure (of isolation layer / upper structure component) is evaluated using an equation of the form (11), where HCLPF(Q) is taken for a of 2° and A_m is replaced by $\tilde{Q}$ (the median of Q). A lower and an upper bound on P_f are also obtained replacing a by a-σ, respectively a+σ in determining HCLPF(Q).

3 CONCLUDING REMARKS

We proposed a modified version of the fragility estimation method presented in [2]. It avoids the use of the reliability index (Eq.(3)), which is not typical for fragility models. Instead, a doubdouble lognormal format is employed, together with HCLPF values for the structural response. The regression coefficients are estimated by the LHS method. Lower and upper regression lines and failure probabilities are determined.

REFERENCES

1 HIRATA K., KOBAYASHI Y., KAMEDA H., SHIOJIRI H.: Reliability analysis for seismically isolated FBR system. Trans. SMiRT 10 1989, Vol.M, 115-120.

2 HIRATA K., YABANA S., ISHIDA K., SHIOJIRI H., YOSHIDA S., KOBAYASHI Y. (1991): Fragility estimation of isolated FBR structure. Trans. SMiRT 11, Vol.M, 235-240.

3 RAVINDRA M.K. and TIONG L.W. (1989): Comparison of methods for seismic risk quantification. Trans. SMiRT 10, Vol.P, 187--192.

4 YAMAGUCHI A. (1991): Seismic fragility analysis of the heat transport system of LMFBR considering partial correlation of multiple failure modes. Trans. SMiRT 11, Vol.M, 91-96.

5 YAMAGUCHI A., CAMPBELL R.D., RAVINDRA M.K. (1991): Bayesian methodology for generic seismic fragility evaluation of components in nuclear power plants. Trans. SMiRT 11, Vol.M, 97--102.

6 HWANG H.H.M. (1989): Determination of HCLPF value for seismic margins study. Trans. SMiRT 10, Vol.M, 179-183.

ACKNOWLEDGEMENTS

The authors wish to express their gratitude to the chairmen of the preceding two SMiRT Conferences, Asadour HADJIAN and Heki SHIBATA for their essential support regarding participation in these conferences. They are also indebted to authors who sent them reprints and other important information : Stanley KAPLAN, Jun KANDA, George APOSTOLAKIS, Robert BOSNAK, A. Der KIUREGHIAN and others.

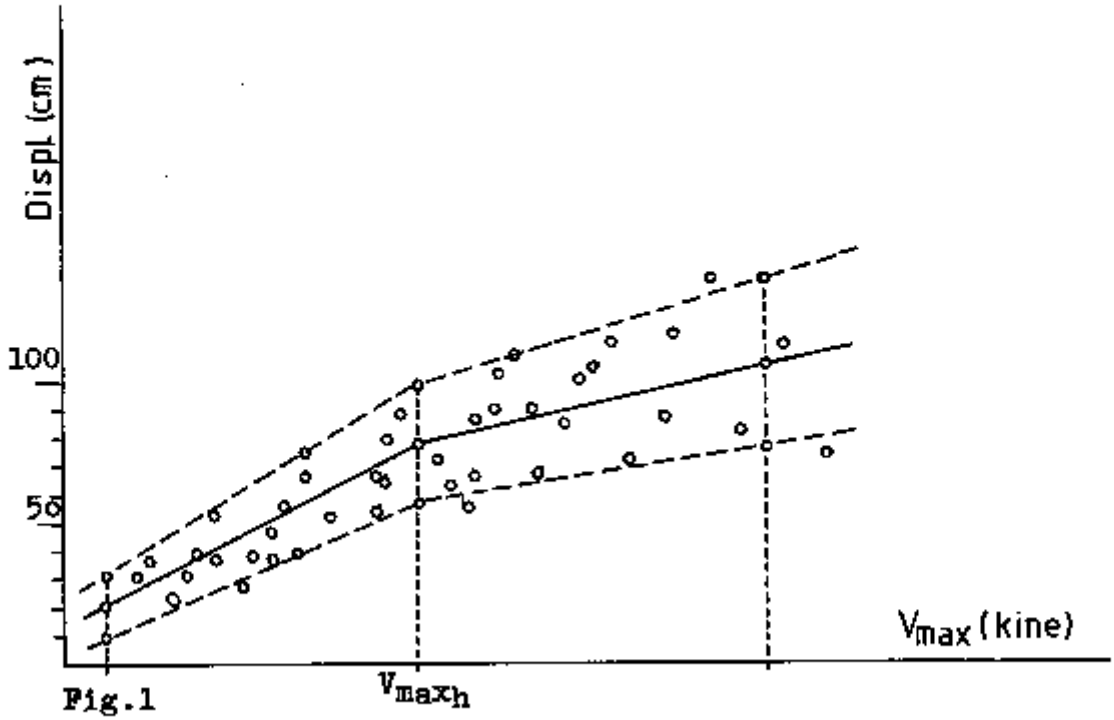

Fig.1

V_{max} vs maximum displacement of isolation layer : Estimated bi-linear regression line and lower / upper bounding lines

SMiRT-12 / K. Kussmaul (Editor)

K23/1

RESPONSE OF SEISMIC ISOLATED FACILITIES: A PARAMETRIC STUDY OF THE ALMR

F.F. Tajirian[1] and M.R. Patel[2]

[1]Bechtel National Inc., San Francisco, CA, USA
[2]General Electric Company, San Jose, CA, USA

ABSTRACT

The seismic response of the isolated Advanced Liquid Metal Reactor (ALMR) is investigated using three-dimensional linear and nonlinear models. Dynamic analyses are performed for earthquake levels ranging from one-fourth the ALMR design safe shutdown earthquake (SSE, 0.075g) to more than six times the SSE (2.0 g input). The results show that the horizontal seismic response of the ALMR is insensitive to variations in modeling techniques, type of analysis (linear or nonlinear), soil flexibility, and the characteristics of the design earthquake. The vertical response is primarily influenced by the soil flexibility and vertical dynamic properties of the isolated structures and components. The effect of stiffening that occurs in elastomeric based isolators at high shear strains on system response is examined. When the increased stiffness is accounted for in the analysis, the computed displacements for extreme events are reduced by up to thirty percent.

1 INTRODUCTION

The ALMR program sponsored by the U.S. Department of Energy (DOE) uses seismic isolation to simplify design, to enhance safety margins, and to support the development of a standardized design for the majority of the available U.S. reactor sites. The ALMR [Quinn et al. 1992], employs compact reactor modules sized to enable factory fabrication, and ease of shipment to a wide range of sites. The isolated structural configuration investigated in this paper consists of a stiff rectangular steel-concrete box structure 52 ft × 91 ft (15.9 m × 27.7 m). It supports the reactor vessel, the containment dome and the reactor vessel auxiliary cooling system stacks. The reactor vessel has a 20 ft (6.1 m) diameter and a height of 62 ft (18.9 m) and is supported from the top. The relatively small diameter of the vessel provides sufficient intrinsic resistance in the vertical direction to minimize amplifications in the vertical ground motions making vertical isolation unnecessary. The isolated structure weighs 13,000 kips (5800 tons) and is supported on 25 seismic isolation bearings. The isolators consist of steel-laminated elastomeric bearings using a high damping compound. The horizontal isolation frequency is 0.75 Hz, and the vertical frequency is greater than 20 Hz. Other ALMR plant configurations are presently under study including a design which supports the steam generator on a larger common isolated platform using 48 bearings.

A comprehensive seismic analysis plan has been developed to confirm the adequacy of the design and to support regulatory licensing activities. In this paper, various factors that may affect the seismic response are investigated. These include nonlinear response of the isolators, effect of the isolators on vertical seismic response, variability in the input earthquake mechanism including the size of the earthquake, and soil-structure interaction effects. The results of linear and nonlinear seismic analyses are summarized.

2 SEISMIC CRITERIA

The ALMR is designed to accommodate the seismic conditions expected at a wide range of sites, from deep soil sites with a minimum shear wave velocity of 1000 fps (305 m/s), to stiff rock sites. The present licensing seismic design basis is a safe shutdown earthquake (SSE) with a maximum horizontal and vertical acceleration (PGA) of 0.3g. The design earthquake is consistent with the U.S. NRC Regulatory Guide 1.60 spectra. However, a PGA of 0.5g is being used to design the nuclear island. Figure 1 shows a comparison of the RG 1.60 design spectrum with the tentative Japanese design spectrum developed specifically for seismically isolated FBRs [Ishida et al. 1989]. It can be seen that for frequencies that are important to the response of isolated structures (0.5 to 1.0 Hz), the two curves are alike. Figure 1 also shows response spectra developed by the Electric Power Research Institute [EPRI 1989] for Central or Eastern USA. Spectra for two siting conditions. The EPRI spectra have lower long period components than the RG 1.60 spectrum which was originally developed from earthquakes recorded in the Western United States. For example at 1 Hz the RG 1.60 spectrum normalized to 1.0g PGA has a spectral acceleration of 1.5g. The equivalent EPRI spectral accelerations are 1g for the soil site and 0.5g for the rock site. Thus, for a given peak ground acceleration, designs of isolated structures based on RG 1.60 spectra will have higher margins at sites where the EPRI spectra are applicable.

3 LINEAR SEISMIC ANALYSIS

A three-dimensional model was developed to represent the isolated ALMR. The seismic platform and reactor model are shown in Figure 2. Input time histories that envelop the RG 1.60 spectra were scaled to 0.3g for the SSE and to 0.1g to represent small earthquakes. Soil-structure interaction (SSI) effects were modeled as frequency independent springs. Composite modal damping was used to include soil damping. Two sites were investigated; a rigid site, and a soft site with a shear wave velocity of 1000 ft/s (305 m/s). The seismic isolators used for the ALMR have nonlinear characteristics. At the low strain levels expected during small eathquakes, their horizontal stiffness is higher than at strains resulting from the design earthquake. The 25 seismic isolators were modeled with beam elements with equivalant linear strain compatible stiffness properties. For the SSE case the isolator horizontal stiffness was equivalent to a frequency of 0.75 Hz. For the smaller earthquake, this stiffness was increased by a factor of 2.5, increasing the isolation frequency to 1.16 Hz. This factor was based on half-scale bearing tests [Tajirian et al. 1992].

For the SSE level input the maximum horizontal accelerations are reduced by the isolators from 0.3g to 0.26g in both horizontal directions. Furthermore, the isolated structure moves as a rigid body and there is very little amplification in horizontal accelerations. Figure 3 compares the response spectra on the lower mat below the isolators with the spectra at the reactor vessel supports. The results for the two horizontal directions and two site conditions are shown. The isolators are very effective in reducing spectral accelerations above 1.2 Hz. The figure shows that the isolated response is not sensitive to variations in the input motion or soil stiffness even though the spectra below the isolators differ significantly above 5Hz. In fact unlike conventional structures, the response of isolated structures is governed by input response in the range between 1 and 3 seconds (0.3 Hz to 1 Hz) and is unaffected by changes that affect frequencies greater than 2 Hz. SSI effects seldom modify response within the applicable low frequency range. This is a major advantage of using seismic isolation over conventional plant design, where significant effort is consumed during the design phase to account for uncertainties in structural response due to changes in input time history and SSI effects. Another advantage is that high frequency motions which control the response of conventional structures are stochastic and can reach very large values (>2g) in extreme cases. Conversely, low frequency components that affect isolated structures are deterministic and can be predicted reasonably well if the overall seismic source parameter values are known [Spudich and Archuleta 1987; Tajirian and Abrahamson 1991; Somerville and Graves 1993]. Furthermore, displacements during an extreme event are bounded by the physical characteristics of the seismic source and thus are numerically more stable.

The vertical spectra below and above the isolators are compared in Figure 4a and 4b. It can be seen that the amplification across the isolators is small for both sites. The peak at about 9 Hz for the soil case corresponds to the vertical foundation-soil frequency and is independent of the vertical stiffness of the isolators. A more detailed SSI analysis is required to accurately quantify the vertical amplifications in foundation response resulting from the flexibility of the soil. It is expected that more accurate modeling of embedment will reduce the amount of amplification calculated in this study. For the rock case the amplifications at frequencies greater than 10 Hz are partly attributed to the vertical flexibility of the isolated concrete platform. These peaks are not present in the soil case because of the beneficial damping effects present in the softer sites.

To study the effect of a small earthquake, the input time history used above was scaled to a maximum acceleration of 0.1g. For this case the maximum horizontal acceleration on the seismic platform was amplified to 0.13g. Such amplifications have also been observed in the response of isolated buildings during small earthquakes [Kelly et al. 1992; Clark et al. 1993]. This phenomenon is well understood and as shown in this study is predictable even with the use of simple equivalent linear models. The horizontal spectra above the isolators are compared with the equivalent spectra for the SSE case widened by plus or minus 15 percent in Figure 5. As shown the smaller earthquake may cause spectral accelerations at about 1.2 Hz to be higher than the SSE widened spectra. The impact of this observation should be considered when evaluating the response of equipment and other components with frequencies less than 2 Hz.

4 NONLINEAR SEISMIC ANALYSIS

The same ALMR configuration analyzed above was also analyzed with a nonlinear representation of the isolators. The objective of this analysis was to evaluate the effects of increases in bearing stiffness at high strains and to compare the results with the equivalent linear analysis. The seismic platform was modeled as an assemblage of rigid beams. The isolators were modeled as individual springs to properly model rocking and torsional effects. In the axial direction, the springs were linear. In the two lateral directions, the springs were nonlinear, and had three stiffness segments as shown in Figure 6. Damping of the isolators was provided as hysteretic damping in the springs. Additional effective damping of about 1 percent was introduced as Rayleigh damping. A single lumped mass spring model was used to represent the reactor system. The site was assumed rigid.

A parametric study was performed to compute the response of the platform. The parameters that were modified included the input time history, the peak acceleration, the ratio of the third stiffness, K_3, to the mid stiffness, K_2, and the horizontal deflection δ_s at which the bearing stiffness increases (see Figure 7).

The analyses were performed for earthquake levels ranging from one-fourth the SSE (0.075g input) to more than six times the SSE (2.0g input). The isolator stiffnesses were adjusted to make them compatible with the input acceleration level. The RG 1.60 input time histories used in the linear analyses were scaled to 0.075g, 0.15g, 0.75g, 1.0g, and 2.0g. For the extreme case, an additional set of time histories was generated through numerical analysis for a hypothetical site in California. It was developed assuming a moment magnitude 8.5 on the San Andreas fault [Tajirian and Abrahamson 1991]. This condition represented an upper bound event for California. The resulting time histories had a maximum horizontal acceleration of 2.0g and a maximum vertical acceleration of 1.2g.

The combined displacements computed for the low level inputs were 1 in. (2.54 cm) for 0.075g and 2 in. (5.08 cm) for 0.15g. It should be noted that the equivalent displacements computed using the equivalent linear approach described in the previous section was 1.29 in. (3.28 cm) for 0.1g input. This compares well with the nonlinear results (1.33 in. obtained by interpolating the nonlinear results). The displacement computed using the linear model compatible with the 0.3g input was 6.23 in., or 2.08 in. (5.28 cm) for 0.1g input. It can be thus concluded that the equivalent linear model used for the small earthquake is more appropriate. For 0.75g and 1.0g inputs the nonlinear solutions give 16.6 in. (42.2 cm) and 21.6 in. (54.9 cm) respectively. Scaling the linear results (0.3g model) to these levels would give 15.6 in. (39.6 cm) and 20.8 in. (52.8 cm) indicating that the model is adequate in the range of input from 0.3g to 1.0g,

which is within the bearing stiffness range that is constant. This finding has also been confirmed by other investigators [Kitamura et al. 1992; Sanò et al. 1992].

To examine the effect of bearing stiffening at high shear strains on limiting extreme displacements, the results for the four different K_3/K_2 ratios defined in Figure 7 are plotted in Figure 8. The input for all for cases is the RG compatible scaled to 2.0g. It can be seen that with no bearing stiffening, the maximum combined displacement is 62.5 in. (159 cm). The displacement decreases as the stiffness ratio increases. For K_3/K_2 of 10 the displacement is reduced to 41 in. (104 cm). Although the increase in stiffness is beneficial in limiting displacements it results in an increase in the forces in the isolated structure. The effect of this on component margins has to be assessed. Another parameter which was varied was the lateral displacement δ_s beyond which the bearing was assumed to stiffen. The K_3/K_2 was held constant at a value of 4.2. The analysis was performed with the extreme input and three value of δ_s, 1.5 ft. (45.7 cm), 2.0 ft. (61 cm), and 2.5 ft. (76 cm). The same analysis was performed with the RG 1.60 input scaled to 2.0g with δ_s of 2.0 and 2.5 ft. The maximum combined displacements for the various cases are compared in Figure 9. It can be concluded from this figure that the displacements are reduced if a bearing design with a shorter rubber stack is used where the stiffness starts increasing at a lower displacement. It can also be concluded from this figure that the two different time histories used result in similar responses. The effects of vertical nonlinearities in the bearings and any coupling with horizontal response will be investigated in future studies.

REFERENCES

Electric Power Research Institute (1989), *Probabilistic Seismic Hazard Evaluation at Nuclear Power Plant Sites in the Central and Eastern United States: Resolution of the Charleston Earthquake Issue*, NP-6395-D, April.

Clark, P. W., Whittaker, A. S., Aiken, I. D., and Egan, J. A. (1993) "Performance Considerations for Isolation Systems in Regions of High Seismicity," *Seminar on Seismic Isolation, Passive Energy Dissipation, and Active Control,* ATC-17-1, Vol. 1.

Ishida, K., et al. (1989), "Tentative Design Response Spectrum for Seismically Isolated FBR," *Transactions of 10th SMiRT Conference*, Vol. K2, Anaheim, California, August.

Kelly, J. M., Aiken, I. D., and Clark, P. W. (1992), "Response of Base-Isolated Structures in Recent Earthquakes," *10th Structures Congress*, ASCE, April.

Kitamura, S., Morishita, M., and Iwata, K. (1992), "3-D Seismic Response of a Base-Isolated Fast Reactor," *IAEA Specialists' Meeting Seismic Isolation Technology*, San Jose, CA.

Quinn, J. E., Boardman, C. E., Thompson, M. L., and Snyder, C. R. (1992), "US ALMR, A Multi-Mission Advanced Reactor Concept for the Next Century," *Int. Conference on Design and Safety of Advanced Nuclear Power Plants*, Tokyo.

Sanò, T., Di Pasquale, G., and Vicaturo, E. (1992), "Linear Analysis for Base-Isolated Structures," *IAEA Specialists' Meeting Seismic Isolation Technology*, San Jose, CA, March.

Somerville, P., and Graves, R. (1993), "Conditions that Give Rise to Unusually Large Long Period Ground Motions," *Seminar on Seismic Isolation, Passive Energy Dissipation, and Active Control,* ATC-17-1, Vol. 1.

Spudich, P. and Archuleta (1987), *Complete Strong Motion Synthetics in Seismic Strong Motion Synthetics*, B. Bolt, ed., Academic Press, pp 153-204.

Tajirian, F. F., and Abrahamson, N. A. (1991), "Response of Seismic Isolated Structures During Extreme Events," *Transactions of 11th SMiRT Conference*, Vol. K2, Tokyo, August.

Tajirian, F. F., Gluekler, E. L., Chen, P., and Kelly, J. M. (1992), "Qualification of High Damping Seismic Isolation Bearings for the ALMR," *IAEA Specialists' Meeting Seismic Isolation Technology*, San Jose, CA, March.

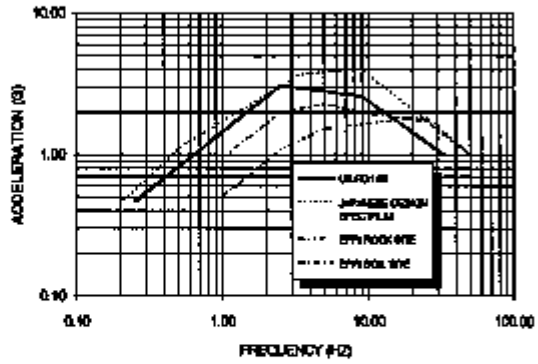

Fig. 1 Comparison of Horizontal Design Spectra 5 Percent Damping.

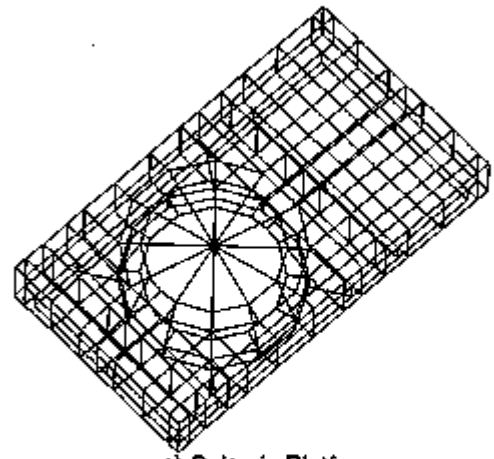

a) Seismic Platform

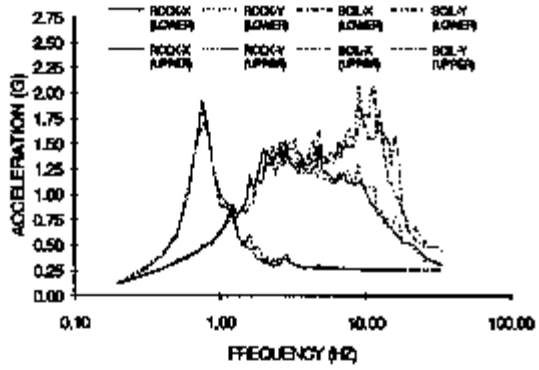

Fig. 3 Comparison of Horizontal Spectra, Lower Mat and R/V Support, 2 Percent Damping

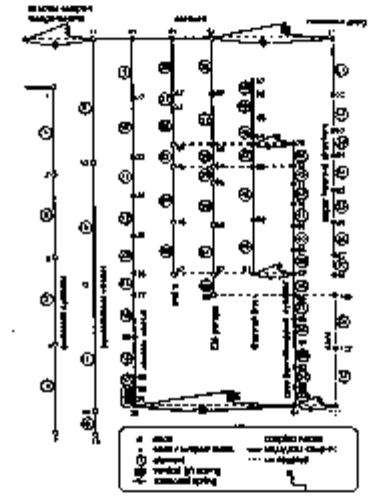

b) Reactor Model

Fig. 2 ALMR Seismic Analysis Model

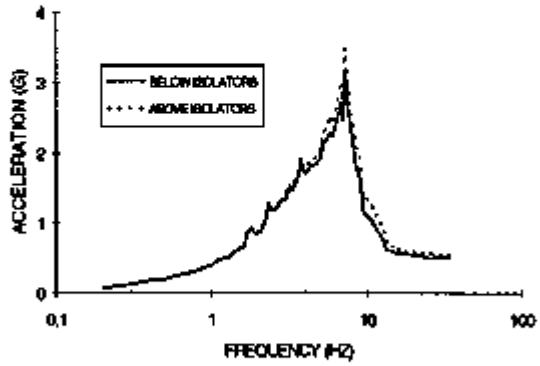

a) Soil Case

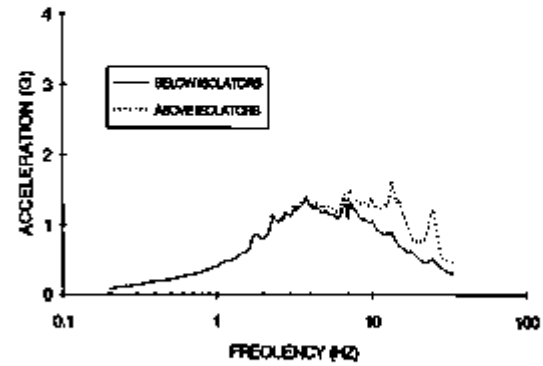

b) Rock Case

Fig. 4 Comparison of Vertical Spectra, Lower Mat and Isolated Platform, 2 Percent Damping

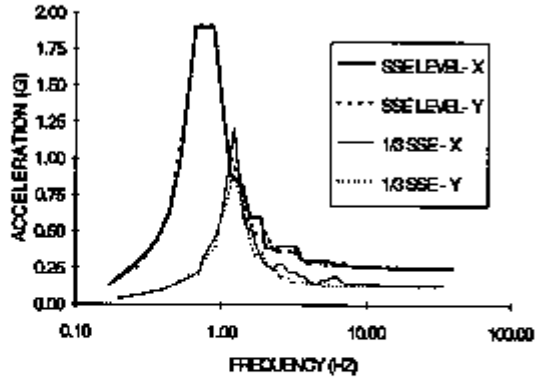

Fig. 5 Comparison of Horizontal Spectra on Isolated Platform for SSE and 1/3 SSE

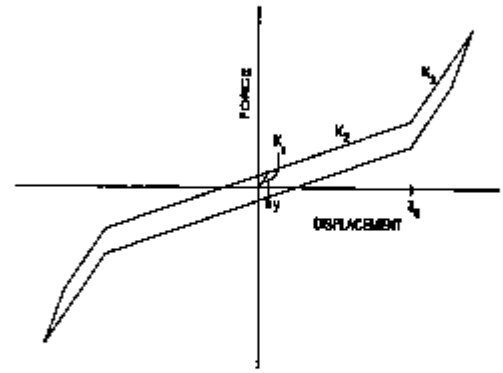

Fig. 6 Isolation Bearing Nonlinear Model

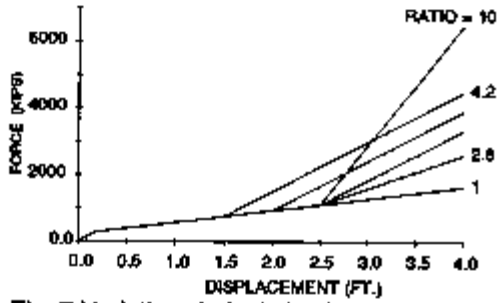

Fig. 7 Variations in Isolation Bearing Spring Properties

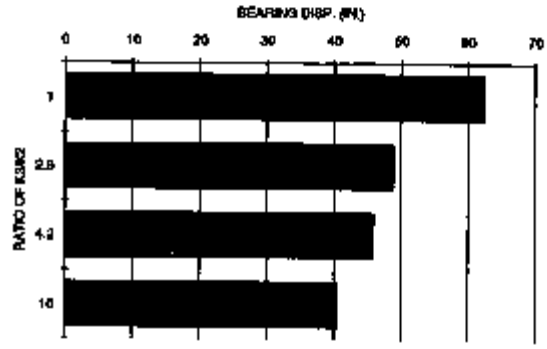

Fig. 8 Effect of Isolator Stiffening on Maximum Displacement, 2.0g Input

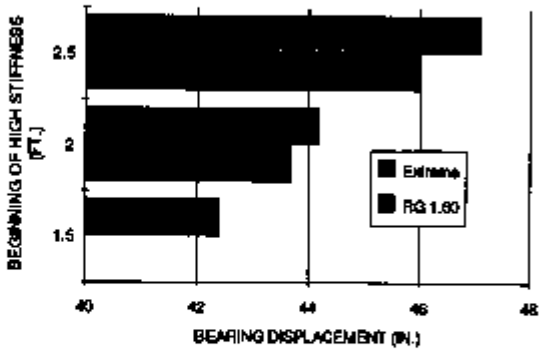

Fig. 9 Effect of Varying Dispacement δ_S on Total Bearing Displacement, 2.0g Input

SMiRT-12 / K. Kussmaul (Editor)
1993 Elsevier Science Publishers B.V.

K24/5

STRUCTURAL SEISMIC ISOLATION BY ANTIRESONANCE LOCY

K. Ishtev[1], E. Zheiliazkov[2], P. Petrov[2] and P. Philipov[2]

[1]Technical University, Department of Automatics and Systemo-Technics, 1756 Sofia, Bulgaria
[2]Bulgarian Academy of Sciences, Central Laboratory of Seismic Mechanics and Earthquake Engineering, Acad. G. Bontchev Str., Bl. 3, 1113 Sofia, Bulgaria

ABSTRACT

The antiresonance and resonance phenomena in structures are investigated by the method of dynamic condensation and by means of the frequency approach. Antiresonance and resonance frequencies are obtained from the structure transfer function. The main structural parameters alteration leads to change of these frequencies. They describe paths in the parameter space. These loci are used for seismic isolation by an optimal choice of the structural parameters. An illustrative example is given.

1. INTRODUCTION.

The structural dynamical behaviour can be investigated in the frequency domain through the well known relation between Fourier spectra of the input excitation $X(j\omega)$, the output reaction $Y(j\omega)$ and the system frequency responce function $W(j\omega)$:

$$Y(j\omega) = W(j\omega)X(j\omega). \tag{1}$$

From the amplification function:

$$A(j\omega) = |W(j\omega)|, \tag{2}$$

the resonance frequenceis ω_{ri} can be obtained (fig.1[a].)

There are frequencies in which opposite phenomena can be observed - considerable vibration damping. Some times such antiresonance frequencies ω_{ai} can be seen in the amplification function $A(\omega)$ [Savidis,1992,fig.6.]. But it is easier to detect them from the logarithmic amplificatin function - fig.1 :

$$L(\omega) = 20 \lg A(\omega). \tag{3}$$

The system property to damp fluctuation in determined frequency range can be used for structure protection from harmonic, seismic or wind loadings. Such an idea is proposed in this paper.

2. ANTIRESONANCE AND RESONANCE FREQUENCIES DETERMINATION.

By means of the finite element method the structures are described by the following equation:

$$M\ddot{Y} + C\dot{Y} + KY = -MR\ddot{X}_g, \tag{4}$$

where M,C,K are mass, damping and stiffnes matrices,R is distributive vector, Y is system displacement vector and $\ddot{X}_g$ is ground acceleration in the place.

After Laplace transformation, equation (4) becomes:

$$[Ms^2 + Cs + K]\,Y(s) = -MR\ddot{X}_g(s), \tag{5}$$

The relation between Laplace transform $Y(s)$ and $\ddot{X}_g(s)$ is:

$$Y(s) = -W(s)\ddot{X}_g, \tag{6}$$

where $W(s)$ is a matrix transfer function:

$$W(s) = \left[Ms^2 + Cs + K\right]^{-1} MR. \tag{7}$$

Usually only a few degrees of freedom are important for a dynamical analysis. In this case it is convenient to obtain the matrix transfer function through a dynamical con densation from equation (5) [Ishtev,1985]. For an arbitrary degree of freedom through single dynamical condensation, $W(s)$ is fraction rational function:

$$W(s) = \frac{b_0 s^{2n-2} + b_1 s^{2n-3} + \cdots + b_{2n-2}}{a_0 s^{2n} + a_1 s^{2n-1} + \cdots + a_{2n}}, \tag{8}$$

where n is the initial system degree of freedom number.

For antiresonance and resonance frequencies obtaining, the factorization form of $W(s)$ it is more conveinient:

$$W(s) = \frac{b_0}{a_0} \frac{\prod_{i=1}^{n-1} (s^2 + g_i s + d_i)}{\prod_{l=1}^{n} (s^2 + e_l s + f_l)}. \tag{9}$$

The frequency response function can be obtained by substituting s with $j\omega$. According to (2) and (9) the amplification function is:

$$A(\omega) = \frac{b_0}{a_0} \frac{\prod_{i=1}^{n-1} A_i(\omega)}{\prod_{l=1}^{n} A_l(\omega)} \tag{10}$$

The logarithmic function according to (3) and (10) assumes the form of the elementary term sums:

$$L(\omega) = \sum_{i=1}^{n-1} L_i(\omega) - \sum_{l=1}^{n-1} L_l(\omega) + \lg \frac{b_0}{a_0}. \tag{11}$$

The antiresonance frequencies are determined from each of the first sum terms. Indeed, the terms of the logarithmic function:

$$L_i(j\omega) = 20 \lg \sqrt{(d_i - \omega^2)^2 + \omega^2 g_i^2}, \tag{12}$$

when $g_i < 2d_i$ have minimum in frquency.

$$\omega_{ai} = \sqrt{d_i - \frac{g_i^2}{2}} \tag{13}$$

If $g_i = 0$, L_i in (12) and respectively L in (11) gets $-\infty$ values which corespond to absolute antiresonance (zero amplification) in the respective frequency ω_{ai}. This means that the described degree of freedom is immovable. In the building structure attenuation $g_i \neq 0$ but normaly $g_i^2 \ll d_i$. In this case the antiresonance is not absolute (the amplification is different from zero) but it exists in frequencies determined by equation (13).

Resonance frequencies are determinated by analogy from the second sum terms in equation (11). These terms, render an account of the minus sign before the sum, obtain a very big (if $e_l = 0$ - infinite) value in the well known resonance frequencies:

$$\omega_{rl} = \sqrt{f_l - \frac{e_l^2}{2}} \tag{14}$$

3. ANTIRESONANCE AND RESONANCE LOCI.

The structures frequency response function depends on its parameters (dimensions, reinforcement and so on). This parameter alteration leads to respective modification in M, C, K matrices. In the final reckoning ω_{ai} and ω_{rl} are alterating - describing loci in the parameter space. Convenient graphics visualization can be received when there is only one essential structure parameter (p) alteration - (fig.2.).

The loci can be used for solving the inverse problem - from desirable antiresonances frequencies value, to obtain essential structure parameters. This problem solution will be important for example in the case of passive seismic isolation of the very important structure element such as a nuclear reactor and so on, when the predominant seismic signal frequency ω_s in the place is known. For this frequency (fig.2.), the searched for parameter values p_{a1} or p_{a2} which ensure antiresonance can be obtained. On the opposite,the parameters p_{r1} or p_{r2} are hardly undesirable bacause of the resonance pheno me na arise risk.

In the case of more than one structure parameters choosing the graphical interpretation is difficult and the solution of this problem can be searched for through the medium of expressions (13) and (14).

4. ILLUSTRATIVE EXAMPLE.

The structure under consideration and designing is shown in fig.3.

In the case of damping neglecting ($C = 0$) equation (4) becomes:

$$mM\ddot{Y} + kKY = -mMR\ddot{X}_g. \tag{15}$$

where $k = \frac{24EJ}{H^3}$ and m are structural parameters for chosing in the design process. The transfer function W_4 for an important degree of freedom Y_4 received by the dynamical condensation is:

$$\frac{s^6 + 6\frac{k}{m}s^4 + 10\left(\frac{k}{m}\right)^2 s^2 + 4\left(\frac{k}{m}\right)^3}{s^8 + 7\frac{k}{m}s^6 + 15\left(\frac{k}{m}\right)^2 s^2 + 10\left(\frac{k}{m}\right)^3 s^2 + \left(\frac{k}{m}\right)^4} \tag{16}$$

The transfer function (16) presented in the form (9) is:

$$\frac{\left(s^2 + 0,5858\frac{k}{m}\right)\left(s^2 + 2,0\frac{k}{m}\right)\left(s^2 + 3,4142\frac{k}{m}\right)}{\left(s^2 + 0,1206\frac{k}{m}\right)\left(s^2 + \frac{k}{m}\right)\left(s^2 + 2,3473\frac{k}{m}\right)\left(s^2 + 3,532\frac{k}{m}\right)}. \tag{17}$$

The antiresonance and resonanse frequences are:

$$\begin{aligned} \omega_{a1} &= 0,7654\sqrt{\frac{k}{m}} & \omega_{r1} &= 0,3473\sqrt{\frac{k}{m}} \\ \omega_{a2} &= 1,4142\sqrt{\frac{k}{m}} & \omega_{r2} &= 1,0000\sqrt{\frac{k}{m}} \\ \omega_{a3} &= 1,8478\sqrt{\frac{k}{m}} & \omega_{r3} &= 1,5321\sqrt{\frac{k}{m}} \\ & & \omega_{r4} &= 1,8794\sqrt{\frac{k}{m}} \end{aligned} \tag{18}$$

In fact there is only one generalized parameter $p = \frac{k}{m}$ - for loci analysis. The antiresonance and resonance loci are shown in fig.4.

The soil amplification function of the geological column from fig.3. is shown in fig.5. If the bed rock signal $\ddot{X}_b$ is white noise, from the relation between the spectral densities in the bed rock $S_{\ddot{x}_b}(\omega)$ and surface signal $S_{\ddot{x}_g}(\omega)$:

$$S_{\ddot{x}_g}(\omega) = |W_{soil}(j\omega)|^2 S_{\ddot{x}_b}(\omega) \tag{19}$$

it follows that the predominant seismic signal density is concentrated around $15[s^{-1}](\approx 2.39Hz)$. For ensuaring the antiresonance frequency $\omega_a = \omega_s$ the generalized parameter $p = \frac{k}{m}$ can be chosen: $p_1 = 384s^{-1}$ (from locus ω_{a1}) or $p_2 = 112s^{-1}$ (from locus ω_{a2}).

or $p_3 = 66s^{-1}$ (from locus ω_{a3}). In fig.6. are shown the structures logarithmic amplification functions for the parameter $p_1 = 384s^{-1}$ and the spectral density of the seismic signal $\ddot{X}_g$.

5.CONCLUSION.

The design of structures and equipment is usually realized in accordance with standards based on the modal analysis. By this method the attenuation is focused on resonance phenomena while the antiresonance phenomena are hardly included. At the antiresonances a significant decreasing of the movement is observed. This can be used for structure stability improvement against seismic effects.

This report is devoted to some studies connected with the antiresonance phenomena and application in design. For investigation of these phenomena the transfer function is used. The numerator of the transfer function determines the frequencies in which a decrease of the system output signal is observed (antiresonance frequencies). The denominator defines natural resonance frequencies. Antiresonance loci can be used in the design process. The essential structure parameters may be determined in a way to ensure minimum dynamical loading in the responsible elements.

Although the enclosed example is illustrative, it shows the potentialities of the considered method for structural design. It is connected whith one typical computational model, which is applied in the majority of the codes. The parameter $\frac{k}{m}$ chosen in the example is of a physical meaning and can by modified in large ranges by the designer. For example inreinforced concrete structures the modification of the $\frac{k}{m}$ can be carried out by chosing of the armature.

The application of the proposed method is connected with a large volume of calculations, which are possible if the respectiv software is available. The elements of such a sortware are in the elaboration and they will be added to the part of CAD system, described in [Ishtev,1993].

6. REFERENCES.

Sarfeld W., S.Savidis,C.Vrettos, 1992.
Concrete frame under incident seismic wave, Earthquake Engineering, Tenth World Conference, Balkema, Rotterdam.

Ishtev K., Z.Bonev, Ph.Philipov, 1985.
Linear Mechanical Modelling Using Dynamical Condensation, SMiRT 8, B10/9, Brussels, Belgium.

Ishtev K., P.Petrov, E. Zheliazkov, Ph.Philipov. 1993.
CAD System for Solving a Wave Propagation Problems and Structural Behaviour under Stochastic Loadings, SMiRT 12,B 02/4.

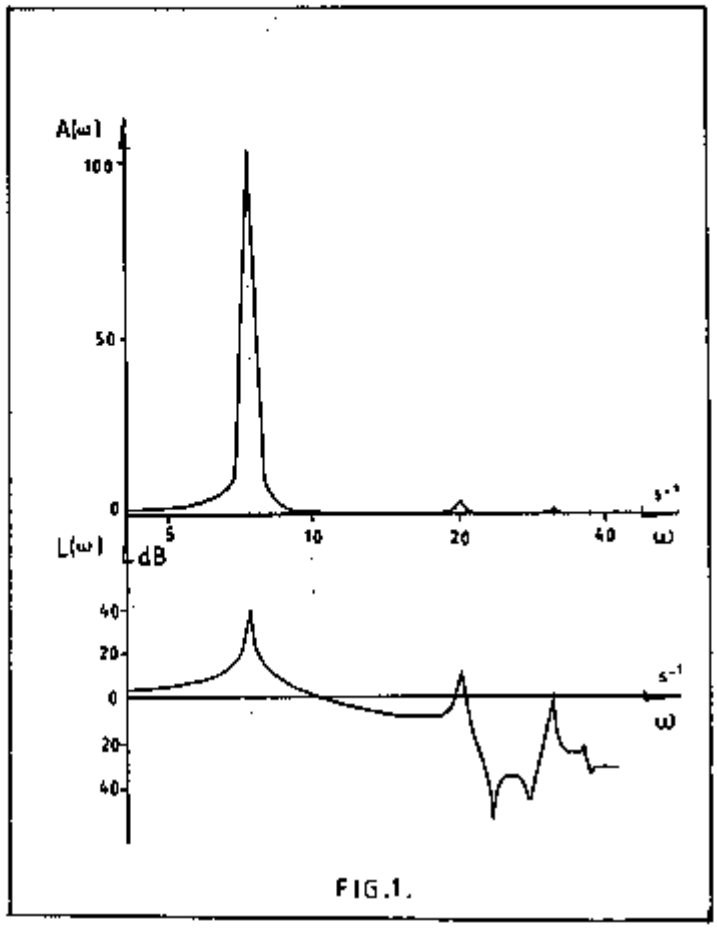

FIG.1.

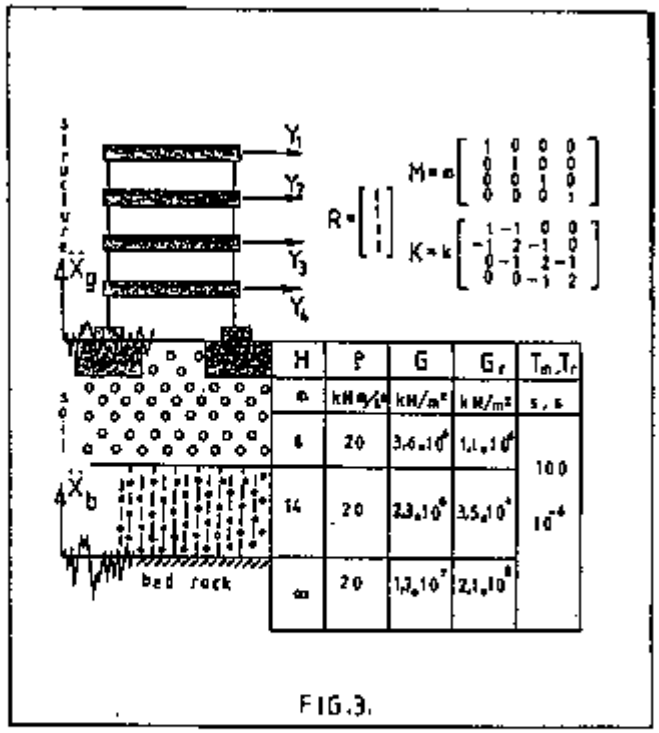

FIG.3.

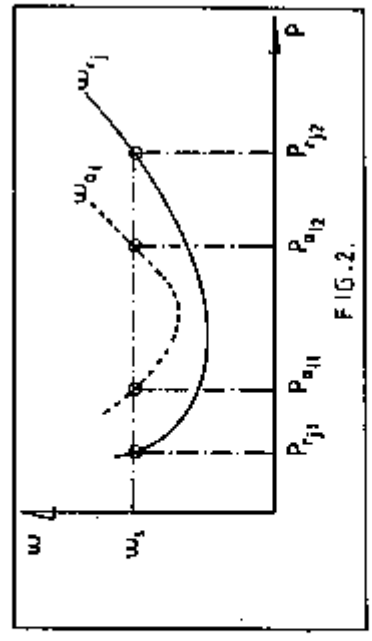

FIG.2.

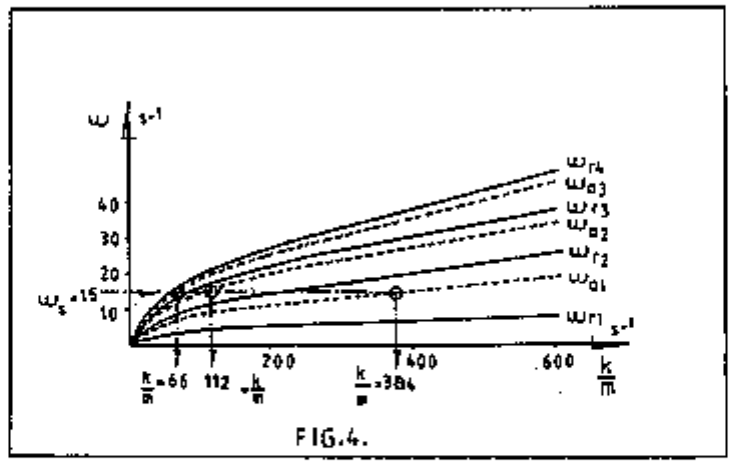

FIG.4.

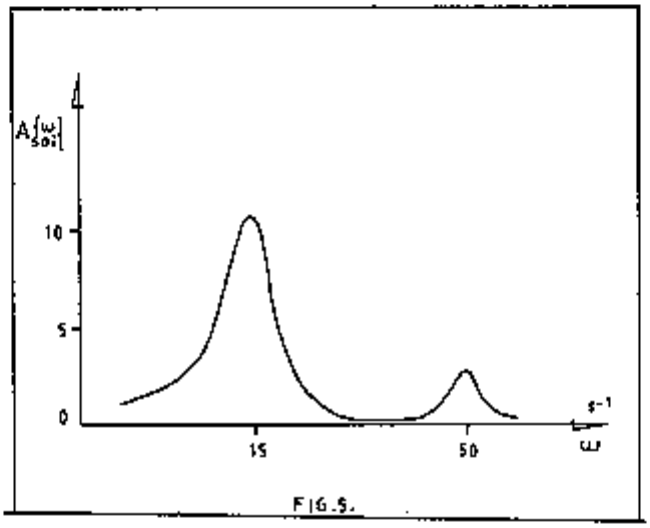

FIG.5.

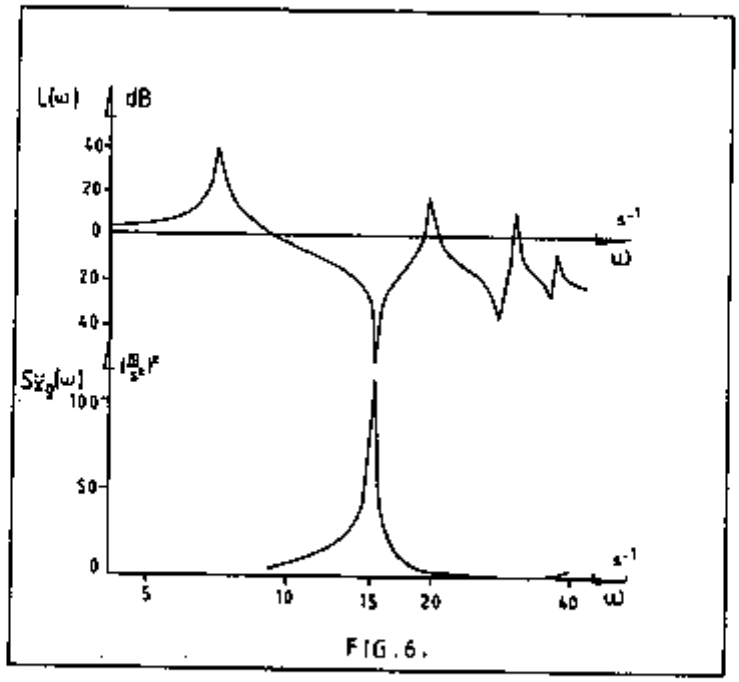

FIG.6.

SMiRT-12 / K. Kussmaul (Editor)

K25/5

BASE-ISOLATION SYSTEM WITH HYBRID LEAD RUBBER BEARINGS

K. Tanaka[1], M. Hirasawa[1], Y. Ishiguro[2], H. Ohyama[1] and Y. Nakamura[1]

[1]Technical Research Institute, Fujita Corporation, Yokohama, Japan
[2]Architectural and Engineering Division of Fujita Corporation, Tokyo, Japan

ABSTRACT

Multi-layer rubber bearings with several kinds of damper are commonly used in base-isolated buildings. Systems with such devices are mainly designed for seismic safety against strong earthquake excitations, so the performance in weak earthquakes is not always sufficient from the view point of habitabilities. In order to get good seismic performances both in weak and strong earthquakes, new isolator device named HLRB have been developed. The mechanical properties of HLRB, the seismic responses of a HLRB building and an application of HLRB system to an existing base-isolated building are presented.

1. INTRODUCTION

In Japan, over sixty base-isolated buildings with multi-layer rubber bearings have been constructed since 1982[1]. The authors have already developed base isolation systems with two kinds of rubber bearings, which have been applied to three buildings. From field seismic observation results of these buildings, some informations have been obtained. Two important informations are as follows. The first is that the performances of all buildings in moderate earthquake excitations were satisfactory. The second is that the performances in weak earthquakes were not always sufficient, especially in case that the ratio of natural period of the building to that of the ground is nearly unity. The performance in weak earthquakes is concerned to "habitability", and the habitability is estimated by floor acceleration.

The authors have developed a new isolator that gives good habitabilities in weak earthquakes and also seismic safety[2] in strong earthquakes. The new isolator is named "HLRB[3]".

In this paper, the mechanical properties of HLRB and its parts obtained from several experiments, the results of seismic response analysis comparing HLRB with LRB building, and an application of this system to an existing base-isolated building are presented.

2. DESCRIPTION OF HLRB

HLRB means hybrid lead rubber bearing. Fig.1 shows a vertical section view of HLRB. This isolator is vertically composed of a Lead rubber bearing (LRB) and a rubber bearing with a stopper (SRB). The lateral stiffness of

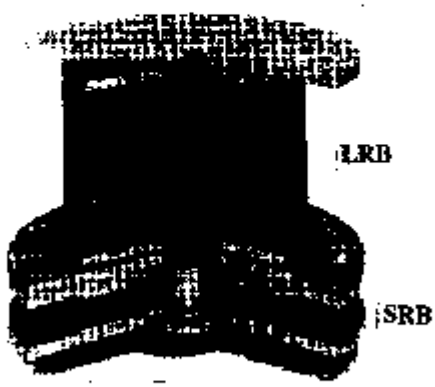

Fig.1 Vertical Section View of HLRB

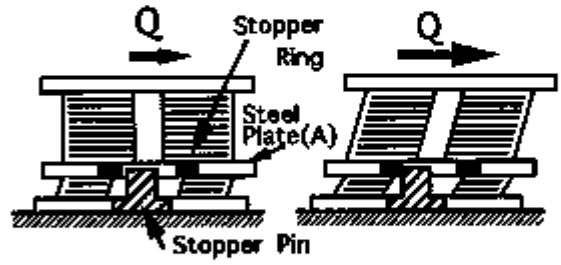

(a) In Weak Earthquake (b) In Strong Earthquake

Fig.2 Mechanical Action of HLRB

the rubber bearing of SRB is designed to be lower than that of LRB. The mechanical actions of HLRB in earthquakes are shown in Fig.2(a)and(b). SRB mainly works in weak earthquakes and LRB in strong earthquakes.The stopper is arranged in a center hole of SRB, and is composed of a steel pin and a ring that is made of glass fiber reinforced plastic(GFRP) and set closely in a steel plate (A) shown in Fig.2. There is clearance between the pin and the GFRP ring. This clearance controls the range that SRB mainly works. The GFRP ring absorbs the impact energy which is generated in collision of pin and ring. The role of the stopper is to restrict lateral displacement of SRB within acceptable level and to transmit shearing force to LRB in strong earthquakes.

The main dimensions of a HLRB that is used in this study are as follows. The design diameter is 450 mm. The thickness of natural rubber layer is 4 mm. The number of the rubber layer of LRB and SRB is 44 and 9 respectively. The thickness of steel layer is 3mm and 4mm, respectively. The diameter of lead plug is 90 mm.

3. MECHANICAL PROPERTY

3.1 STOPPER

Fig.3 shows a contact state of pin and ring. The pin is subjected to bending and shearing force, on the other hand the ring is subjected to contact compression. The dimension of the stopper is designed by Herz equation[4]. Fig.4 shows the relationship between shearing force and displacement from the beginning of contact. The maximum force that acts on the stopper in strong earthquakes is determined by the seismic response analysis which will be shown later. Below the maximum force , the stopper shows nearly linear and elastic hysteretic behaviors.

3.2 SRB and LRB

SRB is composed of a rubber bearing and a stopper, so its hysteretic behavior is modeled by a tri-linear type as shown in Fig.5. This model is made up by the hysteresis of the stopper and the rubber bearing obtained from experiments. The analytical model of SRB is composed of a linear characteristics of the rubber bearing and a higher stiffness property of the stopper.

LRB is composed of a rubber bearing and a lead plug, and has dowel pin joints at both ends. Its hysteresis loop is modeled as shown in Fig.6.

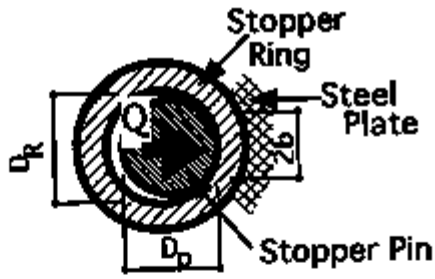

Fig.3 Contact State of Pin and Ring

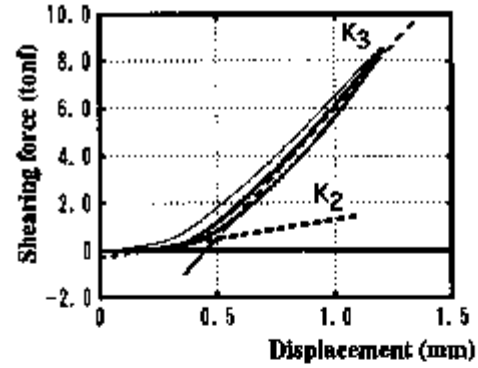

Fig.4 Hysteresis Loop of Stopper after Contact

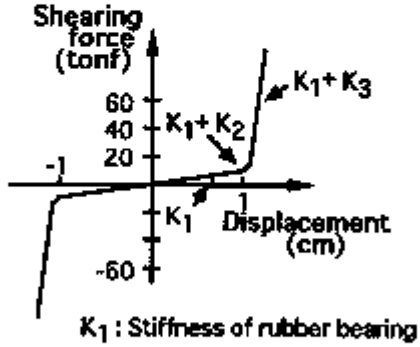

Fig.5 Hysteretic Model of SRB

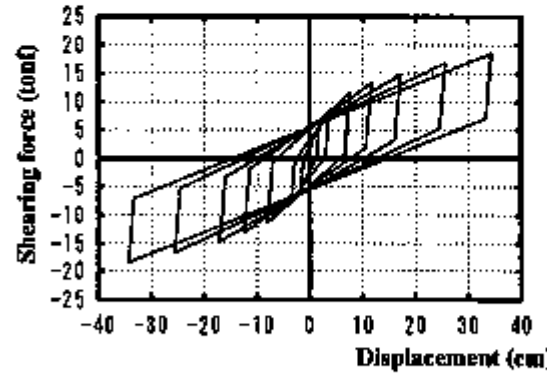

Fig.6 Hysteresis Loop Model of LRB

3.3 HLRB

The lateral stiffness of HLRB can be simulated by an analytical model that connects LRB and SRB in series. The hysteresis loops of HLRB and its two parts(LRB and SRB) obtained from experiments are shown in Fig.7 (a) and (b) with the analytical model. The results of analytical models are well agreed with the experimental results. The variation of the lateral stiffness of HLRB and LRB under various displacement, are shown in Fig.8. The lateral stiffness of HLRB in range of small displacement are lower enough to increase the natural periods of the building. The variation of the vertical stiffness of HLRB under various shearing strain is shown in Fig.9. The decrease of the effective sectional area with increasing lateral displacement is taken into account in the analytical model.

3.4 CONSIDERATION OF SEISMIC SAFETY

Some additional considerations are necessary in the design of HLRB, to ensure seismic safety. Fig.10 shows an equilibrium of overturning of LRB. The resisting arm of overturning :(B1–δ) should be decrease by δc. Distance δc is the maximum displacement of SRB. Fig.11 shows effective sectional area of rubber bearing caused by lateral displacement. This effective area affects the vertical stiffness as shown in Fig.9 and stability of LRB. Therefore in case of estimation of this area, the maximum displacement(δc) of SRB should be considered.

The stopper is subjected to impact force reaction in strong earthquakes. This impact force is estimated by seismic response analysis which is described later. The maximum impact force is calculated by effective mass of HLRB multiplied by maximum acceleration obtained by seismic analysis.

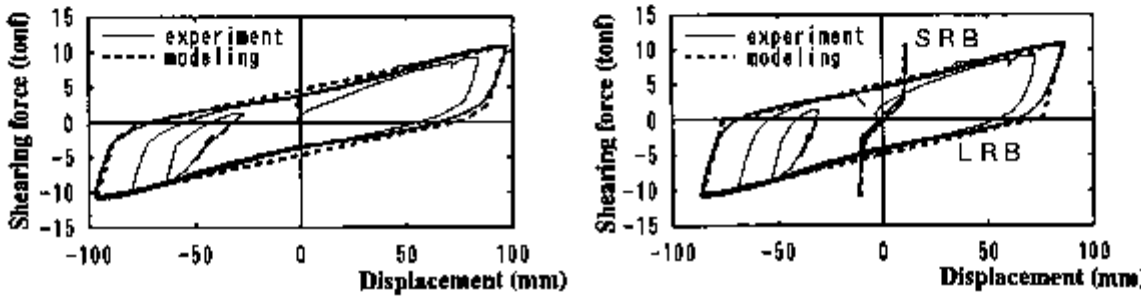

(a) HLRB (b) LRB and SRB

Fig.7 Hysteresis Loop of HLRB and its Parts

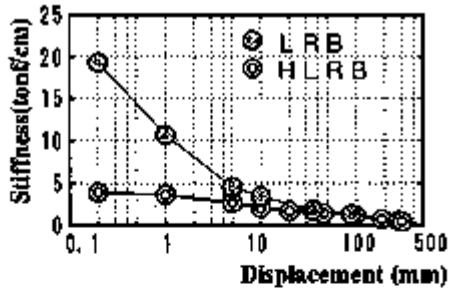

Fig.8 Lateral Stiffness of HLRB and LRB

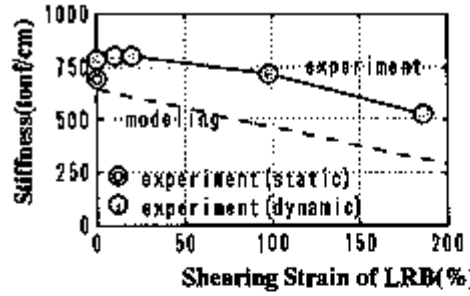

Fig.9 Vertical Stiffness of HLRB

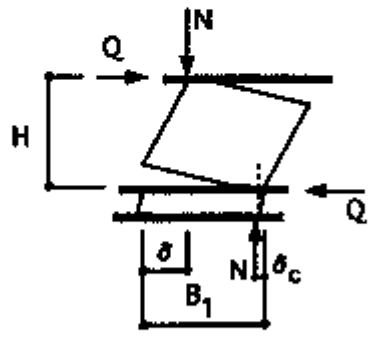

Fig.10 Equilibrium of Overturning

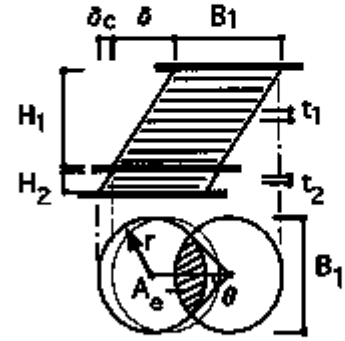

Fig.11 Effective Sectional Area
(hatched region)

4. PRACTICAL APPLICATION

4.1 OBJECTIVE BUILDING

The objective building is an existing three stories base-isolated building with LRBs. Fig.12 shows a section of the building. This building was constructed in 1987 in Technical Research Institute of FUJITA CORPORATION at Yokohama, Japan. This building has a square plan(10.11m x 10.11m) and four columns.

Because the natural period of the ground was longer than the natural period of the Base-Isolated building, the performance in weak earthquake excitations, the strength of which is less than 30 cm/sec^2, was not sufficient. Four new SRBs were installed under existing LRBs in order to lengthen the period of the building and to verify the effectiveness of HLRB system.

4.2 SEISMIC RESPONSE ANALYSIS

Before installing, the seismic responses of a HLRB building and a LRB building against several kinds of earthquake excitations were numerically analysed. The analytical model of the building is shown in Fig.13. The analytical results in case of strong earthquakes shows that the responses of the building with HLRB and LRB are almost the same, however in case of weak earthquakes the maximum acceleration response of HLRB building is

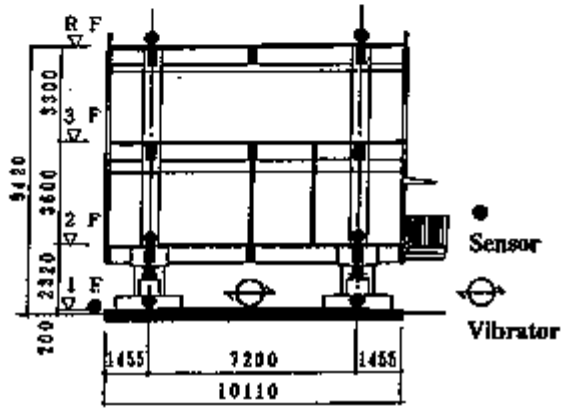

Fig.12 Section of Base-Isolated Building

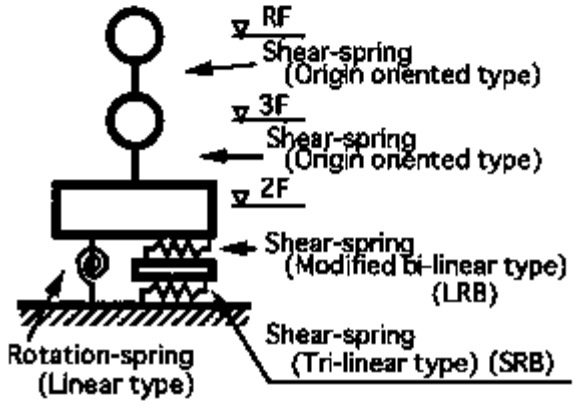

Fig.13 Analytical Model of Base-Isolated Building

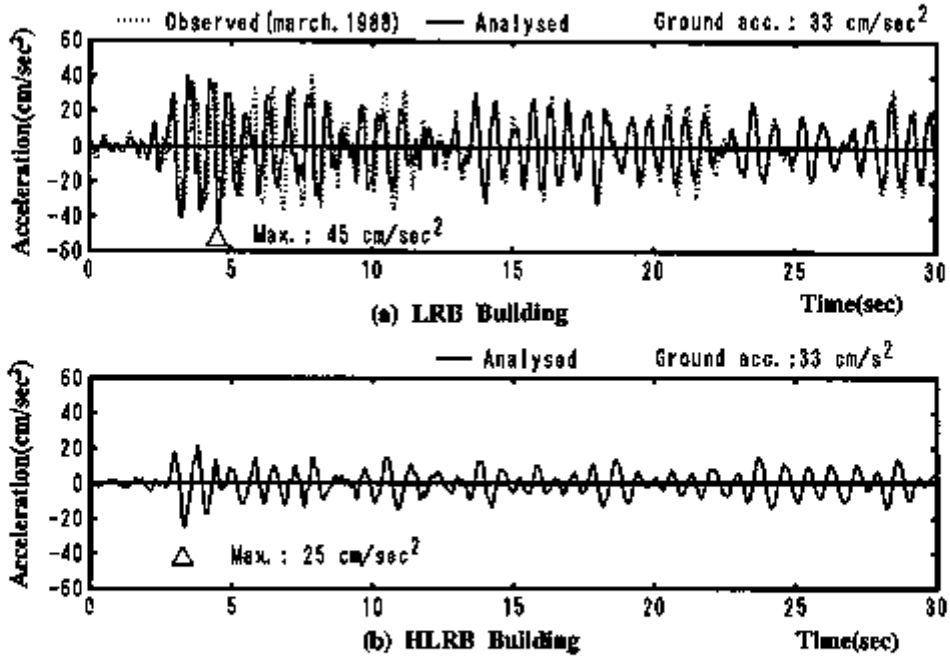

Fig.14 Top Floor Seismic Response of LRB and HLRB Building under the same Ground Motion

reduced to one-half compared to that of LRB building, as shown in Fig.14(a) and (b). Fig.14(a) shows the comparison of the observed results and the analytical results of LRB building. Both results are well agreed. The decreased response of HLRB building is caused by the longer period of that building comparing to that of LRB building in region of small displacement of isolators. This is shown in Fig.15, as the relations between equivalent natural period of the base-isolated building and shearing strain of LRB.

4.3 PROCEDURE OF INSTALLING WORK

Procedure of installing new SRBs are shown in Fig.16 (a),(b) and (c). The lifting up construction system was adopted. The lifting up was done,step by step 5mm at a time, until 200mm, as checking the differences of four levels were less than 5mm carefully. Additionally total weight of the building was measured during this work. The design weight is 311 tonf, but the actual weight is about 280 tonf. This result slightly affected the natural period of the building.

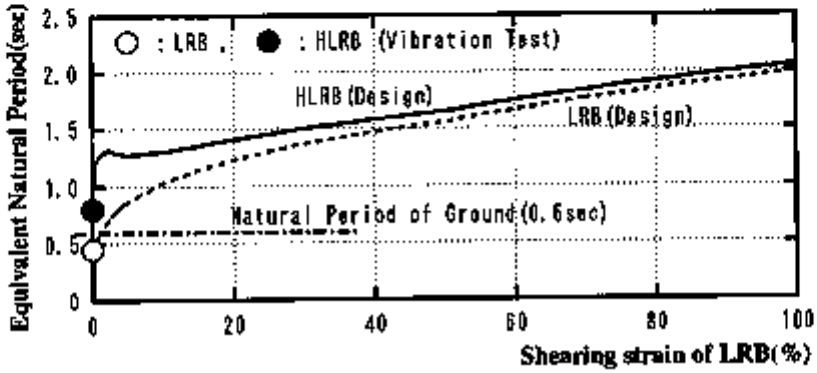

Fig.15 Equivalent Natural Period

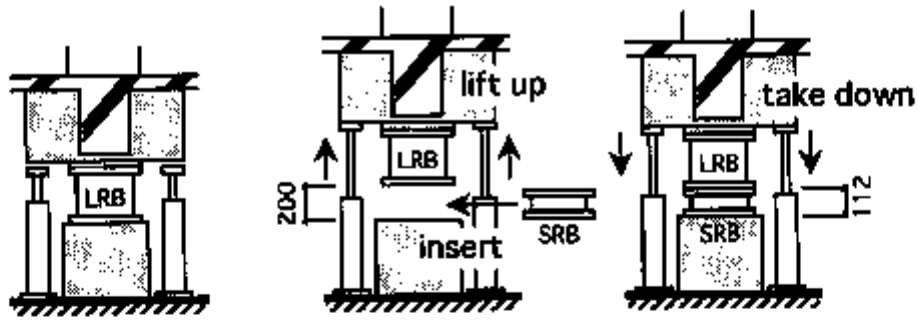

(a) Preparation (b) Lifting up (c) Taking down

Fig.16 Procedure of Installing Work

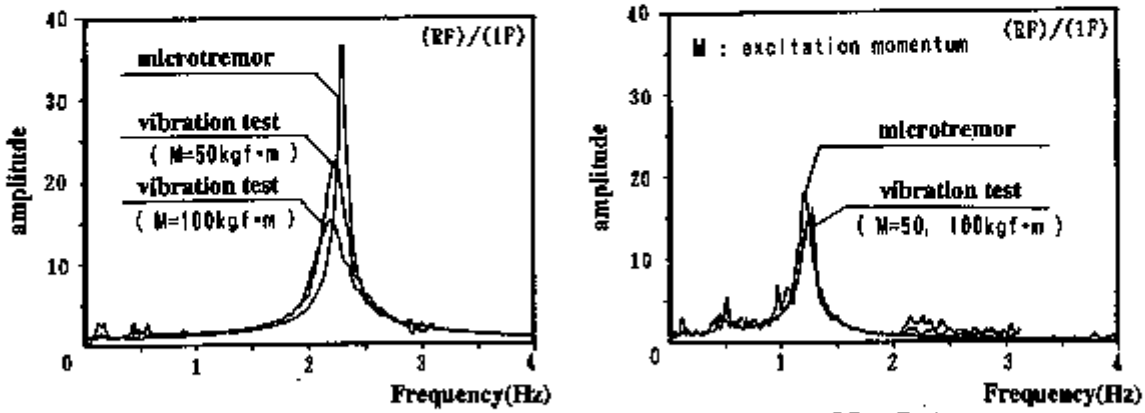

(a) LRB Building (b) HLRB Building

Fig.17 Transfer Function

4.4 VIBRATION TEST AND MICROTREMOR OBSERVATION

Vibration tests and microtremor observations were carried out before/after installing SRBs. The arrangement of vibrator and sensors is shown in Fig.12. The results of the tests are shown in Table 1. At the time that LRB building was constructed, same vibration test was done. Its results is also shown in Table 1. The transfer functions obtained from the vibration tests and microtremor observations are shown in Fig.17(a) and (b).

The natural frequency of the building is clearly decreased after the installing work. The natural periods of the building before the work were 0.45 and 0.42 sec. in X and Y direction, respectively. After installing, these were increased to 0.80 and 0.79 sec. These results are plotted in Fig.15. In this figure, natural period of the ground is also indicated. After installing, the natural period of the building became longer than that of the ground in region of small displacement of isolators. The damping factor is slightly decreased from 4.7 and 5.4 to 3.7 and 4.3, in X and Y respectively.

The LRB building shows that the natural period is not changed but the damping factor is increased in five years.

4.5 SEISMIC OBSERVATION

The field seismic observation of the building has been continued for six years. In regard to weak earthquakes, about eighty records were obtained as LRB building and eight records as HLRB building. The observation results show that the maximum acceleration response at top floor of HLRB building is reduced to 73 % of LRB building in case that the strength of earthquake excitations were in the region of 2.5 to 8 cm/s^2 and 82 % in the region of 0 to 2.5 cm/s^2.

4.6 VIBRATION INDUCED BY WIND

As the stiffness of the building is reduced, the vibration induced by wind for one year return period wind velocity(11.4 m/s) is examined from the view point of habitabilities[5]. The calculated maximum acceleration is 1.12 cm/s^2, which is small enough to keep good habitabilities.

Table 1 Result of Vibration Test

Building name	Test date	Direction	Natural period (sec)	Damping factor (%)
LRB Building	May, '87	X	0.45 (—)	4.2 (-)
		Y	0.42 (—)	3.3 (-)
LRB Building	March, '92	X	0.45 (0.44)	4.7 (1.4)
		Y	0.42 (0.40)	5.4 (1.6)
HLRB Building	March, '92	X	0.80 (0.81)	3.7 (2.6)
		Y	0.79 (0.81)	4.3 (-)

Note : Natural period and Damping factor evaluated from the results of Microtremor observations are also shown in parenthesis.

5. CONCLUSION

The new HLRB base-isolation system is introduced with experimental and analytical studies. Through field observation of a building with HLRB system, it can be concluded that this system is effective in reducing building responses to both weak and strong earthquake excitations. Especially, this system can improve habitabilities in weak excitations. Also, the responses of this HLRB building by wind has no problems from the view point of habitabilities.

ACKNOWLEDGMENTS

The authors sincerely appreciate the helps of Mr. Ikuo Shimoda and Mr. Masayoshi Ikenaga of OILES CORPORATION in experiments, and Mr. Toshio Suzuki, Mr. Yoshio Takasaki and Mr. Kazuo Ishikawa of FUJITA CORPORATION in field observations and installing works.

REFERENCES

[1]Teramoto,T.,Kitamura,H.,Yamane,T.and Yamamoto,H.(1991),"Base Isolated Building in Japan," Proc. of Int.Workshop on Developments in Base Isolation Techniques for Buildings,Tokyo,Japan, pp.243-263.

[2]A.I.J (1989),"Recommendation for the Design of Base Isolated Buildings"(in Japanese).

[3]Tanaka,K.,Hirasawa,M.,Ohyama,H.,Nakamura,Y.,Suzuki,T.,Ishiguro,Y.and Ishikawa,K.(1992),"Development on Base-Isolated System using Hybrid Rubber Bearing," JOURNAL OF FUJITA TECHNICAL RESEARCH INSTITUTE,No.28,pp.55-60 (in Japanese).

[4]Timoshenko,S.P. and Goodier,J.N.(1970),"THEORY OF ELASTICITY -- Third Edition", McGraw-Hill Book Company.

[5]A.I.J (1991),"Guidelines for the evaluation of habitability to building vibration"(in Japanese).

SMiRT-12 / K. Kussmaul (Editor)

K24/3

RESPONSE CHARACTERISTICS OF BASE-ISOLATED STRUCTURE WITH SILICONE RUBBER BEARINGS

S. Hayashi[1], H. Watanabe[1], Y. Nakamura[1], T. Yoshizawa[2] and T. Nakamura[3]

[1]Shimizu Corporation, Tokyo, Japan
[2]Bridgestone Corporation, Tokyo, Japan
[3]Shin-Etsu Chemical Industry Co. Ltd., Tokyo, Japan

1.INTRODUCTION

More than sixty base-isolated buildings have been built in Japan. A number of base-isolation systems were considered in our research, which was intended to establish the effectiveness of base-isolation systems.

We conducted research on silicone rubber bearings. Generally, silicone rubber is durable and its characteristics are not dependent on the temperature within the relevant design range.

The first part of the report covers material and elements testing. After the bearings were installed in the building, we performed forced vibration tests in both the horizontal and vertical directions. These test results form the next section. After several experiments, we carried out earthquake observations. We report on the effectiveness of the system in reducing response acceleration during a small displacement. This system was installed in the building in March 1992.

2.CHARACTERISTICS of SILICONE RUBBER and SILICONE RUBBER BEARINGS

2.1 Material

The fundamental characteristics of the rubber are shown in Table 1. The 25% modulus of the silicone rubber is somewhat low compared to that of the high damping rubbers. It is nearly equal to that of natural rubber, however, the tensile strength of the silicone rubber is low compared to other rubbers. Silicone rubber is equal to the natural rubber in the ultimate elongation.

Certain tests were performed on the silicone rubber material . Fig. 1 shows the shear modulus and the tanδ as a function of temperature. Tanδ is a factor related to damping. The shear modulus and the tanδ of the silicone rubber material are not dependent on the temperature within the relevant design range.

We performed several aging tests to investigate the durability of silicone rubber. Table 2 shows the results. The aging test simulated sixty years of natural aging. The variations in stiffness was +17% and that in ultimate elongation was -7%. Tensile strength remained nearly unchanged.

2.2 Bearing (Scale model)

We used a scale model to test the fun-

Table 1 Material characteristics of rubber

Material	Hardness (JIS A)	25% Modulus (kgf/cm^2)	Ultimate Elongation (%)	Tensile Strength (kgf/cm^2)
Natural Rubber	40±5	3.4±1.0	≥500	≥200
High Damping Rubber (Low Modulus Type)	50±5	4.7±1.0	≥800	≥150
High Damping Rubber (High Modulus Type)	60±5	12.0±2.0	≥650	≥100
Silicone Rubber	45±5	4.0±1.0	≥500	≥90

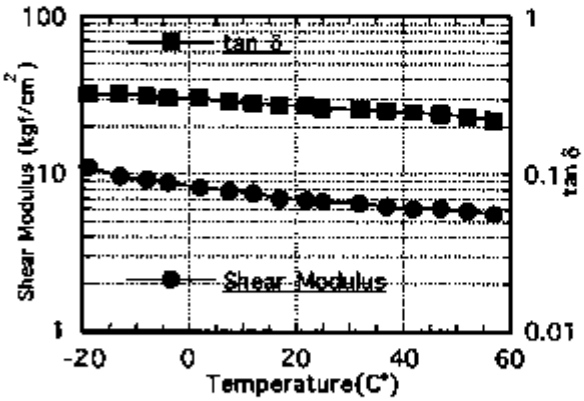

Fig. 1 Dependence on temperature of material

damental characteristics of the silicone rubber bearing.

Fig. 2 shows the influence of vertical stress on the hysteresis characteristics of the silicone rubber bearing. The experiment was performed by varying the vertical stress. As it increases, the loop area expands and the equivalent damping ratio tends to increase. This tendency was evident at small displacements. However, there was almost no change in the shear modulus.

Fig. 3 shows the influence of loading speed on the shear modulus and the equivalent damping ratio of the silicone rubber bearings. The experiment was performed in which the loading speeds were altered. The shear modulus of the silicone rubber bearings did not respond to changes in the vibration frequency within the relevant design range. The damping ratio was influenced by frequency changes.

To investigate the durability of the silicone rubber bearing further, we performed another aging test.

Table 3 shows the results of the aging test. The variation in horizontal stiffness was about +20% and that for the damping ratio was -10%~+20%.

2.3 Bearing (Real scale)

Fig. 4 shows the dimensions of the bearing used in this test. The bearing consisted of 24 layers with a thickness of 6.5-mm and a diameter of 600mm, 23 steel plates with a thickness of 3.1mm, top and bottom flange plates with thickness of 29.6-mm.

Table 4 shows the design values of this bearing. The equivalent horizontal stiffness for a displacement of 10 cm is 663.7 kgf/cm (horizontal frequency is 0.3Hz), and the equivalent hysteresis damping ratio is 0.12.

Before installing the rubber bearings under the building, a static loading test was performed at the laboratory.

A horizontal loading test was carried out under a constant vertical load of 110 tf. The horizontal stiffness and the equivalent damping ratio at each displacement are shown in Fig. 5.

In this displacement range, the horizontal stiffness of the silicone rubber bearing is linear. The values are almost equal to the design values. And the equivalent damping ratio is higher than 15% at displacements under 20cm and 13% at displacement of 30cm in the second cycle. This value is higher than the design value.

Table 2 Material characteristics by aging tests

		Initial Value	Value after Aging Test	Ratio of Variation
Stiffness	kgf/cm^2	8.9	10.4	+17%
Tensile Strength	kgf/cm^2	103	106	+3%
Ultimate Elongation	%	680	630	-7%

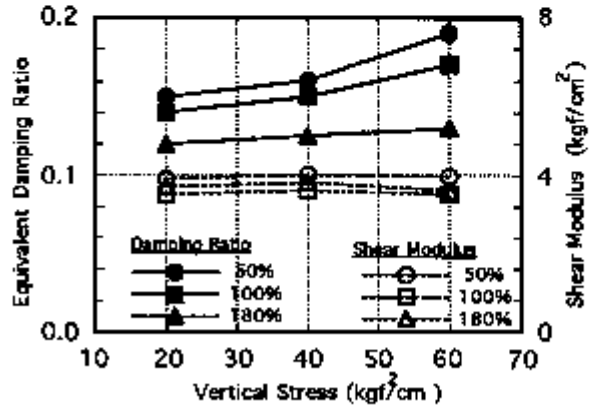

Fig. 2 Dependence on vertical stress of bearing characteristics

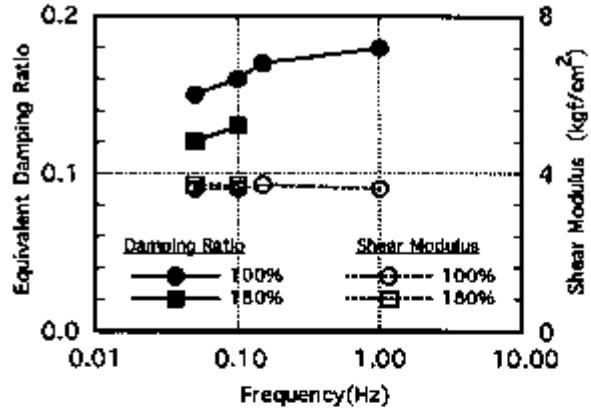

Fig. 3 Dependence on frequency of bearing characteristics

Table 3 Bearing characteristics by aging tests

Aging Tests	Horizontal Stiffness	Damping Ratio
Ordinary states	+20%	-10% ~ +20%
Vertical stress dependency	+13%	-9%
Frequency dependency	0%	+2% ~ 5%
Cyclic dependency	same as the initial state	same as the initial state

3.BUILDING

The building with the silicone rubber bearings is located in Matsuida, Gunma Prefecture, Japan. It is a two story reinforced concrete structure which was completed in March 1992. A general view of the building is shown in Fig. 6.

The building is used as a guard house and PBX (Private Branch Exchange) for the factory. The building is 8.4m by 8.4m, and the total combined area is about 142m2. Total weight of the building is 392tf.

Four bearings were installed. This building was founded on a gravel layer with clay, which has a shear wave velocity of 370m/sec. Construction of the base-isolated building with the silicone rubber bearings had been authorized by the Minister of Construction in Japan.

4.SITE EXPERIMENT

In order to investigate the basic properties of the building, forced vibration tests were carried out immediately after installation of the silicone rubber bearings.

4,1 Forced Vibration Test (Horizontal)

In order to investigate the dynamic properties of the building, a forced vibration test was carried out in March 1992. A vibration exciter was installed in the center of the roof slab and applied horizontal sinusoidal forces to the building. Fig. 7 shows the change in the resonance curves of the building along the X axis, based on the eccentric moment of the exciter. The resonant frequency clearly decreases as the loading force increases, i.e. amplitude of horizontal displacement increases. This tendency also holds for ordinary high damping rubber bearings.

The natural frequencies and the damping ratios in both directions as obtained from the experiment are shown in Fig. 8. These values were affected by the amplitude of the vibrations. As horizontal displacement increased, damping ratio increased and natural frequency decreased. The natural frequency was about 0.8Hz (1mm) ~ 0.9Hz (160μm) and the damping ratio was about 8% (160μm) ~ 12.5% (1mm) in both directions. The damping ratio of the silicone rubber bearing exceeds the design value at the displacements over 1mm.

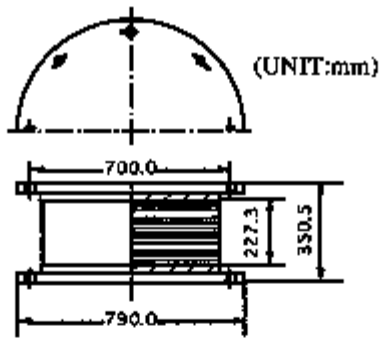

Fig. 4 Dimension of silicone rubber bearing

Table 4 Design value of bearing

Horizontal Stiffness	663.7	(kgf/cm)
Natural Frequency (Horizontal)	0.3	(Hz)
Vertical Stiffness	1170	(tf/cm)
Natural Frequency (Vertical)	12.6	(Hz)
Equivalent Damping Ratio	≥12	(%)

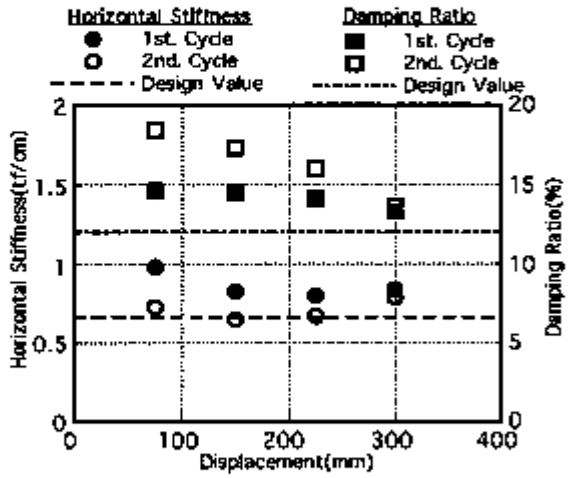

Fig. 5 Horizontal stiffness and Damping ratio by the static loading test

Fig. 6 General view of the building

Fig. 9 shows the results of the natural frequency when the forced vibration test was used on an isolation system with ordinary high damping rubber bearings, lead rubber bearings and the silicone rubber bearings. The natural frequency of the building with the silicone rubber bearings was lower than that of other systems over a small displacement range. The natural frequency of the silicone rubber is 1/3 that of the lead rubber bearing and 1/2 that of the high damping rubber bearing.

Fig. 10 shows the results of the damping ratio when the forced vibration test was used on an isolation system. The damping ratio of the building with the silicone rubber bearing was larger than that of other systems and 1.5 times that of the high damping rubber bearing.

The power spectrum of the micro tremor is shown in Fig.11. The natural frequency is about 1.06Hz.

4.2 Forced Vibration Test (Vertical)

In order to investigate the dynamic properties along the vertical axis of the building, a forced vibration test was carried out in December 1992. A small vibration exciter was installed in the center of the roof slab and applied sinusoidal forces vertically to the building. Force from the exciter was 19.2kgf.

Fig.12 shows the power spectrum of the sum of the response at opposite ends of the first floor and indicates the natural frequency along the vertical axis. The vertical natural frequency of the building with silicone rubber bearings installed is about 14.0Hz. Ordinary systems are over 18Hz.

Fig.13 shows the power spectrum of the difference of the response at opposite ends of the first floor. This shows the natural frequency of the rocking vibration, which are 11.8Hz in the X-direction and 12.0Hz in the Y-direction.

The power spectrum of the micro tremor in the vertical direction is shown in Fig.14. The graph indicates the overlap of the vertical vibration and the rocking vibration.

These results demonstrate that the vertical stiffness of the silicone rubber bearing is 1/2 that of the other materials.

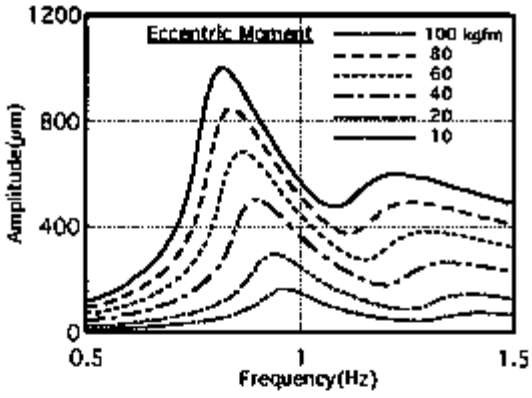

Fig. 7 Resonance curve of different eccentric moment

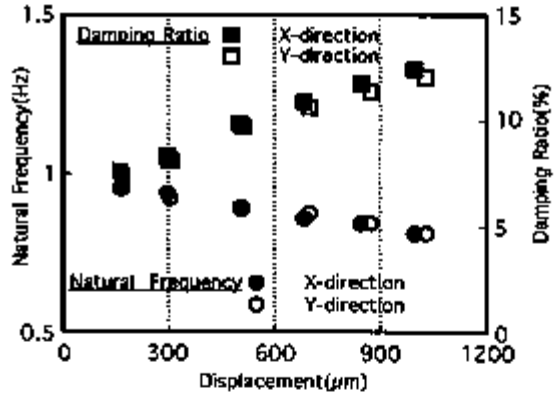

Fig. 8 Damping ratio and natural frequency by the forced vibraton test

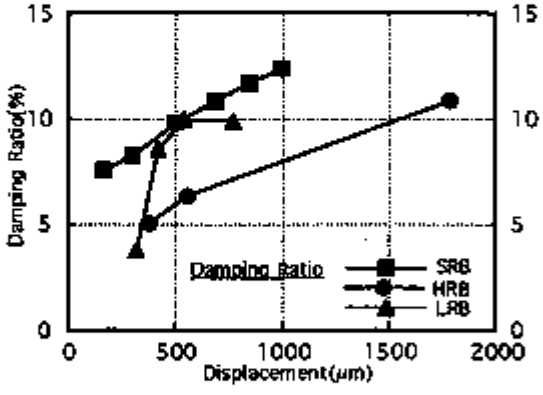

Fig. 9 Damping ratio of several type of bearings by the forced vibraton test

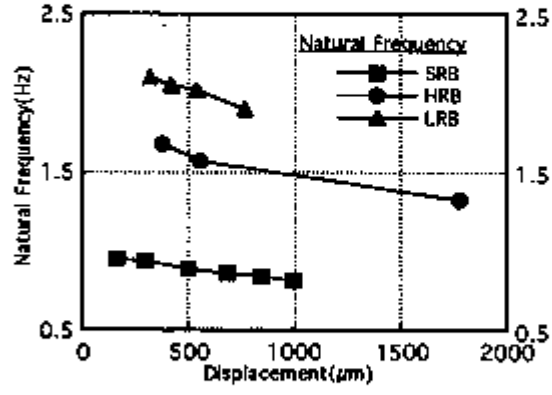

Fig. 10 Natural frequency of several type of bearings by the forced vibraton test

5.EARTHQUAKE OBSERVATION

5.1 Accelerometer setup

After the forced vibration test, an earthquake observation was carried out for the building and the surrounding ground to investigate the dynamic behavior of the building during earthquakes. The response of the building to significant earthquake events is automatically recorded.

Acceleration of five points was observed. The accelerometers were placed in the hard soil stratum(GL-20m), on the surface of ground near by (GL-1m), on the base slab of the base-isolated building, and on the first floor and the roof of the building. In all 16 components of earthquake motion were monitored.

5.2 Recorded earthquake data

Several earthquakes were recorded through June 1992. One of the recorded earthquakes is shown below. The highest acceleration of this earthquake on the ground surface was recorded at about 8 Gal. The maximum accelerations of all accelerometers during the earthquake on April 10, 1992 are shown in Fig.15. The maximum accelerations on the roof of the building was 1.70 Gal in the Y direction and 1.30 Gal in the X direction.

The maximum acceleration value of the first floor of the building is reduced 1/3 that of the basement of the building, and 1/5 that of the ground surface. During small earthquakes, the silicone rubber bearings are clearly effective in reducing the response acceleration.

The accelerograms for X direction at several points are shown in Fig.16. The accelerograms recorded in the building showed a longer period of vibration.

The earthquake response at the 1st floor of the building on this earthquake in the X and Y directions imply a fundamental frequency estimated at about 1Hz. Earthquake response in the Z direction is estimated at 12~15Hz. This value was equal to that produced by the forced vibration tests.

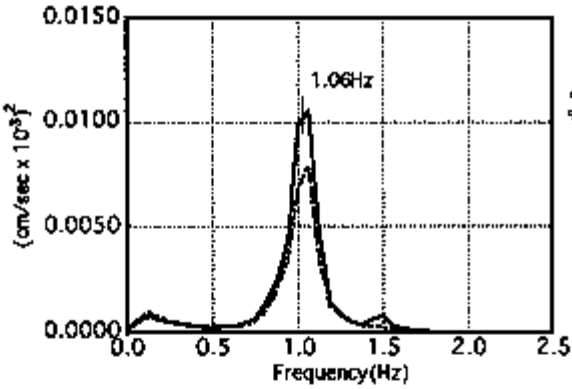

Fig. 11 Power spectrum of the horizontal direction by micro tremor

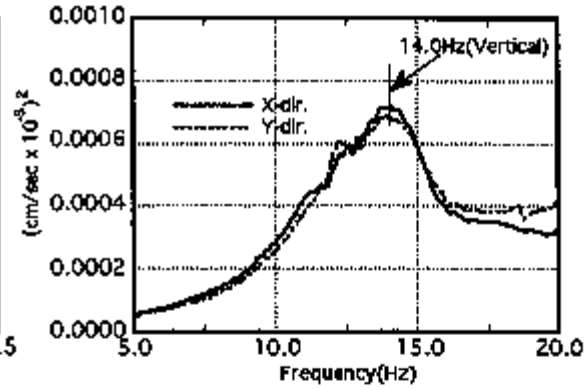

Fig. 12 Power spectrum of the vertical vibration by the forced vibration test

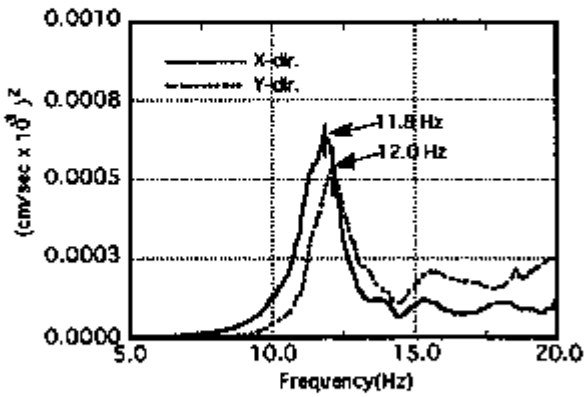

Fig. 13 Power spectrum of the rocking vibration by the forced vibration test

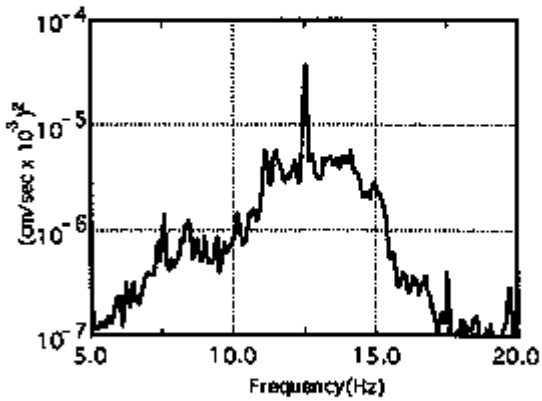

Fig. 14 Power spectrum of the vertical direction by micro tremor

6.CONCLUSION

From the results of the various tests and the earthquake observations, the following conclusions can be made.

(1) The damping ratio of the silicone rubber bearing is a function of horizontal displacement. For displacements under 0.3mm, the damping ratio is 2/3 of the design value. However, the damping ratio exceeds the design value at displacements over 1mm.

(2) The horizontal stiffness of the silicone rubber bearing is non-linear at very small displacements.

(3) The damping ratio of the silicone rubber bearing is about twice that of bearings made from other materials at small displacements.

(4) The horizontal stiffness of the silicone rubber bearing is about 1/3 ~1/2 that of bearings made from other materials at small displacements.

(5) The vertical natural frequency of the building with the silicone rubber bearing installed is 14.0Hz. This value is quite small compared to that for other bearing systems.

(6) The amplification factor of a small earthquake of the base-isolated building with silicone rubber bearings, was small.

ACKNOWLEGEMENT

The authors would like to express their appreciation to Masaaki Saruta for valuable help with the experiments and for helpful discussion, and to Kazuma Momii for providing the data on silicone rubber.

REFERENCE

Tamura K., Yamahara H. and Izumi M. "PROOF TEST OF THE BASE-ISOLATED BUILDING USING FULL-SIZED MODEL", Proc. Seismic, Vibration and Shock Isolation - 1988, ASME, PVP-Vol.147, pp.21-28

Saruta M., Watanabe H. and Izumi M. "PROOF TEST OF THE BASE-ISOLATED BUILDING USING HIGH DAMPING RUBBER BEARING", TRANSACTIONS of the 10th International Conference on SMiRT, Vol.K2, pp.631-636

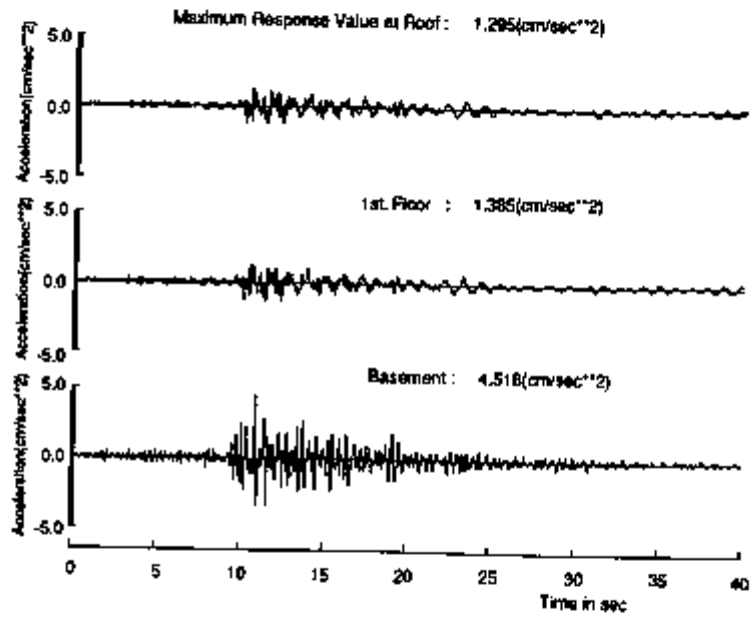

Fig. 16 Time history for X-direction of the earthquake on April 10, 1992

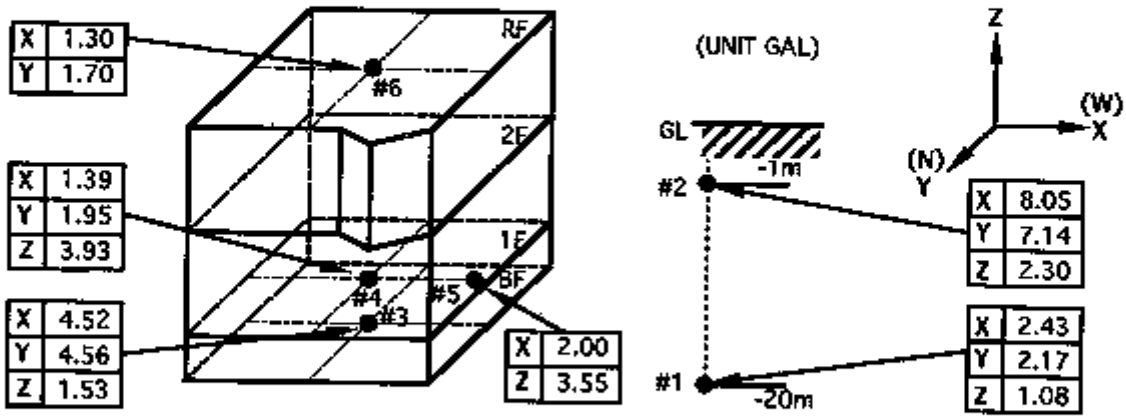

Fig. 15 Maximum acceleration distribution of the earthquake on April 10, 1992

SMiRT-12 / K. Kussmaul (Editor)

K23/4

ANALYTICAL STUDY ON ULTIMATE RESPONSE CHARACTERISTICS OF BASE ISOLATED STRUCTURE

K. Ishida[1], S. Yabana[1], G. Yoneda[2], J. Suhara[3] and K. Yoshikawa[4]

[1]Central Research Institute of Electric Power Industry, Chiba, Japan
[2]Takenaka Corp., Tokyo, Japan, [3]Shimizu Corp., Tokyo, Japan
[4]Kajima Corp., Tokyo, Japan

1. Introduction

In order to make sure of aseismic safety on a base-isolated reactor building, it is important to understand its earthquake response properties not only at the design level, but also at the ultimate state. From this point of view, a shaking table test was conducted to investigate the rupturing characteristics of a laminated rubber bearing and the ultimate response properties of a superstructure. This paper reports the results of a simulation analysis of its shaking table test. The restoring force loops of the rubber bearing were modeled by three different methods; a multi linear model, a smooth function model, and a rate model. It was found that the results of the shaking table test could be simulated quite accurately by any of these analytical models.

2. Outline of the Shaking Table Test

Table 1 shows the similarity law adopted in the test. The acceleration and the stress are equal to those of the prototype. The scale ratio is 1/15. Fig.1 illustrates the shape and the dimensions of the test specimen. The superstructure is a reinforced concrete rigid body with a weight of 17.8 tons. It is supported by 8 sets of lead rubber bearings(LRBs) . The LRB is a 1/15 reduced-scale model of the actual LRB for which the rated design load is 500 tons. The rubber sheet is affixed to the upper and lower flanges. Fig.2 shows the dimensions of an LRB. As an input motion, tentative design seismic motion,S1, is employed. In the tests, the input seismic motion is reduced in time to $1/\sqrt{15}$ according to the similarity law. Excitations are given repeatedly by gradually increasing the acceleration of input seismic motion by approximately 0.25 S1 each time, starting from 1.0 S1 level. Measurements were taken for the following three items. ① Shear and axial forces acting on LRBs ② Horizontal and vertical relative displacements between the shaking table and the superstructure ③ Absolute accelerations of the shaking table and the test specimen. The details of the shaking table test are described in Ref.1.

3. Loading Test of a Single Bearing

Loading tests of a single bearing are carried out by using LRBs that have the same dimensions as those used in the shaking table test. Restoring force characteristics of LRBs are investigated in various stress states created by different combinations of shear and axial forces. Fig.3 shows the results of the loading test of a single bearing. The stiffness in the strain hardening region of the horizontal hysteresis loop is softened in the cyclic loading test, compared with the monotonous loading test. In addition, once an LRB experiences a large deformation, the displacement for starting of strain hardening becomes grater. Equivalent stiffness, Keq, decreases as shear strain increases, until shear strain reaches some 200%. After that, equivalent stiffness increases due to the effects of strain hardening. Shear force at zero displacement, Qd, increases as the amplitude of shear strain increases. It is, however, almost constant over the shear strain of 200%. The equivalent damping ratio, heq, decreases as the amplitude of shear strain increases, until shear strain reaches 300%. When shear strain exceeds 400%, although the area of the hysteresis loop

increases on account of the strain hardening , the equivalent damping ratio, heq, becomes stable at approximately 5%, because the equivalent stiffness, Keq, also increases. In a simulation analysis, it is important to express the above-described restoring force characteristics of an LRB in appropriate models. The details of the loading test of a single bearing are described in Ref.2.

4. Simulation Analysis

4.1 Modeling of Restoring Force Characteristics

Restoring force characteristics of an LRB are modeled by following three different methods.
Multi linear model: As shown in Fig.4, the horizontal restoring force loop is represented by a multi-linear line. It consists of the restoring force due to the effects of the rubber part, and the absolute elasto-plastic restoring force due to the effects of the lead plug. As shown in Fig.3 a), when an LRB is deformed again after experiencing a large deformation, the displacement for starting of the strain hardening becomes larger. This phenomenon is expressed by the following formula.

$$x_s' = x_s + 0.45(x_m - x_s) \qquad \cdots\cdots\cdots (1)$$

In the shaking table test, excitation is given repeatedly by increasing the acceleration of input motion step by step. The maximum horizontal displacement experienced one step before is taken as the initial value of x_m. As shown in Fig.3, the values of K_1 and Q_d depend on the amplitude of the horizontal displacement. Therefore, they are determined according to the maximum horizontal displacement in the shaking table test at each excitation level. The skeleton of a vertical restoring force loop is expressed by a tri-linear line. It is linear in the compression side, but yields in the tension side at the level of $\sigma_2 = 20\ kg/cm^2$.
Smooth Function Model: As shown in Fig.5, horizontal and vertical restoring forces are approximated using a high-order function. Horizontal restoring force loop consists of the skeleton and hysteresis curves. The skeleton curve is expressed as a quadratic function on horizontal displacement, x.

$$Q_s(x) = a_0 \cdot sgn(x) + a_1 x + a_2 x^2 + a_3 x^3 + a_4 x^4 \qquad \cdots\cdots\cdots (2)$$

where, when $x > 0$, $sgn(x) = 1$, and when $x < 0$, $sgn(x) = -1$

The coefficient, a_i ($i = 0 \sim 4$), is determined based on the results of the loading test of a single bearing under static cyclic loading. "a_0" represents shear force Q_d, where horizontal displacement, x, is zero. In the simulation analysis, the value of Q_d is taken as a function on the horizontal displacement amplitude. The hysteresis curve ,$Q_L(x)$, is expressed by a quadratic function on horizontal displacement, x, as is the skeleton curve.

$$Q_L(x) = b_0 \cdot sgn(x) + b_1 x + b_2 x^2 + b_3 x^3 + b_4 x^4 \qquad \cdots\cdots\cdots (3)$$

The coefficient, bi, is determined in the following way. ① The hysteresis curve passes Point (0, $-Q_d$) and Point (x_m, Q_m). ② It is tangent to the skeleton curve at Point (0, $-Q_d$). ③ When the displacement is $\beta \cdot x_m$, the distance between the skeleton and hysteresis curves is r times as large as $2Q_d$. The value of r is defined as a quadratic function on horizontal displacement. The influence of cyclic loading is taken into account by shifting the skeleton curve, as shown in Fig.5 b). The vertical restoring force loop is expressed in a linear form on the compression side and as skeleton and hysteresis curves on the tension side.
Rate Model: As shown in Fig.6, characteristics of horizontal restoring force are expressed by a rate model (Ref.3), and those of vertical restoring force are represented by a non-linear elastic model. The rate model is produced based on the following principles. ① Restoring force characteristics are expressed by a skeleton curve and a hysteresis curve. ② Restoring force loop follows the skeleton curve, when horizontal displacement exceeds the maximum displacement experienced before. Otherwise, it follows the hysteresis curve. ③ The hysteresis curve is determined by the maximum displacement experienced before.
The skeleton curve $Q_s(x)$ is expressed by the following formulas.

$$Q_s(x) = K_{eq}(x_m) \cdot x \qquad \cdots\cdots\cdots (4)$$

$$K_{eq}(x_m) = c_0 + c_1 x + c_2 x^2 + c_3 x^3 \qquad \cdots\cdots\cdots (5)$$

The coefficient, c_i, is determined from Fig.3 b). The hysteresis curve ,Q_L, is expressed by the following formulas.

$$Q_L = Q_1 + Q_2 \qquad \cdots\cdots\cdots (6)$$

$$Q_1 = K_2(\alpha + (1-\alpha)(x/x_m)^6)x \quad \cdots\cdots\cdots (7)$$

$$dQ_2/dt = (K_1 - K_2)\cdot dx/dt \cdot (1 - sgn(dx/dt)\cdot(Q_2/Q_d)) \quad \cdots\cdots\cdots (8)$$

where, $K_1 = (1 - u + u/s)\cdot Keq$ $\quad K_2 = (1-u)\cdot Keq$

$u = Q_d / Q_m$ $\quad q = \pi \cdot heq/2$

"s" represents a solution of $s\cdot(e^{2/s} - 1)(e^{2/s} + 1) = (u-q)/u$

"u" and "q" are expressed by a cubic function on horizontal displacement, based on the results of the loading test of a single bearing.

4.2 Modeling of Dynamic Response Analysis

As shown in Fig.7, the superstructure is modeled by a rigid beam and a concentrated mass. LRBs are modeled as 4 axial springs and a single shear spring. The time-history waveform of acceleration recorded at the surface center of the shaking table is employed as an input motion. Simulation analyses are carried out for input levels of 1.0 S1, 3.0 S1, and 6.0 S1.

4.3. Analytical Result

Fig.8 shows the time histories for an input of 6.0 S1. Analysis is performed on the rate model. In the test, the maximum shear strain of LRBs is 560% and LRBs are just short of rupturing. As the LRB used in the test has a small diameter of 107 mm, it shows rupture shear strain of about 600 %, which is somewhat larger than that of the actual-size LRB. The time-history waveform of the acceleration at the gravity center of the superstructure and the shear force take on sinusoidal forms when input level is low. However, when input level is high, their peaks both in the test and analysis sharpen due to the effects of strain hardening. Fig.9 shows the horizontal hysteresis loops. As remarkably shown in the case of 1.0 S1, the shear force at the point where displacement is zero becomes greater, as displacement amplitude increases. Analyses on the smooth function model and the rate model reflect this tendency. For the input of 6.0 S1, all of the three models simulate a hardening phenomenon of LRBs quite well. Fig.10 shows the relation between the axial strain and the shear strain. The tensile stiffness of LRBs is significantly smaller than its compressive stiffness. Therefore, the center of rocking vibrations shifts to the edge of the test model with an increase of overturning moment. As a result, both in the test and analysis, tensile axial strain caused by up-lift of the test model increases sharply in the area where shear strain reaches the maximum. Fig.11 illustrates the relation between the axial force and the shear strain. Just around the area where shear strain reaches the maximum, compressive axial force rises drastically. This is caused by following two reasons. One is that the increasing rate of shear strain declines and, at the same time, the response acceleration increases on account of the strain hardening. The other is that only those LRBs installed at the edge of the test model are compressive due to the movement of rocking center. The axial force becomes wavy because of the up-lift and drop-down of the superstructure. The analytical results are in good agreement with the test results. Fig.12 shows the acceleration response spectrum at the gravity center. For input of 1.0 S1, it is simulated very accurately. For input of 6.0 S1, there appear some peaks in the high frequency domain , as the peak of the acceleration time history waveform sharpens due to the influence of strain hardening. Also for input of 6.0 S1, simulation analysis results reflect this tendency. As shown in Fig.13, the maximum response values calculated by each modeling method agree quite well with test results at the input level of 1.0S1 and 3.0S1. Even for input of 6.0 S1, the differences are within a range of some 20%.

5. Conclusion

A simulation analysis was carried out on a shaking table test on a base-isolated reactor building model. Characteristics of restoring force of LRBs were expressed in three different models. It was found that the results of a shaking table test from the design level to the ultimate level could be simulated accurately by any of these models. Therefore, these analysis techniques would be very effective in evaluating aseismic safety margin of base-isolated reactor buildings.

Acknowledgement : This study was carried out as a part of the project of the Ministry of International Trade and Industry titled "Verification Tests of Fast Breeder Reactor Technology", which has been conducted since 1987.

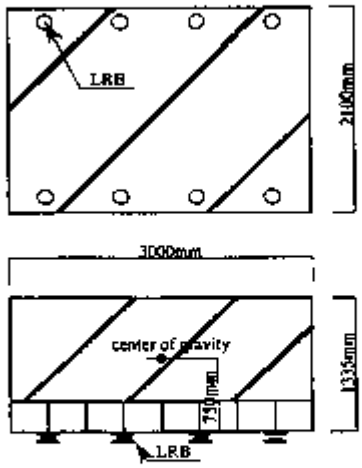

Fig.1 Shape and dimensions of superstructure

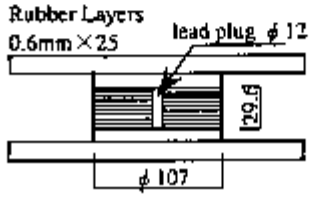

Fig.2 Lead rubber bearing

Table 1 Similitude

Scale of		Similitude
Length	L	$L_p/L_m=\lambda=15$
Acceleration	α	$\alpha_p/\alpha_m=1$
Frequency	f	$f_p/f_m=1/\sqrt{\lambda}=0.258$
Stress	σ	$\sigma_p/\sigma_m=1$
Strain	γ	$\gamma_p/\gamma_m=1$
Force	F	$F_p/F_m=\lambda^2=225$

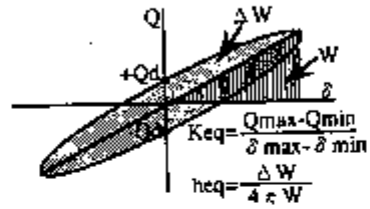

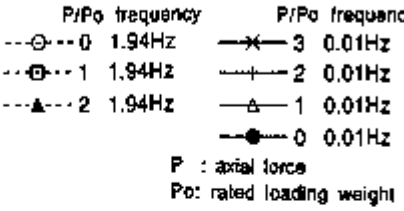

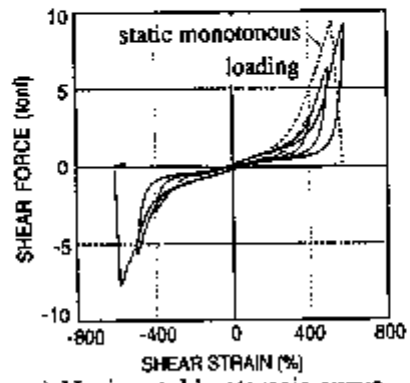

a) Horizontal hysteresis curve

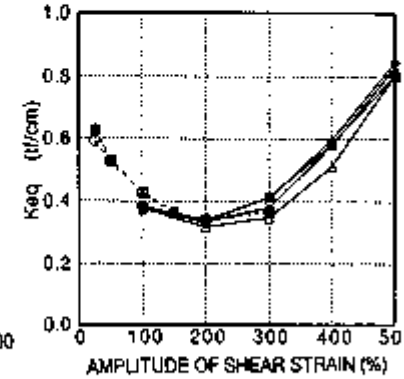

b) Equivalent stiffness Keq

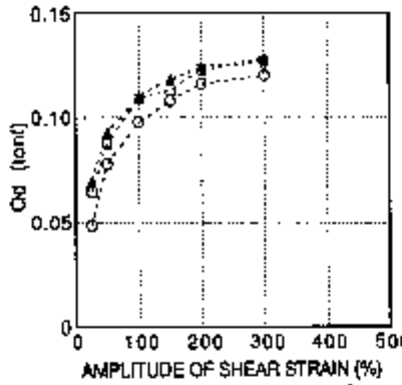

c) Shear force at 0 disp. Qd

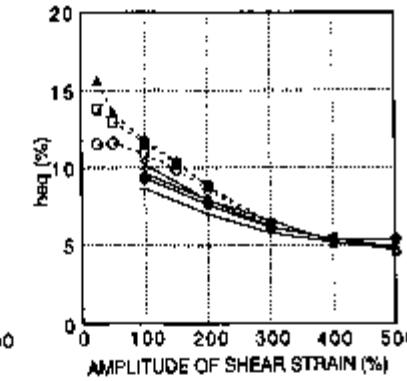

d) Equivalent damping ratio heq

Fig.3 Loading test results of a single bearing

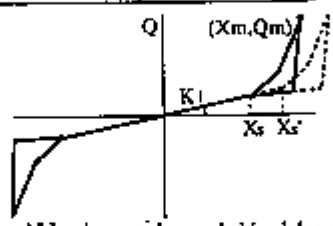

a)Horizontal model(rubber)

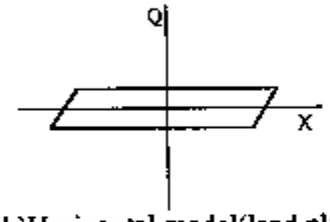

b)Horizontal model(lead plug)

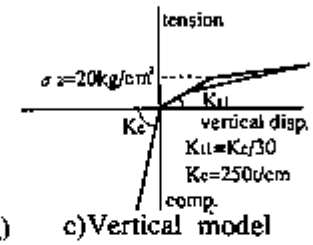

c)Vertical model

Fig.4 Restoring force loop by multi linear model

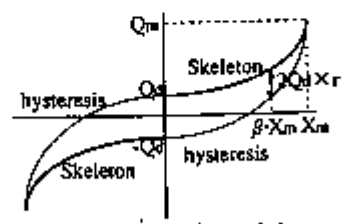

a)Horizontal model

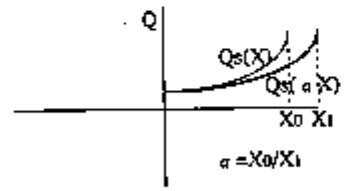

b)Evaluation of dependence on iterative deformation

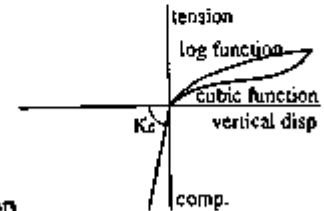

c)Vertical model

Fig.5 Restoring force loop by smooth function model

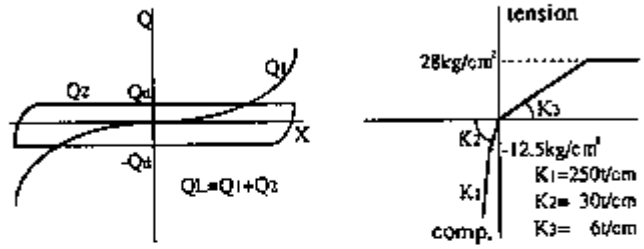

a)Horizontal model(hysteresis) b)Vertical model

Fig.6 Restoring force loop by rate model

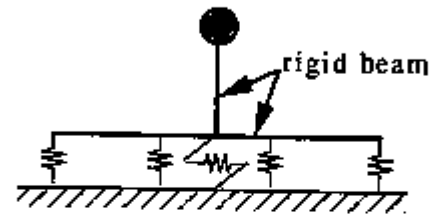

Fig. 7 Simulation analysis model

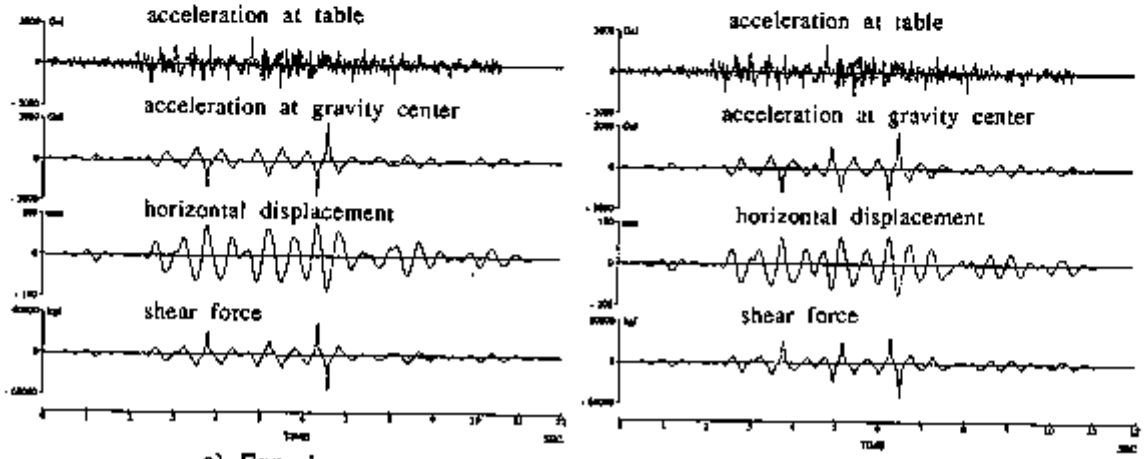

a) Experiment b) Analysis by rate model

Fig.8 Time histories at 6.0S1

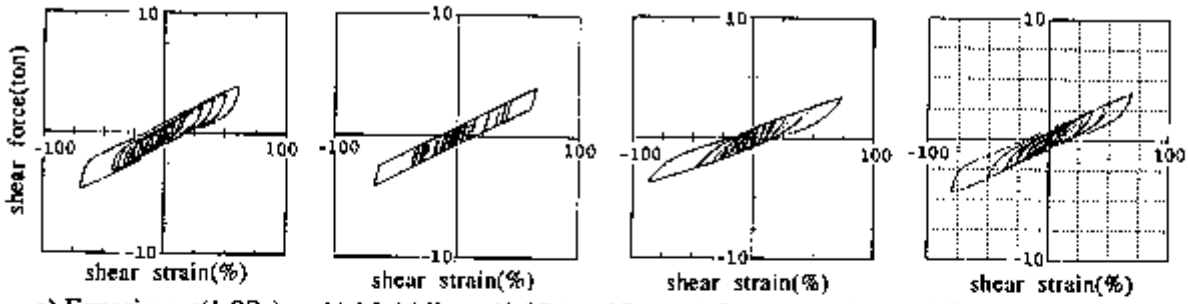

a) Experiment(1.0S1) b) Multi linear(1.0S1) c)Smooth function(1.0S1) d)Rate model(1.0S1)

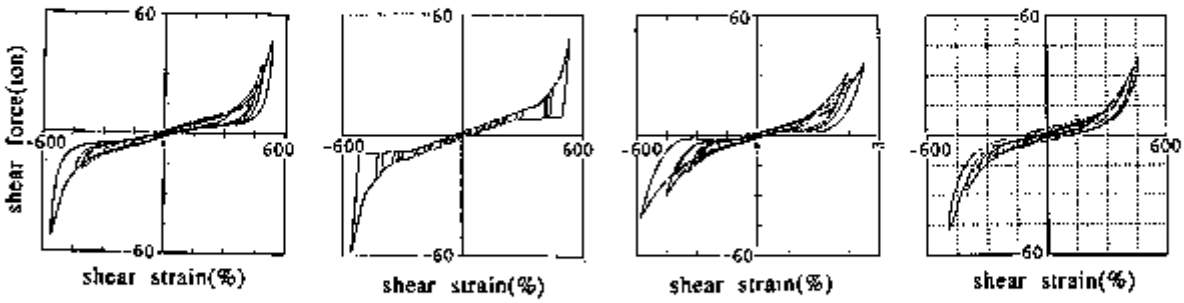

e) Experiment(6.0S1) f) Multi linear(6.0S1) g)Smooth function(6.0S1) h)Rate model(6.0S1)

Fig.9 Relationship between shear force and shear strain

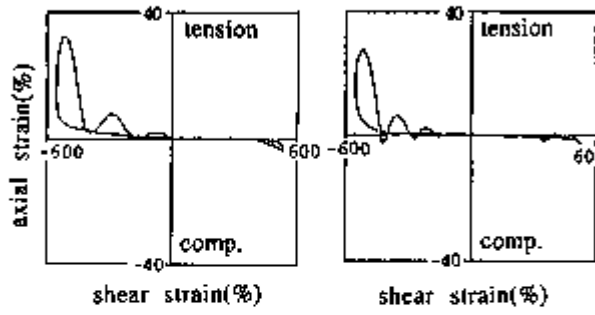

a)Experiment b)Multi linear

Fig. 10 Relationship between axial strain and shear strain (Multi linear model, 6.0S1)

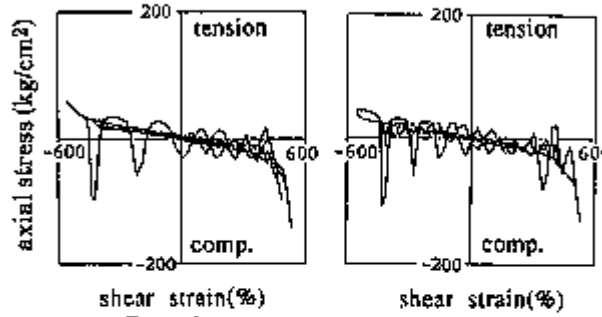

a)Experiment b)Multi linear

Fig. 11 Relationship between axial force and shear strain (Multi linear model, 6.0S1)

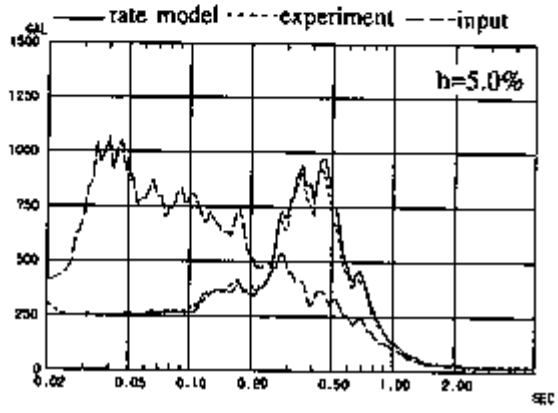

a)at the intensity of 1.0S1

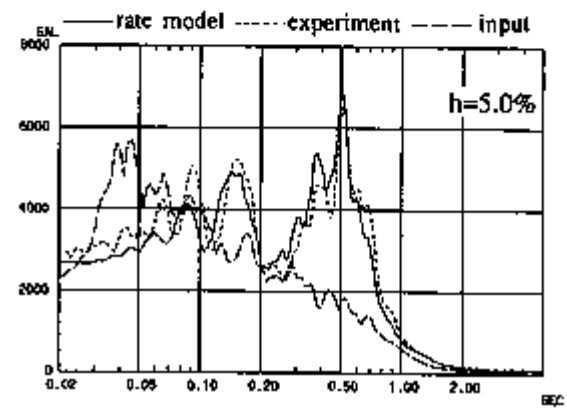

b)at the intensity of 6.0S1

Fig. 12 Response spectra at the center of gravity

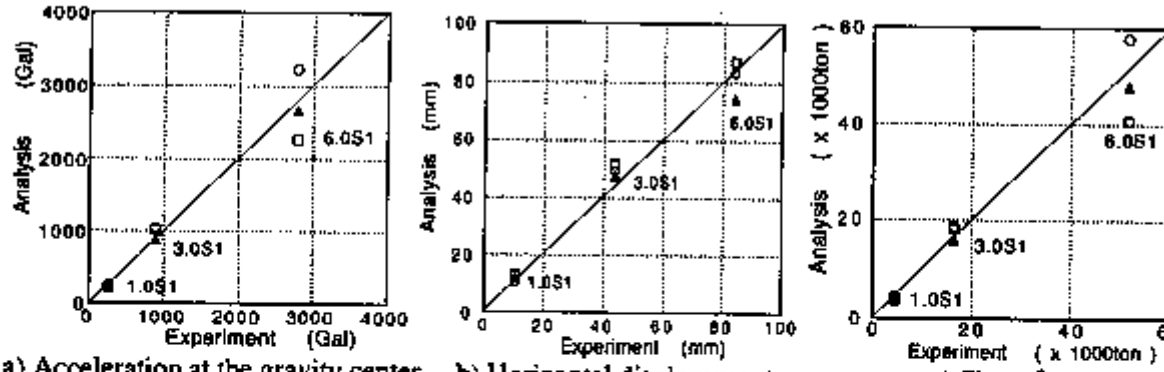

a) Acceleration at the gravity center b) Horizontal displacement c) Shear force

Fig. 13 Comparison between maximum response values of experiment and those of analysis

References
1) Ishida, K., Moteki, M., Yoneda, G., et al., 1992, Shaking table test on ultimate behavior of seismic isolation system Part 1 & 2, 10th WCEE,vol.4, pp2271～2276, pp2411～2416
2) Ishida, K., Iizuka, M., et al., 1991, Failure tests of laminated rubber bearings, 11th SMIRT, vol.K2, pp241～246
3) Fujita, T., Suzuki, S., et al., 1991, Ultimate Strength of Seismic Isolation System Using High Damping Rubber Bearings for Buildings, trans. Jpn. Soc. Mech. Eng., Vol.57, No.544, C

SMiRT-12 / K. Kussmaul (Editor)

K24/4

PERFORMANCE OF BASE-ISOLATED SPENT FUEL STORAGE POOL STRUCTURES

J.K. Kim[1], I.K. Choi[1], J.M. Seo[1], Y.S. Choun[1], J. Kim[1] and D.H. Ha[2]

[1]Korea Atomic Energy Research Institute, P.O. Box 7, Daeduk-Danji, Taejeon, 305-606 Korea
[2]Department of Civil Engineering, Seoul National University, Gwanak-Ku, Seoul, Korea

ABSTRACT

A modal analysis technique is presented for the seismic response analysis of base-isolated spent fuel storage structures taking into account of fluid-structure interaction effects and composite damping characteristics of the base-isolated structural system. Responses of a base-isolated pool structure subjected to 1940 El Centro earthquake load are analyzed by the developed method and compared with the responses of fixed base counter part. An objective function for the optimization of the base-isolated pool structure is proposed which is based on strain energies of the structure and base isolator.

1. INTRODUCTION

Spent fuel assemblies or canisters are usually stored in rectangular reinforced concrete pool structures, which may not be rigid dynamically, in the wet-type interim spent fuel storage facility(ISFSF). It is well recognized that hydrodynamic pressure in a flexible container can be greatly amplified due to the fluid-structure interaction effects between the fluid inside and the flexible walls[1]. But, if base isolators are installed between the base slab and foundation, the earthquake load transmitted to the superstructure can be reduced significantly, and vibration characteristics can be controlled too[2]. The reduced base acceleration of the superstructure will enhance the safety of stored canisters or spent fuel assemblies.

In this paper, a 2-D analysis method of the coupled system is described and its dynamic characteristics under horizontal ground acceleration are investigated.

Since the convective pressure due to the sloshing of the fluid can be practically decoupled and is one order of magnitude less than the impulsive pressure due to the fluid mass moving together with the structure[3], the impulsive mass alone is computed by finite element modeling of the potential flow of the incompressible ideal fluid and added to the structural mass lumped at the nodes. Because of the dominant contribution of the 1st mode, vibration of the fluid-structure system is described by the first mode alone.

Isolators are assumed to be laminated rubber bearing type which can be modeled by a linear spring and a viscous damper. The coupled equation of motion for the fluid-structure-isolator system does not accept classical modal decomposition because of composite damping of the system. In this study modal analysis is made possible by finding equivalent modal damping ratios.

Finally, an objective function for the optimization of the base-isolated pool structure is proposed which is based on strain energies of the structure and base isolator.

2. FINITE ELEMENT MODELING OF FLUID MOTION

Two dimensional motion of invicid and incompressible ideal fluid (Fig. 1) can be expressed in terms of velocity potential. The velocity potential $\phi(x,t)$ satisfies two-dimensional Laplace equation in the fluid region:

$$\nabla^2\phi = \left(\frac{\partial^2}{\partial x_1^2}+\frac{\partial^2}{\partial x_2^2}\right)\phi(x,t) = 0. \tag{1}$$

Applying Galerkin finite element method to Eq. (1), algebraic equations governing fluid motion are derived easily in the following form:

$$[B]\{\ddot{v}\} = \{p\} \tag{2}$$

where $\{p\}$ and $\{\ddot{v}\}$ denote nodal pressure vector and nodal acceleration vector in inertia reference frame defined at the nodes along the wall respectively.

By employing shape functions used to interpolate pressure distribution and acceleration along the boundary of each finite element and by applying virtual work principle, the relationship between nodal force vector, $\{F\}$, and nodal acceleration vector can be derived in the following form:

$$[M_f]\{\ddot{u}\} = -\{F\} - [M_f]\{1\}(\ddot{u}_b+\ddot{u}_g) \tag{3}$$

where $\{\ddot{u}\}$ is nodal acceleration vector relative to the base of the structure, $\ddot{u}_b$ is base acceleration relative to the ground and $\ddot{u}_g$ is ground acceleration.

3. EQUATION OF MOTION FOR THE COUPLED SYSTEM[4]

The motion of dry structure may be described by the next equation:

$$[M_d]\{\ddot{u}\} + [C_d]\{\dot{u}\} + [K_d]\{u\} = -[M_d]\{1\}(\ddot{u}_b+\ddot{u}_g) + \{F\} \tag{4}$$

where $[M_d]$, $[C_d]$, and $[K_d]$ are mass, damping and stiffness matrix of the dry structure model respectively. The governing equation for the coupled fluid-structure system may be easily obtained by combining Eq. (3) and (4):

$$[M]\{\ddot{u}\} + [C]\{\dot{u}\} + [K]\{u\} = -[M]\{1\}(\ddot{u}_b+\ddot{u}_g). \tag{5}$$

Assuming that damping matrix $[C]$ can be diagonalized, the following modal equations are obtained:

$$\{u\} = \eta_n\{\phi_n\}, \tag{6}$$

$$\ddot{\eta}_n + 2\xi_n\omega_n\dot{\eta}_n + \omega_n^2\eta_n = -\Gamma_n(\ddot{u}_b+\ddot{u}_g) \tag{7}$$

where ω_n, η_n, ξ_n, $\{\phi_n\}$ and Γ_n denote the natural frequency, modal amplitude, modal damping ratio , mode shape vector and modal participation factor of the n-th mode respectively. Since the motion of the superstructure will be dominated by the first vibration mode, it may be expressed as follows:

$$\{u\} = \eta_1\{\phi_1\}, \tag{8}$$

$$\Gamma_1\ddot{u}_b + \ddot{\eta}_1 + 2\xi_1\omega_1\dot{\eta}_1 + \omega_1^2\eta_1 = -\Gamma_1\ddot{u}_g \tag{9}$$

The substructure consisting of the base mass and isolator may be modeled mechanically by the following equations:

$$m_b(\ddot{u}_b+\ddot{u}_g) + c_b\dot{u}_b + k_bu_b - F_s = 0 \tag{10}$$

$$F_s = -\{1\}^T[M](\{\ddot{u}\} + \{1\}(\ddot{u}_b + \ddot{u}_g)) \tag{11}$$

where m_b, c_b, and k_b denote base mass, viscous damping and stiffness of the isolator. Introduction of Eq. (8) and (11) into Eq. (9) will render the following equation:

$$(m_r + m_b)\ddot{u}_b + c_b\dot{u}_b + k_b u_b + q_1\ddot{\eta}_1 = -m_t\ddot{u}_g \tag{12}$$

where $q_1 = \{1\}^T[M]\{\phi_1\}, m_r = \{1\}^T[M]\{1\}$, $m_t = m_s + m_b$. Eq. (9) and Eq. (12) constitute the governing equation for the coupled fluid-structure-isolator system, which can be expressed in the (2 x 2) matrix equation:

$$[M_c]\{\ddot{u}_c\} + [C_c]\{\dot{u}_c\} + [K_c]\{u_c\} = -\{q_c\}\ddot{u}_g. \tag{13}$$

Because damping characteristic of the superstructure is quite different from that of the isolator and the matrix, $[C_c]$, in the above equation may not be diagonalizable in general, Eq. (13) can not be solved by the traditional modal analysis method. In order to remedy this shortcoming and make the response spectrum analysis be possible, equivalent modal damping ratios are calculated explicitly as explained in next section.

4. EQUIVALENT MODAL DAMPING RATIOS

It starts from the assumption that modal damping ratios are given as ξ_{1c} and ξ_{2c}. From the assumed modal damping ratios, damping matrix for the system may be composed as

$$[\overline{C_c}] = [\phi_c]^{-T}\begin{bmatrix} 2\xi_{1c}\omega_{1c}M_{1c} & 0 \\ 0 & 2\xi_{2c}\omega_{2c}M_{2c} \end{bmatrix}[\phi_c]^{-1} \tag{14}$$

where $[\phi_c]^{-T}$ is the transpose of the inverse of the mode shape vector matrix, $[\phi_c]$, of Eq. (13) and $M_{nc} = (\phi_{nc})^T[M_c](\phi_{nc})$. Equating $[\overline{C_c}]$ in Eq. (14) with $[C_c]$ in Eq. (13), equivalent modal damping ratios ξ_{1c} and ξ_{2c} can be calculated. Since there are three equations for two unknowns, they can be calculated by least square method or by equating only diagonal elements.

5. OBJECTIVE FUNCTION FOR THE OPTIMIZATION

Earthquake load may not be known deterministically. Therefore base isolation system need be designed to show good performance against varying earthquake loads expected at the particular site. Usually structural optimization is attempted by stochastic analysis method. But stochastic method requires the earthquake load be described in terms of power spectrum. However, since design response spectrum is employed for the design of most nuclear or non-nuclear facilities, it may be more practical to rely on the spectrum analysis for the optimal design of spent fuel storage structures. The objective function proposed is based on the strain energies of the structure and isolator.

The relative advantage of the isolation system is the increased safety compared with the fixed base structure. Therefore this aspect may be taken into account by the following expression:

$$R_s = \frac{E_{si}}{E_{sf}} \tag{15}$$

where E_{sf} is the maximum strain energy in the fixed base structure model and E_{si} is the strain energy in the isolated superstructure model calculated by response spectrum analysis.

For a given isolator the maximum shear deformation may have to be within the design specification. Therefore the increased safety of the isolator may be expressed by the ratio

between the strain energies developed in the isolator:

$$R_\delta = \frac{E_{bs}}{E_{bo}} \tag{16}$$

where E_{bo} means the maximum strain energy based on the allowable shear deformation limit and E_{bs} is the actually developed strain energy in the isolator. Because one may give different weights to the two ratios, more general form of the objective function $R(k_b,c_b)$, may be written as

$$R(k_b,c_b) = \alpha R_b + \beta R_\tau \tag{17}$$

where α and β are weighting factors which depend on the importance consideration. Thus optimization of the isolator may be defined as finding k_b and c_b which produce the minimum value of Eq. (17) within prescribed constraints. The usual constraint is the limit in the base displacement. This kind of constraint can be easily imposed to Eq. (17).

6. PERFORMANCE ANALYSIS

Using the developed program, seismic responses of an isolated pool structure are analysized. The model is described in Fig. 1. The superstructure of the isolated system is identical with that for fixed base model. Mechanical properties of the isolator chosen are given in Table 1.

Table 1. Properties of Isolator

Type	k_b	c_b	ω_b*	ζ_b**
Laminated Rubber Bearing	120.16t/m	11.47t·s/m	3.14r/s	0.15

* $\omega_b = \left[\frac{k_b}{m_d+m_f}\right]^{1/2}$, ** $2\zeta_b\omega_b = c_b/(m_d+m_f)$

m_f = total fluid mass/4, m_d = total mass of the dry structure

Acceleration responses at the top of the dry structure subject to N-S component of 1940 El Centro earthquake records whose peak ground acceleration is scaled down to $0.2g$ are given in Fig. 2. It is easily observed that base isolation system is very effective in reducing acceleration responses. Responses of the pool structure containing fluid excited by the same earthquake input are analyzed. Calculated acceleration responses at the top of the structure are provided in Fig. 3. It is confirmed that isolation system is more effective in the reduction of the seismic responses for the pool structure than for the dry one.

Comparisons of the base displacements in the dry structure with those in the wet one are made in Fig. 4. The maximum base displacement of the wet structure is larger than the dry structure as expected. This may be primarily because of the added fluid mass and increased base shear due to the dynamic fluid-structure interaction effects.

As explained in the introduction section, one of the major concern is determining mechanical properties of the base isolator to show good performance under uncertain earthquake load. Using the objective function defined previously, optimization of the isolator is attempted for the pool structure model. Shown in Fig. 5 is objective function defined by Eq. (17) with $\alpha = \beta = 1$ and $\zeta_b = 0.15$. The independent variable, ω_b, for the calculation is defined in Table 1. The earthquake load is prescribed by site-independent design response

spectrum given in Reg. Guide 1.60[5] with $PGA = 0.2g$. It is observed for the given damping ratio, the optimal ω_s is found to be around $(2\pi)(1.03)$.

7. CONCLUDING REMARKS

A simple modal analysis method of a coupled fluid-structure-isolator system is presented. The final equation has only 2 degrees of freedom. Seismic analysis results for a pool structure indicate that base isolation system is very efficient in reducing the transmitted earthquake load. Also presented is an objective function based on the strain energy consideration. The good behavior of the derived function suggests that it may be utilized in the actual design process. But still further works need be done to include 3-dimensional effects to the dynamic response analysis of the pool structure.

Since free surface sloshing may be another important design concern especially for the spent fuel storage pool structures, the effect may have to be included both in the objective function, possibly in a form of kinetic energy, and in the fluid-structure interaction modeling.

8. REFERENCES

[1] Rammerstorfer, F.G., Sharf, K. and Fisher, F.D., 1990, "Storage Tanks under Earthquake Loading," *Applied Mechanics Reviews*, Vol. 43 : 261-281.

[2] Electric Power Research Institute(EPRI), 1979, *A Review of Seismic Isolation for Nuclear Structures*, EPRI NP-1220-SR.

[3] Haroun, M.A. and Housner, G.W., 1981, "Earthquake Response of Deformable Liquid Storage Tanks," *Journal of Applied Mechanics*, Vol. 48 : 411-417.

[4] Choi, I.K., 1992, *Response Analysis of Structures Using LRB Type Base Isolator Subjected to Earthquake Loading*, M.S. Thesis, Chungnam National University.

[5] U.S. NRC, 1973, *Design Response Spectrum for Nuclear Power Plants*, Regulatory Guide 1.60.

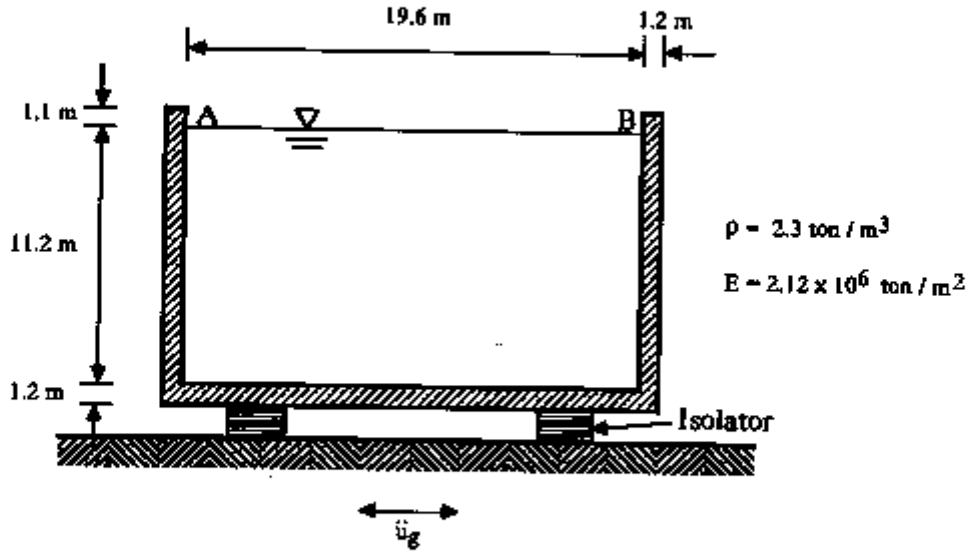

Fig. 1 Spent Fuel Storage Pool Model and Isolators

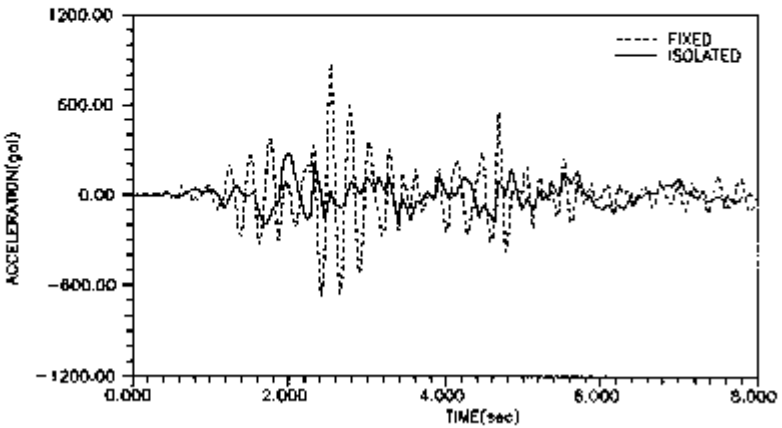

Fig. 2 Performance comparison of dry structure model (Top Acceleration)

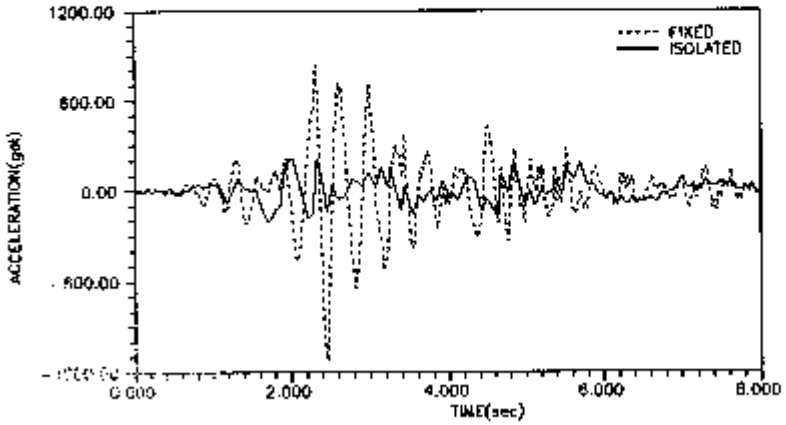

Fig. 3 Performance comparison of the pool structure (Top Acceleration)

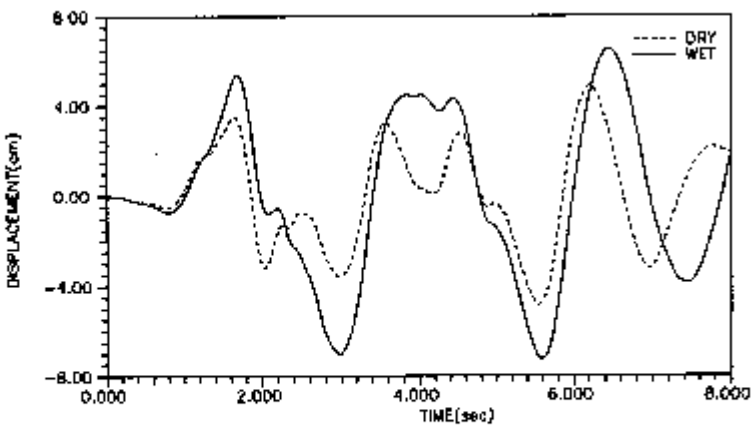

Fig. 4 Comparison of base displacements between dry and wet structure

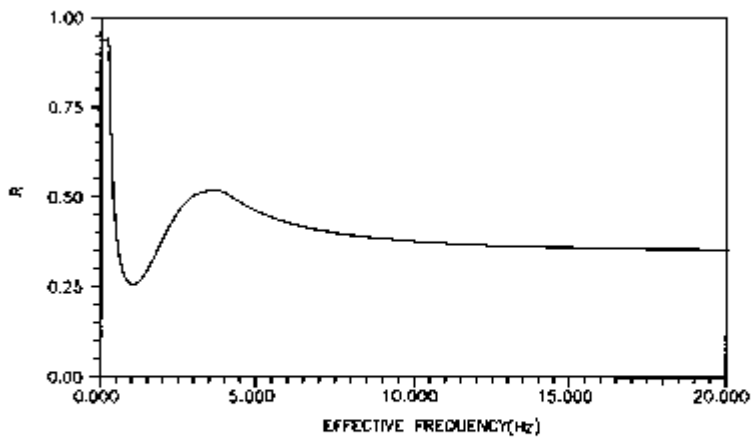

Fig. 5 Objective function under the earthquake load defined by Reg. Guide 1.60 site-independent design spectrum(PGA=0.2g)

SMiRT-12 / K. Kussmaul (Editor)

K19/6

EXPERIMENTAL AND ANALYTICAL STUDY ON CROSSOVER PIPING SYSTEM IN SEISMIC ISOLATION FBR PLANT: (I) MAIN STEAM PIPING

Y. Watanabe[1], M. Kuroha[1], K. Amada[1], A. Nishikawa[2], T. Iijima[3] and H. Shimizu[3]

[1]The Japan Atomic Power Company, Tokyo, Japan
[2]Ishikawajima-Harima Heavy Industries Co. Ltd., Yokohama, Japan
[3]Toshiba Corporation, Yokohama, Japan

1. INTRODUCTION

In the design of crossover pipings between a seismic isolated and a non-isolated buildings of FBR plant, large relative displacement caused by design basis earthquake are imposed on the pipings. A main steam piping, which sustains a high steam pressure in the elevated temperature range, is required to be designed as the crossover piping in the seismic isolated FBR plant that we considered. The design method for the main steam crossover piping was investigated in this study. As a result of the study, it is found that a main steam crossover piping with some reduced stiffness seismic supports and viscous type dampers would be preferable to accomodate large relative displacement in the seismic events.

To confirm the applicability of the conventional design analysis method and the stress evaluation method to the crossover piping, the seismic tests on the main steam piping system was conducted. A 1/2 scale main steam piping model was used in the experiment. The seismic isolated building model was simulated by steel block supported by rubber bearings and installed on a shaking table.

The test results were compared with both predictions by the time historical analysis method and by the modal analysis method. Response spectrum defined on the shaking table and on the seismic isolated building model were used for the modal analysis. The stress evaluation method for the crossover piping was discussed focusing on the stress classifications and allowable limits. Design margines of the design analysis methods for crossover piping was evaluated by comparing with stress measured in the piping.

2. DESIGN OF THE MAIN STEAM LINE CROSSOVER PIPING SYSTEM

The piping layout of main steam line of the seismic isolated FBR plant is shown in Fig.1[1]. The design temperature and design pressure of the piping are approximately 500℃ and 190 atg respectively. Maximum relative displacement (± 390 mm) between the seismic isolated building and non-isolated building appear in the extreme design basis earthquake (S_2). In order to establish the structural integrity of the crossover piping, following considerations on the material and the seismic supports are added to conventional piping design.

Piping material : High strength at elevated temperature range is required. In this study, Mod.9Cr-1Mo steel is applied.

Seismic supports: Coil springs are used to avoid resonance with the seismic isolated building, and velocity proportional type oil dampers are required to reduce seismec responce of the piping system.

A 1/2 scale seismic test model was designed considering the shaking table size. A similarity law was applied to the model piping to simulate the stress appeared in the actual crossover piping under seismic events. The schematic figure of the seismic test piping is shown in Fig.2. The seismic isolated building modelled with an 20 tons of inertial mass structure, supported by four rubber bearings, was connected to the test piping rigidly by weld. The vibrational characteristics of the building model was adjusted by stiffness of the rubber bearings and dampers attached to the seismic isolated building model.

3. EXPERIMENTS

Experiments on following three items were condcted in the facility of the National Research Institute for Earth Science and Disaster Prevention in Tsukuba.

3.1 STATIC LOAD TEST

Static load was applied to the test piping model by the oil actuator and the displacements and strains of the piping were measured. The measured data was put into comparison with analytical results.

3.2 SINUSOIDAL SWEEP EXCITATION TEST

Frequency response functions were measured at various location of the piping system by sinusoidal sweep excitation. Resonance frequencies, mode shapes and damping ratios of each modes were evaluated from the results. The measured data were put into comparison with analytical results.

3.3 SEISMIC EXCITATION TEST

The piping system was excitated at the maximum design basis earthquake (S_1) and the extreme design basis earthquake (S_2) level, and displacements, accelerations and strains of the various locations of the piping system were measured. The data measured in the test were put into comparison with analytical results. Maximum acceleration of the shaking table and maximum relative displacement between the shaking table and the seismic isolated building model are shown in Table 1.

4. NUMERICAL ANALYSES

Static analysis on relative displacement, complex eigen value analysis and time historical response analysis (direct integral method) were conducted using FEM beam elements model and compared with measurements. The FEM analytical model is shown in Fig 3. Stiffness of the coil springs and damping coefficient of the oil dampers evaluated by element tests were applied to the analytical model. The stiffness and damping coefficient of the seismic isolated building model were also evaluated by the building model element test and applied to the analytical model. Since these components showed linear deformation characteristics, linear analysis methods was applied to the piping analyses.

Two conventional seismic analysis methods, the enveloped response spectrum analysis and the milti-response spectra analysis were conducted. Here, the equivalent damping ratio in these response spectra was determined by weightening the modal damping ratios and the participation factors. The stresses obtained by two response spectrum analyses methods were combined with the stresses in the piping by the relative displacement to evaluate total stresses in the piping during seismic excitations.

5. RESULTS OF THE EXPERIMENT AND THE NUMERICAL ANALYSES

5.1 STRESS BEHAVIOR IN THE PIPING UNDER STATIC LOAD

Comparison between mesurements and analysis results of the displacements and stresses in the piping system caused by relative displacement are shown in Table 2. Stresses of the experiment were evaluated from axial and circumferential strains of fhe piping using the formula of plane stress fields. Agreements between measurements and analized values were excellent. Therefore, it was concluded that the piping behavior under relative displacements can be sufficiently predicted by the linear static analysis.

5.2 VIBRATIONAL CHARACTERISTICS

Comparison between measurements and numerically analized values of the resonance frequencies and damping ratios are shown in Table 3. Here, the first mode is dominant frequency of the seismic isolated building model. Responses in the second, therd and sixth mode were too low to measure during the experiments. It is due to their large damping ratios and small participation factors. Other resonance frequencies and damping ratios agreed with analysis results. Therefore, it is also concluded that vibrational characteristics of the piping system can be sufficiently predicted by the complex eigenvalue analysis.

5.3 SEISMIC RESPONSE CHARACTERISTICS

Comparison between measurements and numerically analized time histories of the piping system at S_2 level excitation are shown in Fig.4. Sufficient agreement between measurements and analized time histories of displacements, accelerations and stresses were observed during excitation. Disagreement between measured and analized maximum responses of piping displacements, accelerations and stresses are less than 10%.

The stresses by seismic excitation were devided into stresses caused by relative displacement and stresses caused by inertial force. Each stresses in the time history form are shown in Fig.5. From this figure, it is founded that apporoximately 70～90% of the piping stresses are caused by relative displacement between the seismic isolated building model and the shaking table.

In the conventional design method of the piping system, the stresses by inertial force and the stresses by relative desplacement were analized by response spectrum analysis and static analysis respectively. The applicability of this conventional design method to the crossover piping was considered. Response spectrum defined on the shaking table and on the seismic isolated building model are shown in Fig.6. The damping ratio of each spectrum is assumed to be 4.3%, which is the equivalent damping ratio of the piping system evaluated by the complex eigenvalue analysis. Two response spectrum analysis methods were considered to evaluate stresses caused by inertial force. One was the stress evaluation by using a enveloped response spectrum, other is by using multi-response spectra. The stress evaluation results by both methods are shown in Table 4. From theses results, the stresses obtained from the enveloped response spectrum analysis are approximately 1.7 times of the stresses measured, whereas the stresses by the multi-response spectra analysis are 1.4 times of the measurements. Therefore, it is concluded that even for in the crossover piping design, the conventional design method based on response spectrum analysis and static analysis on ralative displacement gave conservative stress evaluation.

6. CONCLUSIONS

The seismic tests on the main steam crossover piping system of the seismic isolated FBR plant was conducted, and the following results were obtaind;
[1]The seismic response of the crossover piping under seismic events can be

precisely predicted by linear type time historical response analysis.
[2]Under seismic events, the stresses caused by relative displacement are dominant in the crossover piping.
[3]The stresses of the crossover piping system can be conservatively evaluated by combining response spectrum analysis results and static analysis results on relative displacement.

7. ACKNOWLEDGEMENT

Activities in this study has been performed as a part of joint research and development projects for DFBR under sponsorship of nine Japanese electric companies, Electric Power Development Co., Ltd. and the Japan Atomic Power Company.

REFERENCES

[1]Watanabe, Y et al. (1992). Design Study of Piping System to Accomodate Large Displacement of Sismic Isolation FBR Plant. Proc. 1992 Fall Meeting of the Atomic Energy Society of Japan, 575.

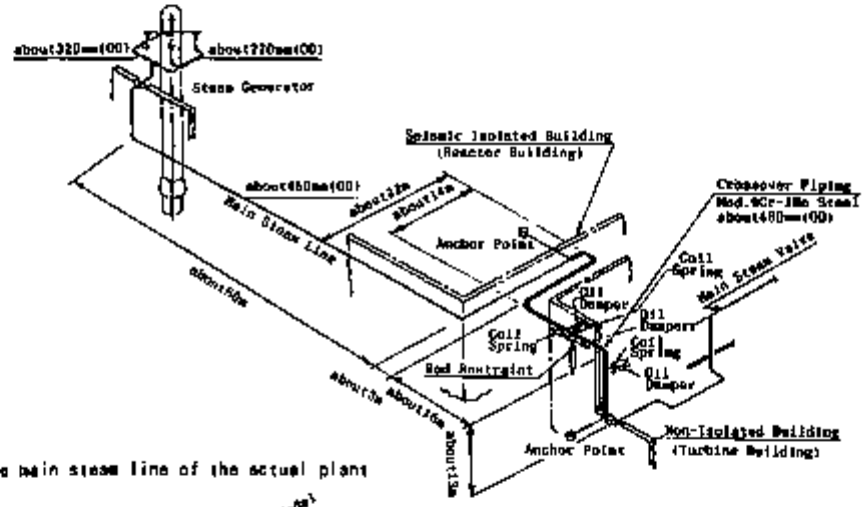

Fig.1 Layout of the main steam line of the actual plant

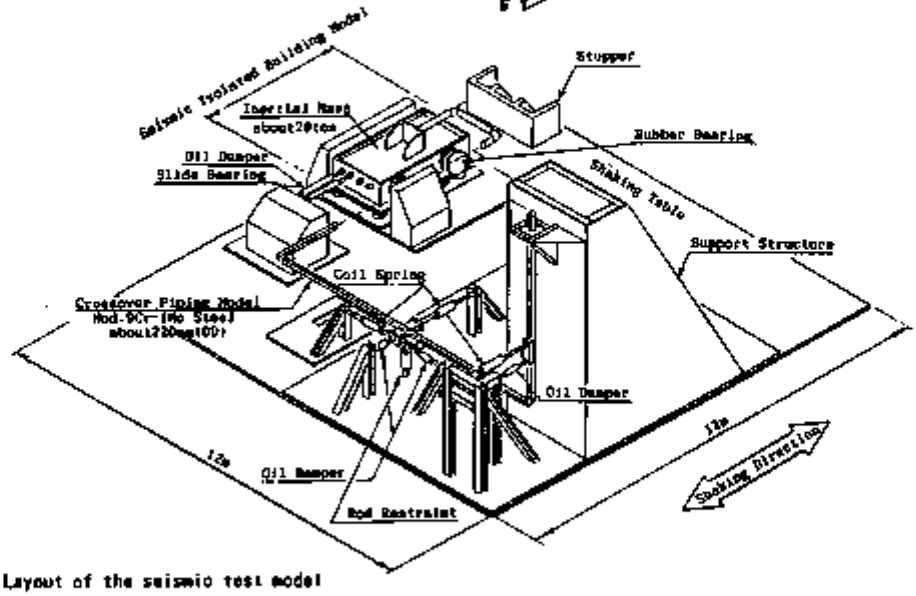

Fig.2 Layout of the seismic test model

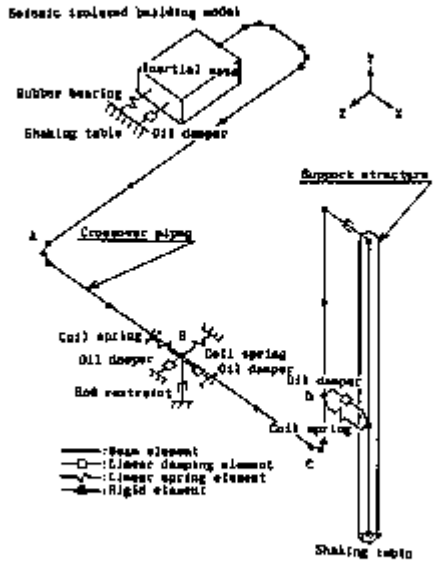

Fig. 3 Analytical model

Table 1 Maximum inputs of the seismic excitation test

Seismic level	Maximum acceleration of the shaking table (G)	Maximum relative displacement between the shaking table and the isolated building model(mm)
S1	1.1	65
S2	1.7	195

Table 2 Behavior of the piping system under relative displacement

Displacement of the isolated building model (mm)	Piping displacement(mm) A Exp.	A Ana.	B Exp.	B Ana.	Piping stress(Kgf/mm²) A Exp.	A Ana.	B Exp.	B Ana.
+285	+272	+276	+128	+123	24.2	26.0	9.5	10.1
-284	-272	-276	-125	-122	25.6	25.9	9.8	10.2

Table 3 Resonance frequencies and damping ratios of the piping system

Mode number	Resonance frequency(Hz) Experiment	Analysis	Damping ratio(%) Experiment	Analysis	Participation factor(--)
1	1.3	1.3	4.4	5.0	2.17
2	---*	4.0	---*	13.5	0.04
3	---*	5.3	---*	19.7	0.07
4	7.1	6.4	0.6	0.1	0.41
5	11.3	11.2	1.7	3.5	0.02
6	---*	12.6	---*	7.6	0.05
7	13.4	13.3	1.0	0.8	0.04
8	15.2	14.0	0.6	0.1	0.62
9	15.8	18.4	4.2	4.1	0.98
10	18.1	20.3	1.2	1.5	0.03

*:These modes were not measured because the damping ratios are large and the participation factors are small.

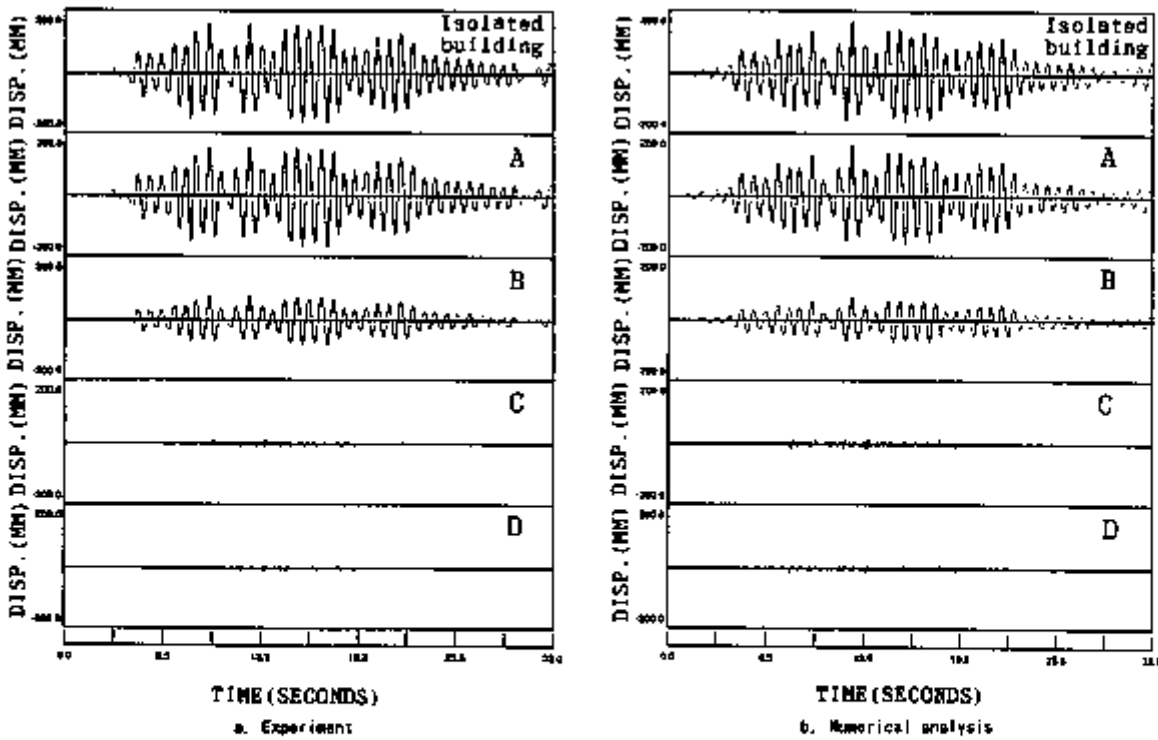

Fig. 4 Time historical seismic response of the piping system (S2 level)

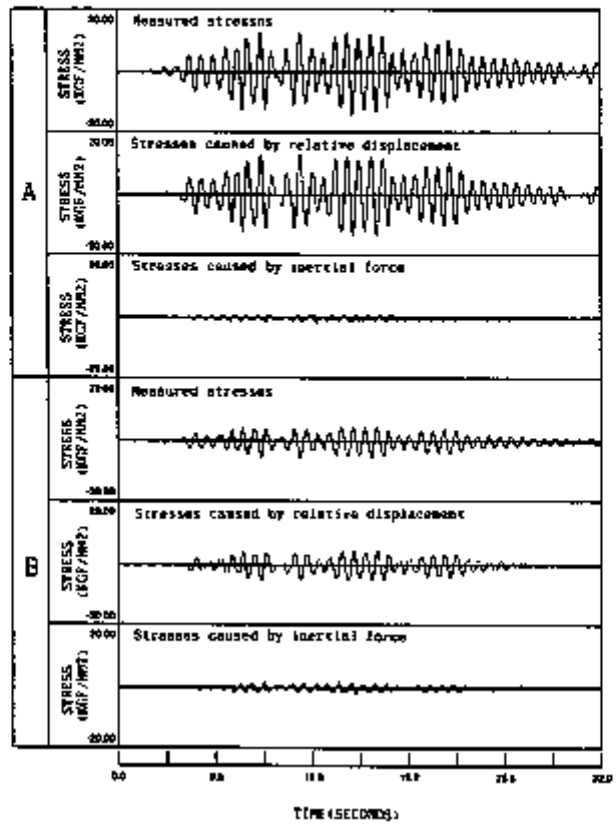

Fig. 5 Devided stress time histories of the piping system

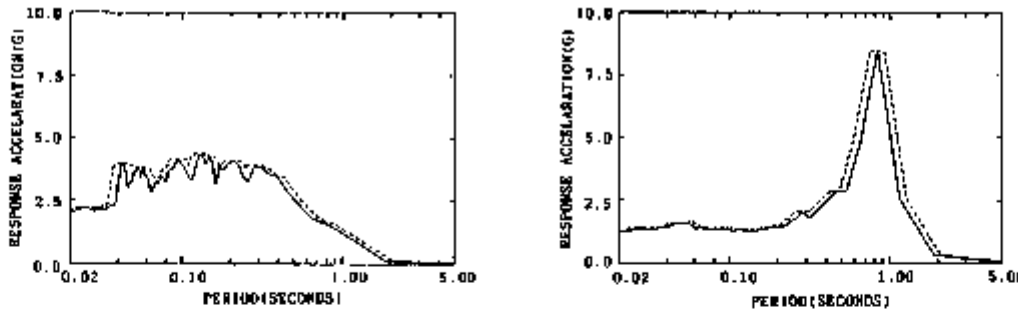

a. Shaking table

b. Seismic isolated building model

Fig. 6 Response spectrum

Table 4 Stress range evaluation results of conventional design analysis (S2 level)

Location	Experiment	Time historical analysis	Multi-response spectrum analysis + Statically relative displacement analysis	Enveloped response spectrum analysis + Statically Relative displacement analysis
A	31.8	35.2 [1.1]*	42.2 [1.3]*	48.0 [1.5]*
B	14.5	14.4 [1.0]*	20.2 [1.4]*	25.2 [1.7]*

*: The number in [ ] show the ratio of the analytical value to the experimental value. The unit of stresses is Kgf/mm².

SMiRT-12 / K. Kussmaul (Editor)

K21/2

MULTI DIRECTIONAL EARTHQUAKE INPUT TEST AND SIMULATION ANALYSIS OF BASE ISOLATED STRUCTURE

M. Kato[1], Y. Watanabe[1], A. Kato[1], T. Hirotani[2], J. Suhara[2] and T. Tamura[2]

[1]The Japan Atomic Power Co., Tokyo, Japan
[2]Shimizu Corporation, Tokyo, Japan

1. INTRODUCTION

In applying base-isolation system to nuclear facilities such as the fast breeder reactor (abbreviated as FBR), it is very important to evaluate the seismic safety margin of the base isolation layer.

From this point of view, dynamic breaking tests on base isolation layer consisting of a group of scaled laminated rubber bearings are conducted on shaking tables.

In the series of the tests, horizontal one-way, horizontal two-way and horizontal-and-vertical simultaneous earthquake input tests are carried out.

The present paper shows the results of horizontal two-way and horizontal-and-vertical earthquake input tests and simulation analysis of horizontal two-way earthquake input tests.

2. HORIZONTAL TWO-WAY EARTHQUAKE INPUT TEST

In horizontal two-way earthquake input tests, NS and EW waves are inputted for X and Y direction respectively. The waves are artificial seismic waves that have the same degrees of power and spectral characteristics. Both waves are made using the phases of horizontal two-way component of actual seismic waves. The input level of NS wave is raised up to three levels as follows. (Same as in the one-way input tests described in Reference 1.)

- Design level : 100 Gal input : laminated rubber bearing stay in linear condition
- Hardening level : 350 Gal input : non-linear behavior
- Target breaking level : 700 Gal input : ultimate state

The acceleration ratio between both waves is kept constant during the test.

The specimen consists of four laminated rubber bearings, two rows of two each, and the super-structure made of reinforced concrete rigid body. Figure 1 shows the outline of specimen.

In excitation at the design level, the two-way responses coincided roughly with the results of superposing on the time-history responses under the individual excitation.

In excitations at above hardening level, the two-way responses showed a trend differing from the one-way input responses due to the effects of orthogonal direction input.

However, it was found that the two-way responses are roughly the same as the one-way responses based on the following results, when the test results were arranged taking the primary axis in the maximum deformation direction that varied with time, as shown in Fig. 2.

First, the shear strain at breaking is shown in Fig. 3 in terms of relationship with the axial force ratio obtained by the horizontal one-way and two-way input tests. In the two-way input tests, the shear strain is evaluated by primary-axis direction deformation D. The two-way test results are equal to those from the one-way tests.

Next, the horizontal-direction hystereses in the X and Y directions at the hardening level obtained in the horizontal two-way input tests are shown in Fig. 4. Disturbance of the hysteresis properties is seen due to the effects of orthogonal direction input. However, these hystereses are converted into more simple style as shown in Fig. 5(1) when organized with primary-axis

direction deformation D, primary-axis direction force F_{PR} and orthogonal-axis direction force F_{TR}. According to the figure, the orthogonal-direction force F_{TR} is sufficiently small compared with the primary-axis direction force F_{PR}. It can be seen that the restoring force characteristics in horizontal two directions may be represented by the primary-axis direction only. Similarly, the result of excitation at the target breaking level is shown in Fig. 5(2). The horizontal-direction hysteresis of the one-way input test in terms of the absolute value is shown in Fig. 6. From a comparison of Figs. 5 and 6, it can be seen that the horizontal two-way restoring force characteristics converted into the primary-axis direction indicate almost the same trend as for the one-way restoring force characteristics including hardening and slipping phenomena.

3. HORIZONTAL-AND-VERTICAL EARTHQUAKE INPUT TEST

The input waves used in horizontal-and-vertical earthquake input test was the NS wave and UD wave. The UD wave is artificial seismic wave made using the phase of the vertical component of the actual wave that is utilized in making the corresponding NS wave.

In Fig. 7, the relationship between shear strain and axial force ratio of the laminated rubber bearings in excitation at the design level is shown in the form of comparison of the result of horizontal-and-vertical simultaneous input test and the superposed result on the respective one-way input test in time histories. It can be seen from this figure that superposition of horizontal and vertical responses, each one-way, at the design level is effective.

In excitation at the target breaking level, UD wave was inputted at almost 1,200 Gal (excitation limit of the shaking table) corresponding to approximately double the extreme design earthquake, but the test result was that there was not much difference from that of horizontal one-way input. Fig. 8 shows the comparison of the horizontal-direction hystereses between horizontal one-way input tests and horizontal-and-vertical input tests. The hysteresis configurations hardly differ and the displacements at which breaking occurred were equal.

4. SIMULATION ANALYSIS OF HORIZONTAL TWO-WAY INPUT TESTS

4.1 Analytical model

To examine analytical techniques for evaluating the ultimate behaviors of base isolation layer, simulation analyses of horizontal two-way earthquake input tests were performed.

The technique of horizontal two-way input response analysis with the nonlinear range has been actively studied in recent years, and Multi-Shear-Spring (MSS) models and fiber models have been proposed. However, there are few horizontal two-way response analysis models that have been proposed for a system of complex stress condition with large influence of repetitions such as hardening phenomena of laminated rubber bearings.

As described in the results of horizontal two-way input tests, findings from tests were that

- Two-way restoring force characteristics can be organized roughly with only the primary-axis directions of deformations at each moment.
- Restoring force characteristics arranged according to primary-axis directions of deformation correspond well with restoring force characteristics at time of one-way input including hardening and slipping phenomena.

Here, the model modifying the MSS model as the restoring force model reflecting these findings will be developed and examined.

In attempting to apply the conventional type of MSS model to the present test results, we found it difficult to reflect the slipping phenomena of restoring force characteristics. This is because each spring independently behaves in a conventional-type MSS model.

Therefore, a restoring force model in which the restoring force characteristics of the individual springs comprising the spring group act interlocked was developed modifying the conventional-type MSS model.

The basic rules are as follows:

- The individual springs comprising the spring group possess common information such as concerning the kink points of the restoring force characteristics at all times.
- With regard to slipping of the restoring force characteristics, the rule for one-way spring is expanded and it is defined that when one spring slips the other springs will also slip as shown in Fig. 9.

The modified MSS model is referred to as "isotropic-hardening-linked MSS" (abbreviated as "IHL-MSS").
The response analysis model, as shown in Fig. 10, is a one-mass-spring model having freedom in horizontal two directions. The base isolation layer is assumed to follow an IHL-MSS model expressed by a group of eight shear springs. The restoring force characteristic of each shear spring shown in Fig. 11 is similar to that of the one-way spring developed in discussion of one-way input tests (Ref. 1). It is set up that the restoring force characteristics as a whole of MSS coincides with the one-way spring as shown in Fig. 12, at the initial rigidity and the skeleton of the restoring force characteristics at infinitely large displacement.

4.2 Analytical results

The analytical results by the IHL-MSS model are shown compared with test results.
The orbit of two-way response displacement in hardening-level excitation is shown in Fig. 13. According to this figure, the response maximum values and response properties in the X and Y directions are reproduced well.
The shear hysteresis in the X direction in hardening level excitation is shown in Fig. 14. As stated in test results, the shear hysteresis of test results is considerably disturbed by the orthogonal input, but this is also reproduced well by the IHL-MSS model.
The orbit of two-way response displacements at target breaking level is shown in Fig. 15. As stated in horizontal two-way test results, breaking of the laminated rubber bearing occurs at primary-axis direction deformation of approximately 5.6 cm (700% for shear strain γ). It can be seen in this figure that the displacement response orbit until $\gamma = 700\%$ is reproduced well in the analytical results.

5. CONCLUSIVE REMARKS

The following results were obtained from the horizontal two-way input tests and horizontal-and-vertical input tests conducted with the purpose of examining the response characteristics of the base isolation layer under multi-directional inputs.

- With regard to input of design level, the response under two-way input can be evaluated by superposition on the time histories of the responses under the respective individual inputs.
- In case of horizontal two-way input, shear strain at breaking evaluated by the primary-axis direction of deformation is equal to that of one-way input.
  Further, the horizontal-direction restoring force characteristics of the primary-axis direction indicate the same trend as that of one-way input.
- In case of horizontal-and-vertical simultaneous input, the horizontal-direction restoring force characteristics and shear strain at breaking are affected very little by vertical motion with the low center-of-gravity building of this case and input of around 1.2 G.

For the simulation analysis of horizontal two-way earthquake input tests, an isotropic-hardening-linked MSS (IHL-MSS) model in which the restoring forces of the individual springs act interlocked was developed modifying the conventional type MSS model.
With this horizontal two-way restoring force characteristics' model, conformity with one-way response was amply taken into consideration, and further, the test results were reproduced well.
Therefore we believe that proposed IHL-MSS model is the powerful tool for the simulation of horizontal two-way ultimate state response such as the base-isolation system.

ACKNOWLEDGEMENT

This study was carried out as a part of the common research study by the electric power companies in Japan, entitled "Technical Study on Feasibility of Isolated FBR Plant.(Part 1)"

REFERENCES

1) Kato, M. Watanabe, Y. & Kato, A. 1992. "Study on failure mode of seismic isolated reactor building". Proc. 10th WCEE : Vol.9, pp4933-4938
2) Kato, M. Watanabe, Y. & Kato, A. 1991. "Study on the seismic base-isolated reactor building for demonstration FBR plant in Japan". Proc. 11th SMiRT : Vol.K2, pp97-102

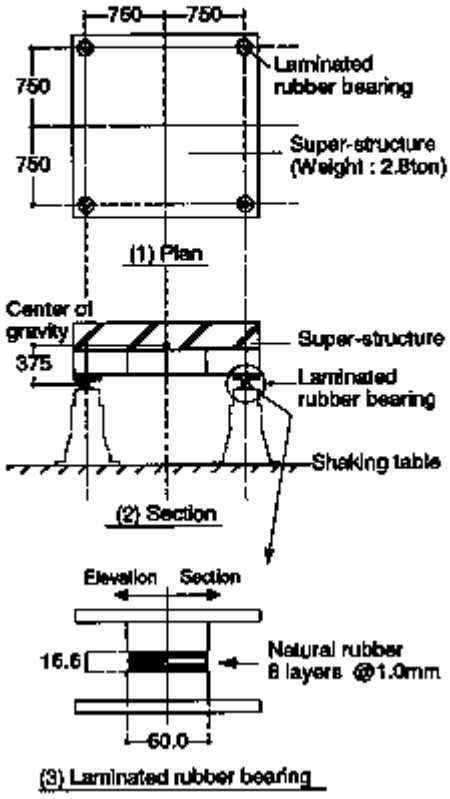

Fig.1 Outline of specimen

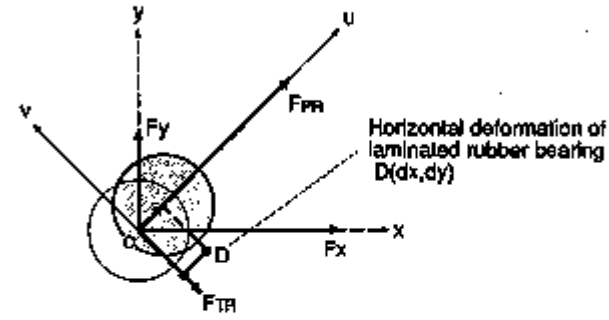

Fig. 2 Transformation of horizontal two-way stress & deformation

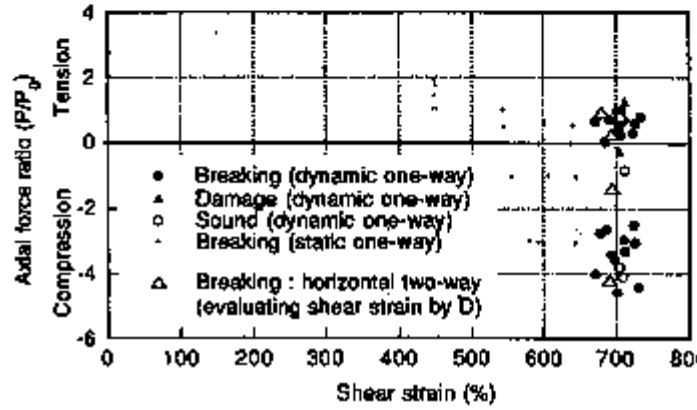

Fig. 3 Comparison of horizontal two-way and one-way test result (Relationship of shear strain and axial force ratio at breaking)

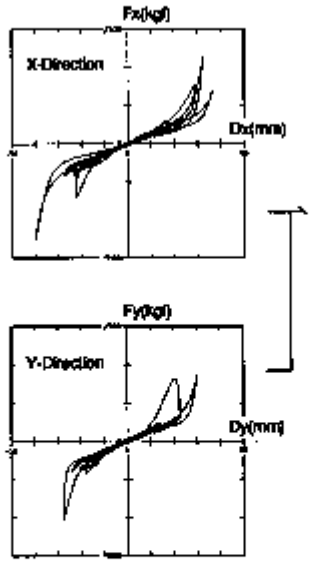

Fig.4 Horizontal hysteresis in X and Y directions under horizontal two-way test (Hardening level excitation)

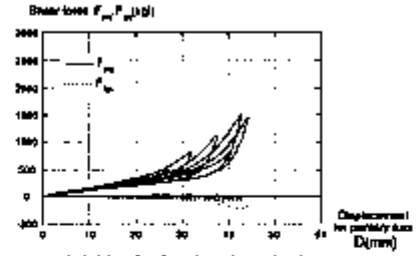

(1) Hardening level excitation

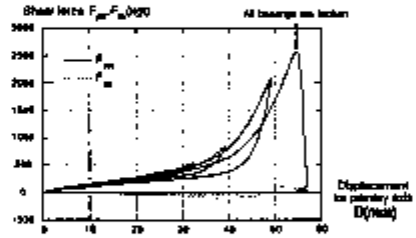

(2) Target breaking level excitation

Fig.5 Hysteresis for primary-axis direction and orthogonal direction under horizontal two-way test
(Primary-axis direction deformation : D
Primary-axis direction force : FPR
Orthogonal direction force : FTR)

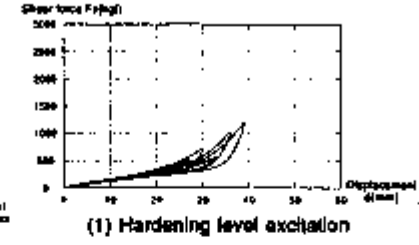

(1) Hardening level excitation

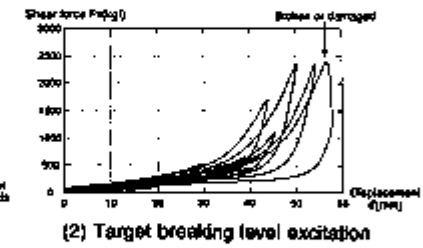

(2) Target breaking level excitation

Fig.6 Horizontal hysteresis under one-way excitation (Arranged based on absolute value)

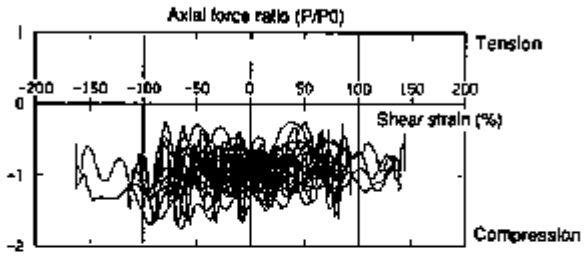

(1) Horizontal-and-vertical simultaneous excitation

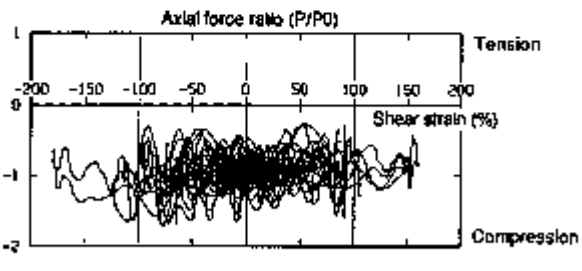

(2) Superposition on the respective one-way excitation

Fig. 7 Comparison of test results by horizontal-and-vertical simultaneous excitation and superposition on the respective one-way excitation. (Relationship between shear-strain and axial-force ratio in design level excitation)

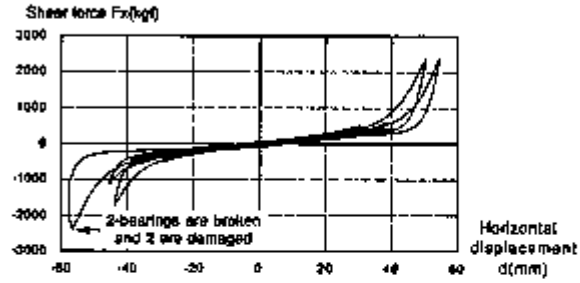

(1) Horizontal one-way excitation

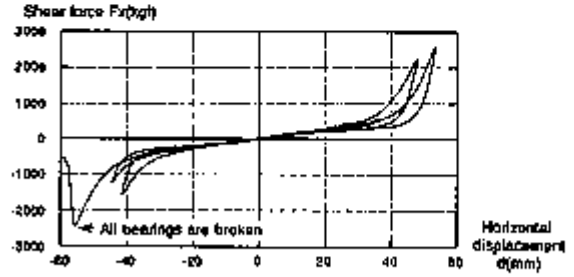

(2) Horizontal-and-vertical simultaneous excitation

Fig. 8 Comparison of test results by horizontal one-way excitation and horizontal-and-vertical simultaneous excitation. (Horizontal-direction hystereses in target breaking level excitation)

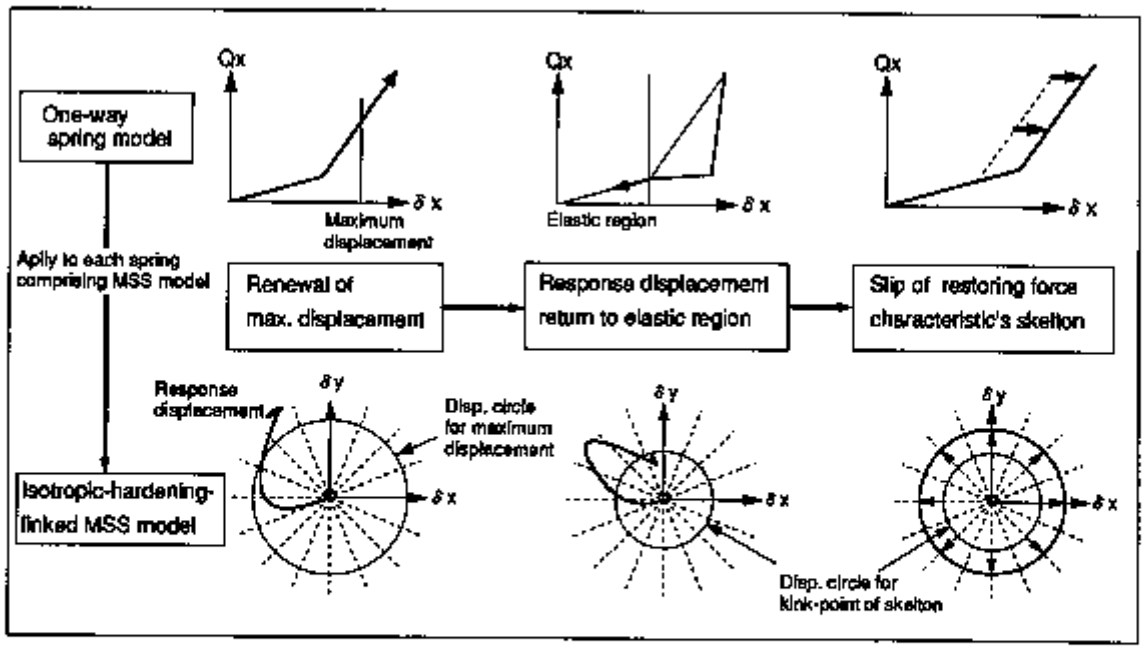

Fig. 9 Expansion of hysteresis rule for one-way spring into Isotropic-hardening-linked MSS model

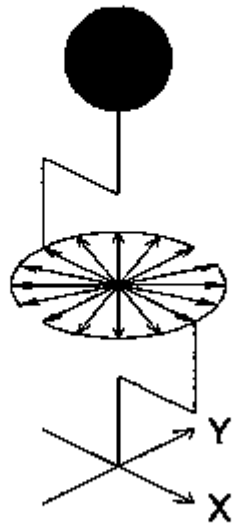

Fig.10 Analytical model by MSS model (Consist of 8 shear spring)

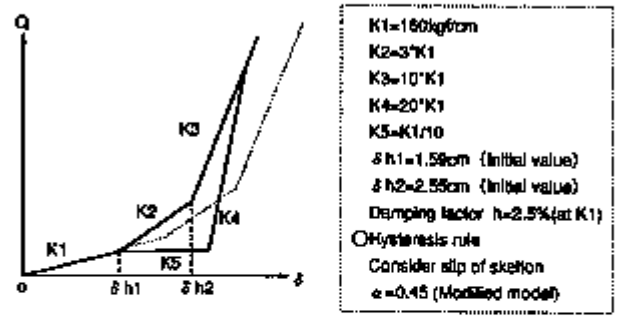

Fig. 11 Restoring force characteristics of each spring comprising MSS model

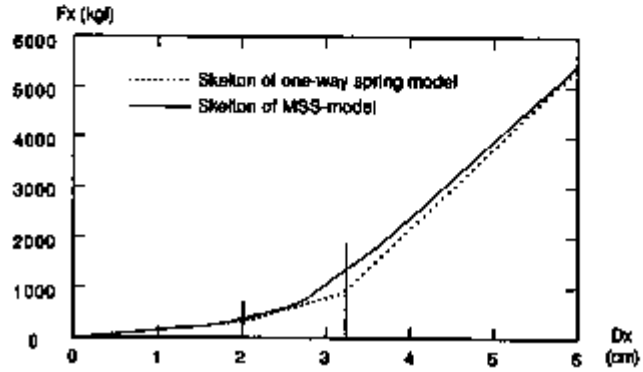

Fig. 12 Comparison of hysteresis skelton between MSS model and one-way shear spring

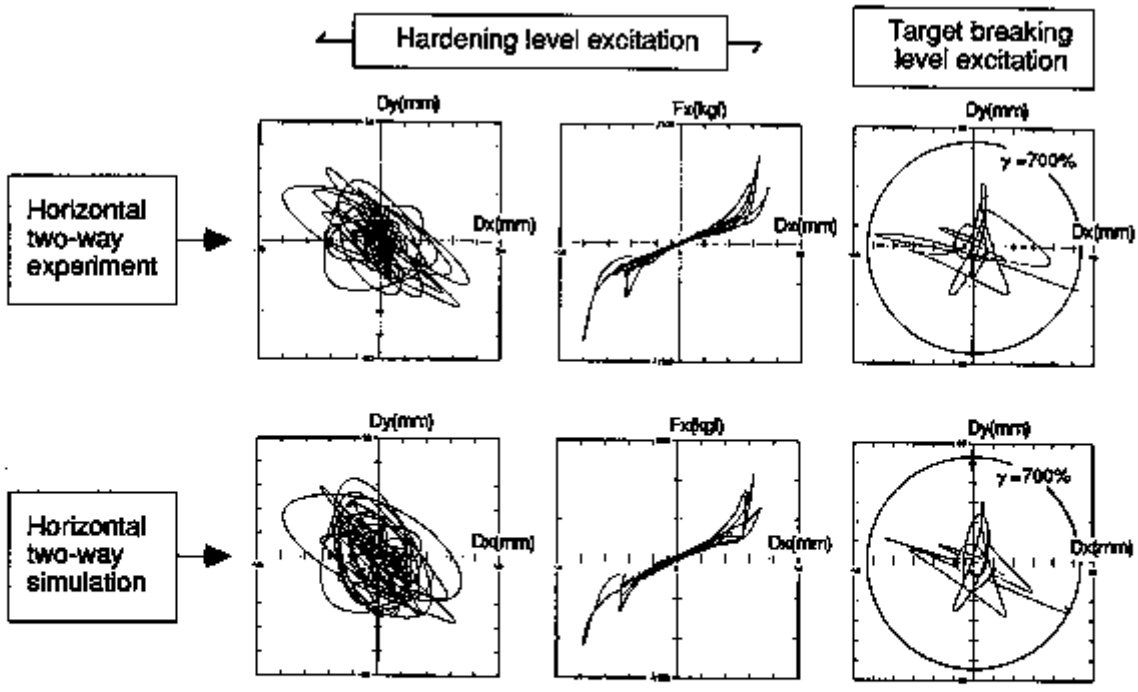

Fig.13 Orbit of two-way response displacement

Fig.14 Horizontal hysteresis (X-direction)

Fig.15 Orbit of two-way response displacement

SMiRT-12 / K. Kussmaul (Editor)

K23/5

STUDY ON ULTIMATE BEHAVIOR OF BASE ISOLATED REACTOR BUILDING

K. Munealdi[1], W. Yukio[1], K. Asao[1], H. Ikuo[2], K. Minoru[2] and W. Masamitsu[2]

[1]The Japan Atomic Power Company, Tokyo, Japan
[2]Taisei Corporation, Tokyo, Japan

1. INTRODUCTION

In a high-seismic country such as Japan, it is important for the practical use of a base isolated plant to comprehend the seismic safety margin. In this study, the ultimate behavior of a base isolated reactor building beyond the design level was investigated using dynamic non-linear analysis in which the design seismic motions with increased amplitude were used. And the effects of the different stiffnesses used in the model of laminated rubber bearing on the ultimate behavior of a base isolated reactor building were also verified.

2. ANALYSIS METHODOLOGY

2.1 Structure

The structure of interest was the base isolated FBR reactor building. The building was planned so as to have low center of gravity and wide basemat to overcome low tensile capacity of the laminated rubber bearing, or to reduce tensile force due to seismic overturning moment.[1] For the isolation devices, the laminated rubber bearings (160 cm in a diameter and 22.5 cm in total thickness of rubber sheet) with a 500 tonf load rating and the Steel Dampers which formed a part of the seismic energy absorption device were provided. Fig.1 gives a summary of this base isolated reactor building.

2.2 Input Seismic Motion

The input motion consisted of seismic waves (S2 level) which contained long period components, as known to have the most influence on the base isolated structures. Fig.2 shows the response spectrum and the acceleration time history of S2 seismic motion.

2.3 Analysis Model

The analysis model is presented in Fig.3. The superstructure was modeled by shear-flexural beams with lumped-masses, where nonlinearity of shear stiffness of RC members was taken into account. The isolation layer consisted of a single horizontal spring and 19 vertical springs. The soil foundation was assumed to be the hard rock with Vs=1500m/s and modeled by sway and rocking springs. The non-linear rocking spring was used taking account of the up-lift of the basemat.

2.4 Modeling the Isolation Devices

The horizontal spring in the isolated layer consisted of the non-linear characteristics

of the laminated rubber bearing and these of the Steel Damper. The horizontal restoring force characteristics of the laminated rubber bearing was modeled by the polygonal lines as shown in Fig.4. In addition, a slip phenomenon in which the value for the horizontal displacement ($\delta 1$) at the beginning stage of the hardening increased due to the influence exerted by cyclic loading was modeled by a repetition influence factor α .[2]

The restoring force characteristics of the Steel Damper was modeled by R-O model as shown in Fig.5.[3]

The vertical springs in the isolated layer, consisting of the laminated rubber bearing, have one non-linear characteristic. The restoring force characteristics of the laminated rubber bearing in the vertical directions were assumed to be asymmetrical (stiffness of the compression side was different from stiffness of tension side) and non-linear, as shown in Fig. 6.[2]

2.5 Cases for Analysis

Tables 1 and 2 show the cases for analysis.

Seismic response analyses were carried out by using the seismic motion amplified by 1.0 ~ 2.75 times the S2 seismic motion in order to determine the ultimate behavior of the base isolated reactor building.

Sensitivity analysis was performed to verify the effects of different stiffnesses used in the model of the laminated rubber bearing on the ultimate behavior of the base isolated reactor building. In sensitivity analysis, the seismic motion of 2.25 x S2 was input, and the values of stiffness in the hardening zone as shown in Fig.7 and the value of the repetition influence factor α were changed.

3. RESULTS

3.1 Seismic Response Analysis

Fig.8 shows the distribution of maximum response acceleration and the maximum response displacement under the influence of seismic motion with varying amplification. Fig.9 gives the relationship between the shear force and the horizontal displacement in the isolated layer (the laminated rubber bearings plus the Steel Dampers) when 2.75 x S2 seismic motion was input. As the amplification was increased, the effect of minimizing the response acceleration by the isolation devices diminished and the response acceleration of the steel structure on top of the reactor building increased. This is because the hysteresis curve of the laminated rubber bearing moves from the linear region into the hardening zone as the seismic motion increases, and the response of the building increases as the response in the short period increases.

Fig.10 shows the maximum response value in the shear force versus the horizontal displacement for the laminated rubber bearings. The hysteresis curves moved from the linear region into the hardening zone when 1.5 x S2 seismic motion was input, and the maximum horizontal displacement increased approximately in proportion to the amplification of input seismic motion. Above the level of 2.0 x S2, the displacement at the beginning stage of the hardening increased due to the effects of repetition, and the skeleton curve began to slip.

Fig.11 shows the maximum response value in the axial force versus the vertical displacement for the laminated rubber bearing. At the level of 1.5 x S2 a tensile force started to act on the laminated rubber bearings, and at the level of 2.75 x S2 the vertical displacement exceeded the turning point of the stiffness in the tension side.

Fig.12 shows the maximum response value in the axial strain versus the shear strain for the laminated rubber bearing. With input seismic motion greater than 2.0 x S2, where the skelton curve of the laminated rubber bearing moved into the hardening zone, the tensile axial strain increased and at the level of 2.75 x S2 the tensile axial strain exceeded the assumed breakage bound. However, since

the reactor building as studied herein had a low center of gravity, the tensile axial strain at the level of 2.75 x S2 was small and about 10%.

3.2 Sensitivity Analysis

Fig.13 shows the comparison of each case in the maximum response.

Even when the stiffness in the hardening zone was varied by ± 20%, the changes in the maximum response acceleration at the support level of the reactor vessel, in the maximum horizontal displacement of the laminated rubber bearing, and in the maximum shear strain of the lowest story of the reactor building were within ± 5%. The effects of different stiffnesses in the hardening zone on maximum response were also small.

If the repetition influence was disregarded (α = 0), the maximum response acceleration at the support level of the reactor vessel and maximum shear strain on the lowest story of the reactor building increased by about 18%, and the maximum horizontal displacement in the isolated layer decreased by about 8% This leads to the conclusion that the repetition influence factor can have some effect on the maximum response. However, when the repetition influence factor α was assumed 0.50, the change in maximum response from the basic case (α = 0.45) was small, being within ± 2%.

4. CONCLUSIONS

In this study, the ultimate behavior of a base isolated reactor building was investigated using dynamic non-linear analysis by using the seismic motion amplified by 1.0 ~ 2.75 times the S2 seismic motion. And the effects of the different stiffnesses used in the model of the laminated rubber bearing on the ultimate behavior of a base isolated reactor building were verified by the sensitivity analysis. The results obtained by these studies may be summarized as follows.

i) With increased amplification of the imput seismic motion, the histeresis curves moved into the hardening zone and the response of the reactor building increased. However, the laminated rubber bearings remained undamaged at the level of 2.75 x S2 seismic motion. Therefore, the base isolated reactor building as studied herein had the sufficient seismic safety margin.

ii) It was understood that the repetition influence factor had some effect on the ultimate behavior of a base isolated reactor building, but the difference in the response was a little less than ± 20%.

5. ACKNOWLEDGMENTS

This study was carried out as a part of the FBR common research of the electric power companies in Japan, having useful advices and suggestions by professors and specialists.

Reference

[1]Watanabe,Y.et al.(1990)"Study on Concept of Seismic Isolation Type Plant for FBR (Part 1 Basic Philosophy for Construction of Plant Image)",Summaries of Technical Papers of Annual Meeting AIJ,Vol B,pp.1437-1438

[2]Terazaki,H.et al.(1992)"Study on Concept of Seismic Isolation Type Plant for FBR (Part 16 Shaking Table Test of Base Isolation System of Ultimate State)",Summaries of Technical Papers of Annual Meeting AIJ,Vol B,pp.1579-1580

[3]Shirahama,K.et al.(1992)"Study on Concept of Seismic Isolation Type Plant for FBR (Part 20 Simulation Analysis of the Experiment on the Steel Damper)", Summaries of Technical Papers of Annual Meeting AIJ,Vol B,pp.1587-1588

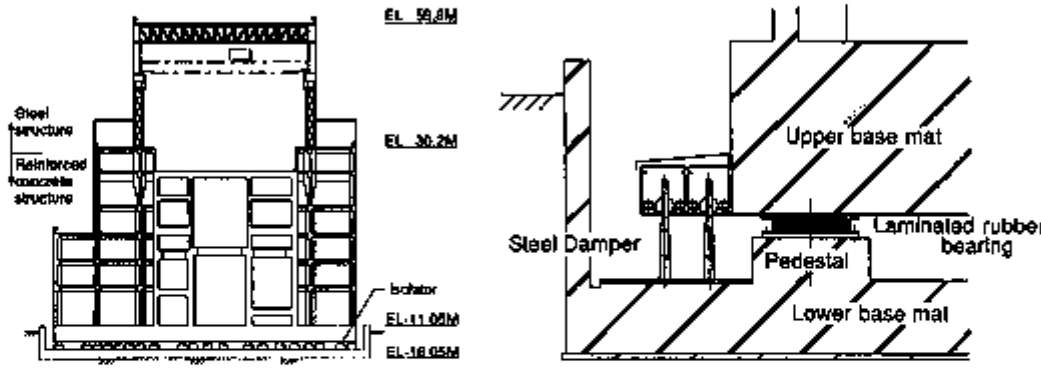

(a) Section (b) Isolation Devices

Fig.1 Summary of base isolated reactor building

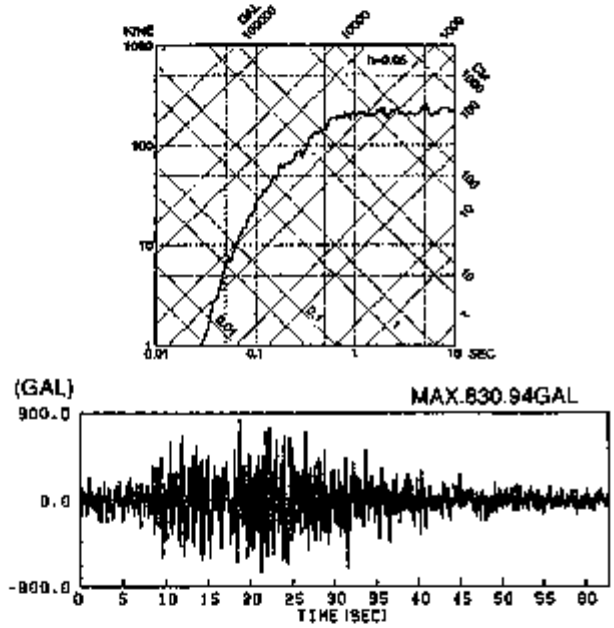

Fig.2 Input seismic motion (S2)

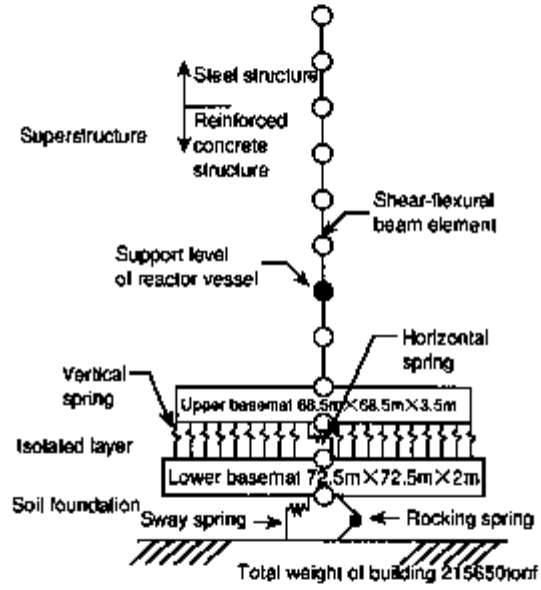

Fig.3 Analytical model

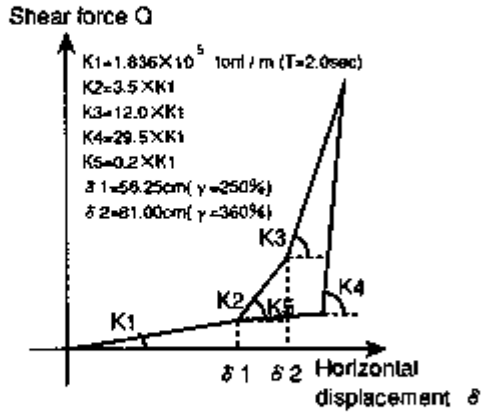

(a) Hysteresis curve

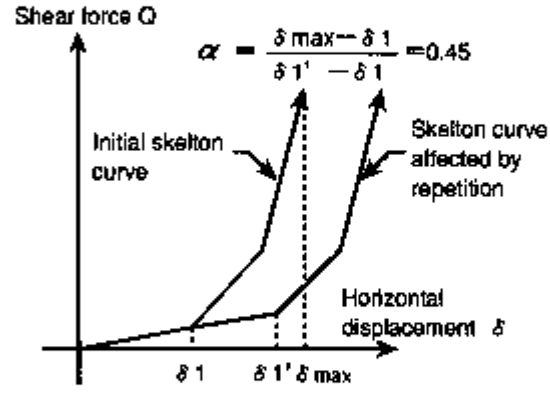

(b) Repetition influence factor α

Fig.4 Horizontal restoring force characteristics of laminated rubber bearing

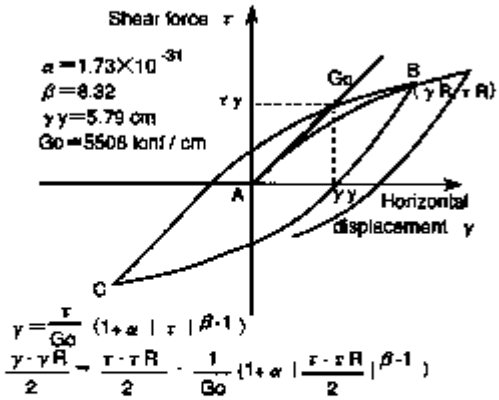

Fig.5 Restoring force characteristics of steel damper

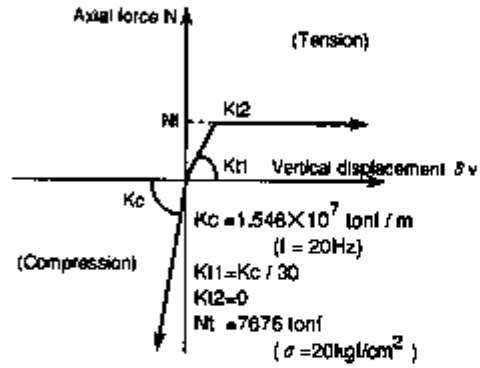

Fig.6 Vertical restoring force characteristics of laminated rubber bearing

Table 1 Cases for seimic response analysis at ultimate behavior

Case No.	Input seismic motion
1	1.0 × S2
2	1.5 × S2
3	1.75 × S2
4	2.0 × S2
5	2.25 × S2
6	2.5 × S2
7	2.75 × S2

Table 2 Cases for sensitivity analysis (Seismic motion of 2.25× S2 input)

Case No.	Stiffness in hardning zone	Repetition influence factor α
Basic case	K2 , K3	0.45
I − 1	1.2 K2 , 1.2 K3	0.45
I − 2	0.8 K2 , 0.8K3	0.45
II − 1	K2	0.0
II − 2	K2	0.50

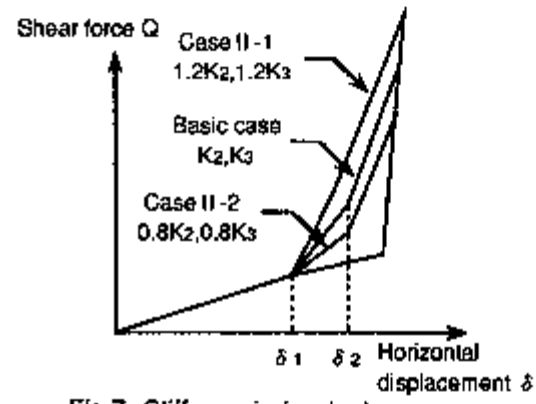

Fig.7 Stiffness in hardening zone for sensitivity analysis

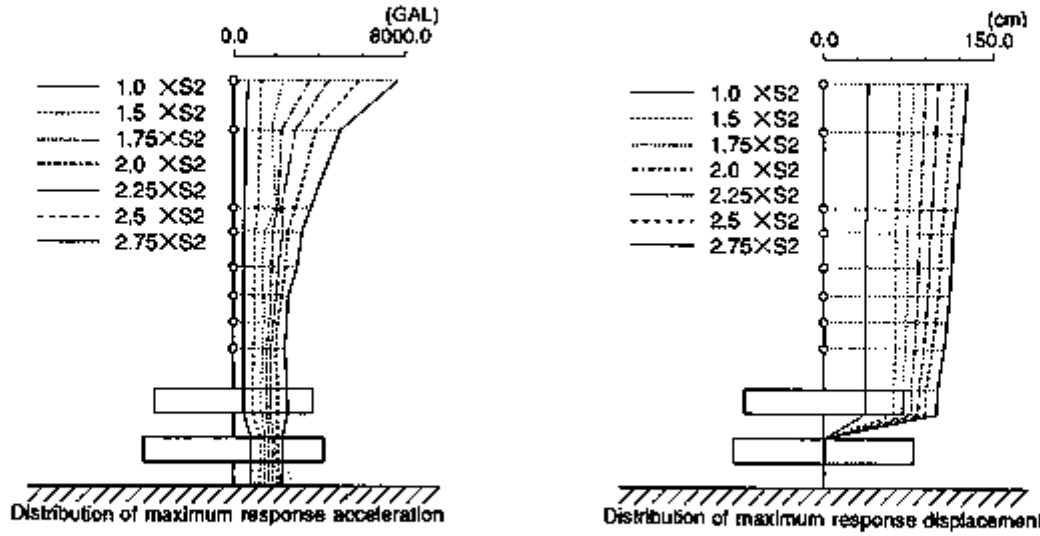

Fig.8 Maximum response

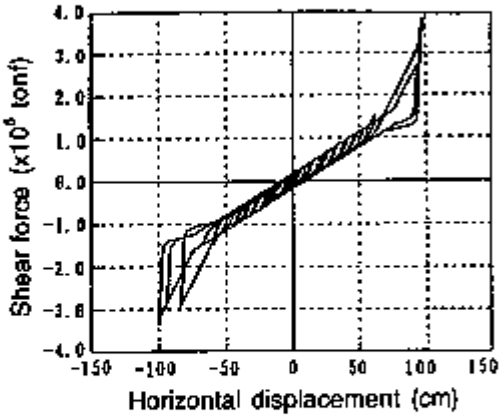

Fig.9 Relationship between shear force and horizontal displacement in the isolated layer (Case7 : 2.75× S2)

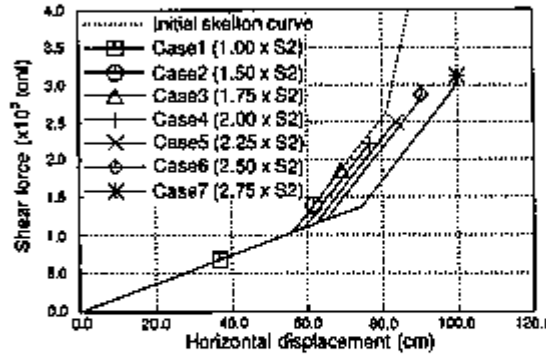

Fig.10 Maximum response value in shear force versus horizontal displacement for laminated rubber bearing

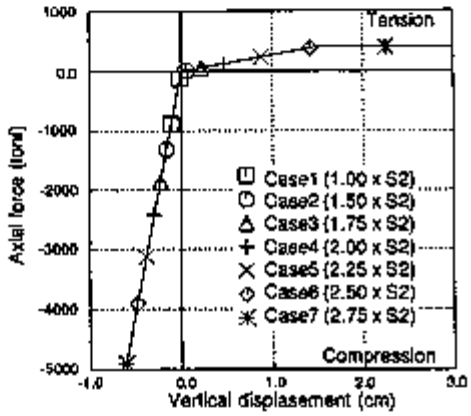

Fig.11 Maximum response value in axial force versus vertical displacement for laminated rubber bearing

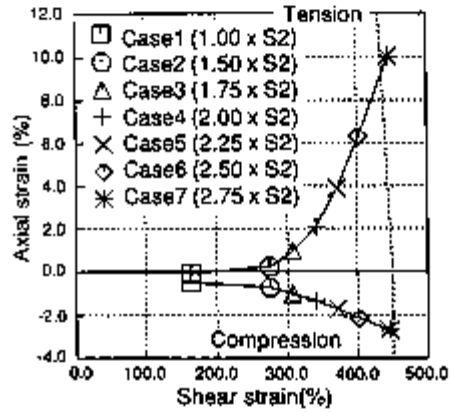

Fig.12 Maximum response value in axial strain versus shear strain for laminated rubber bearing

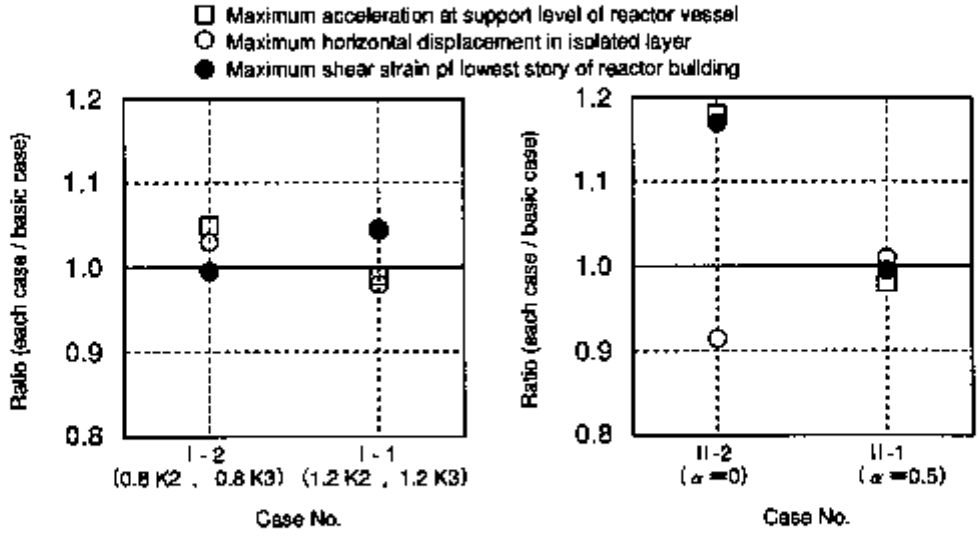

Fig.13 Comparison of each case with basic case in maximum response

SMiRT-12 / K. Kussmaul (Editor)

K25/1

STUDY ON THE APPLICATION OF SEISMIC ISOLATED FLOORS FOR NUCLEAR POWER PLANTS

K. Kuroda[1], T. Nakatogawa[1], M. Yokoyama[1], T. Fujita[2], I. Ichihashi[3], H. Sakuda[3], H. Kurabayashi[4] and T. Omi[4]

[1]Mitsubishi Atomic Power Industries Inc., Tokyo, [2]University of Tokyo, Tokyo, [3]Kansai Electric Power Co. Inc., Osaka, [4]Mitsubishi Steel MFG, Co. Ltd., Tokyo (Japan)

1. INTRODUCTION

To improve the safety of nuclear power plants during an earthquake, it has been proposed to install seismic isolated floors in parts of a plant which are difficult to strengthen sufficiently to withstand seismic forces. As a typical area of this kind we selected the main control room, designed 3-dimensional seismic isolated floors for it, and made a layout study. Vibration tests were carried out on a model to confirm the effectiveness of the seismic isolated floors.

2. EVALUATION OF THE EFFECTIVENESS AND DESIGN OF SEISMIC ISOLATED FLOORS FOR NUCLEAR POWER PLANTS

The CRTs in the main control board are not qualified to withstand S_2 earthquakes in present plants. If we install seismic isolated floors in the main control room, the CRTs can withstand the forces of S_2 earthquakes, and we can take credit for their use after an S_2 earthquake.

In order that the CRTs in the main control board can continue to function after S_2 earthquakes, it is necessary to reduce the response accelerations in both the horizontal and vertical directions to less than 250gals.

We evaluated the function and the performance of seismic isolated floors during S_2 earthquakes(input acceleration:about 500 gals) by analyses using a single mass model. (reference(1)) The results of the horizontal response analyses are shown in Fig. 1. The target is to reduce the acceleration to less than 180 gals for conservatism because the maximum accelerations measured in tests exceeded those of the analyses by a factor of about 1.3 in a past study.(reference (2)) (250/180≒1.38) The allowable displacement is less than 40 cms and the allowable damping coefficient is less than 70%. These limiting the conditions can be

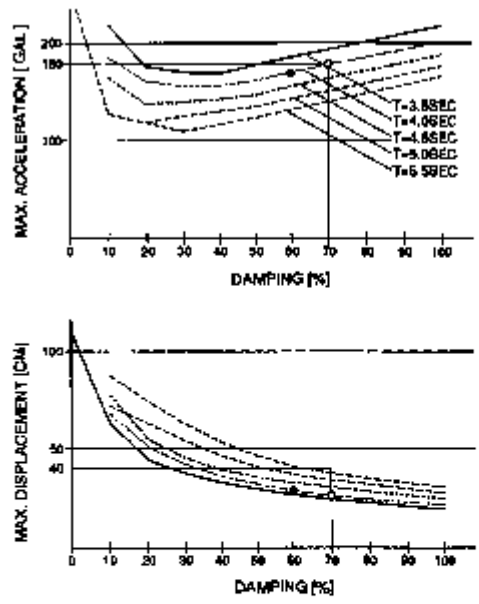

Fig. 1 Results of horizontal response analyses

satisfied for some range of damping coefficients if the natural period of the isolated floors is between 3.5 to 5.5 secs. In the diagram, the point marked ○ gives the minimum displacement in the allowable range of damping coefficients and natural periods. The point marked ● was selected for the design of the floors to allow for variations in the damping coefficient. Vertical analyses were performed, and evaluated in the same way. Based on the simulation analyses of the isolated floors, the design specifications were decided as shown in Table 1.

Table 1. Design specifications of the isolated floors

item	horizontal	vertical
natural period	4 sec	1 sec
damping coefficient	60 %	40 %
friction coefficient	0.01	0.04

3. THE LAYOUT STUDY OF ISOLATED FLOORS FOR NUCLEAR POWER PLANTS

We studied a suitable layout for the main control room of the next PWR plant under design, and designed the 3-dimensional seismic isolated floors.

The resultant layout of the seismic isolating devices is shown in Fig. 2, and a cross section is shown in Fig. 3. We must consider the seperation between A train and B train safety cables and between safety and non-safety cables to provide fire protection. So, we installed the floor cable ducts,made of concrete as in the present design, on the isolating devices. As the seismic isolation can allow a relative displacement of 40 cms, we provided a gap of 1 m between the isolated floors and the outer concrete wall and installed friction panels between them. It is difficult technically to use 3-dimensional isolated floors for the whole area of the main control room and there are also design difficulties in adopting friction panels to the main control board.

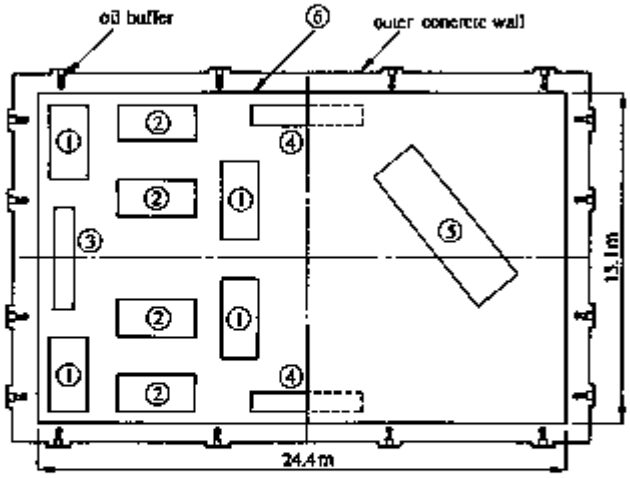

layout of horizontal devices

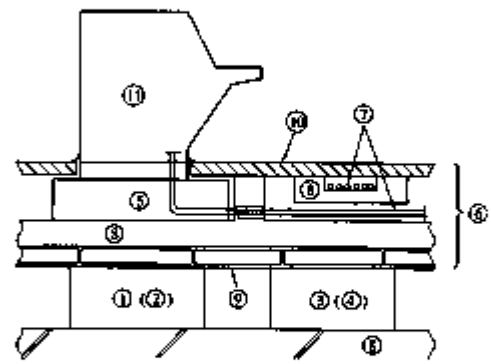

layout of vertical devices

Fig. 3 Cross section

Fig. 2 Layout of seismic isolating devices

Therefore, the isolating devices for the horizontal direction are installed for the whole area of the main control room(area⑥), and the devices for the vertical direction are installed for two main control boards. (⑤) Also, we install oil buffers around the isolated floor in case the displacement exceeds the design value. We installed spring and damper units separately in order to reduce the height of the floor. The horizontal isolating devices consist of spring units(①, ②), and damper units(③, ④)for the X and Y directions. Each unit has an orthogonally coupled linear motion mechanism,therefore, the upper parts of the units can move in any horizontal direction. The details of the spring unit and the damper unit are shown in Fig. 4 and Fig. 5 respectively. The details of the vertical isolating units are shown in Fig. 6. Links and guide rollers prevent rocking motion of the vertical isolating devices.

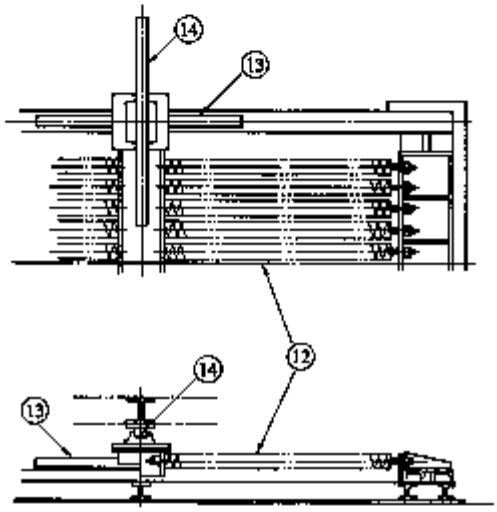

Fig. 4 The details of the spring unit

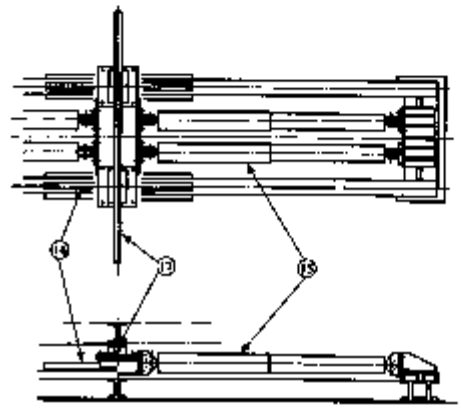

Fig. 5 The details of the damper unit

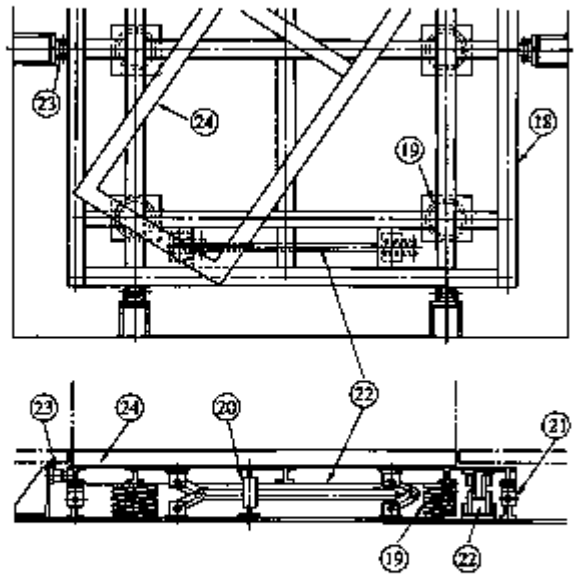

Fig. 6. The details of the vertical isolating unit

①:spring unit for x direction
②:spring unit for y direction
③:damper unit for x direction
④:damper unit for y direction
⑤:vertical isolating unit
⑥:horizontal isolating area
⑦:cables
⑧:concrete
⑨:H-beam
⑩:floor panel
⑪:main control board
⑫:horizontal spring
⑬:rail roller for x direction
⑭:rail roller for y direction
⑮:horizontal oil damper
⑯:rail roller for x direction
⑰:rail roller for y direction
⑱:frame
⑲:vertical spring
⑳:vertical oil damper
㉑:vertical friction damper
㉒:link
㉓:guide roller
㉔:frame

4. VIBRATION TEST OF A MODEL

We designed and manufactured a test model for the 3-dimensional floor isolating devices, and performed sinusoidal characteristic and seismic response vibration tests in the Chiba Experiment Station of University of Tokyo.

4.1 TEST MODEL CONFIGURATION

The fundamental configuration of the test model for the 3-dimensional floor isolating devices is shown in Fig. 7. The experimental setup for the vibration test using a two dimensional shaking table is shown in Fig. 8. The size of the table is 3m × 3m. Due to its limitations, the test model is a combination of spring and damper units, but, the natural period, damping coefficient, and friction coefficient of the test model are the same as those of the main control room of an actual plant. A model which simulates the weight and vibration chacteristics of a main control board is loaded on the test model.

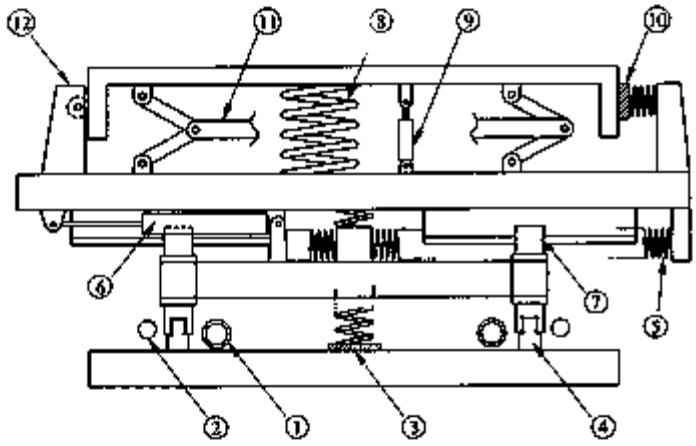

①:spring for x dir.
②:oil damper for x dir.
③:friction damper for y dir.
④:rail roller for x dir.
⑤:spring for y dir.
⑥:oil damper for y dir.
⑦:rail roller for y dir.
⑧:spring for z dir.
⑨:oil damper for z dir.
⑩:friction damper for z dir.
⑪:link
⑫:guide roller

Fig. 7 The fundamental configuration of the test model

Fig. 8 Experimental setup of the vibration test

4.2 VIBRATION TEST AND RESULTS

The location of instruments for the vibration test is shown in Fig. 9. Typical expreimental data are shown in Fig. 10. Fig. 11 shows the horizontal and vertical response accelerations and displacements of the test model. As shown in Table 2, the response accelerations of the test model are less than the allowable 250 gals, and, we could comfirm the acceptable performance of the isolated floors during an earthquake.

Table 2. Performance of the isolating devices

Wave name	S_2 earthquake input acceleration	Maximum response acceleration	Allowable acceleration
EL CENTRO NS	450 gals	98 gals	250 gals
EL CENTRO EW	450 gals	96 gals	250 gals
AKITA NS	450 gals	150 gals	250 gals
AKITA EW	450 gals	113 gals	250 gals
EL CENTRO UD	779 gals	218 gals	250 gals
AKITA UD	366 gals	175 gals	250 gals

* For the vertical direction,the floor response waves were used in the analysis.

4.3 REFLECTION OF THE TEST RESULTS INTO THE DESIGN

Based on the experience of these tests, changes in each of the parameters relative to the design conditions can be expected as follows:

- natural period: same as the design condition
- damping coefficient: $\pm 15\%$
- friction coefficient: $-12\% \sim +25\%$

We should reflect the fluctuations of such parameters into the design of the isolated floors of an actual plant.

5. AKNOWLEDGEMENTS

The authors would like to express great appreciation to Professor H.Shibata, Yokohama National University, for his good advice, Mr.M.Shimazaki, University of Tokyo, for his helpful support in the vibration tests, and the persons concerned in MAPI for their work in the layout study.

This study was carried out as a joint research project by The Kansai Electric Power Co., Hokkaido Electric Power Co., Shikoku Electric Power Co., Kyushu Electric Power Co., The Japan Atomic Power Company, and Mitsubishi Heavy Industries, Ltd.

6. REFERENCES

(1) Fujita,T.&Hattori,S. 1981. An earthquake isolation floor using pre-tensed or pre-compressed springs(6th report:Analysis for actual earthquake isolation floors-part 1-). Seisan-Kenkyu Vol.33,No.7:339-342

(2) Fujita,T.,Yogo,k.&Omi,T. 1983. An earthquake isolation device using linear motion mechanism(2nd report:Seismic excitation tests and response analysis). Seisan-Kenkyu Vol.35,No.5:212-215

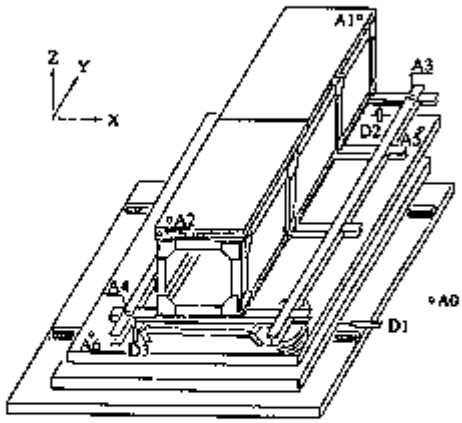

A0:acceleration on the shaking table
A1,A2:acceleration on the model which simulates a main control board
A3,A4:acceleration on the vertical isolating device
A5,A6:acceleration on the horizontal isolating device
D1:relative displacement between the horizontal isolating device and the shaking table
D2,D3:relative displacement between the vertical isolating device and the horizontal isolating device

Fig. 9 Location of measuring instruments for the viblation test

EL CENTRO EW

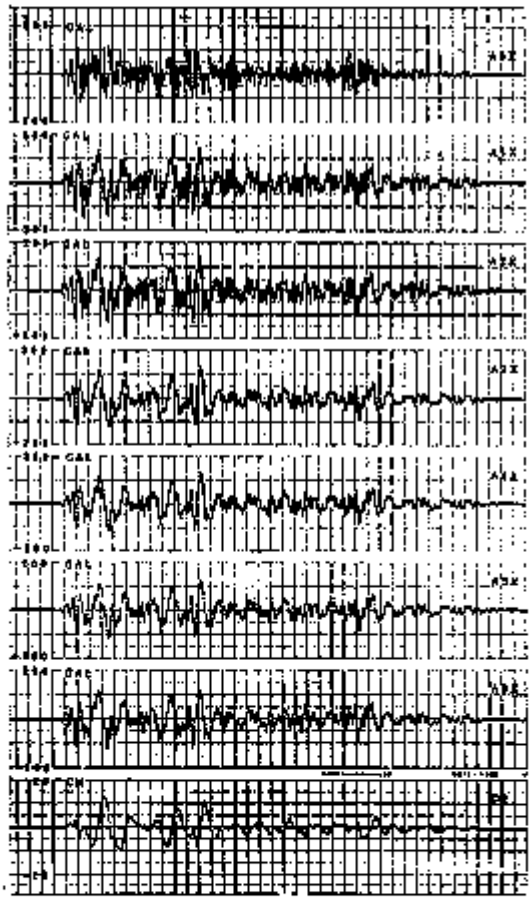

Fig. 10 Typical experimental data

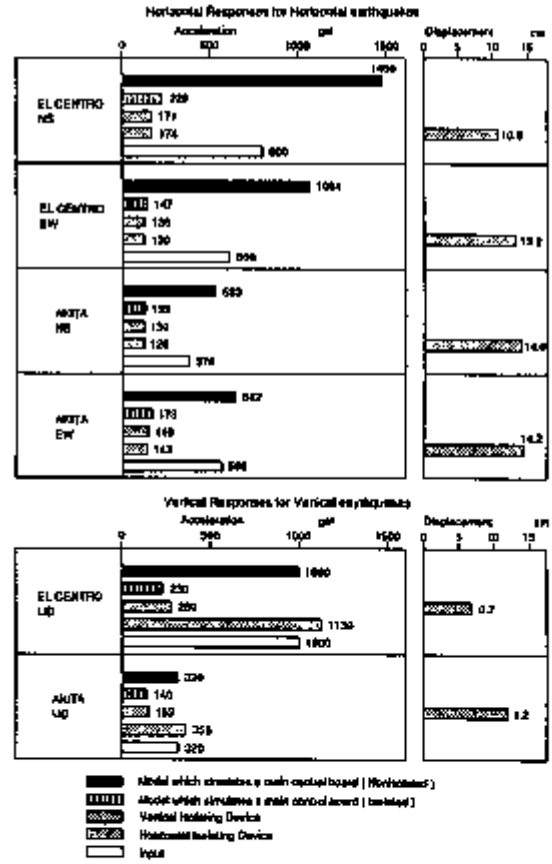

Fig. 11 Horizontal and vertical response accelerations and displacements of the test model

SMiRT-12 / K. Kussmaul (Editor)

K19/7

EXPERIMENTAL AND ANALYTICAL STUDY ON CROSSOVER PIPING SYSTEM IN SEISMIC ISOLATION FBR PLANT: (II) CCWS-SEA WATER PIPING

Y. Watanabe[1], M. Kuroha[1], K. Amada[1], M. Kohda[2], K. Arai[2] and S. Kajii[3]

[1]The Japan Atomic Power Company, Tokyo, Japan
[2]Mitsubishi Atomic Power Industries, Tokyo, Japan
[3]Mitsubishi Heavy Industries, Ltd., Takasago, Japan

1. Introduction

In a seismic isolation FBR plant, crossover piping, which is the piping that crosses the open space around the seismically isolated building, is subjected to large relative displacements and inertia forces during earthquakes. Sea water piping of the Component Cooling Water System (CCWS), which is a safety-related system of an FBR plant, is one of such systems.

In order to accommodate extremely the large displacements caused by seismic loads, hinged bellows expansion joints are an important feature of this piping system. There is no experience of such piping system in nuclear power plants in Japan, now. This system aims at achieving a rational (short length) piping route design, by considering its low pressure and low temperature conditions. First a design study was made which showed this piping system would maintain its structural integrity during the extreme design basis earthquake (S_2 earthquake). Then two kinds of vibration tests were carried out to examine the analysis methods, and to demonstrate the feasibility of this piping system. Based on the test results, some analysis models were examined and conventional seismic piping stress evaluation analyses were performed.

The objectives of this study are to examine and demonstrate the following items based on analyses and tests, and then, to demonstrate the feasibility of the new piping system in the seismic isolation plant.

(1) The feasibility of a piping system which employ bellows to accommodate large displacements during earthquakes.
(2) The acceptability of the conventional analytical method by using some general piping analysis models and modal analysis with response spectra, for such type of piping system.

2. Design of CCWS

The design conditions of the sea water piping are ① Seismic class: As (the highest class). ② Component classification: ASME Code Class 3 piping. ③ Line size: 16 inches. ④ Material: ASME Code SA 106 Gr.B. ⑤ Design pressure/temperature: 7.0kg/cm^2/ 50℃, and ⑥ Displacement due to earthquakes: 129mm for the maximum design basis earthquake (S_2 earthquake) /387mm for the S_2 earthquake.

An "L" shaped pipe routing configuration was adopted, which employs three hinged bellows expansion joints (with three, four and five convolutions, respectively) to adequately accommodate the large relative displacement caused by the S_2 earthquake. The layout of the sea water piping of an actual plant is shown in Fig.1. By adopting this new piping design, a great deal of space can be saved.

3. Experiments

3.1 Individual test of a bellows unit

(1) Test scope

This test was to obtain the rotational stiffness of the bellows which was essential for the analytical models.

The schematic drawing of the test is shown in Fig.2. The test apparatus used 1/1.9 scale models. Vibration tests for three kinds of bellows were carried out. The specifications of the bellows are shown in Table 1. The bellows unit (with three convolutions) which was used for the test is shown in Fig. 3.

(2) Test results

The relation between the rotational stiffness and the angles of rotation under two pressure conditions (7.0 kg/cm^2 or 0 kg/cm^2) are shown in Fig.4. In the case of 7.0 kg/cm^2, it is noticeable that the rotational stiffness becomes greater as the angle of rotation is decreased. This is because, internal pressure has an effect on the pin joint of the bellows, so that the rotational friction factor around the pin increases. Fig.5 is an example of the dissipated energy.

3.2 Vibration test of the piping system

(1) Test scope

The schematic drawing of the piping system vibration test is shown in Fig.6. Fig.7 shows the piping analysis model. The tests were carried out using a 1/1.9 scale model using a large mass to simulate the dynamic behavior of the isolated building on the shaking table. Inertia type shaking equipment was installed on the large mass to simulate vibration behavior (damping factor etc.) of the seismic isolated building.

Sinusoidal wave sweep vibration tests and several kinds of earthquake wave vibration tests were carried out. In addition static load tests were also carried out in which loads on the test apparatus were caused by static displacements.

(2) Test results

Acceleration, displacement, strain, and pressure were measured at several points of the test piping. Because of the alignment of the bellows relative to the direction of the seismic input, the rotational angle of bellows "A" (with three convolutions) was very small. The vibration behavior of the piping was measured by the rotational angles of bellows "B" (with five convolutions) and bellows "C" (with four convolutions). The rotational angles were obtained from the bellows's strain data and the calibration curves, obtained from the individual bellows test. The time history stress of a typical point (point "a") is shown in Fig.8. In Fig.8, the stress is divided into two components, one being the primary stress caused by inertia forces and the other being the separated stress caused by relative displacements. For the bellows "B", both the rotations measured during the time history, and the rotations caused by relative displacements which were obtained from the static load test results, are shown in Fig.9.

The test results demonstrated that the structural integrity of this piping system would be maintained during earthquakes.

4. Analysis to simulate the test

The results of the simulation study identified the following points which should be taken into consideration.

① The rotational stiffness of the bellows depends on the angle of rotation. It is necessary to change the rotational stiffness of the bellows for each test and/or each analysis. Thus, the rotational stiffness of the piping is non-linear with respect to the responses (forces and displacements).

② The friction factor of the vertical support structure should be considered.

③ The damping ratio of this piping system is very large.

The simulation, therefore, was carried out by employing linear models that were equivalent to the non-linear test piping. We constructed two kinds of linear models. One model yields the inertia forces that agree with the test results and the other yields the same large relative displacements as the test piping. Static analysis, eigenvalue computation, and dynamic analysis were conducted iteratively until the responses converged.

The analytical models used to simulate the tests are shown in Table 2. These were called "model (a)" models. The vibrational behavior of the piping system could be simulated, using these models. The natural frequency and damping ratio were estimated to be 20.4 Hz and 15.0 % for the S_1 earthquake model, and 17.25 Hz and 8.8 % for the S_2 earthquake model.

5. Seismic analysis method

5.1 Scope of analysis

(1) Analysis model

The above "model(a)" models were complex and had no generality. Therefore two kinds of simplified analysis models were made which were generally applicable. One was "model(b)" in which the values of EJMA (STANDARDS OF EXPANSION JOINT MANUFACTURERS ASSOCIATION, INC.) stiffness were used for the rotational stiffness, because they represent stiffness very well as shown in Fig. 4. The other was "model (c)" in which bellows could rotate freely to calculate the largest bellows rotations. The specifications of "model (b)" and "model(c)" are shown in Table 2.

(2) Seismic input conditions

The response spectra were made from time history response accelerations and damping factors were obtained, by the Newmark-β method. The response spectra were broadened by ± 10 %. The response spectra of the S_2 earthquake are shown in Fig. 10.

(3) Seismic analysis method

For the purpose of analyzing inertia forces, the "Enveloped response spectrum analysis method" and the "Independent input response spectrum analysis method" were used. On the other hand, for the purpose of analyzing displacements, a static forced displacement analysis was performed. The total piping stress and the total rotational angle of the bellows were evaluated by means of an absolute summation method.

5.2 Results

Table 3 shows a comparison of piping stresses as calculated in the analysis and as measured in the tests. Table 4 shows similar information for angle of bellows rotation. The following points can be seen. First, the "Enveloped response spectrum analysis method" has a tendency to give larger piping stresses and rotational angles than the "Independent input response spectrum analysis method", as was expected. Second, the analytical results are almost in agreement with the test results or are conservative, except for one stress evaluation point, when calculated by the "Independent input response spectrum analysis method". The total piping stress and the total rotational angle of analytical results from the three models are in close agreement.

6. Conclusions

The new piping system which employs hinged bellows expansion joints, is useful for a seismic isolation plant. The piping vibration tests demonstrated that the structural integrity of this piping system could be maintained under the large relative displacements and inertia forces caused by earthquakes. The conventional analytical method using some general piping analysis models and the modal analysis with response spectrum, was applied to this study. By comparing these analysis results with the test results, it was confirmed that the conventional analytical method was acceptable.

7. Acknowledgement

This study was performed as part of a joint research and development project for the DFBR under the sponsorship of the nine Japanese electric power companies, Electric Power Development Co., Ltd. and the Japan Atomic Power Company.

Table 1 Specifications of the test bellows

bellows		A	B	C
design pressure	(kgf/cm²)	7.0		
design temperature	(℃)	50		
material		SUS345(SALB2 F316 as ASME Code)		
outside diameter	(mm)	365		
convolution depth	(mm)	30		
bellows pitch	(mm)	25		
thickness	(mm)	1.0		
total number of convolutions		3	5	4
length	(mm)	375	430	480

Table 2 Specifications of simulation models and simplified models

analysis model	earthquake	objective of analysis	rotational stiffness of bellows (kgf-mm/deg.) A	B	C	spring const. of rigid support (kgf/mm)
simulation model(a)	S_1	inertia force relative displ.	5.05×10^4 5.05×10^4	3.40×10^4 1.93×10^4	2.79×10^4 2.22×10^4	173
	S_2	inertia force relative displ.	5.05×10^4 5.05×10^4	1.13×10^4 1.05×10^4	7.27×10^3 1.34×10^4	58.3
simplified model(b)	S_1,S_2	inertia force and relative displ.	1.59×10^4	9.46×10^3	1.18×10^4	—
simplified model(c)	S_1,S_2	inertia force and relative displ.	∞	∞	∞	—

Table 3 Comparison of piping stress from test results and analytical results (kgf/mm²)

point			a		b	
earthquake			S_1	S_2	S_1	S_2
test results		inertia forces	0.1	0.0	0.5	0.8
		relative displ.	0.1	0.4	0.1	0.3
		total stress	0.2	0.4	0.6	0.8
analytical results of Enveloped response spectrum analysis method	model(a)	inertia forces	1.0	2.4	0.6	1.0
		relative displ.	0.4	0.7	0.0	0.0
		total stress	1.4	3.1	0.6	1.0
	model(b)	inertia forces	1.8	2.9	0.6	1.0
		relative displ.	0.2	0.6	0.0	0.1
		total stress	2.0	3.5	0.6	1.1
	model(c)	inertia forces	1.8	3.0	0.6	1.0
		relative displ.	0.0	0.0	0.0	0.0
		total stress	1.8	3.0	0.6	1.0
analytical results of Independent input response spectrum analysis method	model(a)	inertia forces	0.6	1.1	0.3	0.4
		relative displ.	0.4	0.7	0.0	0.0
		total stress	1.0	1.8	0.3	0.4
	model(b)	inertia forces	0.7	1.3	0.2	0.5
		relative displ.	0.2	0.6	0.0	0.1
		total stress	0.9	1.9	0.2	0.6
	model(c)	inertia forces	0.7	1.3	0.2	0.4
		relative displ.	0.0	0.0	0.0	0.0
		total stress	0.7	1.3	0.2	0.4

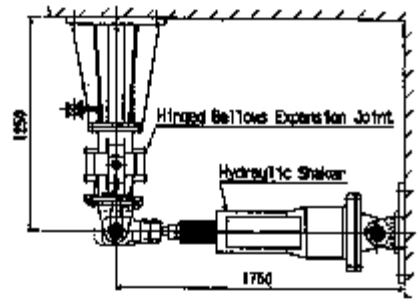

Fig.2 Test apparatus for individual bellows unit test

Table 4 Comparison of bellows rotations from test results and analytical results (deg.)

bellows			B		C	
earthquake			S_2	S_1	S_2	S_1
test results		inertia forces	0.2	0.3	0.1	0.1
		relative displ.	3.2	8.8	3.2	8.0
		total angle	3.4	9.1	3.3	8.1
analytical results of Enveloped response spectrum analysis method	model(a)	inertia forces	0.3	0.6	0.1	0.2
		relative displ.	3.2	8.9	3.2	8.9
		total angle	3.5	9.5	3.3	9.1
	model(b)	inertia forces	0.5	0.6	0.1	0.2
		relative displ.	3.2	8.8	3.2	8.9
		total angle	3.7	9.6	3.3	9.1
	model(c)	inertia forces	0.5	0.8	0.1	0.2
		relative displ.	3.2	8.9	3.2	8.9
		total angle	3.7	9.7	3.3	9.1
analytical results of Independent input response spectrum analysis method	model(a)	inertia forces	0.2	0.3	0.1	0.1
		relative displ.	3.2	8.9	3.2	8.9
		total angle	3.4	9.2	3.3	9.0
	model(a)	inertia forces	0.2	0.3	0.1	0.1
		relative displ.	3.2	8.8	3.2	8.9
		total angle	3.4	9.1	3.3	9.0
	model(b)	inertia forces	0.2	0.3	0.1	0.1
		relative displ.	3.2	8.9	3.2	8.9
		total angle	3.4	9.2	3.3	9.0

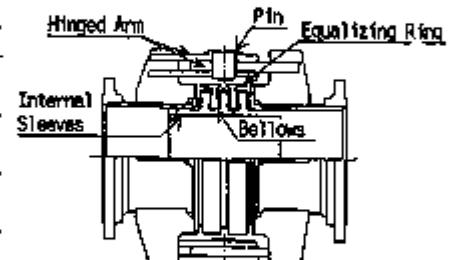

Fig.3 Bellows unit used for tests (three convolutions)

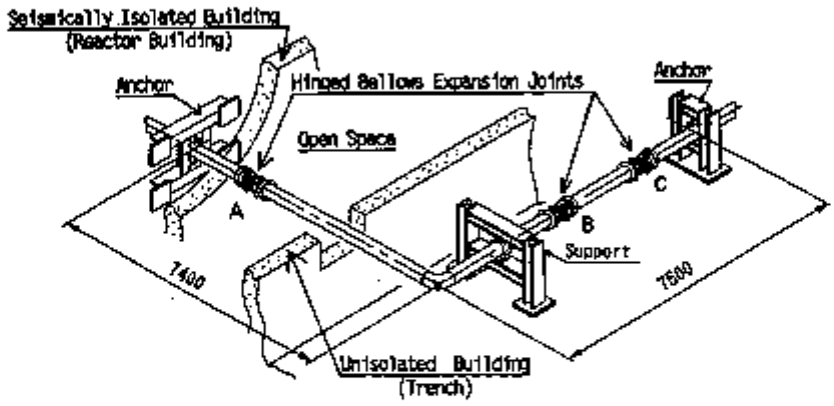

Fig.1 Layout of sea water piping of an actual plant

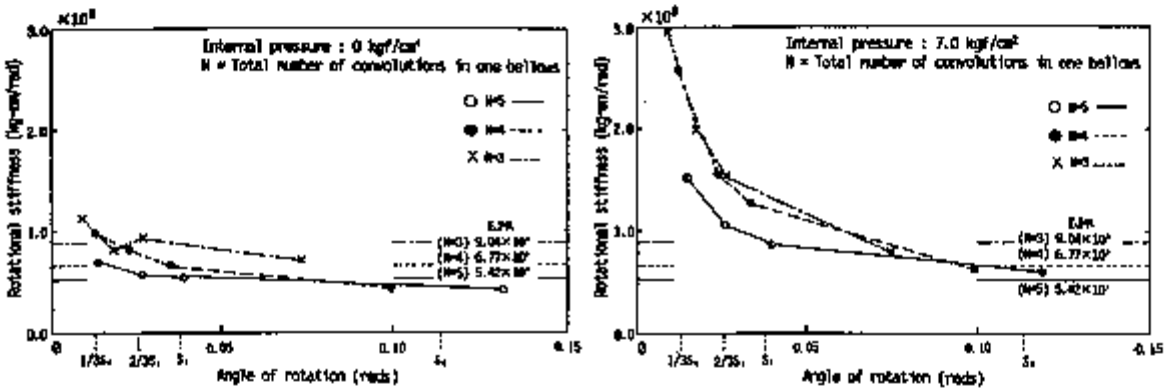

Fig.4 Relation between rotational stiffness and angle of rotation (left: internal pressure is 0 kgf/cm², right: 7.0 kgf/cm²)

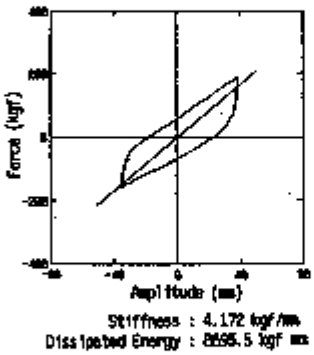

Fig.5 Hysteresis loop for dissipated energy of a bellows (four convolutions, S_2 earthquake)

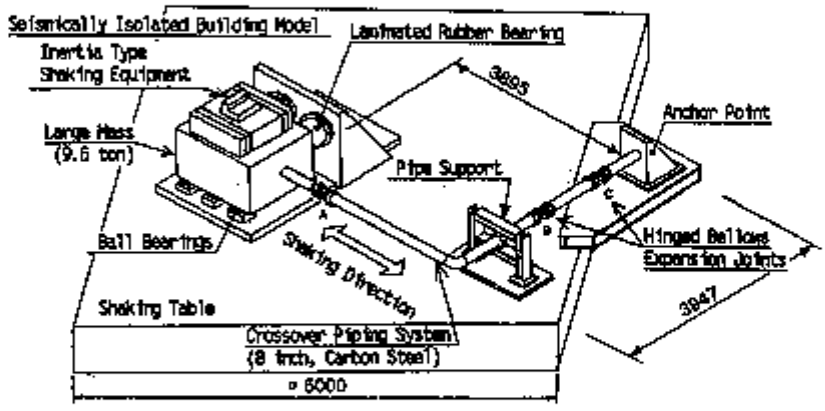

Fig.6 Test apparatus for piping system vibration test

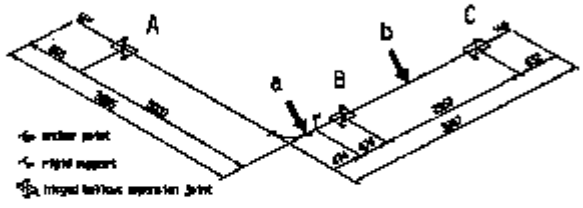

Fig.7 Piping analysis model

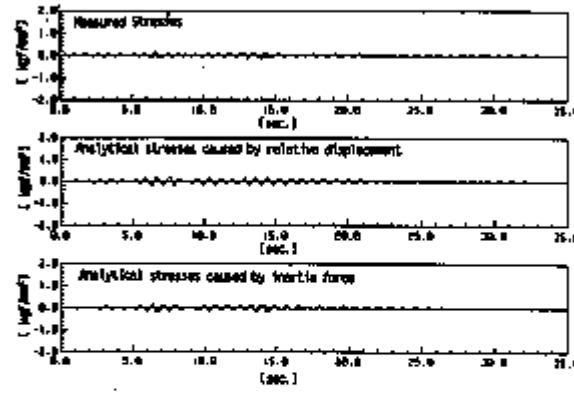

Fig.8 Time history piping stress at point "a" (S_2 earthquake)

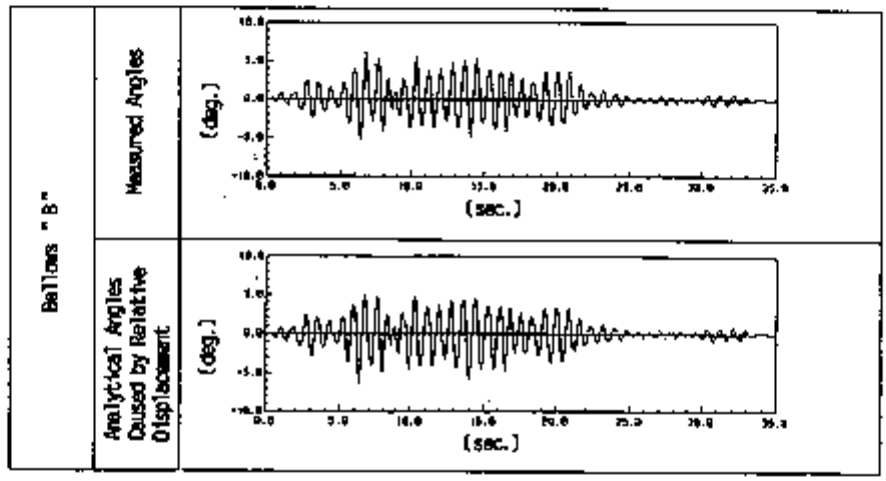

Fig.9 Time history bellows rotations of "B" (S_2 earthquake)

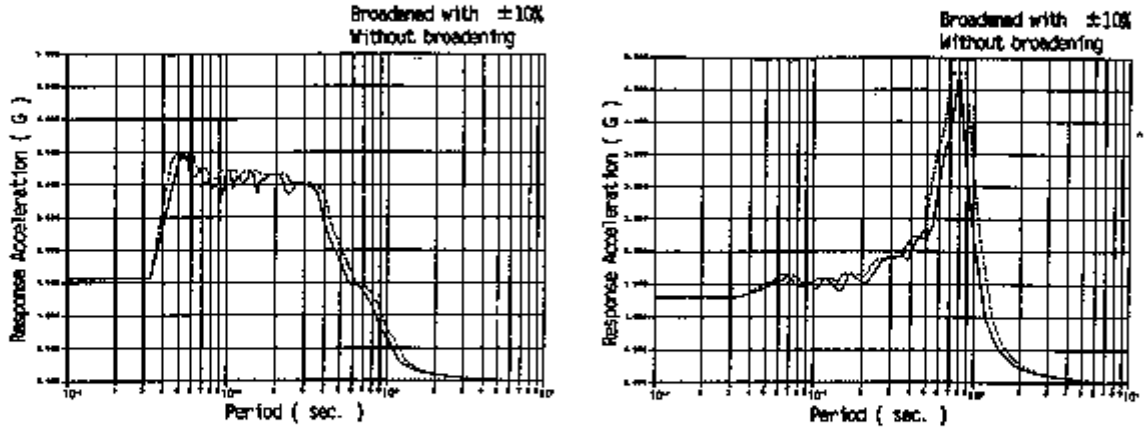

Fig.10 Response spectra of S_2 earthquake (damping ratio: 8.8%)
(left: unisolated building, right: isolated building)

SMiRT-12 / K. Kussmaul (Editor)

K21/1

MOST RECENT EXPERIMENTAL AND NUMERICAL STUDIES PERFORMED IN ITALY ON SEISMIC ISOLATION

M. Forni[1], A. Martelli[1], B. Spadoni[1], G. Vernoni[1], F. Bettinali[2], A. Marioni[3], G. Bonacina[4], C. Mazzieri[5], F. Vestroni[6]

[1]ENEA, Department of Innovative Reactors, Bologna, Italy, [2]ENEL, Hydraulic and Structural Research Center, Milano, Italy, [3]ALGA S.p.A., Milano, Italy, [4]ISMES S.p.A., Bergamo, Italy, [5]ANSALDO-Ricerche, Genova, Italy, [6]University of L'Aquila, Italy

ABSTRACT

In order to verify the applicability of seismic isolation to high risk plants such as nuclear reactors, static and dynamic tests have been performed in Italy on isolation rubber bearings, rubber specimens, isolated structure mock-ups and actual isolated civil buildings since 1989. Simplified and detailed numerical models of isolators and isolated structures have also been developed and applied, and considerable work has been made for the preparation of design guidelines for isolated structures. This paper summarizes the main features and results of R&D activities, focussing on those performed after the 11th SMiRT Conference.

1 INTRODUCTION

The use of techniques capable of reducing the seismic loads acting on structures (isolation and passive energy dissipation) began in Italy in 1974. The first applications concerned bridges and viaducts; in 1983, the construction of seismically isolated buildings also began. At present, passive energy dissipation and seismic isolation systems are being used in more than 150 Italian bridges and viaducts, while 8 isolated buildings have been completed and 5 are in advanced construction in Italy (Martelli et al. 1993a). Preliminary design analysis has also been performed by Bonacina et al. (1993) to support the application of seismic isolation to conventional energy production plants. Detailed studies for the development of seismic isolation began in Italy in 1988, in order to permit the safe use of this technique in civil buildings and in view of its possible adoption for industrial facilities, including high risk nuclear and chemical plants. Indeed, in spite of the very encouraging results that had already been obtained, further research and development (R&D) work was considered to be still necessary to fully verify the adequacy of seismic isolation for high risk plants. In addition, the development of appropriate design rules was also judged essential, because of both the key role of isolation system for plant safety and its important effects on the structure design. It is noted that a fairly large amount of information needed for the use in high risk plants can (and will be) provided by the experience gained on the design and behaviour of isolated civil buildings.

2 STUDIES IN PROGRESS IN ITALY

Italian studies concern: (a) preparation of design guidelines and national standards for isolated

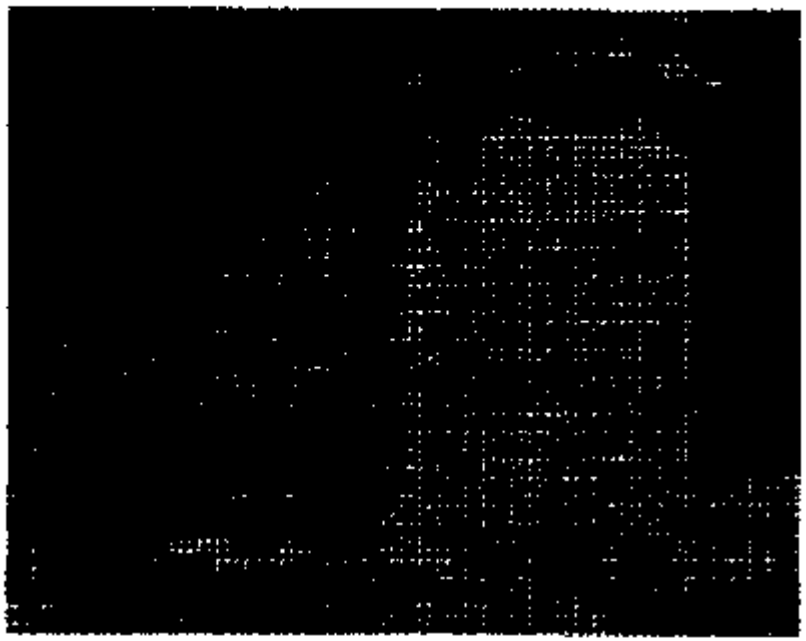

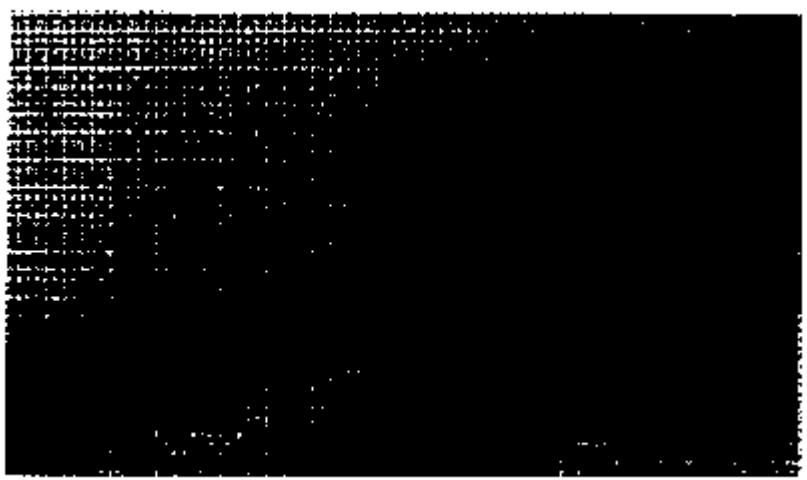

Fig. 1. View of the isolated SIP building at Ancona which was subjected to in-situ tests and detail of the isolation system (October 1990).

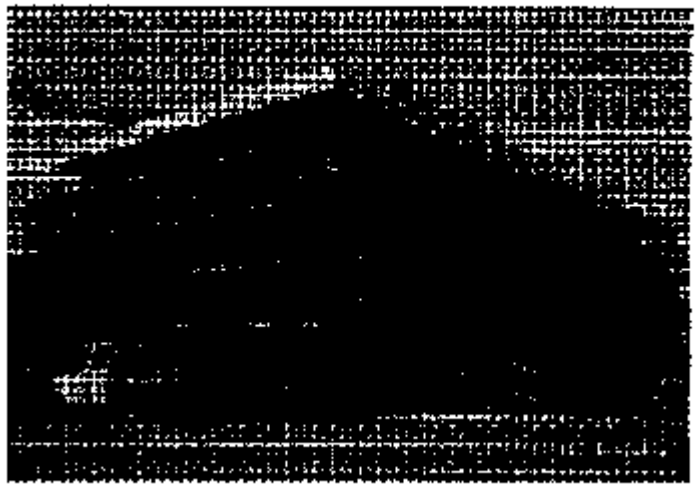

Fig. 2. View of the isolated house at Squillace Lido, at the time of in-situ tests (June 1991).

structures; (b) development of isolation and energy dissipation systems; (c) laboratory tests on rubber specimens, individual isolators and isolated structure mock-ups; (d) in-situ tests of isolated buildings; (e) seismic monitoring of such buildings; (f) development of simple and detailed numerical models for isolators and isolated structures. These studies are being jointly performed by several organizations and universities, in the framework of the activities of the Italian Working Group on Seismic Isolation (GLIS).

It is noted that in-situ tests were performed on both one of the five large isolated buildings of the Administration Center of the National Telephone Company (SIP) at Ancona (Fig. 1), and the twin three-story houses (one being conventionally founded, the other being seismically isolated) which were constructed at Squillace Lido, Calabria, South of Italy (Forni et al. 1991a&b, see Fig. 2). Both SIP buildings and twin houses at Squillace have just been provided with seismic monitoring systems (Forni et al. 1993).

This paper provides a short overview on the R&D work which is being performed in Italy, focussing on the most recent, namely on that performed after the 11th SMiRT Conference (thus, integrating the information given there by Martelli et al. 1991a&b and Forni et al. 1991a&b). Information on the progress on guidelines development is given by the separate paper of Martelli et al. (1993b). Only a few recent R&D results are shown here; more details will be presented by Forni et al. (1993) at the Post-SMiRT Conference Seminar on Isolation, Energy Dissipation and Control of Vibrations of Structures (Capri, Italy, August 23 to 25, 1993).

3 BEARINGS USED IN THE EXPERIMENTS

Several types of energy dissipation and seismic isolation devices have been used in Italy for brigde applications, while, with regard to buildings and plants, applications (Martelli et al. 1993a) and R&D studies in progress in Italy are at present mainly based on the high damping steel-laminated rubber bearing (HDRB).

R&D work was undertaken in 1989. At present, it is being jointly performed by ENEA, ENEL, ISMES, ALGA and ANSALDO-Ricerche. This work concerns both experimental and numerical studies of HDRBs, bearing materials and isolated structures. Tests have been performed at ISMES and the ENEA/ANSALDO Centre of Boschetto (Genova) on rubber specimens, bearings in various scales, structure mock-ups isolated by means of such bearings, and the previously mentioned isolated SIP and Squillace buildings.The first tests were based on one (the 500 mm diameter) of the two HDRB types used in SIP buildings. These are characterized by a horizontal displacement equal to 144 mm at 100% shear strain, and a "containment" system for bearing attachment (Martelli et al. 1991a). Several bearings in full scale and 1/2, 1/3 and 1/4 scales were fabricated and tested. Tests followed a very detailed acceptance campaign of SIP HDRBs.

In the second phase of tests (which is still in progress), use is being made of modified (full and half scale) bolted and dowelled isolators and modified rubber materials (Fig. 3).

Some bearings equal to those used in the isolated house at Squillace (Fig. 8) were also fabricated and tested: these isolators have diameters of 400 mm and 500 mm, a total rubber height of 136 mm, and an attachment system similar to that used for the SIP bearings at Ancona.

4 TESTS ON RUBBER SPECIMENS

Tests on rubber specimens are being performed by ENEA in cooperation with ALGA and ANSALDO, with the aim of improving fabrication processes, controling bearing quality and determining rubber properties. Shear tests on rubber specimens preceded all experiments on bearings and isolated mock-ups. These were carried out for all bearing batchs, to mainly measure

Fig. 3. View of the modified SIP-type bearings in full and half scales.

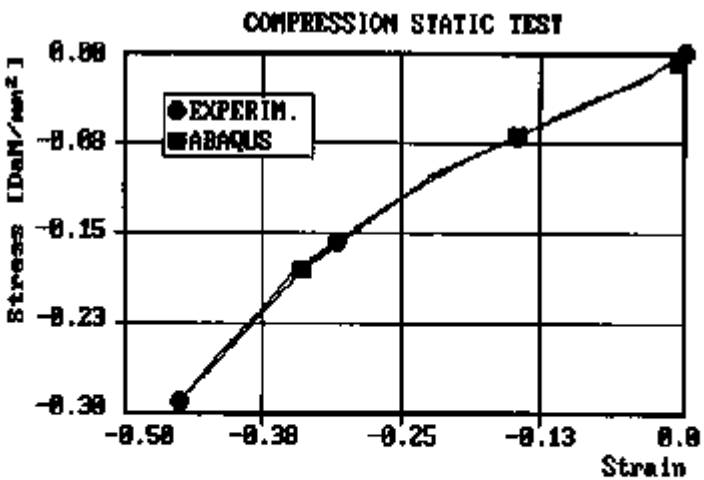

Fig. 4. Comparison between the results of tests on specimens with compression loads and ABAQUS calculations with a hyperelastic model.

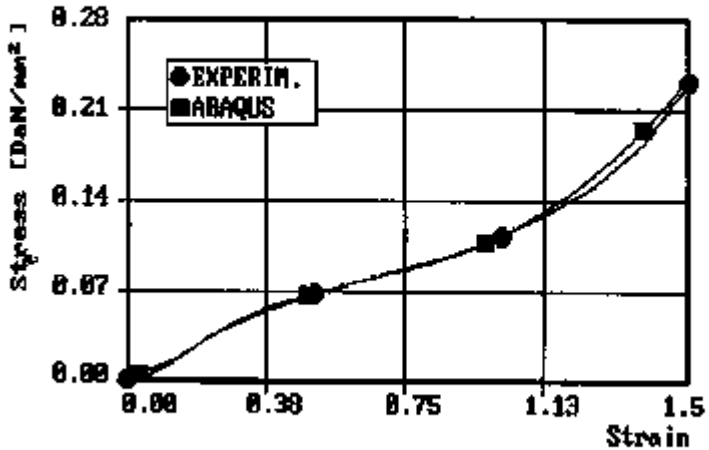

Fig. 5. Comparison between the results of tests on specimens with tensile loads and ABAQUS calculations with a hyperelastic model.

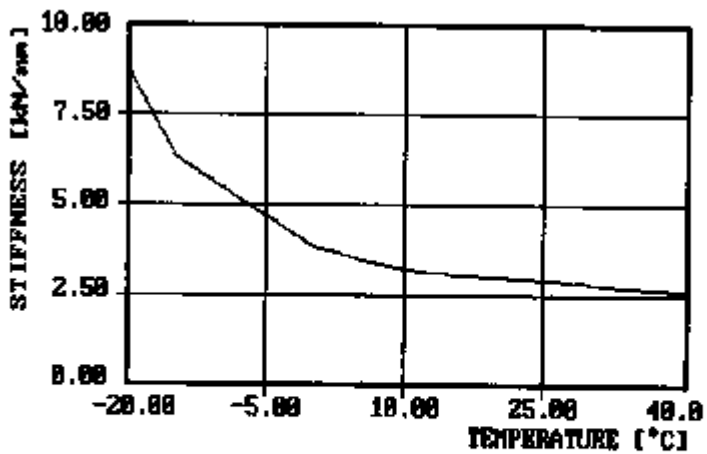

Fig. 6. Temperature effects on stiffness, measured in shear tests of rubber specimens using the HDRB compound of SIP bearings.

the shear modulus of elasticity, G; they stressed the importance of an adequate G measurement.

Tests on specimens formed by new rubber materials allowed for the definition of three HDRBs with improved rubber-steel bonding and different compounds (Forni et al. 1993), and for the assessment of a hyperelastic model of the rubber (Figs. 4 and 5).

Accelerated aging experiments on specimens formed by the compound used in the SIP HDRBs, performed by ALGA, showed that the isolator life is larger than 110 years (Forni et al. 1993), and tests carried out at the Boschetto Centre demonstrated that temperature does not produce any permanent modification of compound features, but has a non-negligible effect on horizontal stiffness at the low values (Fig. 6).

5 TESTS ON ISOLATION BEARINGS

Tests of individual bearings have been performed at ISMES using the SISTEM machine (designed and fabricated by ENEA, see Fig. 7). Those completed on the SIP-type bearings were already mostly described by Martelli et al. (1991a) and Forni et al. (1991b). They include: (a) quasi-static vertical compression tests; (b) cyclic quasi-static shear tests under vertical design load; (c) sustained compression tests; (d) quasi-static shear tests under different vertical loads; (e) four sets of quasi-static tests for the analysis of natural aging effects, performed on bearings mantained in actual installation conditions; (f) sinusoidal horizontal excitation tests at fixed frequencies; (h) one quasi-static cyclic failure test.

As mentioned in Sect. 3, static and dynamic tests were also performed (on behalf of ENEL) on Squillace bearings, and some first ENEA tests were carried out on the modified SIP bearings.

The results of more recent tests confirmed the conclusions of Martelli at al. (1991a) and Forni et al. (1991b) and provided further important data for the development of design guidelines, the development and validation of numerical models, and comparison with the results of tests on isolated structure mock-ups and actual buildings. In particular, it has been confirmed that: (a) large horizontal stiffness variations with displacement occur to about 50% shear strain; (b) damping nature is mostly hysteretic; (c) equivalent viscous damping ratio is larger than 10% for the HDRBs used; (d) creep effects are limited; (e) the effects, on vertical stiffness, of dynamic excitation are small; (f) sufficient margins exist before failure. Furthermore, no effects of natural aging were detected, yet, on SIP-type bearings after more than two years, during which some of these bearings were mantained under the actual vertical load (cooperation for the analysis of these effects has been started by ENEA and the owner of SIP Center, SEAT).

As to margins before failure, we remember that the quasi-static test mentioned by Martelli et al. (1991a) concerned a 1/2 scale bearing without lateral rubber cover: for this isolator some damage had began at about 160% shear strain, although the bearing was still capable of sustaining the vertical load - in spite of very severe damage - at 260% shear strain (test had been interrupted at this level). The reasons for damage beginning at a relatively low displacement and the subsequent severe damages at larger displacements were attributed by Martelli et al. (1991a) to some initial damage caused by bearing reworking performed to remove the lateral rubber cover. This explanation was later confirmed by the results of a dynamic test of a 400 mm diameter Squillace bearing (Fig. 8). This test was performed at a frequency of 0.45 Hz under the design vertical load of 700 kN, by gradually increasing displacement (every five cycles) from the initial value of 13 mm to the maximum force compatible with SISTEM capabilities (corresponding to about 290 mm, i.e. more than 210% shear strain, see Fig. 9). Only very limited damage occurred to this displacement: it began at about 200% shear strain, probably also due to the large number of cycles and friction between bearing borders and the containing steel plates (see the time-history of the applied force in Fig. 9, which might also have been affected by temperature raise inside bearing, due to cycling).

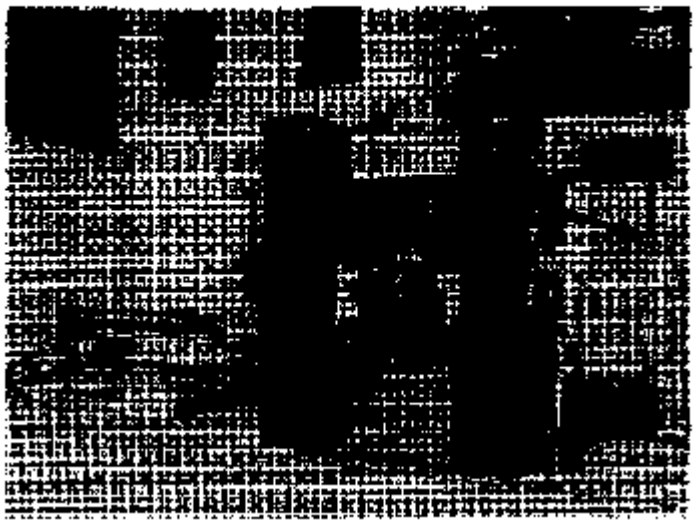

Fig. 7. View of SISTEM after modifications to allow for tensile vertical loads and better guide of vertical jack.

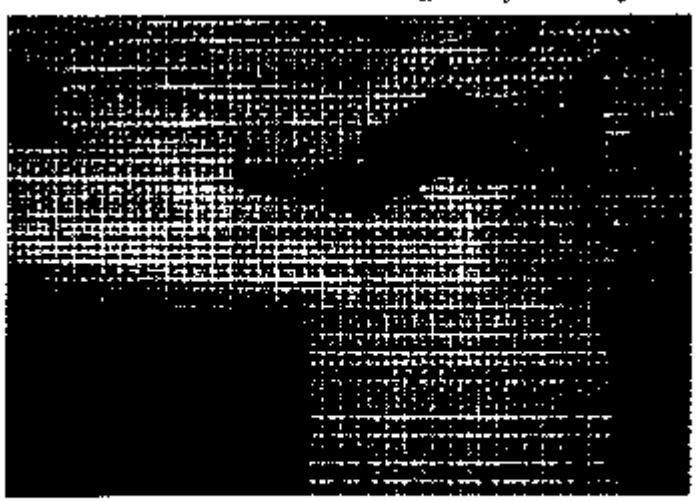

Fig. 8. View of an isolator in the house at Squillace.

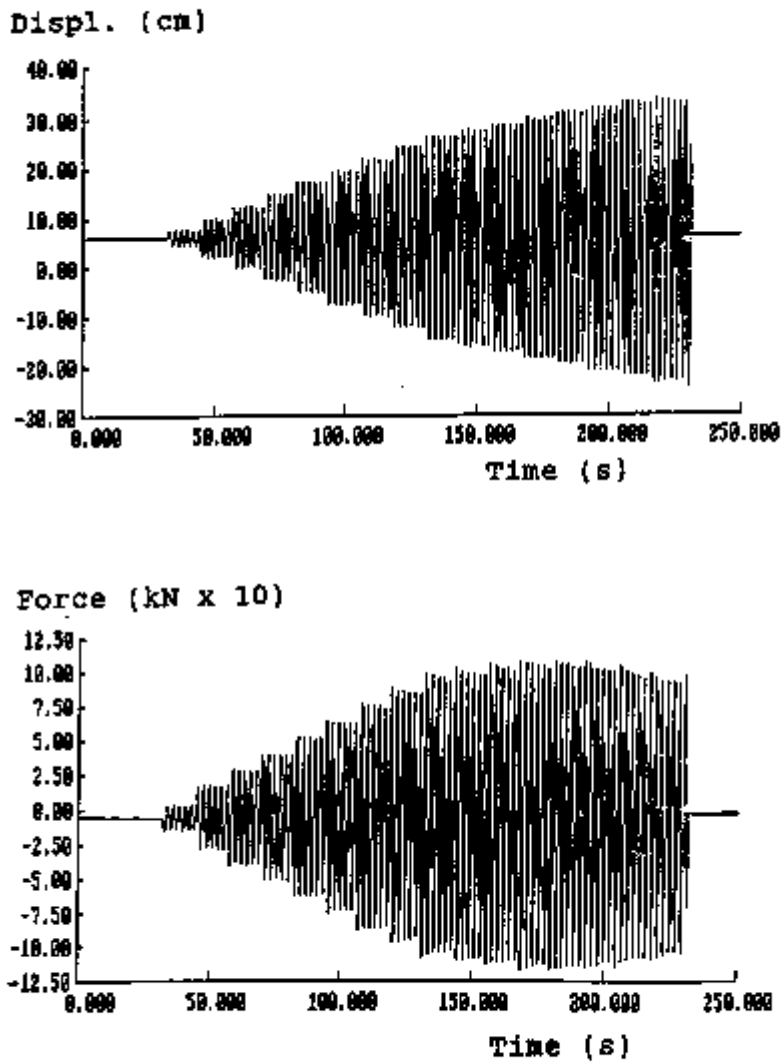

Fig. 9. Displacement and horizontal force time-histories in a dynamic test of Squillace bearings.

Finally, as to the experimental analysis of the effects of bearing attachment and compound features, the first results indicated some (hardly explainable) non-negligible effects: these must be verified through further tests in progress (the results of experiments performed later at Boschetto on a seismically isolated structure mock-up did not confirm such effects - see Sect. 6).

6 TESTS ON ISOLATED STRUCTURE MOCK-UPS

The mock-ups used in the laboratory tests performed to date, at both ISMES and Boschetto, were such as to only reproduce the mass of actual structures, being characterized by very large stiffness (reference was made to SIP buildings). Forni et al. (1991a&b) already mentioned that experiments at ISMES concerned: (a) snap-back tests of a full-scale mock-up (weighting 9,500 kN), supported by six SIP bearings, with a maximum initial displacement of 85 mm (more than 60% shear strain); (b) snap-back, sinusoidal, and one-directional (1d), 2d and 3d simultaneous seismic excitation tests - corresponding to rigid, medium and soft soil conditions in Italy - of a 1/4 scale mock-up (weighting 394 kN) supported by four 1/4 scale bearings, which was tested on the six-degrees-of-freedom (6-dof) MASTER shaking table with a maximum initial displacement of about 36 mm (100% shear strain).

Experiments recently carried out at Boschetto (November-December 1992) consisted of snap-back tests on a half-scale mock-up formed by the inertial mass of SCORPIUS shake table (weighting about 1,600 kN), which was supported by four 1/2 scale SIP-type bearings. The effects of the original and the dowelled attachment systems have been tested to date, by increasing the initial displacement to 150% shear strain (Fig. 10).

The results of the full-scale mock-up tests have already been presented in detail by Forni et al. (1991a&b), together with some data concerning the 1/4 scale mock-up. A detailed description concerning the 1/2 scale mock-up tests will be presented by Forni et al. (1993), while more information on the 1/4 scale mock-up tests is separately given to this Conference by Serino et al. (1993).

We can state here in general that all mock-up tests provided essential information on the behaviour of isolated structures and isolation systems and for the assessment and validation of calculation procedures. In all snap-back tests, the motion in the initial displacement direction lasted very few seconds only (about 3 s), and consisted in three appreciable cycles only (see Forni et al. 1991a&b and Fig. 10). Residual displacements of some millimeters (partly recovered within some hours and never additive with respect to those of previous tests) were always detected at ISMES at test conclusion: these can be attributed to the presence of later rubber cover (which can be deformed), quite long time necessary to reach the initial displacement and attachment type (which allows for a small gap between bearing and the borders of the containing steel-end plate). On the contrary, tests at Boschetto (Fig. 10) have correctly shown some effects (but more limited due to the much faster loading phase) for the original attachment system only; no other effects of dowels have been found.

The first response frequency increased considerably during motion, as displacement amplitude decreased (see Forni et al. 1991a&b and Fig. 10). This behaviour is consistent with the non-linear correlation which exists between bearing elastic forces and displacements. For similar reasons it was impossible to define an unique damping value for each entire test. The assumption of equivalent viscous damping (ß), and use of the logarithmic decrement technique, led to ßs that were rather larger than those obtained in single bearing tests, due to the strong increase of ß with decreasing displacement during each test and the hysteretic nature of energy dissipation.

In seismic tests of the 1/4 scale mock-up, large amplifications of the actual ground motion were necessary to attain 100% shear strain for medium soils (a factor 2.5 for the Tolmezzo records of 1976 Friuli earthquake), and especially, for rigid soils (such as for the San Rocco record of the

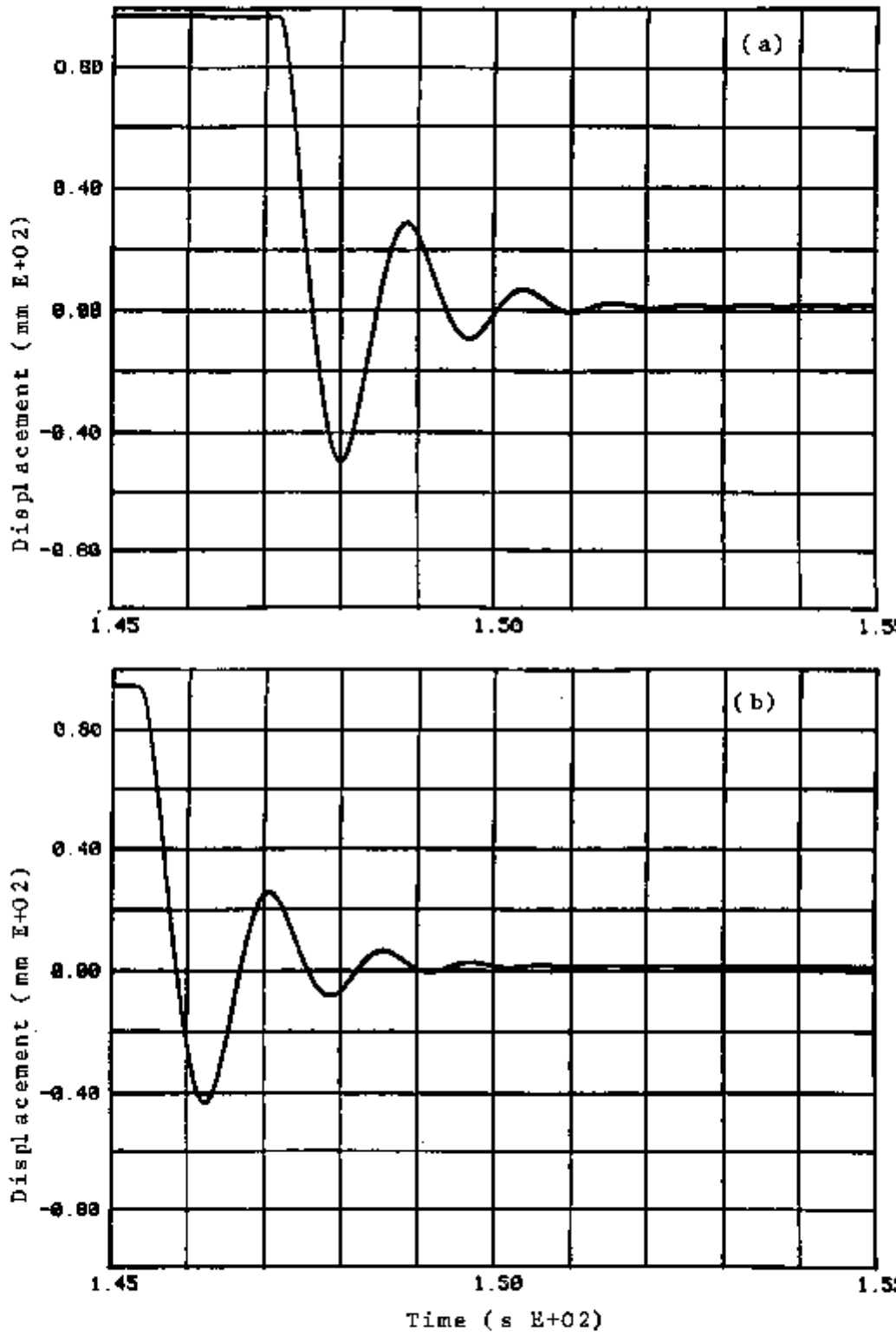

Fig. 10. Displacement time-histories measured in snap-back tests at Boschetto: initial displacements corresponding to 150% shear strain; "containment"-type (a) and dowelled (b) attachments.

same earthquake, for which the application of a factor 7 produced a displacement of some millimeters only). Even for relatively soft soils, margins - although obviously rather reduced - still exist (the design displacement was reached by increasing the Calitri record of 1980 Irpinia earthquake by a factor 1.12). A significant reduction of the motion through the isolation system was obtained (peak accelerations was reduced by 85% for San Rocco records, 90% for Tolmezzo records and 60% even for Calitri records). 2d and 3d interaction effects on isolation bearings were found very small. Peak response acceleration varied almost linearly versus the scale factor applied to each input acceleration record in the various tests concerning each of the three eathquakes (despite the strongly non-linear behaviour of bearings). Also, no residual displacements were detected, according to the fast load application in shake table tests.

Finally, reproducibility of test results was successfully verified for all mock-ups.

7 IN-SITU TESTS OF ACTUAL ISOLATED BUILDINGS

Forni et al. (1991a&b) presented the main features and results of the in-situ dynamic tests of the SIP building (Fig. 1) and the related numerical analysis. These tests had been performed by ENEL, ENEA and ISMES in 1990. We recall that the building had been subjected to both forced excitation and snap-back tests. Maximum initial displacement attained in the latter had been 107 mm (75% shear strain). The results demonstrated the safety of isolated buildings and confirmed those obtained for the mock-ups, as to variation and level of horizontal stiffness, damping, residual displacements and reproducibility of data; they showed that the building quasi exclusively behaves as a rigid body and demostrated the adequacy of the isolation system. Forced excitation tests - performed by use of a mechanical vibrator installed on the building roof - allowed for the dynamic characterization of the superstructure and verification of design and pre-test analysis.

Forni et al. (1991b) also presented the main features of in-situ tests performed by ENEL and ISMES on both twin houses at Squillace (Fig. 2) in 1991. These houses were subjected to both forced excitation tests (by use of a mechanical vibrator located on the roof) and ambient vibration measurement of wind-, truck- and train-induced microtremors. We recall here that test results confirmed the large, beneficial effects of seismic isolation (an example of comparison between the responses of the isolated building and the conventional is shown here by Fig. 11).

8 NUMERICAL ANALYSIS OF INDIVIDUAL BEARINGS

Both simple bearing models and detailed finite-element (f.e.) three-dimensional (3D) models were set up (Martelli et al. 1991b and Forni et al. 1991b). Simple models have been based on the results of single bearing tests: models formed by a spring in parallel to a viscous damper, where both horizontal stiffness and viscous damping ratio vary with displacement, have been developed by ENEA; models based on hysteretic damping have also been developed at ISMES (Serino et al., 1993).

Detailed (3D) bearing models, to be used for design and the analysis of the effects of defects, have been considerably improved by ENEA with respect to some first attempts described by Martelli et al. (1991b). The details of these improvements will be reported by Forni et al. (1993). We note here that models are now consisting of separate 8-node solid elements for the rubber and 4-node shell elements for steel, which have been implemented in ABAQUS for both the original and modified SIP-type bearings (Fig. 12). While three axial subdivisions of each rubber layer have been found sufficient to correctly calculate bearing horizontal stiffness and vibrational behaviour, at least six were found necessary for the vertical.

Calculations by use of both an elastic bearing model and a hyperelastic model of the rubber

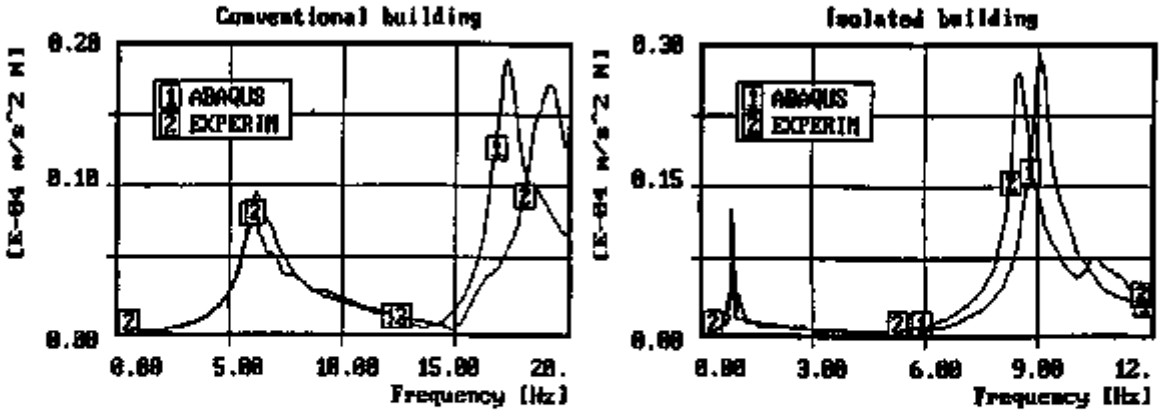

Fig. 11. Measured and calculated transfer functions at the roof of Squillace buildings.

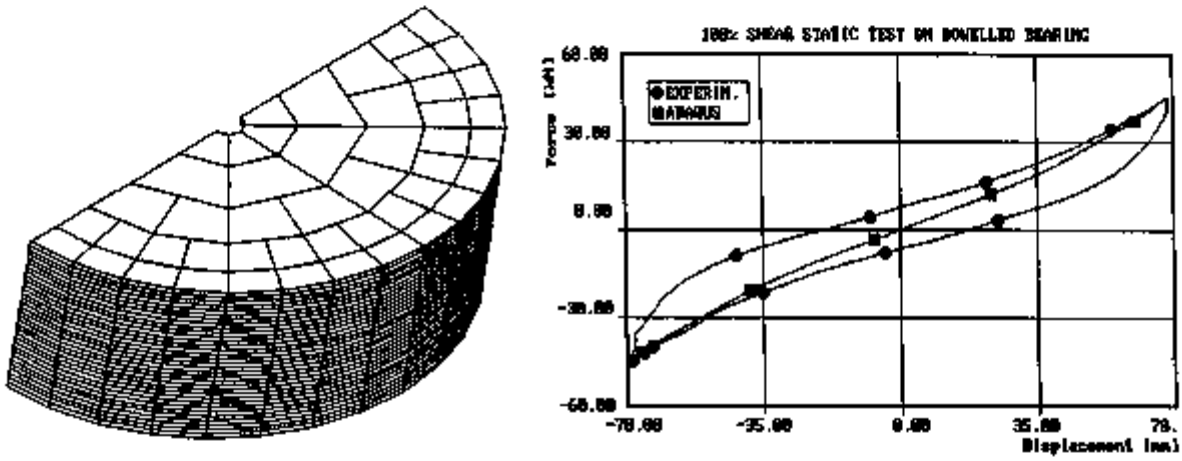

Fig. 12. 3D hyperelastic isolator model: comparison between measured & calculated response.

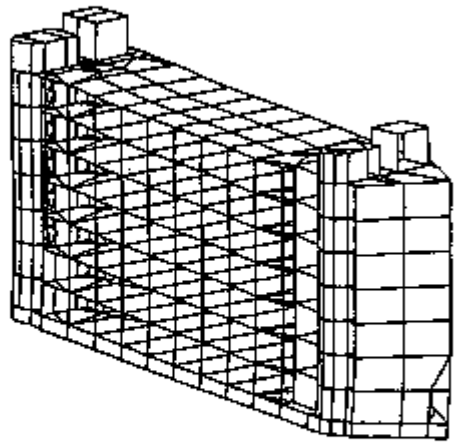

Fig. 13. First vibration mode computed with ABAQUS for the superstructure of the SIP building subjected to in-situ tests at Ancona in 1990.

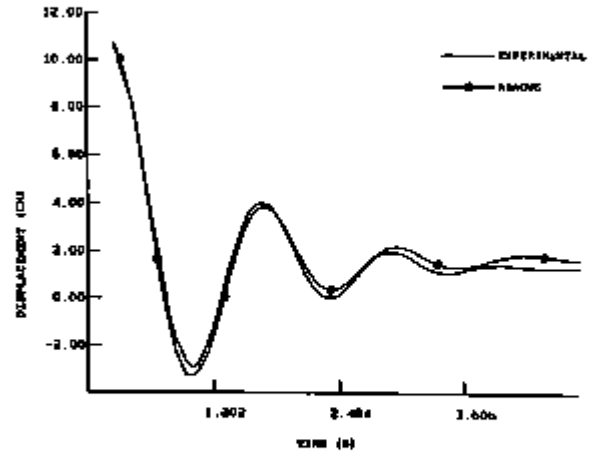

Fig. 14. Measured and calculated displacement of SIP building in the most severe snap-back test (single isolator stiffness; damping measured for the 9,500 kN mock-up).

(based on the results of tests on specimens) have been performed, to evaluate natural frequencies and stiffnesses of bearings. Moreover, an elastic-plastic model has also been used for steel. Mesh simplifications have been analysed, to limit the computer time which was necessary to calculate horizontal stiffness, to acceptable values, without significantly affecting the results. The effects of steel plastic behaviour has been found negligible to 100% shear strain. The use of the rubber hyperelastic model has already led to excellent results regarding both the behaviour of specimens in the different loading conditions (Figs. 4 and 5) and the horizontal stiffness of bearings to 100% shear strain (Fig. 12). Further specimen tests at large shear strain are initiating: they will also allow for a correct evaluation of bearings vertical stiffness. Studies are also in progress to implement an adequate damping model in ABAQUS.

9 NUMERICAL ANALYSIS OF ISOLATED STRUCTURES

Finite-difference programs were set up by Martelli et al. (1991b) and Forni et al. (1991b) for the analysis of isolated structures, in the case that they can be represented by sets of 1-dof oscillators. The program ISOLAE includes the aforementioned simple bearing model of ENEA, where both stiffness and damping depend on displacement and the effects of viscous creep are accounted for. In ISOLAE, the structure can be now represented by a system of 1-dof viscous linear oscillators, which represent the fundamental vibration modes. A similar program has been based by Serino et al. (1993) on the bearing model developed at ISMES.

ISOLAE analysis performed by Forni et al. (1991b), concerning test results for both isolated structure mock-ups and isolated buildings, demonstrated the applicability of single bearing test data (stiffness and damping dependences on displacement) to analyse the dynamic behaviour of isolated structures. The good agreement obtained by Forni et al. (1991b) for the SIP building also, confirmed that buildings can be really considered as rigid bodies, to evaluate their main seismic motion, if deformation frequencies of the superstructure are sufficiently larger than the rigid body values of the isolated construction.

Furthermore, as already mentioned by Martelli et al. (1991b), f.e. models with constant viscous damping were implemented by ENEA in ABAQUS, and have also been used for the analysis of all tested isolated structures. ABAQUS calculations have included both the analysis of experimental data and the evaluation of building responses to the previously mentioned Italian earthquakes corresponding to rigid, medium and relatively soft soil conditions (the latter has accounted for simultaneous excitation effects also); they have been based on both models where a very large stiffness was assumed for the structure, and for buildings, sophisticated 3D f.e. models of the superstructure, as well. The 3D f.e. model of the SIP building (Fig. 13) has been derived from that used for design analysis and pre-test calculations. 3D models of the twin Squillace buildings will be described in detail by Forni et al. (1993).

Studies concerning the mock-ups tested at ISMES and both twin houses tested at Squillace have already been completed, while the analysis of the Boschetto test results and the data concerning SIP buildings is in progress. Forni et al. (1991b) already showed that mock-up and building calculations performed with ABAQUS by use of a rigid mass model have led to results which are very similar to those obtained by ISOLAE. As to the SIP building, 3D calculations by use of direct integration (Fig. 14) have already led to results which also agree with the experimental data and are very similar to those obtained by assuming the building as infinitely rigid. Good agreement between calculations and measurements has also been obtained for both twin houses at Squillace (Fig. 11), together with the demonstration that the isolation system used is effective in the case of severe Italian earthquakes.

10 CONCLUSIONS

This paper has shown that great efforts are in progress in Italy for the development and application of seismic isolation to nuclear and non-nuclear structures. The importance, for nuclear reactors, of information acquired on isolated civil buildings has been stressed. Some more details and some extensions of the work will be described by Forni et al. (1993). It has been mentioned that the development studies are being carried out in the framework of wide-ranging national collaborations, such as those foreseen by GLIS. They also take advantage of international cooperations: within these it is worth citing the organization of International Post-SMiRT Conference Seminars on seismic isolation and other innovative antiseismic design techniques: the third of these ("Isolation, Energy Dissipation and Control of Vibrations of Structures") will be held at Capri (Italy) on August 23 to 25, 1993.

REFERENCES

Bonacina, G., Venturuzzo, M., and Bettinali, F. 1993. *Seismic Isolation of Non-Nuclear Power Plants in Italy.* Proc. of the Post 12th SMiRT Conference Seminar on Isolation, Energy Dissipation and Control of Vibrations of Structures. Ascoli Piceno, Italy: CREA.

Forni, M., Martelli, A., Spadoni, B., Bonacina, G., Pucci, G., and Zola, M. 1991a. *Dynamic Experiments Performed in Italy on Seismically Isolated Structure Mock-Ups in the Framework of the R&D Studies for the Innovative Nuclear Reactors.* Proc. of the 11th SMiRT Conference. Tokyo: Atomic Energy Society of Japan. Vol. K2: 205-210.

Forni, M., Indirli, M., Martelli, A., Masoni, P., Spadoni, B., Bettinali, F., Bonacina, G., Pucci, G., Serino, G., Giuliani, G.C., and Marioni, A. 1991b. *Most Recent Results of R&D Studies in Progress in Italy on Seismic Isolation.* Proc. of the 11th SMiRT Post Conference Seminar on Seismic Isolation of Nuclear and Non-Nuclear Structures: 263-293. Tokyo: Shimizu Corp.

Forni, M., Indirli, M., Martelli, A., Spadoni, B., Di Pasquale, G., Pugliese, A., Sanò, T., Bettinali, F., Marioni, A., Bonacina, G., Mazzieri, C., Serino, G., Grassi, L., Sobrero, E., and Vestroni, F. 1993. *Most Recent Developments on Seismic Isolation of Nuclear Facilities in Italy.* Proc. of the Post 12th SMiRT Conference Seminar on Isolation, Energy Dissipation and Control of Vibrations of Structures. Ascoli Piceno, Italy: CREA.

Martelli, A., Forni, M., Spadoni, B., and Bonacina, G. 1991a. *Static and Dynamic Experiments Performed in Italy on Seismic Isolation in the Framework of the R&D Studies for the Innovative Nuclear Reactors.* Proc. of the 11th SMiRT Conference. Tokyo: Atomic Energy Society of Japan. Vol. K2: 199-204.

Martelli, A., Bettinali, F., Sanò, T., Bonacina, G., Giangreco E., and Marioni, A. 1991b. *Overview on the Activities in Progress on Seismic Isolation in Italy and Future R&D Work.* Proc. of the 11th SMiRT Post Conference Seminar on Seismic Isolation of Nuclear and Non-Nuclear Structures: 29-43. Tokyo: Shimizu Corporation.

Martelli, A., Parducci, A., and Forni, M. 1993a. *State-of-the-Art on Development and Application of Seismic Isolation and Other Innovative Seismic Design Techniques in Italy.* Proc. of the ATC-17-1 Seminar on Seismic Isolation, Passive Energy Dissipation, and Active Control. Redwood City, California: Advanced Technology Council.

Martelli, A., Carpani, B., Forni, M., Di Pasquale, G., Sanò, T., Bonacina, G., Olivieri, M., Marioni, A., Cesari, G.F.. 1993b. *Extension of Guidelines for Seismically Isolated Reactors.* Proc. of the 12th SMiRT Conference. Amsterdam: Elsevier Science Publishers B.V.

Serino, G., Bonacina, G., and Bettinali, F. 1993. *Proposal and Experimental Validation of Analytical Models for Seismic and Vibration Isolation Devices in Nuclear and Non-Nuclear Facilities.* Proc. of the 12th SMiRT Conference. Amsterdam: Elsevier Science Publishers B.V.

SMiRT-12 / K. Kussmaul (Editor)

K24/2

EXTENSION OF GUIDELINES FOR SEISMICALLY ISOLATED REACTORS

A. Martelli[1], B. Carpani[1], M. Forni[1], G. di Pasquale[2], T. Sano[2], G. Bonacina[3], M. Olivieri[4], A. Marioni[5] and G.F. Cesari[6]

[1]ENEA, Department of Innovative Reactors, Bologna, [2]ENEA, Directorate for Nuclear Safety and Health Protection, Roma, [3]ISMES S.p.A., Bergamo, [4]ANSALDO-Ricerche, Genova, [5]ALGA Sp.A., Milano, [6]University of Bologna (Italy)

ABSTRACT

The preparation of a proposal for design guidelines for seismically isolated nuclear reactors has been initiated with the sponsorship of the Commission of European Community. This work aims at (a) updating an existing document which covers the case of high damping steel-laminated rubber bearings, and (b) extending it to the other isolator types of interest.

1 INTRODUCTION

Forni et al. (1993a) have stressed in a separate paper that considerable efforts have been devoted in Italy for some years to the development and application of seismic isolation for both civil structures and industrial plants, including nuclear reactors. Studies in progress concern both experimental and numerical research, and the preparation of design guidelines for isolated structures. This paper reports on the state of activities on guidelines development, focussing on those for nuclear reactors (research work has been presented by Forni et al., 1993a).

2 EXISTING PROPOSAL FOR DESIGN GUIDELINES FOR NUCLEAR REACTORS

As mentioned by Forni et al. (1993a), the preparation of a proposal for design guidelines for nuclear power plants using high damping steel-laminated elastomer bearings (HDBRs) to provide horizontal isolation (i.e. HDRBs which are very stiff in the vertical direction) began in 1988, in the framework of a cooperation between the ENEA Department of Innovative Reactors (RIN) and GE Nuclear Energy, and with the support of experts of the ENEA Directorate for Nuclear Safety and Health Protection (DISP), ISMES and Bechtel National Inc. The reason for choosing the HDBR was that this isolator type was considered to be one of the most innovative and suitable for application to advanced nuclear reactors, and that it was used in the first applications of seismic isolation to large buildings in Italy (Forni et al., 1993a).

The guidelines document was prepared taking into account the most recent information available at the time on seismic analysis of nuclear reactors in general and the state-of-the-art of engineering design of isolated structures. One of its purposes was to identify items which required further R&D. It mainly dealt with items different from non-isolated systems. Although particular attention was paid to the case of Liquid Metal Reactors (due to their sensitivity to earthquakes), the proposal also aimed at fully covering other types of nuclear reactors that are

isolated by means of HDRBs. The proposal consisted of the following sections: (a) definition of ground motions; (b) design requirements and analysis methods for isolated buildings and isolation support structure; (c) design and performance requirements of overall seismic isolation systems; (d) design requirements and analysis methods for isolated structures, systems and components; (e) design requirements and analysis methods for interface components; (f) design requirements for individual isolation devices; (g) qualification of seismic isolation bearing and isolation system; (h) acceptance testing of isolation devices; (i) seismic isolation reliability; (j) seismic safety margin; (k) seismic safety and monitoring systems. In addition, two appendices were included: (A) simplified methods for design of isolation bearings; (B) proposed procedure for establishing design parameters for seismic isolator bearings.

The document was published by Martelli et al. (1990) in a tentative form to allow for a broad review. Its main features were also summarized by Martelli et al. (1992), together with some first information on the R&D studies which had been undertaken at the time to allow for a more complete proposal. In fact, as expected, some safety factors to be used in the design, some test parameters and some details of qualification and analysis procedures were not defined, yet, in the document of Martelli et al. (1990): these were indicated there as TBD, i.e. "To Be Determined", because the exact definition of these items required specific R&D work.

3 GUIDELINES DEVELOPMENT FOR NON-NUCLEAR ISOLATED STRUCTURES

Activities also soon began in Italy to prepare national guidelines concerning the use of seismic isolation and passive energy dissipation systems in civil structures. These activities take advantage of wide-ranging collaborations which had been established, such as those of the Italian Working Group on Seismic Isolation (GLIS, see Forni et al., 1993a). More precisely:

(a) The preparation of a proposal concerning the isolation bearings and passive energy dissipation systems which have been judged of interest for buildings and bridges was undertaken by specific groups established by the Italian Standard Authority (UNI) and was later entrusted to Italian experts by the European Community (CEN TC 167/SC1: Structural Antiseismic Devices). ENEA, ISMES, ANSALDO-Ricerche and other GLIS members are participating in these activities .

(b) The preparation of a guidelines document to be used by designers of isolated buildings (to get the approval for contruction by the High Council of Public Works) was undertaken by the National Seismic Service, in cooperation with ENEA, ENEL and ISMES (Dolce et al., 1993).

Both documents are being completed (February 1993). Finally, a specific subgroup of GLIS was formed: its tasks are to collect, analyse, comment and if necessary, integrate the available guidelines documents and regulations (Forni et al., 1993b). It is noted that the contribution of ENEA and ISMES to the development of documents concerning civil structures took great advantage from the experience gained through the preparation of the proposal of Martelli et al. (1990). In turn, both guidelines development work and research performed for civil structures have been very useful to clarify items applicable to nuclear reactors also.

4 UPDATE AND EXTENSION OF THE EXISTING PROPOSAL FOR DESIGN GUIDELINES FOR NUCLEAR REACTORS

Martelli et al. (1990 & 1992) stated that their proposal would have been periodically updated to include comments and to reflect the advances of seismic isolation technology developments. A first revision of the document has already been prepared according to comments officially received by ENEA-DISP, the American Society of Civil Engineers and Malaysian Rubber

Producers' Association. This revision has been submitted to GE Nuclear Energy.

Furthermore, work to update and extend this document to nuclear reactors using bearings different from the HDRB and energy dissipation devices has been initiated by ENEA, within studies sponsored by the Commission of the European Community (CEC) in the framework of the Study Contract ETNU-CT-91-0031. Work for the CEC is being performed in cooperation with ALGA, ISMES, ANSALDO-Ricerche and the Nuclear Engineering Laboratory (LIN) of the Bologna University. It consists of the following activities:

(a) Revision of the document based on further comments and updated analysis of the state-of-the-art on design of isolated nuclear and non-nuclear structures in Europe.

(b) Extension of the document to: (b1) other horizontal isolation systems of interest for the European projects (neoprene bearings, sliding devices, etc.); (b2) the other types of horizontal isolation systems of general interest (other elastomeric isolators, including lead plug and low damping rubber bearings, etc.); and (b3) three-directional isolation.

(c) Identification of items to be precised through further R&D and specification of the related necessary work.

These activities take into account the other available proposals and recommendations for design guidelines for isolated structures, and take advantage of the co-operations existing between ENEA and other national and foreign organizations. At the time being (Ferbruary 1993), phase (a) is in progress. Work consists in a careful re-analysis of the document revision, made by ENEA, ISMES and ANSALDO-Ricerche, which accounts - among others - for the results of experiments and numerical analyses described by Forni et al. (1993a). Par. 5 reports the main comments (if any), to the different sections of the proposal published by Martelli et al. (1990), which were later included or suggested. It also points out items which are still TBD.

5 REMARKS ON THE EXISTING PROPOSAL FOR DESIGN GUIDELINES FOR NUCLEAR REACTORS

In general, it was suggested that, because of the large number of referenced documents, the most important information of these shall be included in comments. Also, some references shall be updated; in particular, reference should be made to the Appendix SEAOC-1991 or even to the 1991 Uniform Building Code. Finally, the Appendix of Martelli et al. (1990) shall be re-written according to recent of ISMES and ENEL work.

5.1 Definition of Ground Motions (§ 5)

Probabilistic evaluations of SSE and OBE were suggested, together with specification of OBE requirements similar to those adopted in the USA for some ALWRs (§§ 5.1.1-5.1.2). The requirement that design response spectra in the frequency range to 1 Hz shall be equal at least to that specified by R.G. 1.60 was changed to a suggestion (§ 5.1.3). Specific requirements concerning the features of design time-histories (according to App. D of NUREG/CR 5374) were moved from § 6.8.3 to § 5.1.6 and better precised there. Specification of criteria for the choise of time-histories or spectra was suggested (§§ 5.1.6-5.1.8). The need for a characterization of ground motion rotational components, if necessary, was specified (§ 5.1.8).

5.2 Requirements & Methods for Isolated Buildings & Isolation Support Structures (§ 6)

Account for accidental eccentricity due rotational ground motion component was suggested to

determine Reference Displacement (§ 6.1.2). Requirements concerning the calculation of the Design Displacement were modified, suggesting the use of 90% the Reference Displacement in the second criterion of § 6.1.4 (comments to such a reduction were later suggested). Requirements concerning the definition of gaps were also modified, suggesting the use of 80% the sum of the absolute values of structures' Reference Displacements, in the second criterion of § 6.5.1; it was also specified there that gaps shall remain free in every design condition (e.g. flood). The maximum damping ratio which can be assumed at SSE was modified to 15% (§ 6.7.2). It was suggested to refer to foundation rigidity instead of foundation flexibility, in § 6.7.5. The use of SRSS method, to combine results of separate one-directional analyses, was replaced by the Absolute Sum method, and requirements concerning the contribution of rotational components of the input motion where introduced in § 6.8.1. A further modification of § 6.8.3, so as to include the possibility of using a single set of input time-histories, was suggested (by moving there the contents of § 8.5 and the last sentence of § 8.4).

Some TBD values remain as to features of fail-safe systems and safety factor for gaps between separately isolated adjacent structures. Furthermore, a new TBD value was introduced concerning which contribution of rotational effects makes it necessary to account for this effect.

5.3 Requirements for Overall Seismic Isolation Systems (§ 7)

Modification of § 7.1.1 (by simply referring to § 6.1.4) was suggested. The minimum value of isolation frequency range to be chosen was lowered from 0.5 Hz to 0.33 Hz (§ 7.2.1.1). It was suggested to specify, in § 7.2.1.2, that vertical stiffness shall be sufficiently high to avoid not only vertical amplification, but also rocking. The value of 10% was specified as to the minimum equivalent viscous damping ratio which shall correspond to design displacement (§ 7.2.2.1); however, a careful evaluation of this item was later suggested. The need for investigating the effects of so called "minor earthquakes" was stressed (§ 7.2.5.3).

TBD values remain for safety factors applicable to horizontal displacement and maximum design vertical load to be used for the design of isolation system (the first being equal to that to be used for gaps), as well as to permissible variations of isolation system stiffness and damping.

5.4 Requirements & Methods for Isolated Structures Systems & Components (§ 8)

Reference to the NUREG/CR-1161 Report, as to simplified rules to evaluate sloshing motion, was included as comment to § 8.7.

5.5 Requirements for Individual Isolation Devices (§ 10)

The need that vertical load capacity shall account for buckling effects was stressed (§ 10.2). Safety factors were specified for the maximum horizontal displacement (2), and vertical load and horizontal displacement at which the isolator shall be designed to be stable (both 1.7) (§§ 10.3.1-10.3.2). The requirement that safety factors shall account for roll-over - if relevant - was introduced (§ 10.3.3). As to § 10.4.4, it was recalled that large temperature effects were measured below 0 C by Forni et al. (1993a). The reduction to three, of the number of cycles for the evaluation of damping, was suggested (§ 10.6). A criterion to evaluate fatigue life was proposed, the very large number of cycles at large shear strain before failure in US tests was stressed, and a requirement such as that foreseen in the IEC-980/1989 document was suggested (§ 10.7.2). The requirement that environmental conditions shall also include various chemical and

biological attacks was specified, and tests for the evaluation of aging due to thermal and radiation effects were suggested, together with the specification of engineering solutions to reduce the risk connected to fire attack (§ 10.8). The need for defining the temperature at which creep effects shall be evaluated was stressed (§ 10.9). Finally, requirements that degradation due to aging shall not reduce safety factors below specified values, and that isolators shall survive the faulted condition at the end of their design life were introduced (new §§ 10.10.1 and 10.10.2).

Several TBD values remained, for instance for environmental effects, tests to be performed to evaluate the maximum offset, uplift and rocking, disengagement of dowelled bearings and tests to be performed on the rubber compound (although the latter were suggested).

5.6 Qualification of Seismic Isolator Bearings (§ 11)

It was suggested to cancel the possibility of analytical qualification of single isolators, to consider that isolator qualification shall not be limited to seismic effects, and to include reference to IEC standards (e.g. IEC 780-1984 and IEC-980-1989) in comments to §§ 11.1.1-11.1.3 and to IEEE Std 323-1983 in § 11.1.3. The requirement that the manufacturing process of isolation bearings shall be qualified was introduced (§ 11.1.5). It was suggested to extend the use of tests on scaled bearings according to the US seismic bearing qualification program presented at the 1992 IAEA Meeting on Seismic Isolation Technology (§ 11.2), and also, to use § 11.2.1 for general requirements, thus adding that qualification is necessary every time that isolators with new features are developed and defining acceptance criteria according to Dolce et al. (1993); it was also stressed that § 11.2.1 shall require the repetition of the same tests on four aged bearings, as those performed before in their virgin conditions. It was suggested to only outline, as requirements of § 11.2.2, tests to be performed (according to Dolce et al. 1993) and to include proposed details of tests procedures as comments (detailed definition shall be carried out in the framework of test procedures and specifications). Environmental effects such as temperature were introduced among those to be considered and it was suggested to repeat qualification tests after artificial aging globally accounting for environmental conditions (§ 11.2.3). It was suggested to refer to Dolce et al. (1993) for tests concerning the evaluation of vertical load variation on horizontal parameters (§ 11.2.5). Some questions arose on the difficulty, in some cases, of performing shake table tests on scaled isolated structure mock-ups (§ 11.3.1), and real need for multifrequencial simultaneous three-directional excitations (§ 11.3.2). The recommendation of performing forced excitation tests - if feasible - on isolated structures, in the case that snap-back tests cannot be performed, was added in § 11.3.3; further recommendations concerned the use of snap-back tests on scaled mock-ups if those on actual structures are not feasible; however, it was later suggested to only make a generic recommendation that in-situ tests should be performed, in the requirements of § 11.3.3, and to cite the different techniques as comments.

5.7 Acceptance Testing of Isolation Devices (§ 12)

It was suggested: to require the measurement of vertical stiffness for all bearings (§ 12.1.1); to include tolerance classes for some geometrical sizes as a comment to § 12.2.1; to replace - where feasible - the destructive controls required on isolators in § 12.2.3 by controls during the assembly phase (those foreseen by Martelli et al. 1990 are very costly, due to the limited number of bearings per batch); to move, to comments, the detailed description of compression tests and combined compression and shear tests (§ 12.2.3 and § 12.2.5), and not to suggest any procedure (only the important topics shall be outlined). A TBD fraction of the isolator heigh measured during qualification tests (which if exceeded determines isolator rejection) was introduced in §

12.2.4 concerning sustained compression tests; however, it was later suggested to cancel the entire section (because undesirable effects may be detected during qualification or measurement of vertical stiffness), or at least, to limit tests to 20% of the isolators (to be selected using statistical criteria). It was finally suggested to comment, in § 12.2.6, that tensile tests are required only if tension is foreseen in the design (it is noted that TBD values remain as to such tests).

5.8 Seismic Isolation Reliability (§ 13)

Reference to finite-element analysis as to the evaluation of phenomena affecting the bearing reliability was cancelled, together with the entire § 13.4.2, concerning submission of the in-service inspection program to the Licensing Authorities (otherwise, reference to these Authorities should be also made for other items). It was specified in § 10.4.3 that OBE is the "significant earthquake" after which tests shall be performed on a larger numbers of bearings (this number, however, remains TBD, together with the number of bearings to be usually tested and time interval for more detailed controls).

5.9 Seismic Safety Margin Assessment (§ 14)

Comments to § 14.1.1 were moved to prescriptions. However, it was later commented that the entire § 14 is too detailed, thus it was suggested to shorten it considerably, by making reference to the documents describing PRA and SME procedures and limiting requirements to specific items caused by the adoption of seismic isolation (definition of seismic input, isolation effects on the response to beyond SSE earthquakes, evaluation of the seismic capability/fragility of the isolation system itself).

6 CONCLUSIONS

This paper has summarized activities in progress in Italy on the development of design guidelines for isolated structures, focussing on those concerning nuclear reactors. Information has been provided on work in progress to update and extend the proposal of Martelli et al. (1990). Advancements will be reported by Forni et al. (1993b).

REFERENCES

Dolce, M., et al. 1993. *Linee Guida per il Progetto di Edifici con Isolamento Sismico*. Roma, Italy: Servizio Sismico Nazionale della Presidenza del Consiglio dei Ministri (in Italian).

Forni, M., et al. 1993a. *Most Recent Experimental and Numerical Studies Performed in Italy on Seismic Isolation*. Proceedings of the 12th SMiRT Conference. Amsterdam: Elsevier.

Forni, M., et al. 1993b. *Most Recent Developments on Seismic Isolation of Nuclear Facilities in Italy*. Proceedings of the Post 12th SMiRT Conference Seminar on Isolation, Energy Dissipation and Control of Vibrations of Structures. Ascoli Piceno, Italy: CREA.

Martelli, A., et al. 1990. *Proposal for Guidelines for Seismically Isolated Nuclear Power Plants - Horizontal Isolation Systems Using High Damping Steel-Laminated Elastomer Bearings*. Energia Nucleare. 1: 67-95.

Martelli, A., et al. 1992. *Development of Design Guidelines for Seismically Isolated Nuclear Reactors and R&D Work Performed by ENEA*. Nuclear Technology. 97: 153-169.

SMiRT-12 / K. Kussmaul (Editor)
1993 Elsevier Science Publishers B.V.

K23/6

SEISMIC RESPONSE OF A BASE-ISOLATED BUILDING WITH HIGH DAMPING-LOW SHEAR MODULUS ELASTOMERIC BEARINGS

C.Y. Wang[1], Y.W. Chang[1], R.F. Kulak[1], R.W. Seidensticker[1]T. Kuroda[2] and M. Kobatake[2]

[1]Reactor Engineering Division, Argonne National Laboratory, 9700 S. Cass Avenue, Argonne, IL 60439, USA
[2]Nuclear Power Division, Shimizu Corporation, Tokyo, Japan

ABSTRACT

This paper deals with an investigation of seismic responses of a base-isolated building subjected to actual earthquakes. The isolation system consists of six medium shape factor, high damping, low shear modulus bearings designed by ANL and manufactured in the United Kingdom. The objective is two-fold: (1) to study the effectiveness of the isolated bearings through responses of the test building under actual earthquakes, and (2) to validate the 3-D SISEC program.

Results obtained from the earthquake observations indicate that the advantage of the base-isolation system in mitigating the acceleration of the superstructure is very pronounced. For earthquakes #42 and #44, the accelerations at the roof level of the isolated building are only 20% to 30% of the ordinary building accelerations. Also, for both ordinary and base-isolated buildings the computed accelerations agree reasonably well with those recorded.

1 INTRODUCTION

Seismic isolation is gaining attention worldwide for use in a wide spectrum of structures and critical facilities, including bridges, office buildings, hospitals, computing and telecommunication centers, as well as nuclear facilities. Today there are over 125 structures worldwide which are isolated and the numbers have been increasing steadily in the past few years. Also, substantial research efforts have been devoted to the designs, testing of isolation bearings, as well as development of analytical methods for predicting the responses of isolated structures.

An international cooperation program was initiated in September, 1988 by Argonne National Laboratory (ANL) of the USA and Shimizu Corporation of Japan for studying the response of isolated structures under actual earthquakes. Within the program agreement, Shimizu provided their test facility and earthquake data collection while ANL supplied the isolation bearings to be installed at the test facility and performed most of the analytical simulations utilizing the ANL developed 3-D computer program, SISEC (Seismic Isolation System Evaluation Code) (Wang et al., 1991).

To ensure the accuracy of the analytical simulation, recorded data of full-size reinforced concrete structures are used as the benchmarks for comparisons of code simulations with observations. Also, numerical calculations were carried out for the ordinary building, aimed at studying the relative responses of these two structures.

Two high-damping isolation systems, designed by ANL, were installed in the isolated building of the test facility. The first one, installed in April 1989, was a high shape factor, high shear modulus rubber bearing system aimed for medium and large earthquakes. From April 1989 to July 1990 thirty-seven (37) earthquakes have been recorded. Detailed responses of the test facility were analyzed and reported (Wang & Gvildys 1991; Uras 1993). The second one was a medium shape factor, low shear modulus bearing system designed for a wide range of earthquakes, including small earthquakes. This system was installed in October 1990. This paper addresses the response of the low shear modulus bearing system.

From November 1990 to March 1991, seven earthquake motions were observed at the test facility (Kuroda et al., 1991). Complete records of two representative earthquakes, #42 and #44, are used in this paper. In the analysis, 3-D models were developed for simulating the seismic responses of the ordinary and isolated structures. Correlations of observed and calculated accelerations at all instrument locations are made. The advantage of the base-isolation system in reducing the seismic accelerations is also discussed.

2 TEST FACILITY

Two test buildings, one conventionally designed and the other base-isolated, were constructed side-by-side at Tohoku University in Sendai, which is located in the northern part of Japan. The test buildings consist of two full-size, three-story reinforced concrete structures as shown in Fig. 1. The dimensions and construction details of the superstructure were exactly the same for both buildings. The buildings were constructed as rigid frame structures with outer walls made of light weight concrete panels. The test buildings were completed in May 1986.

The isolation system of the base isolated building consists of six identical bearings (Fig. 2) designed with a medium shape factor and molded with a high damping, low shear modulus rubber. These bearings are laminated composites with 12 layers of rubber and 11 layers of steel plates (shims) manufactured by Rubber Consultants, UK. Note that the U.S. bearings previously installed in the Sendai isolated building between April 1989 and July 1990 were high-shape-factor bearings (Wang & Gvildys, 1991) with 33 rubber layers and 32 shims.

3 MATHEMATICAL MODELS

Three-dimensional frame models are used in numerical simulations for both convention and base-isolated buildings. In the analyses, beams, columns, and girders are all modeled by 3-D beam elements with six degrees of freedom per node to account for the translations and rotations generated from seismic events. Stiffnesses of the outer walls and partitions that are not structurally connected to the beams and girders are neglected in the calculation. However, their masses are appropriately lumped to the element nodal points, so that their inertia effects are included in the analysis.

The mathematical models of both ordinary and base-isolated buildings are given in Fig. 3. These two models are almost identical except that different modeling techniques are used for the substructure connecting the basement slab and the first floor. More specifically, the major difference (in the models) is in the middle portion of the support columns where the isolator is located. For the ordinary building, each basement column is represented by three beam elements in which the stiffness of the basement reinforced concrete wall is included. For the isolated building, on the other hand, the isolator is modeled by two spring elements; one linear spring and one nonlinear elastoplastic spring to simulate, respectively, the vertical and horizontal

responses of the isolator. Two beam elements, similar to those columns of the superstructure are then utilized above and below the isolator to model the reinforced concrete pedestals.

In calculating the horizontal response of the isolator a bilinear force-displacement constitutive equation is used for the nonlinear spring element. This relationship is determined from the dynamic tests of the ANL bearings conducted by the University of California at Berkeley (Kelly, 1991).

4 RESULTS AND DISCUSSIONS

In simulating the responses of ordinary and isolated buildings, the X (transverse) and Y (longitudinal) direction accelerations observed at the center of the basement of the isolated building are utilized as input to the basement structural nodes. The computed accelerations are then compared with the recorded observations.

For simplicity, comparison of observed and calculated peak accelerations at the first floor and the roof level of both the ordinary and isolated buildings are given in Table 1. As seen from this table, the maximum accelerations obtained from recorded data and SISEC simulations agree satisfactorily with each other. In fact, for both earthquakes (#42 and #44), the deviation between the calculated and observed accelerations at both the first floor and the roof levels of the isolated building is within 21%.

To study the effectiveness of the base-isolation system, Table 1 further lists the acceleration ratio, i.e., the acceleration of the isolated building A_I divided by the acceleration of the ordinary building A_O. The advantage of the base isolation system in mitigating the seismic response is quite evident. For earthquake #42, the simulated transverse acceleration at the first floor of the isolation building is about 54% of the ordinary building, whereas in the recorded data it is about 66%. At the roof level, the advantage of base isolation becomes more pronounced. The analytical results indicate that, in the transverse and longitudinal directions, the accelerations of the isolated building are about 23% and 27% of the ordinary building. In the observation data the acceleration ratios are about 26% and 33%. This further demonstrates that as the floor elevation increases the degree of acceleration reduction also increases.

To illustrate the effect of the isolation system, Fig. 4 compares both observed and calculated accelerations in the transverse direction at the roof level for earthquake #44. As can be seen, the accelerations are greatly reduced for the isolated building.

5 CONCLUSIONS

From the results of this study several conclusions can be drawn:

(1) With the use of high damping-low shear modulus elastomeric bearings the advantage of isolation system in mitigating the acceleration response is very significant even for small earthquakes.

(2) The ANL developed SISEC code can produce the general shape of the acceleration responses of the isolated building. The analysis accurately predicts the peak accelerations and the arrival times.

(3) The ANL designed isolation bearings are very effective for reducing the earthquake hazard.

ACKNOWLEDGMENTS

This work was supported by the U.S. National Science Foundation, Agreement No. CES-8800871.

REFERENCES

Wang, C. Y. et al. (1991). System Response Analyses of Base-Isolated Structures to Earthquake Ground Motions, Trans. SMiRT-11, paper K26/6, August 18-23, Tokyo, Japan.

Wang, C. Y. and Gvildys, J. (1991). Comparison of SISEC Code Simulations with Earthquake Data of Ordinary and Base-Isolated Buildings, SMiRT-11, paper K 27/4, August 18-23, Tokyo, Japan.

Uras, R. A. (1993). Seismic Response of Base-Isolated Building Using a Viscoelastic Model, Trans. SMiRT-12, paper K23/3, August 15-20, Stuttgart, Germany (to be published).

Kuroda, et al. (1991). Outline of Study and Test on Characteristics of Individual Bearing, ANL/Shimizu, SHUM-006, Rev. 0.

Kelly, J. M. (1991). Mechanical Characteristics of Low Modulus High Damping Natural Rubber Isolators for a Base Isolated Demonstration Building, ANL/Shimizu, ANL-004.

Table 1. Comparison of accelerations of isolated and ordinary buildings

			Ordinary Bldg., A_0		Isol. Bldg., A_1		Accel. Ratio, A_1/A_0	
Eq. No.	Loc.	Dir.	Obs. (gal)	Cal. (gal)	Obs. (gal)	Cal. (gal)	Obs.	Cal.
42	Roof	T	7.18	6.96	1.87	1.59	0.26	0.23
		L	7.29	7.16	2.46	1.94	0.33	0.27
	1st Floor	T	2.10	2.45	1.39	1.33	0.66	0.54
		L	2.79	3.58	1.90	1.70	0.68	0.47
44	Roof	T	8.73	8.56	1.44	1.34	0.16	0.16
		L	5.43	5.27	1.09	0.86	0.20	0.16
	1st Floor	T	1.66	1.95	1.19	0.97	0.71	0.50
		L	1.43	2.05	0.93	0.76	0.65	0.37

Note: T: Transverse L: Longitudinal

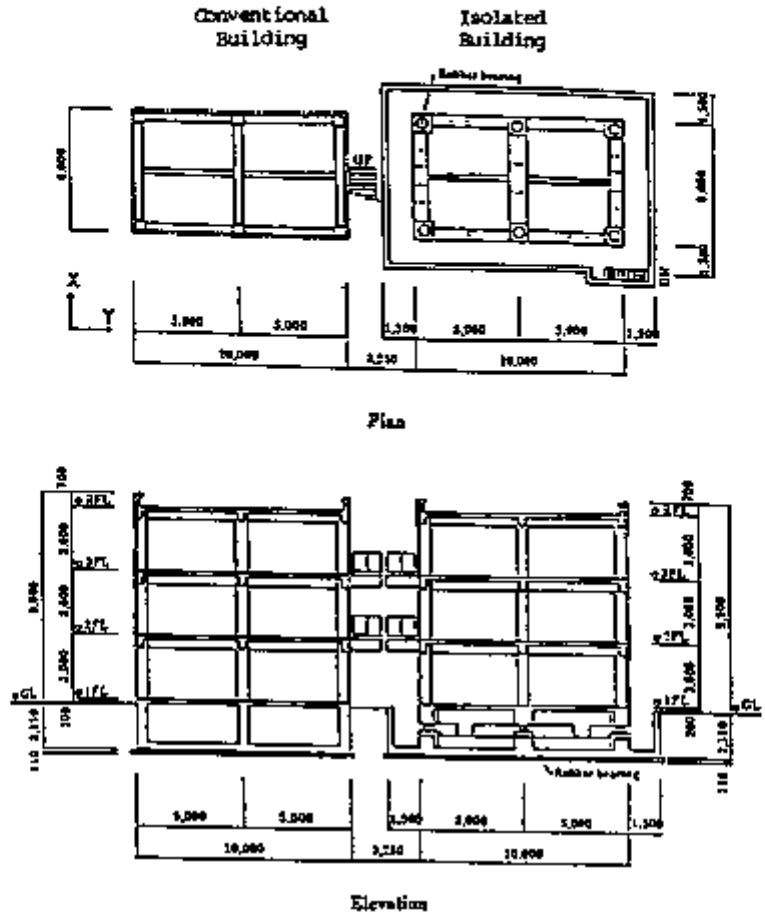

Fig. 1 Plan and Elevation of Test Buildings

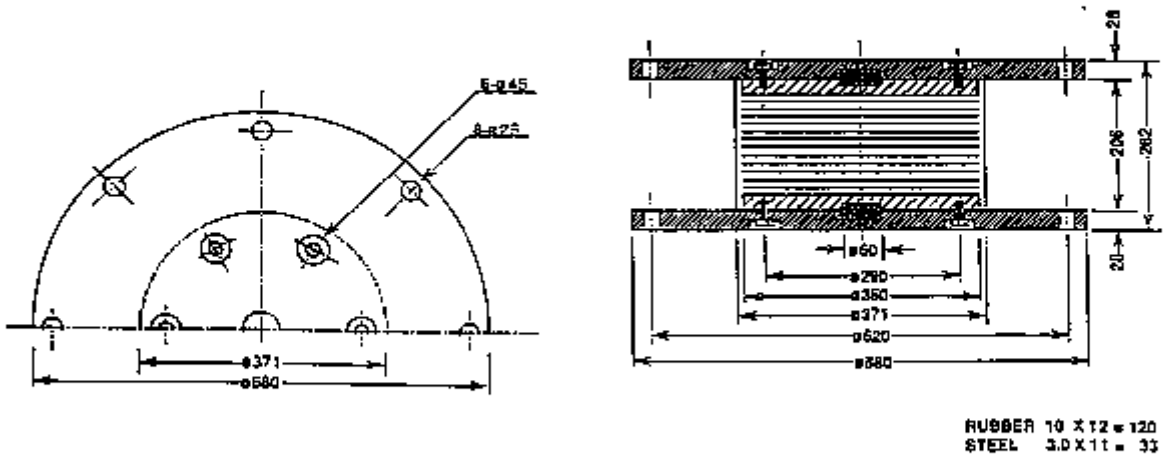

Fig. 2 Bearing Dimensions (unit: mm)

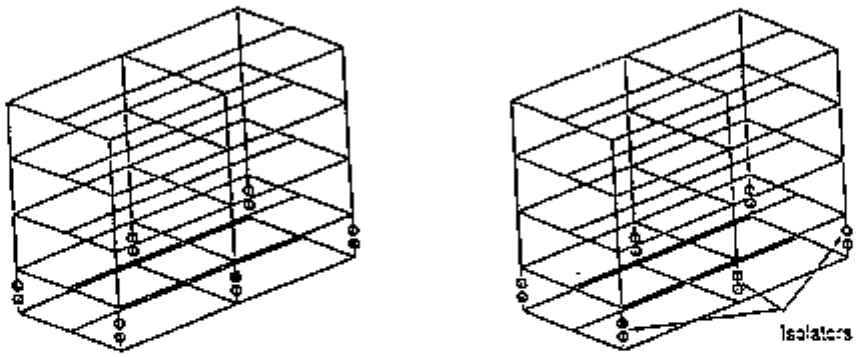

NO ISOLATION WITH ISOLATION

Fig. 3 Mathematical Model of Ordinary and Isolated Buildings

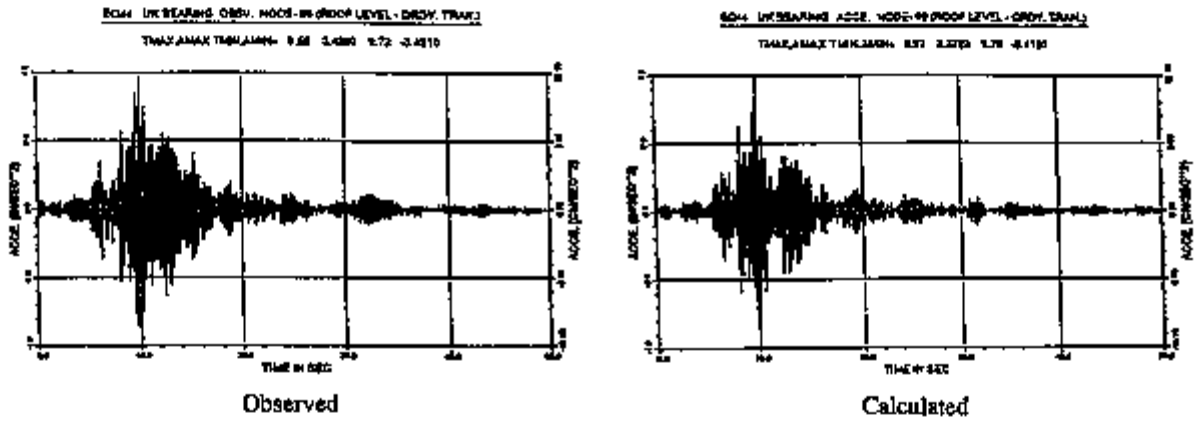

Observed Calculated

Ordinary Building

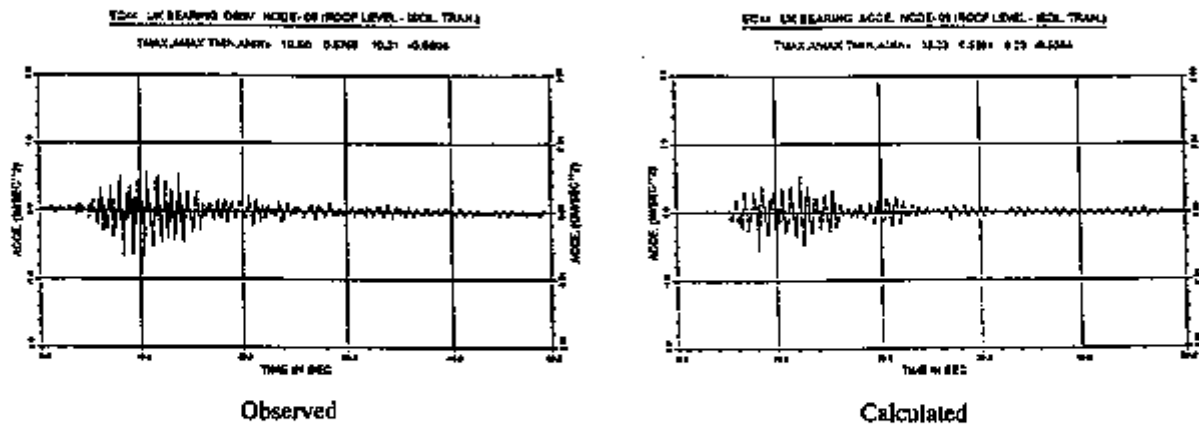

Observed Calculated

Isolated Building

Fig. 4 Comparison the Observed and Calculated Transverse Accelerations at the Roof Level (Eq. #44)

SMiRT-12 / K. Kussmaul (Editor)

K25/2

THREE-DIMENSIONAL SEISMIC ISOLATION FLOOR SYSTEM USING AIR SPRING AND ITS INSTALLATION INTO A NUCLEAR FACILITY

M. Uriu[1], M. Yamamoto[1], K. Shinzawa[1], Y. Yamazaki[1], N. Tokuda[2], A. Kashiwazaki[2], M. Iwama[2], S. Matumoto[3], J. Yokozawa[3] and A. Hara[3]

[1]Power Reactor and Nuclear Fuel Development Co., Tokai, [2]Ishikawajima-Harima Heavy Industries Co. Ltd., Yokohama, [3]Ishikawajima-Harima Heavy Industries Co. Ltd., Tokyo (Japan)

1. INTRODUCTION

As high-precision equipments such as computer systems have been highly advanced in the nuclear field, it is important to protect them from earthquakes. The use of seismic isolation system may provide a practical solution for the object [1].

Research on the use of laminated rubber bearings as seismic isolators has been primarily focused on the development of base-isolated buildings. The laminated rubber bearing shows excellent seismic isolation performance to horizontal directions. However, it cannot reduce the response due to vertical seismic motion. Strength of buildings is usually sufficient to vertical earthquake motion, but high-precision equipments inside of buildings are easily resonant to vertical motion as well as horizontal one. Hence, the use of three-dimensional isolators is necessary to protect them from earthquakes.

Development of three-dimensional isolators for base-isolated buildings may not be practical because of its high cost and of the difficulty in suppressing a rocking motion. One of the practical methods for protecting these equipments may be use of a three-dimensional seismic floor isolation system, on which they are set up.

A three-dimensional seismic isolation floor system has been developed, where the isolator is constructed by the combination of an air spring and a laminated rubber bearing [2,3]

In genaral, isolated structure should be sufficiently stiff relative to an isolator. In three-dimensinal seismic isolation floor systems, however, vertical stiffness of floor structure is limited as compared with an isolator, and load distribution on the isolated floor is non-uniform. Therefore, bending deformations of floor structure is easily caused by vertical seismic motion. The use of air springs as vertical isolators enables to attain uniform vertical motion without bending deformations, because its vertical stiffness is propotional to air pressure i.e. its suppoting load.

The present three-dimensional seismic isolation floor system has been installed into a part of the central control room of the Tokai Vitrification Facility (TVF) of Power Reactor and Nuclear Fuel Development Corporation (PNC). In this paper, we discribe an outline of the above system, the design conditions and the results of performance test using a three-dimensional shaking table.

2.BASIC CONCEPT OF THE PRESENT SYSTEM

2.1 OUTLINE OF THE SYSTEM

The system consists of three-dimensional isolators, viscous dampers and automatic floor level controller and so on, as shown in Fig.1.

The three-dimensional isolator, the main device of the system, is constructed by the combination of an air spring and a laminated rubber bearing. Vertical vibration is absorbed by the air spring, while horizontal one is primarily by the laminated rubber bearing. Fig.2 shows a cross-section of the isolator.

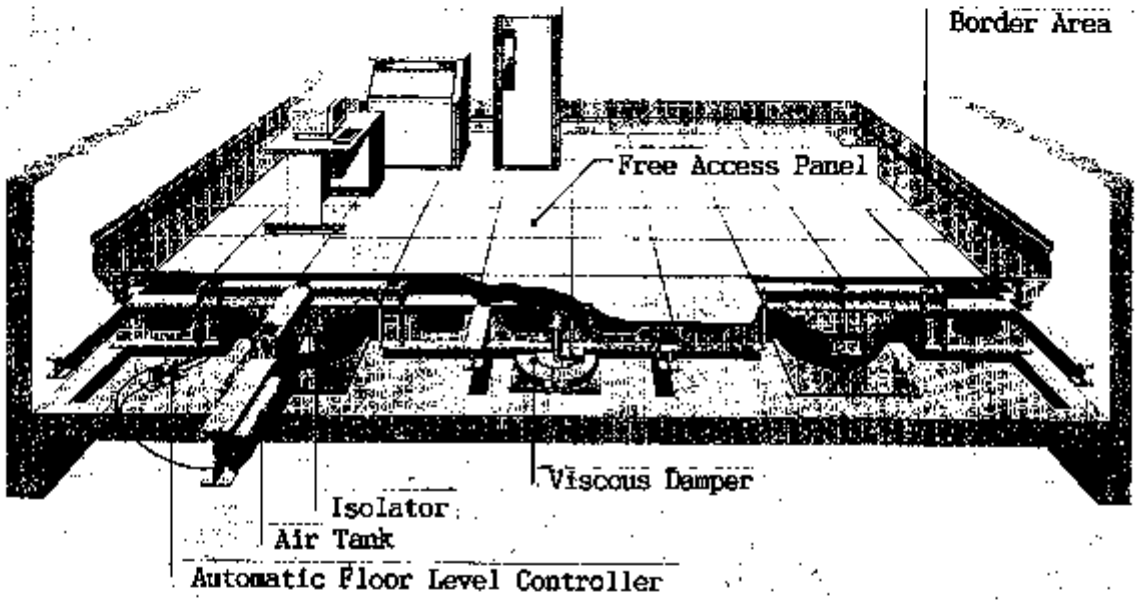

Fig.1 Three-dimensional Isolation Floor System

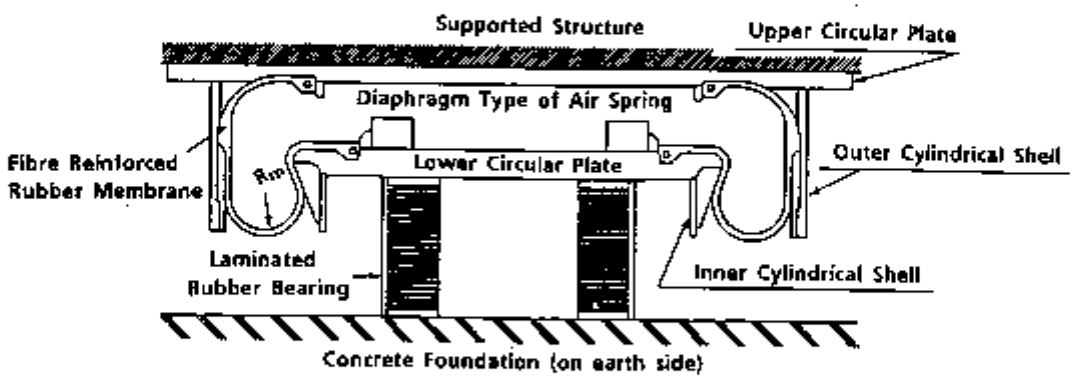

Fig.2 Three-dimensional Isolator

A viscous damper is adopted to reduce horizontal response displacement. It utilizes the shear resistance of highly viscous material located in the gap beetween the base plate of the vessel of the damper and the sliding plate. And an air damper utilizing the feature of an air spring is adopted to vertical damper, which will be discribed later.

2.2 MERIT IN USE OF AIR SPRING

One of the technical difficulty in three-dimensional seimic floor isolation system may be to attain the response in uniform translational motion to vertical seismic motion. In general, supporting load of each isolator varies due to non-uniform load distribution on the isolated floor, i.e. non-uniform arrangement of equipments. And vertical stiffness of floor structure is not sufficintly stiff so that bending deformations of floor structure are easily caused by vertical seismic motion. The use of air springs as vertical isolators enables to attain uniform vertical motion without bending deformations, because its vertical stiffness is propotional to air pressure i.e. its suppoting load. It should be noted that this specific feature of the air spring cannot be given by the use of a conventional coil spring.

Another merit of an air spring is to utilize air damping as a vertical damper with the auxiliary use of air tank. The air damping force is obtained from the resistance generated at an orifice equiped with the connecting part of the air spring with the air tank. The mechanism of air damper is simple as shown in Fig.3, and provides riliable high damping performance, which is independent of temprature.

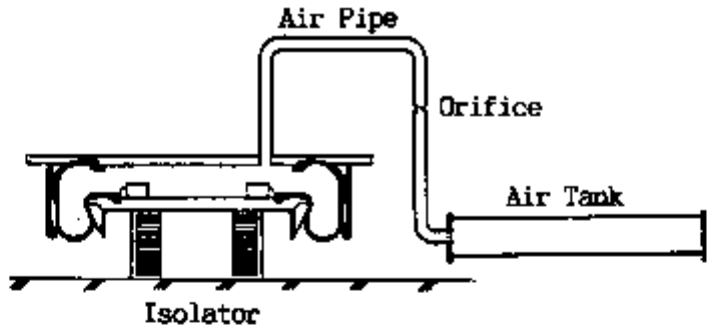

Fig.3 Air Damper

3. ISOLATION FLOOR SYSTEM INSTALLED INTO TVF

The present three-dimensional isolation floor system has been installed into TVF of PNC, in Tokai, Japan. TVF was constructed in 1992, to bear the mission of demonstrating the technology of radioactive liquid waste vitrification. The isolation floor system is installed into a part of the central control room on the second floor of the Technical Developement Building in TVF (Fig.4), with the aim of further increasing the reliability of contral equipments.

The TVF's isolation floor system is shown in Fig.5. The floor area of system is about $100m^2$, supported by four isolators. Natural frequencies, damping ratios and maximum allowable displacements of the system are shown in Table 1.

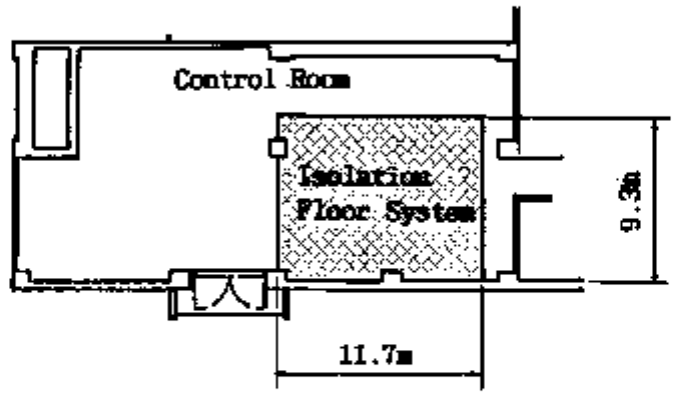

Fig.4 Arrangement of Isolation Floor System

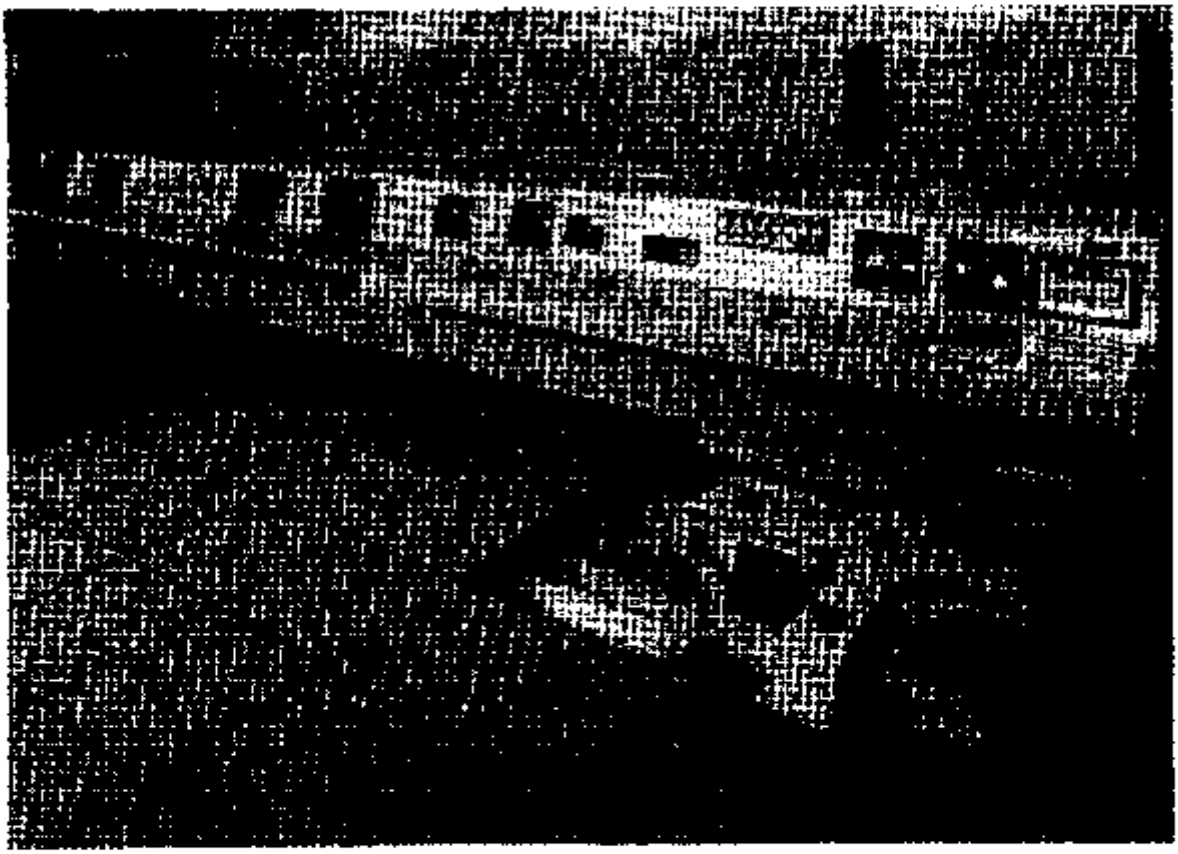

Table 1 Characteristics of TVF's Isolation System

	Natural Frequency	Damping Ratio	Allowable Displacement
Horizontal	0.7 Hz	20 %	± 150 mm
Vertical	1.2 Hz	20 %	± 40 mm

In floor isolation systems it is important to compromise reducing the response acceleration and suppressing large displacement relative to non-isolation part, as compared with the base isolation system. Because available area in control room is reduced by the increase of the border area which absorbs the above displacement smoothly. From the point of view, the frequency of 0.7Hz and damping ratio of 20% in horizontal direction were designed, respectively. Under these conditions, response displacement caused by the design base seismic motion is about 50mm. Maximum allowable displacement is ensured to be about three times of response displacement, which it may be sufficient under the design base earthquake.

Moreover, for the purpose of preventing serious damages under the seismic motion over the design base, a stopper device is adopted to the TVF's system. The stopper is made of rubber block, which suppresses the excessive displacement.

4.PERFORMANCE CONFIRMATION TEST

With the purpose to verify performance of the present system, shaking tests were performed using a floor model. A three-dimensional shaking table of 35tf in IHI Earthquake-Proof Engineering Laboratory was used for seismic isolation performance test. General view of the test model is shown in Fig.6. Four isolators of real size were used in the test model, while its floor area was reduced due to the restriction of the size of the shaking table.

An example of seismic isolation performances to El Centro-NS floor response waves is shown in Fig.7. The input waves were floor response wave at the second floor of the Technical Developement Building. Ground level motion is normalized to a maximum acceleration of 180cm/sec^2 . The seismic isolation performance for the other typical seismic waves were also confirmed in the test.

5.CONCLUDING REMARKS

A three-dimensional isolation floor system has been developed, where the three-dimensional seismic isolator combining an air spring and a laminated rubber bearing is used. And it has been installed into the central control room of PNC's TVF. By using an air spring, the system has various practical specific features including excellent seismic isolation performance. We plan to observe the seismic behavior of the system to confirm the seismic isolation performance from the results of these observation.

Fig.6 Test Model

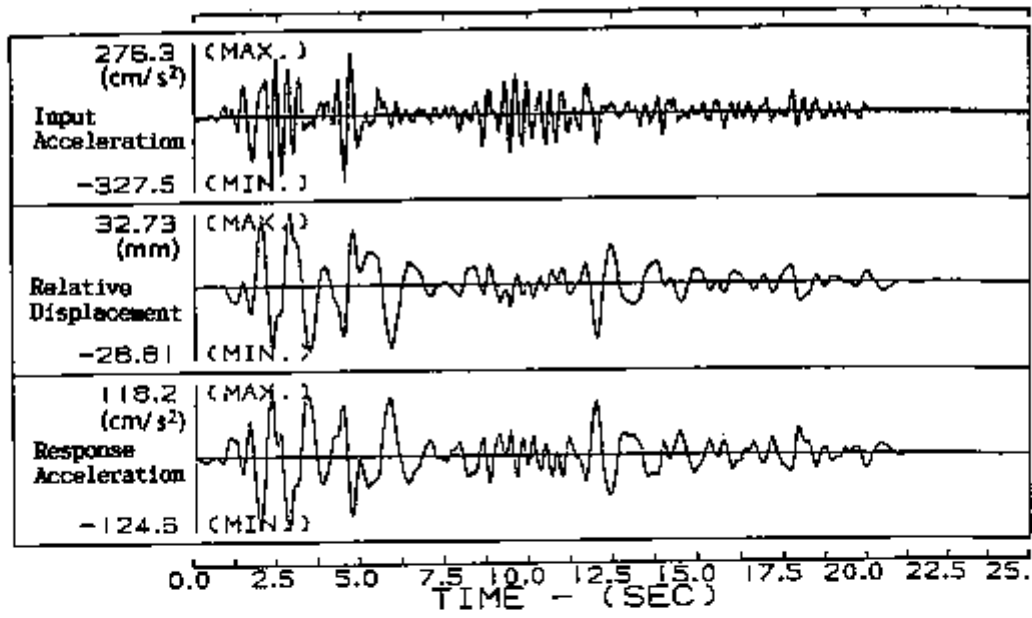

Fig.7 Example of Test Results (El Centro-NS Floor Response Wave)

REFERENCES

[1] Fujita,T. 1985. Earthquake Isolation Technology for Industial Facilities-Reserch, Development and Applications in Japan.
Bulletin of the Newzealand National Society for Earthquake Engineering 18-3

[2] Kashiwazaki,A.Tanaka,M.and Tokuda,N. 1988. Shaking Test of Seismic Isolation Floor System by Using 3-dimensional Isolator.
Procedings of Ninth World Conference on Earthquake Engineering V-p845

[3] Tanaka,M.et al 1989. Developement of Earthquake and Microtremor Isolation Floor System Utilizing Air Springs and Laminated Rubber Bearings.
IHI Engineering Reviw 22-2